2015-07-01

Large-Scale Testing of Passive Force Behavior for Skewed Bridge Abutments with Gravel and Geosynthetic Reinforced Soil (GRS) Backfills

Amy Fredrickson

Brigham Young University - Provo

www.manaraa.com

Large-Scale Testing of Passive Force Behavior for Skewed Bridge Abutments

with Gravel and Geosynthetic Reinforced Soil (GRS) Backfills

Amy Fredrickson

A thesis submitted to the faculty of
Brigham Young University
in partial fulfillment of the requirements for the degree of

Master of Science

Kyle M. Rollins, Chair
Kevin W. Franke
Paul W. Richards

Department of Civil and Environmental Engineering

Brigham Young University

July 2015

ABSTRACT

Large-Scale Testing of Passive Force Behavior for Skewed Bridge Abutments
with Gravel and Geosynthetic Reinforced Soil (GRS) Backfills

Amy Fredrickson
Department of Civil and Environmental Engineering, BYU
Master of Science

Correct understanding of passive force behavior is particularly key to lateral evaluations of bridges because plastic deformation of soil backfill is vital to dissipation of earthquake energy and thermally-induced stresses in abutments. Only recently have studies investigated the effects of skew on passive force. Numerical modeling and a handful of skewed abutment tests performed in sand backfill have found reduced passive force with increasing skew, but previous to this study no skewed tests had been performed in gravel or Geosynthetic Reinforced Soil (GRS) backfills. The goal of this study was to better understand passive force behavior in non-skewed and skewed abutments with gravel and GRS backfills. Prior to this study, passive pressures in a GRS integrated approach had not been investigated. Gravel backfills also lack extensive passive force tests.

Large-scale testing was performed with non-skewed and 30° skewed abutment configurations. Two tests were performed at each skew angle, one with unconfined gravel backfill and one with GRS backfill, for a total of four tests. The test abutment backwall was 11 ft (3.35 m) wide, non-skewed, and 5.5 ft (1.68 m) high and loaded laterally into the backfill. However, due to actuator loading constraints, all tests except the non-skewed unconfined gravel test were performed to a backfill height of 3.5 ft (1.07 m). The passive force results for the unconfined gravel test was scaled to a 3.5 ft (1.07 m) height for comparison.

Test results in both sets of backfills confirmed previous findings that there is significant reduction in passive force with skewed abutment configurations. The reduction factor was 0.58 for the gravel backfill and 0.63 for the GRS backfill, compared to the predicted reduction factor of 0.53 for a 30° skew. These results are within the scatter of previous skewed testing, but could indicate that slightly higher reduction factors may be applicable for gravel backfills.

Both backfills exhibited greater passive strength than sand backfills due to increased internal friction angle and unit weight. The GRS backfill had reduced initial stiffness and only reached 79% to 87% of the passive force developed by the unreinforced gravel backfill. This reduction was considered to be a result of reduced interface friction due to the geotextile. Additionally, the GRS behaved more linearly than unreinforced soil. This backfill elasticity is favorable in the GRS-Integrated Bridge System (GRS-IBS) abutment configuration because it allows thermal movement without developing excessive induced stresses in the bridge superstructure.

Keywords: passive force, skewed abutment, bridge abutment, pile cap, geosynthetics, geotextile, GRS, IBS, gravel, large-scale, earthquake, seismic

ACKNOWLEDGEMENTS

TABLE OF CONTENTS

LIST OF TABLES

LIST OF FIGURES

xiii

xiv

xv

xvi

xvii

www.manaraa.com

1　Introduction

1.1　Background

The passive force behavior of soil backfills behind bridge abutments affects the stress, strain, and displacement of bridge decks when subjected to seismic forces or thermal expansion (Shamsabadi et al., 2006). Correct understanding of passive force behavior is particularly key to seismic evaluations of bridges because nonlinear plastic deformation of soil backfill is vital to dissipation of earthquake energy in the abutments (Shamsabadi et al., 2006). While passive force behavior of non-skewed bridge abutments has been tested in numerous studies, (Mokwa and Duncan 2001; Rollins and Cole 2006; Rollins et al. 2010; Rollins and Sparks 2002), testing of the behavior behind skewed abutments has not been performed until recently. Non-skewed large-scale tests indicate that peak passive force can be accurately predicted using the log-spiral method and is usually achieved at a longitudinal deflection of 3% to 5% of the backwall height (Rollins and Cole 2006) and that the passive force-deflection is roughly hyperbolic. Methods for approximating the passive force-deflection curve as a hyperbola have been developed by Shamsabadi et al. (2007) and Duncan and Mokwa (2001). However, for simplicity in design, most specifications recommend a bilinear relationship (AASHTO 2014; Caltrans 2010).

Approximately 40% of bridges in the U.S. are skewed (Nichols, S., 2012, personal communication). Furthermore, current bridge design practices assume the peak passive force is the same for skewed bridges as for non-skewed bridges (AASHTO 2014; Caltrans 2010).

However, field evidence clearly indicates poorer performance of skewed abutments during seismic events (Apirakyorapinit et al. 2012; Elnashai et al. 2010; Shamsabadi et al. 2006; Unjoh 2012) and distress to skewed abutments due to thermal expansion (Steinberg and Sargand 2010). Stresses in bridge systems are complex so cause and effect is difficult to isolate by observation (Steinberg and Sargand 2010). Therefore, large-scale testing is vital to understanding behaviors such as passive force.

The effects of skew on backfill passive force behavior of bridge abutments has recently been the focus of numerical modeling by Shamsabadi et al. (2006) and laboratory testing by Rollins and Jessee (2013). Definitive reduction in passive force was observed with increasing skew angle. Using data obtained from these studies, Rollins and Jessee (2013) proposed the correction factor, R_{skew}, given by Equation (1-1) which defines the ratio between the peak passive force for a skewed abutment ($P_{P\text{-skew}}$) and the peak passive force for a non-skewed abutment ($P_{P\text{-no skew}}$) as a function of skew angle in degrees, θ.

$$R_{skew} = P_{P-\,skew} / P_{P-no\,skew} = 8.0 * 10^{-5}\theta^2 - 0.018\theta + 1.0 \qquad (1\text{-}1)$$

Now several large-scale tests have also been performed on skewed bridge abutments in various configurations to confirm the validity of Eq. (1-1). In laboratory testing, backfill was confined along the planes of the sides of the scaled abutment (Rollins and Jessee, 2013). In field testing, backfill configurations included unconfined (Marsh, 2013; Palmer, 2013), with Mechanically Stabilized Earth (MSE) wingwalls (Franke, 2013), and with reinforced concrete (RC) wingwalls (Smith, 2014). All these tests were performed with clean sand backfill. Previous testing involving lateral loading of a non-skewed pile cap in gravel backfill performed by Pruett (2009) demonstrated that gravel has greater passive resistance capacity compared to clean sand (Cummins, 2009) owing to the higher friction angle. The higher friction angle could potentially

2

change the transverse shear resistance on the abutment wall and lead to differences in passive force for a skewed abutment relative to that predicted by Eq. (1-1).

An increasingly common backfill design configuration behind bridge abutments is Geosynthetic Reinforced Soil (GRS) backfill. According to the Federal Highway Administration (FHWA), GRS backfill refers to closely-spaced geotextile sheets placed in alternating horizontal layers with compacted granular backfill soil (Adams et al., 2011). The FHWA designed an Integrated Bridge System (IBS) using GRS for both an abutment and integrated approach backfill as a low-cost, accelerated bridge construction technique for shorter-span bridges. The GRS backfill spreads vertical loading from the abutment in order to reduce settlement and, therefore, the "bump" at the end of the bridge. While one study investigated the geotechnical effects of GRS-IBS thermal expansion, more severe lateral loads have not been investigated very thoroughly, and no testing has been done with GRS backfills in skewed configurations. This is the first passive pressure test of its kind in GRS backfill.

1.2 Research Objectives

The objectives of this research study are to:

1. Determine the passive-force deflection relationships for a skewed and non-skewed abutment with gravel backfill relative to sand backfill.

2. Determine the passive-force deflection relationships for a skewed and non-skewed abutment with Geosynthetic Reinforced Soil (GRS) backfill relative to conventional gravel backfill.

3. Investigate the effect of skew angle on reduction in passive force for gravel and GRS abutments.

www.manaraa.com

4. Evaluate methods for predicting passive-force deflection behavior of gravel and GRS abutments.

1.3 Scope of Work

To more fully understand the relationship between skew angle and reduction in peak passive force in gravel and GRS backfill, four large-scale tests were conducted to determine the passive force-deflection curves at skew angles of 0° and 30°. These tests were conducted using an existing 11-ft (3.35-m) wide by 5.5-ft (1.68-m) high by 15-ft (4.57-m) long pile cap which has been used for a number of previously conducted lateral load and passive force-deflection tests (Rollins et al. 2010; Rollins and Sparks 2002; Strassburg 2010).

Previous tests performed at these angles at this site used sand backfill (Franke 2013; Marsh 2013; Palmer 2013) and will be used as comparisons. Two tests in this study, one at 0° and one at 30° skew, were performed with a gravel backfill. The other two tests used a GRS backfill, which used the same gravel material alternated with closely-spaced woven polypropylene geotextile, again with one at 0° and one at 30° skew. Other passive force studies involving gravel backfill include Duncan and Mokwa (2001), Rollins and Cole (2006), and Pruett (2009), but none of the tests used a skewed pile cap. No other published tests involved GRS backfill against extensive lateral loading, so these tests are the first of their kind. The 0° and 30° skew tests for this study were conducted in a similar fashion to the tests conducted by the previous researchers at the same test site.

1.4 Outline of Presentation

This paper will report on the objectives outlined above in the following manner: Chapter 2 will outline the current state of knowledge of topics pertinent to this testing and its desired

objectives. Chapter 3 will specify how the large-scale testing was performed. Chapters 4 and 5 will show the results of the testing for the gravel and GRS backfills, respectively. Chapter 6 will contain the analysis of the results, including comparisons between the gravel and GRS tests and comparisons to previous studies. It will also include computer program analyses. Chapter 7 will summarize the conclusions of this paper and outline recommendations for future research.

2 Literature Review

2.1 Passive Earth Pressure Theories

Lateral Earth Pressure theories attempt to describe how soil behaves under lateral forces and movements. Generally, lateral pressures on soil are different than their vertical pressures, for which difference Lateral Earth Pressure Theory accounts by multiplying the vertical pressure, σ_v with a coefficient of lateral earth pressure, K, to find the horizontal earth pressure, σ_h. This expression is shown in Equation (2-1). Generally the total vertical stress at a given depth is the weight of the soil, γ, multiplied by the height of soil (H) above that point. Thus vertical stress, and therefore lateral earth pressure, increases with depth.

$$\sigma_h = K\sigma_v = K\gamma H \tag{2-1}$$

There are three cases of lateral earth pressure: active, at rest, and passive. Soil exhibits greater strength in compression (passive case) than in tension (active case) or at rest. In other words, any structure moving laterally when embedded in homogenous soil will feel much more resistance against movement from the passive pressure of the soil being compressed than from the active pressure from the soil acting on the opposite side of that structure. In design, higher passive pressures are generally favorable because they restrict movement in the structure being pushed into the soil. Therefore, it has traditionally been considered more conservative to underpredict passive pressures than to overpredict them. However, in cases of lateral spreading, lower passive pressures are favorable, and underprediction would actually be non-conservative.

7

Since this study is focused on passive force behavior, this section discusses the current state of knowledge about predicting passive pressure and the several factors which affect it.

2.1.1 Summary of Passive Theories

A study by Duncan and Mokwa (2001) discusses three widely-used passive earth pressure theories and compares them. The Rankine Theory, the simplest of the methods, is based on stresses and oversimplifies most cases of passive pressures mainly by ignoring soil friction angle. The Coulomb Theory non-conservatively overpredicts passive pressure whenever the ratio of the interface friction angle to the soil friction angle (δ/φ) is greater than 40%. Duncan and Mokwa (2001) found the Log Spiral Theory to be the most accurate for predicting ultimate passive resistance when corrected for 3D effects. A study by Cole and Rollins (2006) confirmed these conclusions to be correct when comparing the passive earth theory predictions to the actual passive resistance attained in their testing, as will later be shown in Table 2-3.

2.1.2 Passive Force Equation

In cohesive soils, the inter-particle cohesion affects the lateral earth pressure, as shown in Figure 2-1, and creates an additional term in the lateral earth pressure equation seen in Equation (2-1). The general earth pressure equation as applied for passive pressure is shown in Equation (2-2).

$$\sigma_P = \gamma H K_P + 2c'\sqrt{K_P} \qquad (2\text{-}2)$$

where

σ_p = Total Resisting Passive Force

γ = Specific Weight of the Backfill

8

H = Height of the Backfill

K_p = Coefficient of Passive Lateral Earth Pressure

c' = Backfill Cohesion
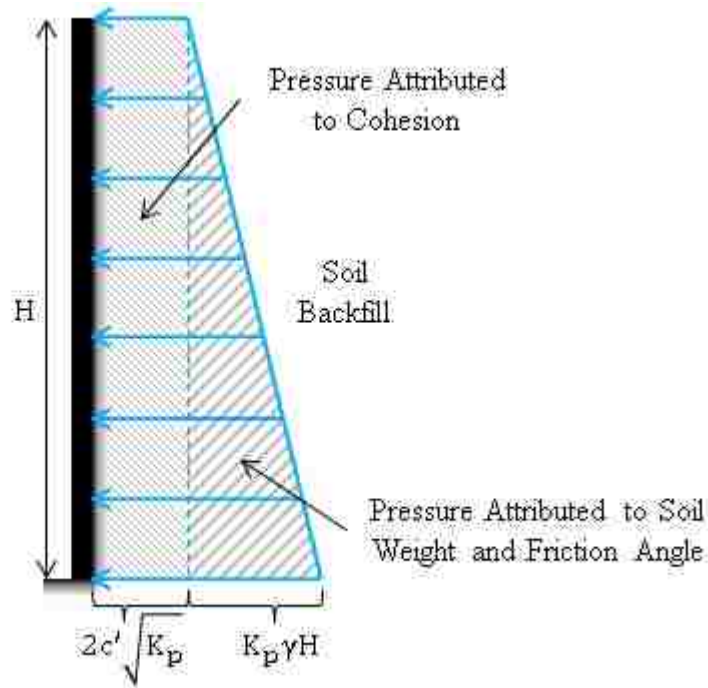
Figure 2-1. Lateral pressure distribution for soil (Smith, 2014).

To find the resultant passive force of a backfill from a given structure, the average pressure is multiplied by the total effective resisting area. The resulting passive force equation is shown as Equation (2-3).

$$P_P = \frac{1}{2}\gamma H^2 K_P B_e + 2c'HB_e\sqrt{K_P}$$ (2-3)

where

P_p = Total Resisting Passive Force

B_e = Effective Width of Failure Surface (Brinch Hansen, 1966) = $B * R_{3D}$

As discussed in 2.1.1, K_P is most accurate when found using the log spiral method, which is most often performed graphically. In the log spiral method, K_P is a factor of internal friction angle (φ), the ratio of wall friction angle to the internal friction angle (δ/φ), and the slopes of the backfill and the backwall (AASHTO, 2014). Potyondy (1961) gathered approximate values for the wall to internal friction angle ratio. The minimum values from his study are summarized in Table 2-1. Potyondy's study did not directly address interface friction angles with gravel, but in general practice because sand and gravel are both granular, the sand values are used for gravel. AASHTO (2014) gives approximate values for interface friction angles, including between formed concrete and gravel, which are summarized in Table 2-2. Conservatively, AASHTO's values are significantly lower than Potyondy's; Potyondy's are more generally used in practice.

Table 2-1: Minimum Values for δ/φ (Potyondy, 1961)

Soil Type	Structural Material		
	Steel (δ_{max}/φ)	Concrete (δ_{max}/φ)	Wood (δ_{max}/φ)
Sand	0.54	0.76	0.76
Silt and clay	0.54	0.50	0.55

Table 2-2: Friction Angle for Dissimilar Materials (AASHTO, 2014)

Interface Materials	Friction Angle, δ (degrees)
Formed or precast concrete against the following soils:	
• Clean gravel, gravel-sand mixture, well-graded rock fill with spalls	22 to 26
• Clean sand, silty sand-gravel mixture, single-size hard rock fill	17 to 22
• Silty sand, gravel or sand mixed with silt or clay	17
• Fine sandy silt, non-plastic silt	14

10

2.1.3 Factors of Passive Resistance Development

As outlined by Duncan and Mokwa (2001), four factors control the development of passive earth pressures. The four factors are movement of the structure, soil strength and stiffness, interface friction and adhesion, and shape of the structure. Each of these factors is described below in greater detail.

2.1.3.1 Structure Movement

When soil fails in lateral loading, the failure wedge moves both horizontally and vertically from the loading. This explains one reason why soil heaves when it is failed laterally. Figure 2-2a illustrates this failure wedge. Because of the vertical components, including the shear of the ascending soil against the structure face, the actual passive pressure resultant acts at an angle to the horizontal plane or to whatever plane is perpendicular to the soil-structure interface.

2.1.3.2 Soil Strength and Stiffness

The behavior of the passive resistance with increasing load is largely governed by the strength and stiffness of the soil backfill (Duncan and Mokwa, 2001). The strength of the soil will govern the peak passive resistance. The stiffness of the soil will govern how great of a movement is necessary to reach a given resistance.

Additionally, undrained conditions apply in passive earth pressure if the load is applied quickly and the soil has low permeability. Otherwise drained conditions dictate soil behavior. Cohesion and friction both affect passive resistance (Duncan and Mokwa, 2001).

2.1.3.3 Interface friction and adhesion

Figure 2-2 shows the free body diagrams illustrating the equilibrium of forces for both the moving backwall structure—an anchor block in the case shown—and the soil behind such a

11

structure. As shown in (b) and (d), the passive force, E_p, is a reaction to horizontal loading of the structure, T, and the weight of the structure, W_{ab}. Sub-figure (d) shows that the interface friction angle at which the passive force acts is δ_{mob} from the horizontal load. The reaction force of the soil beyond the failure plane, R, acts at a friction angle φ_{mob} from perpendicular to the failure surface, shown as a Rankine failure surface in this figure.
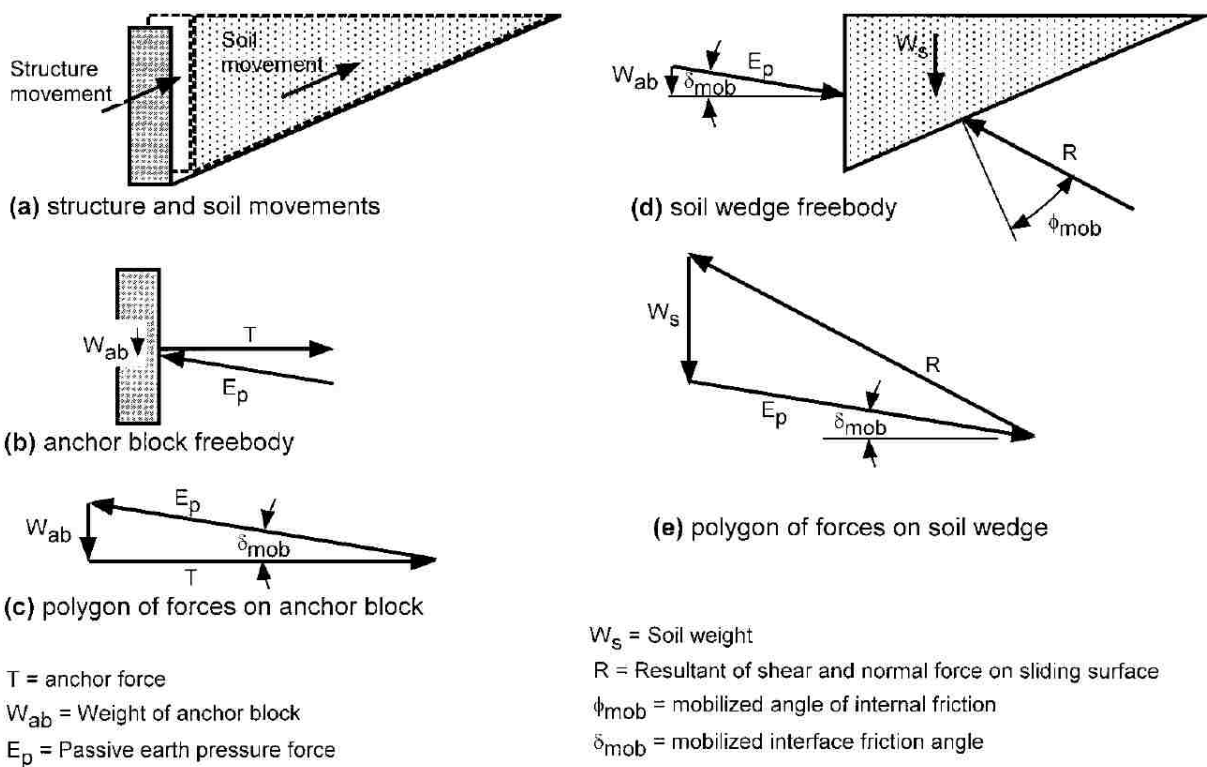
Figure 2-2. Movements, forces, and geometry of passive pressure conditions, taken from Duncan and Mokwa (2001).

Both δ_{mob} and φ_{mob} are less than δ_{max} and φ_{max}, respectively. φ_{max} is governed by soil type and δ_{max} is governed by both the soil type and the roughness of the interface (Duncan and Mokwa, 2001). Furthermore, the minimum movement required to reach full interface friction δ_{max} ranges typically within 0.1-0.25 in (0.25-0.64 cm) (Duncan and Mokwa, 2001). Note that

www.manaraa.com

once maximum friction angles dictated by both the soil and interface are reached, further loading results in failure along the log-spiral failure plane (not shown) and uplift of the structure if it is not sufficiently heavy. Therefore, soils with higher friction angles are generally stiffer and develop greater passive resistance before failure. Also, in the case where the structure is lifted, interface friction would not be fully mobilized before failure. Bridge abutments using pile group foundations are heavy enough to avoid this.

Duncan and Mokwa (2001) also suggest that adhesion to the interface by cohesive structures would also affect the soil-structure interface behavior. The adhesion would increase the shear stresses at the interface. Adhesion is expressed as $\alpha = c_a/c$, where c_a is the active cohesion and c is the maximum cohesion in the soil. Ranges for α start at 0.5 for stiff soil up to 0.9 for soft soils (Duncan and Mokwa 2001).

2.1.3.4 Structure Shape

Corrections for 3D effect are necessary because earth pressure theories generally assume a 2D plane-strain condition (Cole and Rollins 2006). However, when the structures are not very long, as is common in bridge abutments, the geometry around the edges of the structure significantly affects the overall passive pressure behavior. This is due to the width of the failure surface extending beyond the edges of the structure. In shorter structures, the extra width is a more sizeable portion of the passive force and affects the amount of passive resistance proportionally. Tests by Ovesen (1964) confirmed that the passive force for laterally short structures is significantly higher than plane-strain assumptions predict. Based on Ovesen's tests, Brinch Hansen (1966) developed a method for short structures to correct solutions from the conventional passive pressure theories using the plane-strain assumption. Duncan and Mokwa (2001) use the Ovesen-Brinch Hansen 3D correction factor in their PYCAP program, which will

13

be explained in Section 2.3.3. Thus their program can analyze either short or long structures (Duncan and Mokwa, 2001).

2.2 Abutment Configurations

There are three types of commonly constructed abutment configurations in the United States: conventional, integral, and semi-integral (Warren et al., 2014). Conventional bridges are tradition seat and elastomeric bearing pad systems that allow for thermal shrinkage and expansion without placing forces on the abutment. There is also a joint on the ends of the superstructure that allows thermal movement, but differential settlement between the bridge, supported by a deep foundation, and the embankment under the approach slab causes a "bump" at the end of the bridge.

In an attempt to eliminate the "bump," integral bridge abutments do not have joint, seats, or bearing pads. The girders, abutment, and approach slab are all one integrated body. However, a "bump" still develops at the end of the approach slab (Warren et al., 2014). Also, the rigidity of the integrated system requires that the abutment backfill absorb some of the stresses induced by the daily and seasonal expansion and contraction of the bridge. The thermal movement also causes bridge rotation over time (Horvath, 2005). Thus understanding of passive force behavior is particularly important for integral bridges. Semi-integral abutment configurations seek to eliminate the limitations of integral abutments. They use a combination of both conventional and integral abutments: a flexible substructure and a jointless superstructure (Warren et al., 2014).

Integral as well as semi-integral bridges have grown in popularity in recent decades, but because of the rigid connections in integral and semi-integral bridges, the understanding of soil-structure interaction has become more important (Burke Jr. & Gloyd, 1997). Figure 2-3 demonstrates how passive pressures develop with integral abutments.

14
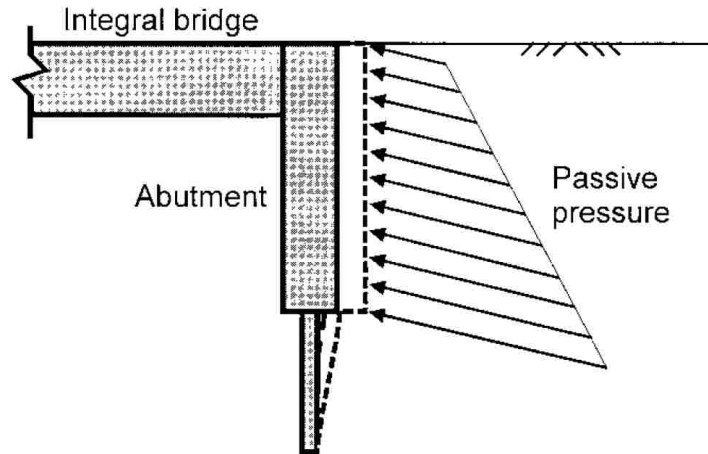
Figure 2-3. Diagram of passive pressure interaction with integral abutment configuration (Duncan & Mokwa, 2001).

2.3 Current Design Methods

To save time and money from doing a detailed soil analysis when designing bridge abutments, simplified methods for calculating the backfill passive force-deflection relationship have been developed for structural engineers. The California Department of Transportation (Caltrans) and the American Association of State Highway and Transportation Officials (AASHTO) have each developed a simplified bilinear method to approximate the passive force-displacement behavior. Additional prediction methods have been developed which are calculated using computer programs, including a hyperbolic method (Duncan & Mokwa, 2001) and a modified hyperbolic method (Shamsabadi et al., 2007). Each of these four methods is briefly described in this section.

2.3.1 Caltrans Method

Caltrans (2010) approximates the passive force-displacement behavior of the backfill with a bilinear relationship comprised of two static parameters of initial stiffness and ultimate passive force. The method is based mainly on the results from a large-scale abutment test done at

UC Davis (Maroney, 1995) and reaffirmed by similar testing done at UCLA (Stewart et al., 2007). The initial stiffness, K_i, of the backfill is approximated to be 50 kip/in (28.70 kN/mm) per ft (m) of wall width for embankment fill dense enough to meet Caltrans specifications as outlined in their seismic design manual and about 25 kip/in/ft (14.35 kN/mm/m) otherwise. K_i is then adjusted proportionally to the backwall/diaphragm height and width as shown in Equation (2-4):

$$K_{abut} = \begin{cases} K_i \times w_e \times \left(\dfrac{h_e}{5.5 \text{ ft}}\right) & \text{US units} \\ K_i \times w_e \times \left(\dfrac{h_e}{1.7 \text{ m}}\right) & \text{SI units} \end{cases} \tag{2-4}$$

where

K_{abut} = Adjusted initial stiffness for the abutment

h_e = Effective height based on abutment type

w_e = Effective width, corrected for skew when needed

Note that the effective height and width are as specified by the figures in the Caltrans (2010) Seismic Design Criteria, and do not correspond with the Brinch Hansen (1966) 3D corrective effective width described in Section 2.1.3.4. From this point the ultimate passive force is determined using Equation (2-5):

$$P_P = \begin{cases} A_e \times 5.0 \text{ ksf} \times \left(\dfrac{h_e}{5.5}\right) & \text{(ft, kip)} \\ A_e \times 239 \text{ kPa} \times \left(\dfrac{h_e}{1.7}\right) & \text{(m, kN)} \end{cases} \tag{2-5}$$

where

P_P = Passive pressure force

A_e = Effective abutment wall area = $h_e \times w_e$

16

The height proportioning and maximum passive pressure of 5.0 ksf (239 kPa) in Equations (2-4) and (2-5) are based on the large-scale testing done at UC Davis (Maroney, 1995) on which the Caltrans method is based. The force-deflection plots demonstrating the Caltrans (2010) passive force prediction method are shown in Figure 2-4.
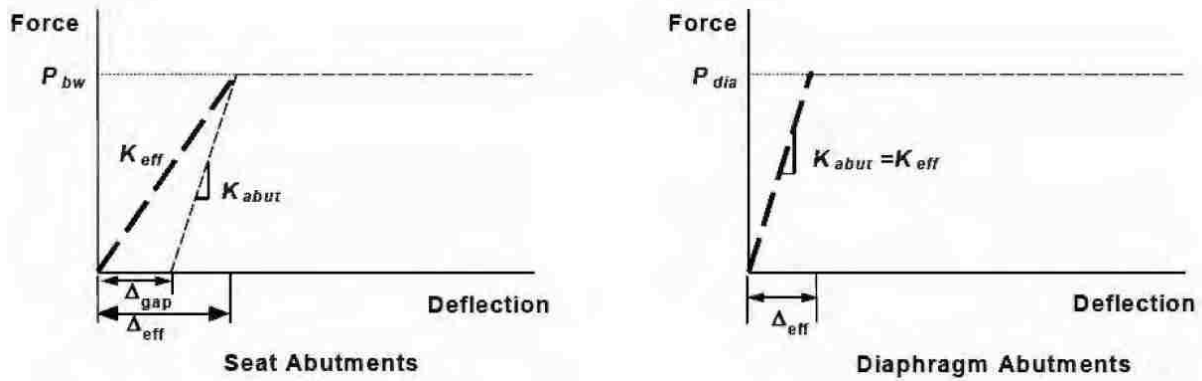
Figure 2-4. Caltrans (2010) passive force-deflection bilinear design curves.

Cole and Rollins (2006) compared their measured peak passive force in four different soil types to predicted passive force values based on three passive pressure theories and the Caltrans 2001 method. The 2001 Caltrans method used 20 kip/in rather than the 25 kip/in required by the 2010 manual as a more conservative approximation, but the ultimate passive force equation has not changed. The results are shown in Table 2-3. Caltrans was somewhat close to the measured values of the clean sand and fine gravel but was overly low for the coarse gravel and silty sand. As discussed in Section 2.1.1 of this chapter, the Rankine theory was grossly low and underestimated in all four cases, the Coulomb theory greatly overestimated in all but silty sand, and the log spiral theory was within about 15% of all four measured results (Cole and Rollins, 2006).

17

Table 2-3: Comparison of Measured and Predicted Peak Passive
Force (Cole and Rollins, 2006)

Method	Peak passive force (kN)			
	Clean sand	Fine gravel	Coarse gravel	Silty sand
Measured	1,090	774	1,997	1,428
Caltrans	914	914	914	914
Coulomb[a]	1,577 (1,577)[b]	1,149 (824)[b]	3,464 (2,224)[b]	1,575 (351)[b]
Log spiral[a]	922	817	1,688	1,210
Rankine[a]	357 (357)[b]	405 (300)[b]	719 (474)[b]	804 (194)[b]

[a]Method includes Brinch Hansen (1966) 3D (R) correction factors (see Table 4).
[b]Cohesion contribution computed using trial wedge for Coulomb and $2c\sqrt{K_p}$ for Rankine; numbers in parenthesis neglect cohesion contribution.

Though Table 2-3 uses the 2001 Caltrans design specifications, the 2010 Caltrans method maintains the same bilinear and rather static characteristics shown. Because there are many backfill types, each with different stiffnesses and a large range of ultimate passive force capacities, the 2010 Caltrans design method is extremely limited in its simplification of passive force-deflection design.

2.3.2 AASHTO Method

The AASHTO (2014) method is also a bilinear design method. The ultimate passive force (P_{ult}) is determined by log spiral theory as discussed in Section 2.1.1. The initial stiffness is not specifically defined, but the maximum deflection required to reach ultimate passive pressure is defined by soil type using values from Clough and Duncan (1991), or 5% to be conservative. However, Clough and Duncan's (1991) values do not include a maximum deflection for reaching ultimate passive force in gravel, but suggest a Δ_{max}/H value of 0.01 for dense sand. Figure 2-5 illustrates the AASHTO (2014) bilinear method. Because AASHTO uses the log spiral method

and Δ_{max}/H values as discussed, it does account for soil type in its passive force-deflection predictions, where Caltrans (2010) does not.
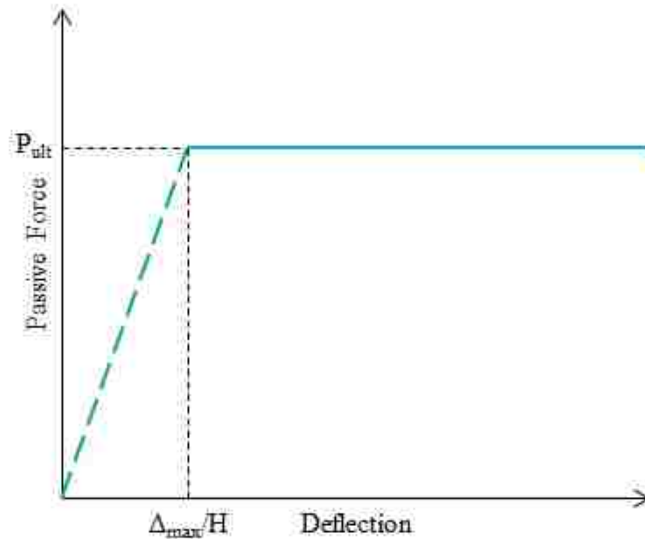
Figure 2-5. AASHTO (2014) bilinear passive force-deflection prediction curve.

2.3.3   Duncan and Mokwa (2001) Hyperbolic Method - PYCAP

Since actual passive force-deflection behavior is more curvilinear, Duncan and Mokwa (2001) created an approximation using a hyperbolic shape. This hyperbolic method was verified by the testing done by Cole and Rollins (2006), as discussed in Section 2.1.3.4. Duncan and Mokwa (2001) created a Microsoft Excel spreadsheet entitled PYCAP to predict the failure surface and force-deflection curve by numerical analysis. PYCAP is based on the log spiral method of lateral earth pressure prediction, and is built exclusively for vertical walls, a horizontal ground surface, and uniform surcharge. Because it can also account for 3D effects using a correction factor from Ovesen-Brinch Hansen (1966), the spreadsheet is not limited to wide structures.

The hyperbolic relationship for force-deflection curves, as introduced by Duncan and Mokwa (2001), is expressed with Equation (2-6):

19

$$P_P = \frac{y}{\left[\frac{1}{K_{max}} + R_f \frac{y}{P_{ult}}\right]}$$

(2-6)

where

 y = Pile cap deflection

 K_{max} = Initial soil stiffness

 R_f = Failure ratio = 0.75 to 0.95

 P_{ult} = Maximum passive soil resistance.

K_{max} is calculated using the soil properties as described by inputs of initial Young's modulus, E_i, and Poisson's ratio, v. Common values for the initial tangent modulus at shallow depths are presented in Table 2-4. Poisson's ratio is traditionally calculated using the soil friction angle, φ, as shown in Equation (2-7). P_{ult} is calculated using the relationship found in Equation (2-8).

$$v = \frac{1 - \sin \varphi}{2 - \sin \varphi}$$

(2-7)

$$P_{ult} = E_p Mb$$

(2-8)

where

 E_p = Passive resistance per unit width

 M = Brinch Hansen 3D correction factor

 b = Pile cap width

Table 2-4: E_i Values for Sands and Gravels at Shallow Depths (2-5 ft or 0.6-1.5 m)
(Duncan and Mokwa, 2001)

Density	D_r	N_{60}	Normally loaded	Preloaded or compacted
Loose	40%	3	$E_i = 200 - 400$ ksf	$E_i = 400 - 800$ ksf
Medium	60%	7	$E_i = 300 - 500$ ksf	$E_i = 500 - 1000$ ksf
Dense	80%	15	$E_i = 400 - 600$ ksf	$E_i = 600 - 1200$ ksf

E_i = initial tangent modulus   1 ksf = 47.9 kPa

D_r = relative density

N_{60} = Standard Penetration Test blow count, adjusted to 60% hammer energy

The Duncan and Mokwa (2001) hyperbolic method is illustrated in Figure 2-6. While there are more input parameters than either bilinear method, the PYCAP program inputs are values that could likely be obtained from a backfill supplier or inferred from approximations based on soil type, such as was demonstrated with Table 2-4 for E_i.
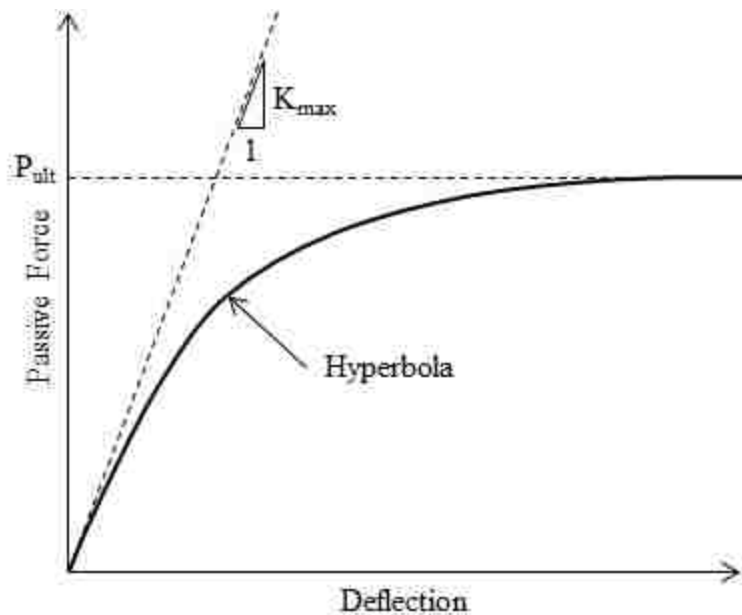
Figure 2-6. Duncan and Mokwa (2001) hyperbolic passive force-deflection curve.

2.3.4 Shamsabadi et al. (2007) LSH Method- ABUTMENT

Shamsabadi et al. (2007) developed a modified hyperbolic model, also based on the log spiral method (LSH). It is based on stress-strain limit equilibrium analysis of log-spiral failure planes and executed in a computer program, ABUTMENT, which has been calibrated with eight field tests using different pile cap configurations and backfills.

The LSH method is based on top down failure as observed by James and Bransby (1971) and Rollins and Cole (2006). In particular, James and Bransby noted that prior to the development of an ultimate shear passive failure plane, smaller shear failure planes are mobilized, as illustrated in Figure 2-7. Thus, each intermediate displacement Δ_i mobilizes a passive failure wedge and results in an intermediate passive force F_i. On the backwall surface this progression develops from the top down as discussed.
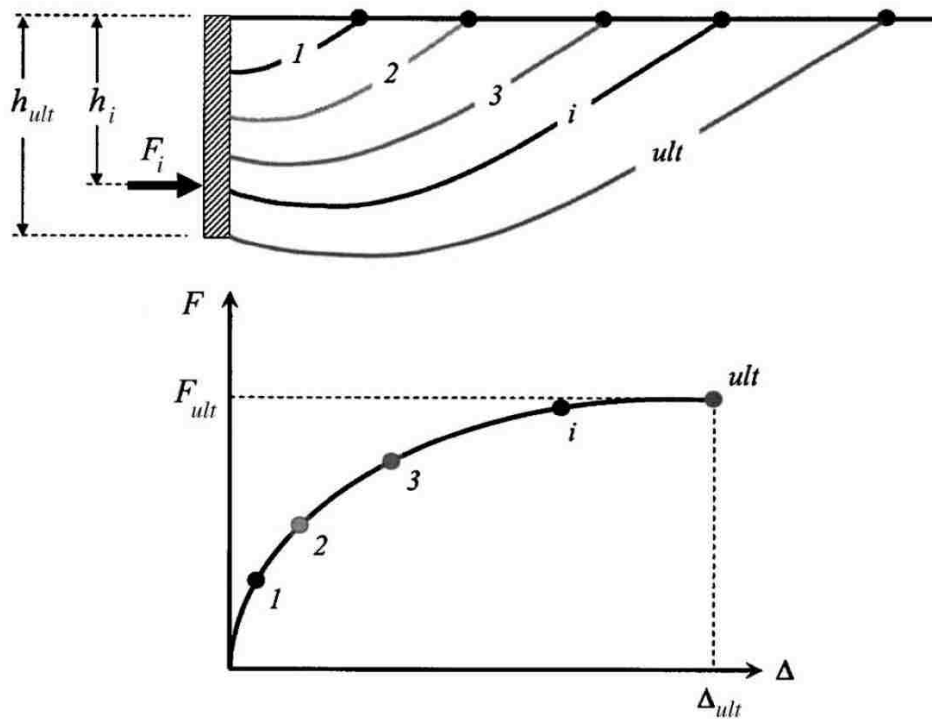
Figure 2-7. Progressive passive shear failure planes and the force-displacement relationship (Shamsabadi et al., 2007).

22

The hyperbolic stress-strain relationship used by the LSH method originates from Duncan and Chang (1970). The equation for the LSH method developed by Shamsabadi et al. (2007) is stated in Equation (2-9).

$$SL(\varepsilon) = \frac{\varepsilon}{\frac{\varepsilon_{50}}{R_f} + \left(2 - \frac{1}{R_f}\right)\varepsilon} \tag{2-9}$$

where

$SL(\varepsilon) = $ Deviatoric stress ratio

$\varepsilon = $ Soil strain (final or intermediate)

$\varepsilon_{50} = $ Strain at which 50% of the failure strength is achieved

$R_f = $ Failure ratio $= \dfrac{\text{deviatoric stress at failure}}{\text{ultimate (asymptotic) deviatoric stress}}$

The terms ε_{50} and R_f are inputs in the ABUTMENT program. Note that the failure ratio R_f is also used by Duncan and Mokwa (2001) in PYCAP. However, Shamsabadi et al. recommend using higher values for R_f, ranging from 0.94 to 0.98 with a recommended value of 0.97. The ε_{50} term can be determined with laboratory testing or estimated by soil type, as shown in Table 2-5. The recommended ε_{50} for gravel ranges from 0.001 to 0.005. The six remaining inputs in ABUTMENT are all based on backfill soil type: soil and wall friction angles, soil cohesion and abutments adhesion, and density; the sixth, Poisson's ratio, is based on friction angle according to Equation (2-7).

23

Table 2-5: Suggested ε_{50} Values for LSH Method (Shamsabadi et al., 2007)

	ε_{50}	
Predominant soil type	Range	Presumptive value
Gravel	0.001–0.005	
Clean sand (0–12% fines[a])	0.002–0.003	0.0035
Silty sands (12–50% fines[a])	0.003–0.005	
Silt	0.005 (nonplastic)–0.007 (plastic)	
Clay	0.0075	0.007

[a]Fines is the percentage by weight of soil grain sizes smaller than 0.075 mm.

The form of Equation (2-9) is expressed in more traditional macroscopic soil properties instead of in terms of stress and strain, particularly for use by structural engineers. Equation (2-10) states the simplified hyperbolic force-displacement (HFD) equation and Figure 2-8 illustrates it.

$$F(y) = \frac{y}{\dfrac{y_{max}}{2Ky_{max} - F_{ult}} + \dfrac{2(Ky_{max} - F_{ult})}{F_{ult}(2Ky_{max} - F_{ult})}y} \tag{2-10}$$

where

y = Abutment displacement

y_{max} = Maximum displacement

K = Average soil stiffness

F_{ult} = Maximum abutment force

24
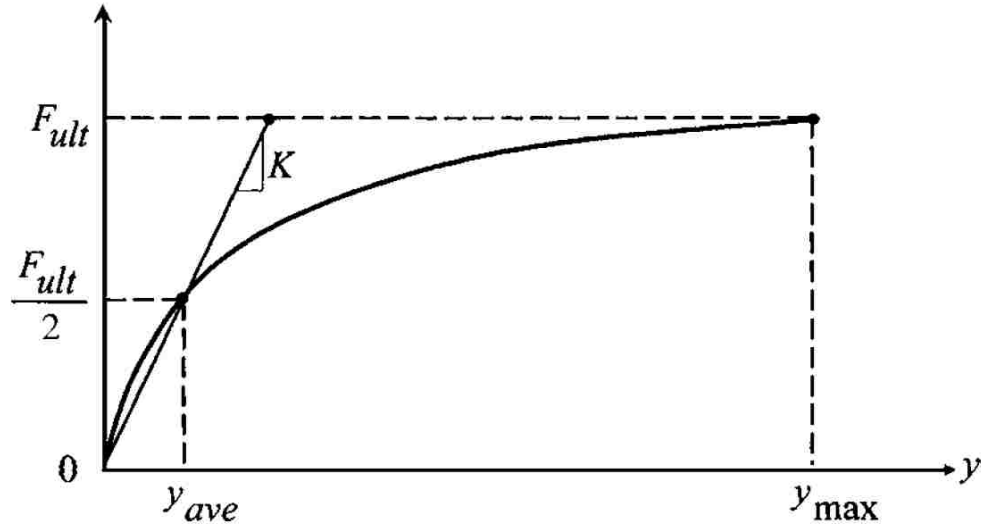
Figure 2-8. Hyperbolic force-displacement formulation for HFD method (Shamsabadi et al., 2007).

Equation (2-10) originates from the general hyperbolic equation shown in Equation and only applies if the following three conditions are met for each passive force limitation (FL), as shown in Figure 2-8.

$$F(y) = \frac{y}{A + By}, \text{where A and B are constants} \tag{2-11}$$

- Condition I $FL = 0$ at $y = 0$

- Condition II $FL = \frac{F_{ult}}{2}$ at $y = y_{ave}$

- Condition III $FL = F_{ult}$ at $y = y_{max}$

The variables in Equation (2-10) are usually supplied to the structural engineer by the geotechnical engineer. Shamsabadi et al. (2007) provides generic recommendations if more specific soil data is unavailable, shown in Table 2-6.

25

Table 2-6: Suggested Values for K and y_{max}/H for Abutment Backfills
(Shamsabadi et al., 2007)

Abutment backfill type	K kN/cm/m (kip/in/ft)	y_{max}/H
Granular	290 (50)	0.05
Cohesive	145 (25)	0.10

Both the LSH method performed by ABUTMENT and the HFD method, like PYCAP and the other design methods, seek to conservatively approximate the passive force-deflection curve of a given backfill and abutment configuration to make safe designs while saving money by minimizing the creation of overconservative designs. All the methods in this section are simple ways for structural bridge engineers to predict the magnitude of passive force resistance and displacements from the backfill. While all designs seek traditional conservatism as discussed in Section 2.1, none account for reduction of passive force results from skewed bridge abutments (Rollins and Jessee, 2012). This study will compare the test results from gravel and GRS backfill, particularly for the skewed tests, with the design curves produced from these methods.

2.4   Non-Skewed vs. Skewed Bridges

This section contains discussion on passive force-deflection curves for non-skewed and skewed bridge abutments.

2.4.1   Non-Skewed Bridge Abutments

Numerous studies have investigated the contribution of a non-skewed pile cap to lateral resistance. Mokwa and Duncan (2001) ran 31 lateral tests on piles and pile groups with and without pile caps, with varying embedment depths, and with either natural soils or granular backfill behind the pile cap. The results clearly indicated that pile caps were responsible for a

considerable portion of lateral resistance, up to 50% in some cases. The greatest two factors affecting the passive contribution of the pile cap were its embedment depth and the stiffness and strength of the backsoil resisting it.

Rollins and Cole (2006) tested a 4×3 pile group with a 10-ft high by 17-ft wide pile cap under cyclic loading in 7 different configurations. Of these, 4 were full backfill tests, each with a different backfill. The 4 tests were compared against the no-fill tests in order to calculate the contribution of passive resistance from the backfill versus the total resistance. As shown in Table 2-7, the study found that the peak passive resistance of the pile cap contributed 33-47% of the total lateral resistance of the pile system. Gravel spanned the full range of variation, with passive force in fine gravel contributing 33% of total lateral resistance versus contributing 47% in coarse gravel, almost half of the entire lateral capacity of the pile group.

Table 2-7: Rollins and Cole (2006) Backfill Passive Force Contribution

Backfill Soil Type	Passive force contribution to total pile cap resistance at Δ_{max}/H (%)
Clean Sand	40
Silty Sand	33
Fine Gravel	33
Coarse Gravel	47

2.4.2 Cyclic Loading

Smith (2014) performed cyclic loading with the same BYU test site and setup as this study, but with reinforced concrete wingwalls and sand backfill. The cyclic loading was performed on the 45° skew 5.5 ft (1.68 m) backfill test configuration and extended ±0.25 in (0.64 cm) from its original position. Figure 2-9 shows the total force-deflection cyclic results

27

from Smith (2014). After the first cycle, resistance decreased noticeably, but subsequent cycles showed only slight decreases in resistance.
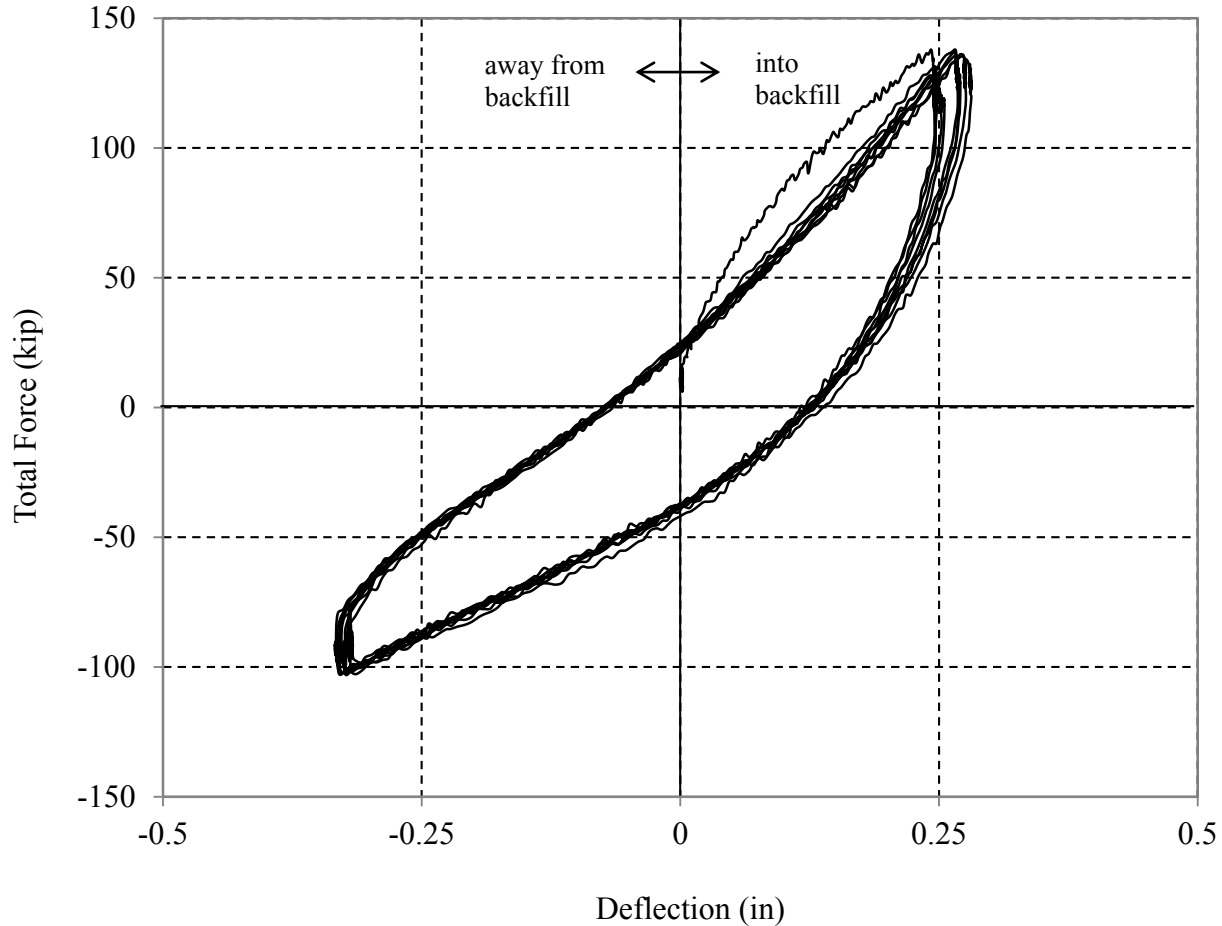
Figure 2-9. Hysteresis loop showing total actuator force vs. deflection (20 cycles) (Smith, 2014).

2.4.3 Skewed Bridge Abutments

This subsection outlines the studies performed on skewed abutments thus far. It describes the forces inherent in a skewed bridge abutment configuration. It also describes the passive force results of laboratory and field testing performed on skewed abutments. No skewed testing thus far has been performed with gravel or GRS backfills.

28

2.4.3.1 Burke Jr. (1994)

Burke Jr. (1994) described the forces which act on a skewed bridge using a figure similar to that shown in Figure 2-10 and in the equations following. As the deck of the bridge moves against the soil and exerts force P_L on the soil due to thermal expansion or earthquake loading, the soil resists compression with passive force P_p perpendicular to the wall of the abutment. Thus the skewed angle, θ, of the backwall creates an imbalance of forces that tends to rotate the bridge, in this case, counterclockwise due to the transverse component of the longitudinal force P_T. Resisting the rotation due to P_T is the frictional force of the soil against the abutment backwall, P_R. Equations (2-12), (2-13), and (2-14) mathematically define P_p, P_T, and P_R. As mentioned in Section 2.1.2, the relationship of the concrete-soil interface friction angle to the soil's internal friction angle, δ/φ, is minimally 0.76 for sand according to Potyondy (1961). The eccentricity between the passive forces on each side of the bridge is the length of the bridge, L, multiplied by $\sin \theta$.
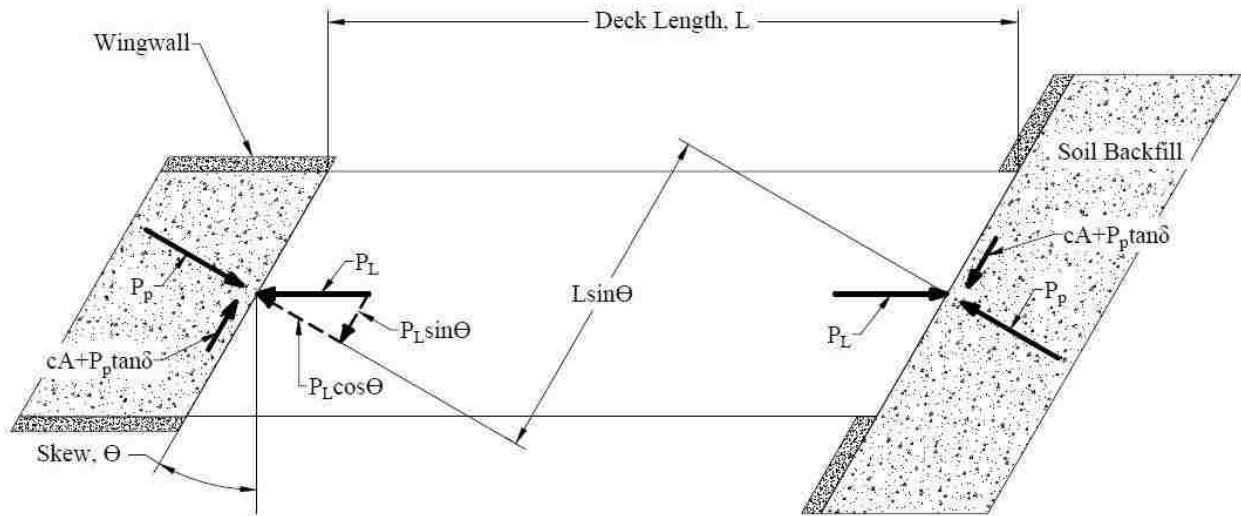
Figure 2-10. Typical distribution of forces on a bridge with skewed abutments, adapted from Burke, Jr. (1994).

$$P_P = P_L\cos\theta \qquad\qquad\qquad (2\text{-}12)$$

$$P_T = P_L\sin\theta \qquad\qquad\qquad (2\text{-}13)$$

$$P_R = cA + P_P\tan\delta \qquad\qquad\qquad (2\text{-}14)$$

where

θ = skew angle of backwall

c = soil cohesion

A = backwall area

δ = angle of friction between backfill soil and abutment wall

L = length of bridge deck

In order to keep the abutment at each end of the bridge deck from sliding in relation to the soil, the frictional resistance of the soil-abutment interface divided by the factor of safety against rotation must be greater than the transverse force resulting from longitudinal force, P_L, as illustrated in Equation (2-15). Also, the frictional resistance will further prevent the bridge from rotating if its moment is greater than the moment caused by the passive force, as shown in the criteria expressed in Equation (2-16).

$$\frac{cA + P_P\tan\delta}{F_s} \geq P_L\sin\theta \qquad\qquad\qquad (2\text{-}15)$$

$$\frac{(cA + P_P\tan\delta)L\cos\theta}{F_s} \geq P_P L\sin\theta \qquad\qquad\qquad (2\text{-}16)$$

where

F_s = factor of safety

30

As discussed in Duncan and Mokwa (2001), the at-rest resistance is greater than the mobilized resistance, and thus, bridge translation or rotation will likely shift the distribution of forces in the bridge system. Also, Burke Jr. (1994) points out that in a truly cohesionless backfill, Equation (2-16) simplifies so that with a factor of safety of 1.5 and a design structural interface friction angle of 22°, a bridge skew of 15° would be unstable even without any driving longitudinal force.

2.4.3.2   Shamsabadi et al. (2006)

Shamsabadi et al. (2006) developed a 3D finite element model that showed that a skewed bridge tends to rotate around a centrally-located vertical axis. The model shows that the rotation develops an asymmetrical passive wedge in the backfill, with the greatest resistance found against the obtuse corner of the abutment. The model confirmed the relationships developed by Burke Jr. (1994) concerning bridge rotation. According to the study, key factors for determining the mobilized passive resistance against bridge abutments are the bridge displacement, bridge geometry (skew angle, deck width and height), the soil stress-strain properties of the backfill, and the characteristics of the ground motion itself.

Shamsabadi et al. (2006) ran the 3D model at skew angles of 0, 15, 30, 45, and 60 degrees. The results from the modelling showed greatly reduced passive force with increasing skew angle. The results are shown in the next subsection with the laboratory testing results from Rollins and Jessee (2013) (see Figure 2-13).

2.4.3.3   Rollins and Jessee (2013)

Rollins and Jessee (2013) performed laboratory tests on compacted clean sand backfills for skew angles of 0°, 15°, 30°, and 45°. The backfill geometry was confined to a 2-dimensional

www.manaraa.com

plane-strain geometry with a pair of parallel longitudinal sidewalls, each lined with double-layered plastic sheeting.

Figure 2-11 shows the plan and profile view of the test setup. An actuator loaded the concrete backwall into the sand backfill. Displacements were measured with string potentiometers. The passive force-displacement results for each of the four skew angles are shown in Figure 2-12. Passive force was calculated using Equation (2-12) of Burke Jr's equations using the longitudinal force measured by the actuators.
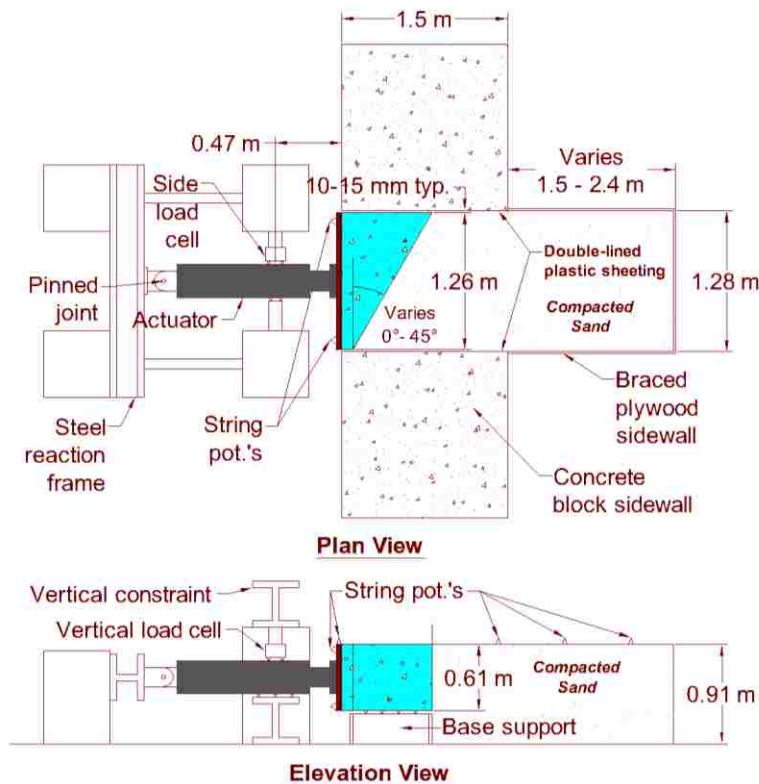
Figure 2-11. Schematic drawings of lab test layout (Jessee, 2012) (NOTE 1 m = 3.281 ft).

Results from the lab tests were normalized to a reduction factor, R_{skew}, for each test by dividing its peak passive force by the peak passive force of the non-skewed tests. When plotted against results from the finite element modeling by Shamsabadi et al. (2006) in Figure 2-13, the

correlation is remarkable. As such, Rollins and Jessee (2013) proposed a correlation equation for R_{skew} based on their lab results and the finite element model results from Shamsabadi et al. (2006). Although stated in Chapter 1, the equation is restated here as Equation (2-17) and included on the plot in Figure 2-13:

$$R_{skew} = P_{P-skew} / P_{P-no\ skew} = 7.79 * 10^{-5}\theta^2 - 0.018\theta + 1.0 \qquad (2-17)$$
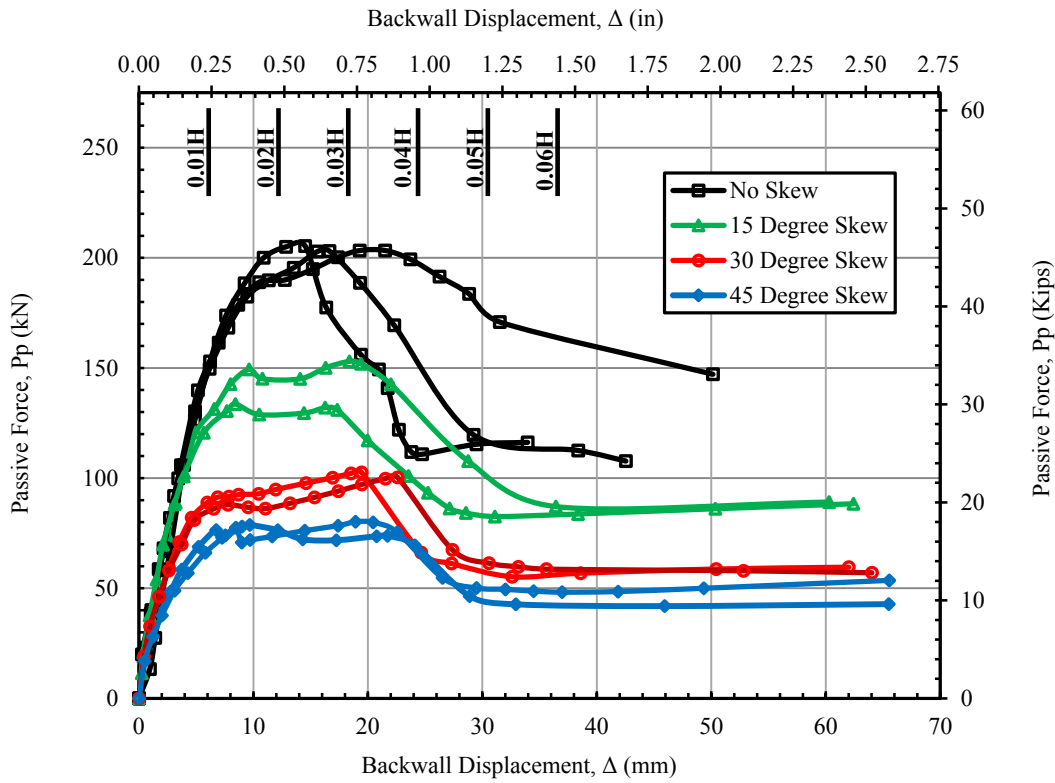
Figure 2-12. Passive force-deflection curves for lab tests (Rollins and Jessee, 2013).

33
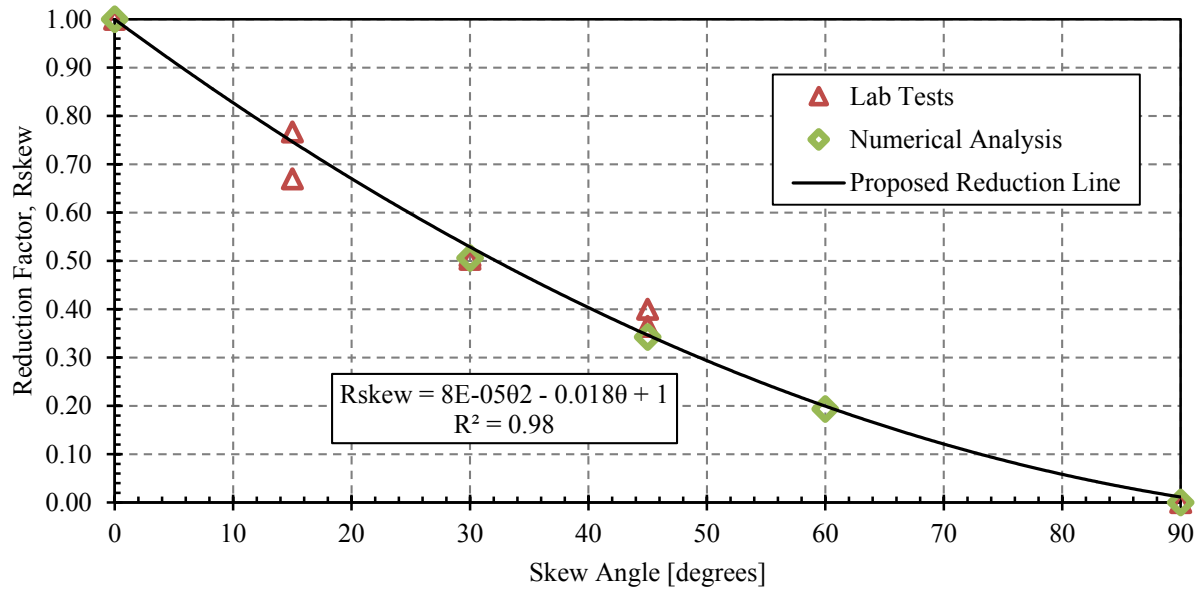
Figure 2-13. R_{skew} vs. increasing skew angle using results from numerical analyses (Shamsabadi et al., 2006), lab tests and proposed reduction line (Rollins and Jessee, 2013).

2.5 **Passive Force-Displacement Tests in Gravel**

Previous testing involving lateral loading of a non-skewed pile cap in gravel backfill performed by Pruett (2009) demonstrated that gravel has greater passive resistance capacity compared to clean sand (Cummins, 2009) owing to the higher friction angle. Only a few passive force tests have been conducted in gravel (Duncan & Mokwa, 2001; Rollins and Cole, 2006; Pruett, 2009). Generally, because sand and gravel are both granular, tests conducted in sand are applied to gravel backfills. While both materials do generally behave similarly, they are not the same. Gravel generally has higher stiffness than sand. Therefore, tests in gravel are invaluable to designing gravel backfills.

Passive force-deflection data from several studies at BYU was gathered by Meyer (2012) with dense and loose gravel backfill (Rollins and Cole, 2006; Pruett, 2009), dense sand backfill (Rollins and Cole, 2006; Valentine, 2008; Cummins, 2009; Strassburg, 2010; Rollins and Jessee, 2013), and loose sand backfill (Runnels, 2007, Cummins, 2009; Strassburg, 2010). The data was

then normalized to find patterns in the passive force-deflection curves. Because there was a good deal of data on sands and less data for gravel, both sets of data will later be compared with the results of this study. The sands are grouped as dense and loose generally depending on their relative density (D_r), which in most cases was estimated from the modified Proctor compaction (R) relationship for granular materials developed by Lee and Singh (1971) using Equation (2-18), where D_r and R are measured in percent.

$$R = 80 + 0.2D_r \qquad\qquad (2\text{-}18)$$

The deflections on the x-axis were normalized by wall height (y/H) and the passive forces on the y-axis were normalized by the maximum measured passive force ($P_p/P_{p\text{-max}}$).

The normalized plot for dense and loose gravels is shown in Figure 2-14. The normalized plots for dense and loose sand are shown respectively in Figure 2-15 and Figure 2-16. In both gravel and sand, the curve of the denser materials curves exhibits a more hyperbolic shape while the looser material curves are more flat. All tests shown also failed or nearly failed at deflections between approximately 2-5.5% of their respective wall heights.
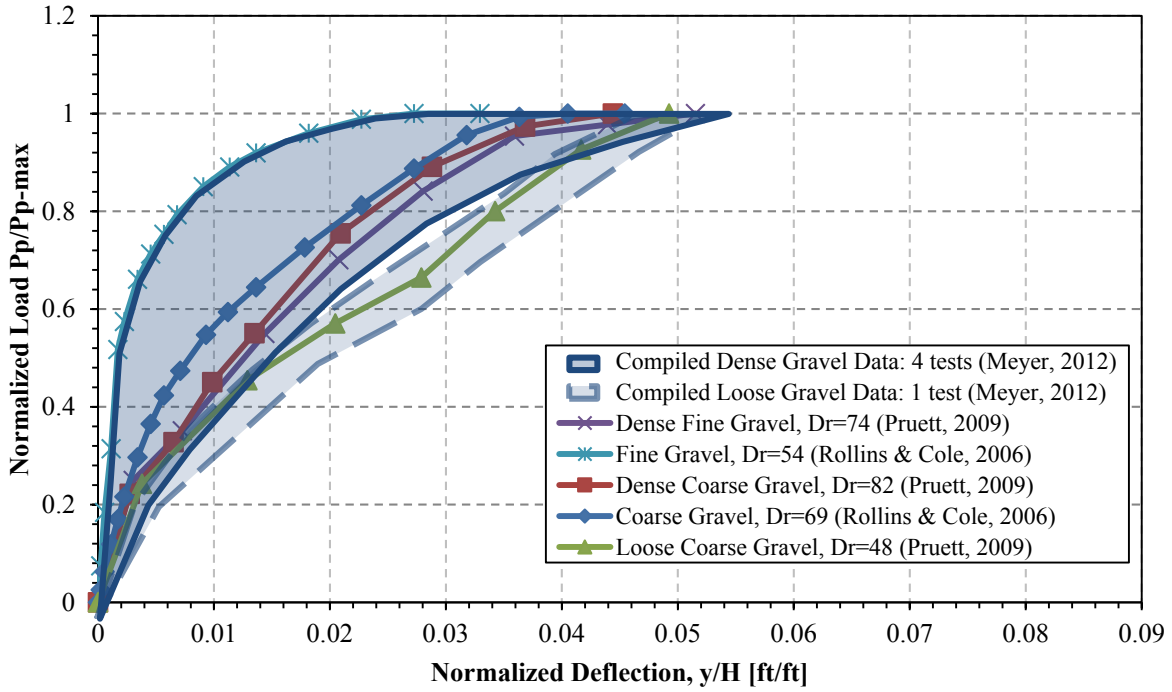
Figure 2-14. Compilation of passive force-deflection data for dense and loose gravels, normalized on both axes (Meyer, 2012). Relative densities listed are percentages.
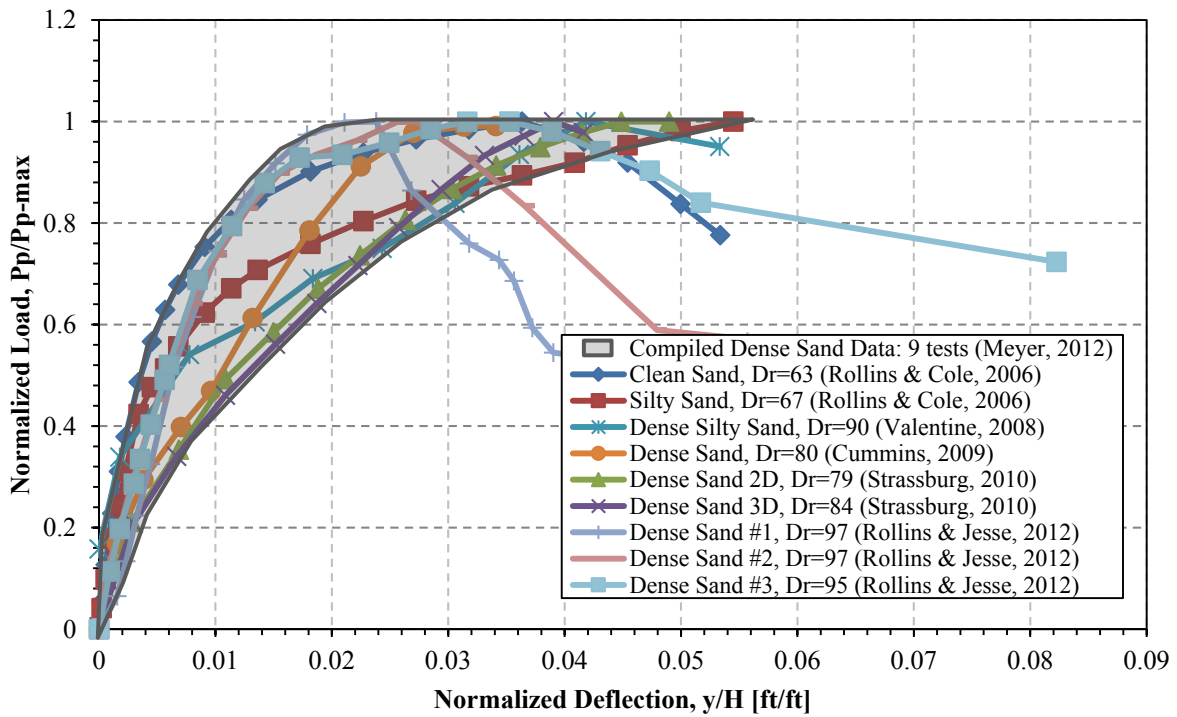
Figure 2-15. Compilation of force-deflection data for dense sands, normalized on both axes (Meyer, 2012). Relative densities listed are percentages.

36
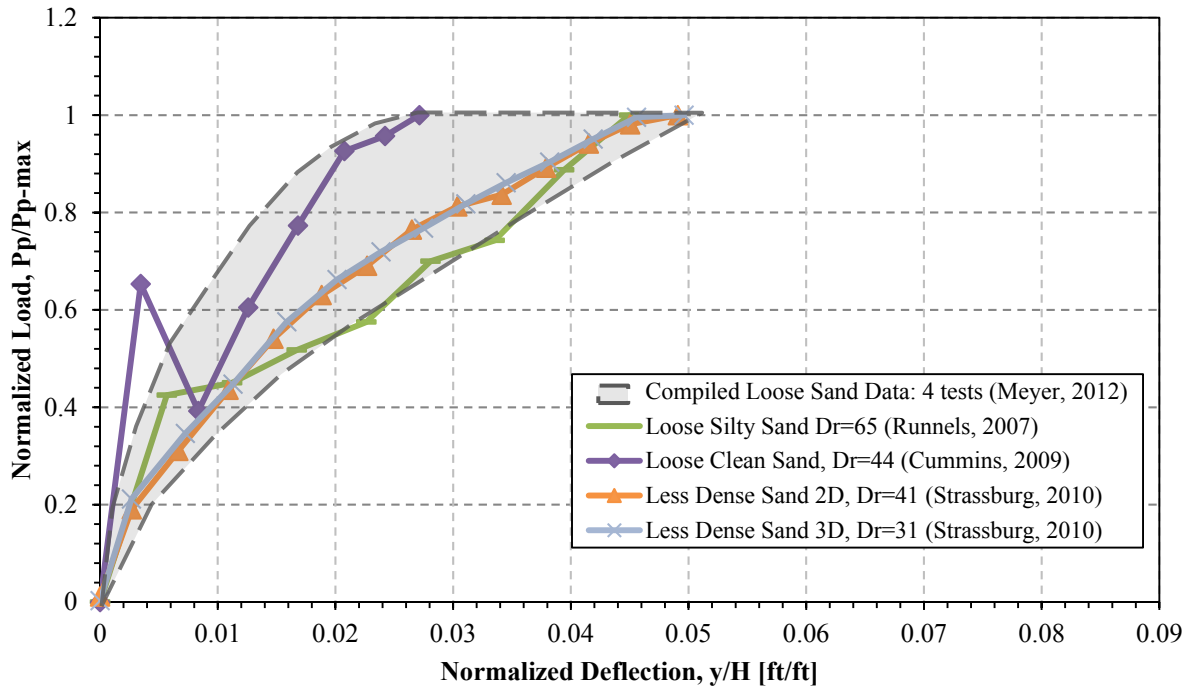
Figure 2-16. Compilation of force-deflection data for loose sands, normalized on both axes (Meyer, 2012). Relative densities listed are percentages.

2.6 GRS Backfill

Geosynthetic Reinforced Soil (GRS) is a compacted granular fill with closely spaced geosynthetic reinforcement layers (Adams et al., 2011). It is a technology developed by the Federal Highway Administration (FHWA) and is now used as part of an Integrated Bridge System (IBS) as a low-cost, accelerated bridge construction technique for shorter-span bridges. GRS backfill is used to spread vertical loading from the abutment in order to reduce settlement and, therefore, the "bump" at the end of the bridge. It also minimizes overturning moment by reinforcing across potential failure planes. This section will briefly describe FHWA and UDOT guidelines on the installation of GRS backfill.

2.6.1 Construction Design of GRS Backfill

GRS technology has generally been used with spans less than 100 ft. However, there have been GRS-IBS structures constructed with spans up to 140 ft (42.7 m) (Adams et al., 2011). FHWA recommends limiting GRS-IBS spans to less than 140 ft (42.7 m) until further research on longer spans is conducted. GRS has been specified for vertical or near vertical faces up to 30 ft (9.1 m) in height. Bearing stress is limited to 4,000 psf (192 kPa), and the tolerable vertical and lateral strain, respectively, are 0.5 and 1 percent. The two rules of GRS construction are good compaction (95 percent of maximum dry unit weight) and closely spaced reinforcement (12 inches [0.3 m] or less).

As shown in Figure 2-17, there are three main components in GRS-IBS: the reinforced soil foundation (RSF), the abutment, and the integrated approach (Adams et al., 2011). All three components use compacted granular fill and geotextile. The RSF has been proven to be an effective alternative to deep foundations in soft soils. The abutment has closely spaced reinforcement less than 1 ft (0.3 m) apart. The facing elements, typically 8 in (0.2 m) tall, serve as guides for spacing in construction but do not hold structural load; the loading is internally contained by the compacted fill and geotextile. They also provide an aesthetic, protective wall. The blocks resist movement due to a frictional connection with the geotextile. The abutment is constructed without any cast-in-place concrete or joint. Lastly, and most important to this study, the integrated approach uses geotextile at regular intervals, with the sheets against the beam face wrapped over the overlying compacted layer, as illustrated in Figure 2-18. Unlike the original figure suggests, however, there is no soil between the extra geotextile material from the layer below and the next geotextile layer.

38
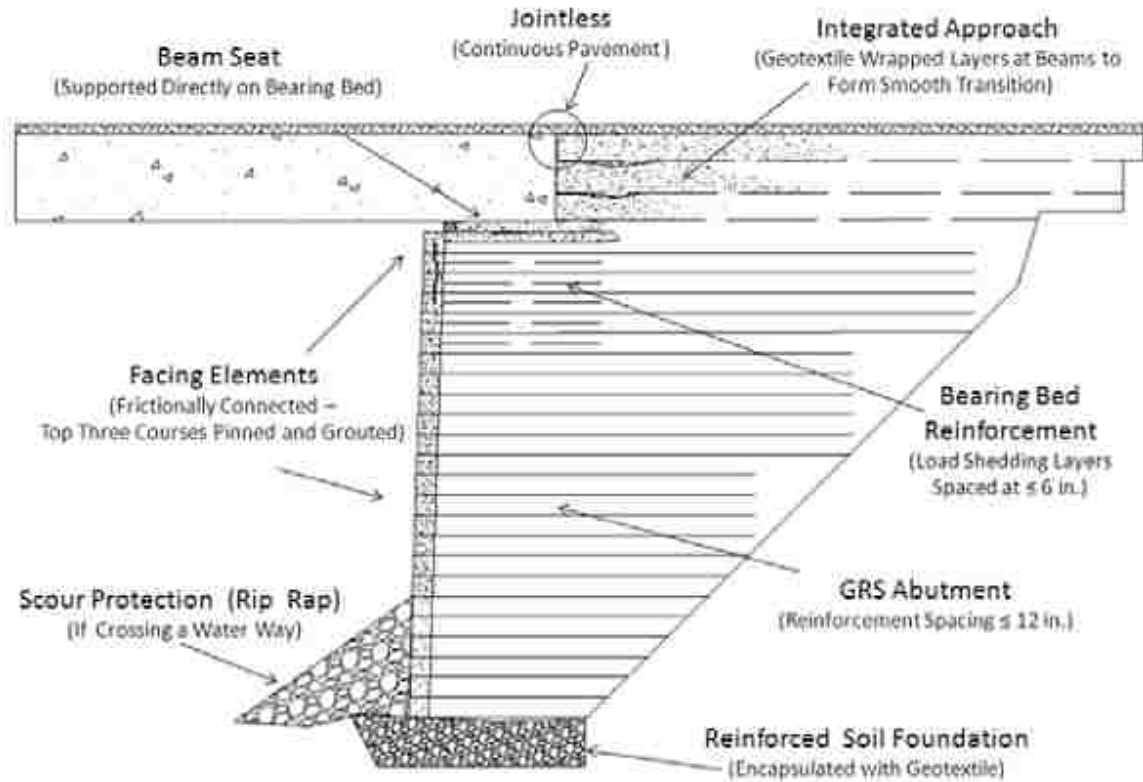
Figure 2-17. Typical GRS-IBS cross-section (Adams et al., 2011).
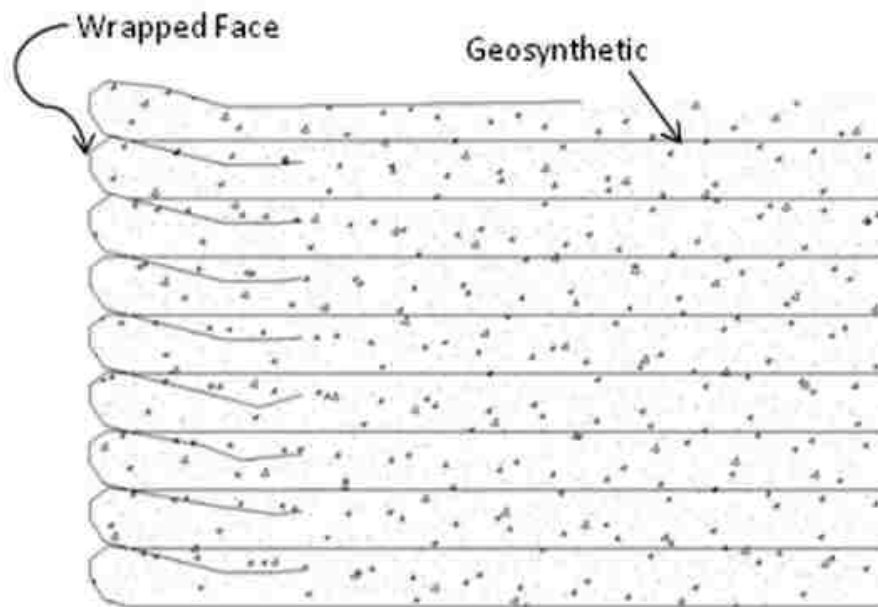
Figure 2-18. Geotextile wrapping at the face of a GRS integrated approach (Adams et al., 2011).

39

The FHWA (Adams et al., 2012) design specifies the granular backfill material must have an internal friction angle greater than or equal to 38° (Nicks et al., 2013) and a maximum Plasticity Index (PI) of 6. Gradation requirements for a well-graded material specify maximum grain size as 0.5-2 in (1.3-5.1 cm) and the maximum passing the No. 200 sieve as 12%. Lifts shall occur in 8 in (0.2 m) lifts, which is the size of the modular block facing in the abutment design.

FHWA (2012) specifies polypropylene, high-density polyethylene, or polyester geogrid or geotextile. The material can be uniaxial or biaxial, but with uniaxial materials, the higher-strength axis must be placed perpendicular to the wall face. The minimum ultimate tensile strength must be 4,800 lb/ft (70 kN/m). Geosynthetic is placed directly on the compacted horizontal fill.

Utah Department of Transportation (UDOT, 2012) also specifies maximum PI as 6, but the internal friction angle must be greater than 42°. UDOT gradation specifications is more specific than FHWA and is shown in Table 2-8. Maximum lift height is 10 in (25.4 cm). UDOT specifies high-density biaxial, woven, polypropylene resin, polymer tensile fabric. The material must have a minimum ultimate strength of 4800 lb/ft (70 kN/m) and grab tensile strength of 300 lb (1.3 kN). A minimum 12 in (0.30 m) of overlap should be used when required.

Table 2-8: GRS Select Backfill Gradation (UDOT, 2012)

Sieve Size	Percent Passing
2 in (5.08 cm)	100
1 in (2.54 cm)	85 - 100
3/8 in (0.95 cm)	60 - 75
No. 10	30 - 42
No. 40	14 - 24
No. 200	6 - 12

40

Compaction is to be 95% of maximum dry density for well-graded fills. Moisture content shall be within 2% of optimum moisture content.

FHWA's seismic design guidelines (Adams et al., 2012) for GRS-IBS recommend checking external stability. FHWA recommends increasing the base width of the wall and increasing the length of the reinforcement at the top of the abutment to increase overall external stability and bearing capacity for seismic loads. However, only one study, a National Cooperative Highway Research Program (NCHRP) study (Helwany et al., 2012), has been conducted concerning the seismic behavior of GRS-IBS. This study suggests that GRS abutments are suitable for low to medium seismic accelerations. However, this study only investigated the GRS abutment portion with the modular facing blocks; no testing has been performed on large lateral forces on the GRS integrated approach and its interaction with the girders and bridge deck.

2.6.2 Lateral Earth Pressures in GRS-IBS Induced by Thermal Expansion

Warren et al. (2014) conducted a study on the bridge superstructure-backfill interaction on a GRS-IBS bridge. An operating bridge in Ohio was instrumented for 3.5 years. They found that shrinkage of the bridge caused active lateral forces and expansion causes passive forces. However, passive pressures did not increase over time. The GRS behaved like a composite material and acted elastically without any failure states. It also remained engaged with the superstructure. Warren et al. (2014) also found that the GRS eliminated the "bump" at the end of the bridge.

41

2.6.3 Geotextile Properties of Note

The woven polypropylene (PP) geotextile used in this study is a common material for transportation applications particularly for use in areas with poor subgrade material. The effects of lateral earth pressures on geosynthetic reinforced soil are not well studied. A literature search produced studies on axial testing of geotextiles and other geosynthetics and lateral testing performed of geogrids (Bathurst et al., 2005; Shinoda & Bathurst, 2004) but none on lateral testing of geotextiles except a couple on GRS previously mentioned. This study is the first large-scale study of passive force in backfill with woven polypropylene (PP) geotextile reinforcement. However, some properties of the woven PP geotextile that have been investigated in sand are applicable to lateral testing in gravel.

Tuna and Altun (2012) performed several interface direct shear tests using woven and nonwoven PP geotextiles in sand. They found that the sand-reinforcement interface friction angle was generally lower than the internal sand friction angle. Their results are shown in Table 2-9. The stress-strain plot for the geotextile materials used in their testing is shown in Figure 2-19. The woven PP geotextiles used in their study had a much higher tensile strength (W1 had 5480 lb/ft [80,000 N/m] and W2 had 1710 lb/ft [25,000 N/m]) than the nonwoven PP geotextiles (170-710 lb/ft [2,500-10,300 N/m]). Higher tensile strength resulted in higher stiffness for one of the samples with woven reinforcement, as shown in Figure 2-20, but not for the other. However, the ultimate shear capacities were comparable to the samples with nonwoven geotextiles and the unreinforced sand, despite the woven geotextiles having 2-10 times the tensile strengths as the nonwoven geotextiles. The study concluded that increased tensile strength was not related to improved interface friction. Tuna and Altun also found that in the reinforced sand, there was little to no post-peak reduction of shear strength, in contrast to a loss of strength observed in their

42

unreinforced sand tests, as was shown in Figure 2-20. They also found that higher confining stresses produced higher interface friction angles.

Table 2-9: Results of Direct Shear Tests on Reinforced Well-Graded Sand (SW) from Tuna and Altun (2012)

Interface type	Normal stress/peak shear stress (kPa)			Cohesion (kPa)	Interface friction angle (°)
	27.20	54.50	109.00		
SW–SW	39.00	71.10	128.60	36.00	36.50
SW-W1	45.60	75.00	104.70	39.00	32.00
SW-NW2-b	49.10	67.50	124.40	48.00	38.40
SW-NW2-a	44.60	77.00	115.10	55.00	35.60
SW-NW1	24.70	51.50	102.90	13.00	35.60
SW-W2	67.20	69.20	106.80	40.00	33.70

Note: SW-SW is sand only, W1 and W2 are woven geotextile, NW1 and NW2-a and NW2-b are non-woven geotextiles

1. Polypropylene woven geotextile
2. Polypropylene, non-woven, heat-bonded geotextile
3. Polypropylene, non-woven, needle-punched geotextile
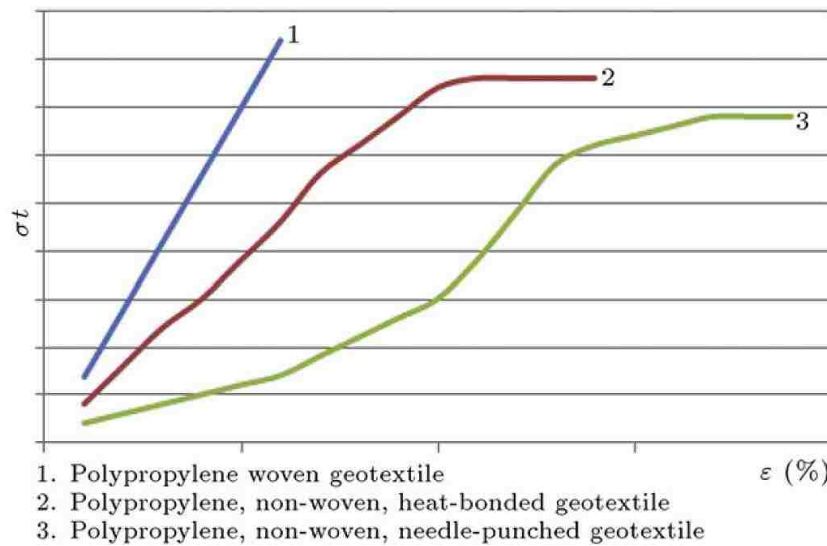
Figure 2-19. Stress-strain behavior of woven PP geotextiles (Tuna & Altun, 2012).
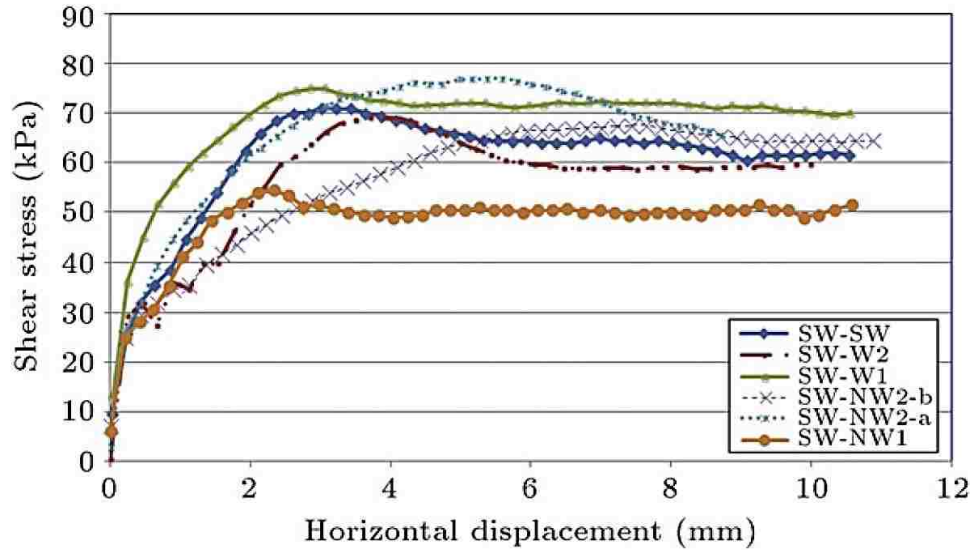
Figure 2-20. Shear stress vs. horizontal displacement in interface direct shear tests performed by Tuna and Altun (2012) with geotextiles in well-graded sand. SW-SW is sand only; SW-W1 and SW-W2 are with woven PP geotextile (Note: 1 kPa = 20.9 psf and 1 mm = 0.039 in).

2.7 Literature Review Summary and Conclusions

As the focus of several studies, good progress has been made in understanding passive force-deflection prediction in backfills of non-skewed abutments. A handful of skewed abutment tests have been performed in sand backfill, but none in gravel or GRS backfills. These tests are the first to investigate passive pressures of the GRS integrated approach. Gravel backfills also lack extensive passive force tests. This study seeks to better understand passive force behavior in non-skewed and skewed abutments with gravel and GRS backfills. The study will also compare results against current design methods. The comparison will look at the skewed test results in particular because no current design methods account for the reduction of passive force resulting from skew in their methods.

3   Field Testing Methods

3.1   Site Description

The large scale lateral testing site was located in a lot north of the air traffic control tower by the Salt Lake City International Airport in Utah, just southeast of the Great Salt Lake (see Figure 3-1). The geologic profile underlying the site is Holocene clay, silt, and very fine sand deposited in ancient Lake Bonneville of which Great Salt Lake is a remnant (Bryant, 1990). The site has been used in several other studies (Rollins and Sparks, 2002; Johnson, 2003; Christensen, 2006; Taylor, 2006; Rollins et al., 2010; Smith, 2014), and many used the same pile cap (Marsh, 2013; Franke, 2013; Palmer, 2013). The four tests for this study were performed as part of a series of 10 tests performed during May and June 2013, which included tests reported by Smith (2014).

3.2   Geotechnical Site Characterization

Figure 3-1 shows a CPT profile from the test site. The clean sand in the upper 8 ft is artificial backfill. A couple layers of lean clay are in the upper 16 ft and the rest of the profile down to 50 ft consisted of alternating layers of sandy silt and silty sand. Prior to testing, the water table was approximately 5 ft (1.5 m) deep, or a few inches above the base of the pile cap. Therefore, two small sump pumps removed water nearly continuously to bring the water table down to about 6.5 ft (2.0 m) deep while testing was being performed.

Figure 3-1. Satellite view of the test site, which was located at 40.799° N 111.986° W, near the control tower of the Salt Lake City International Airport. Taken from Google Earth.
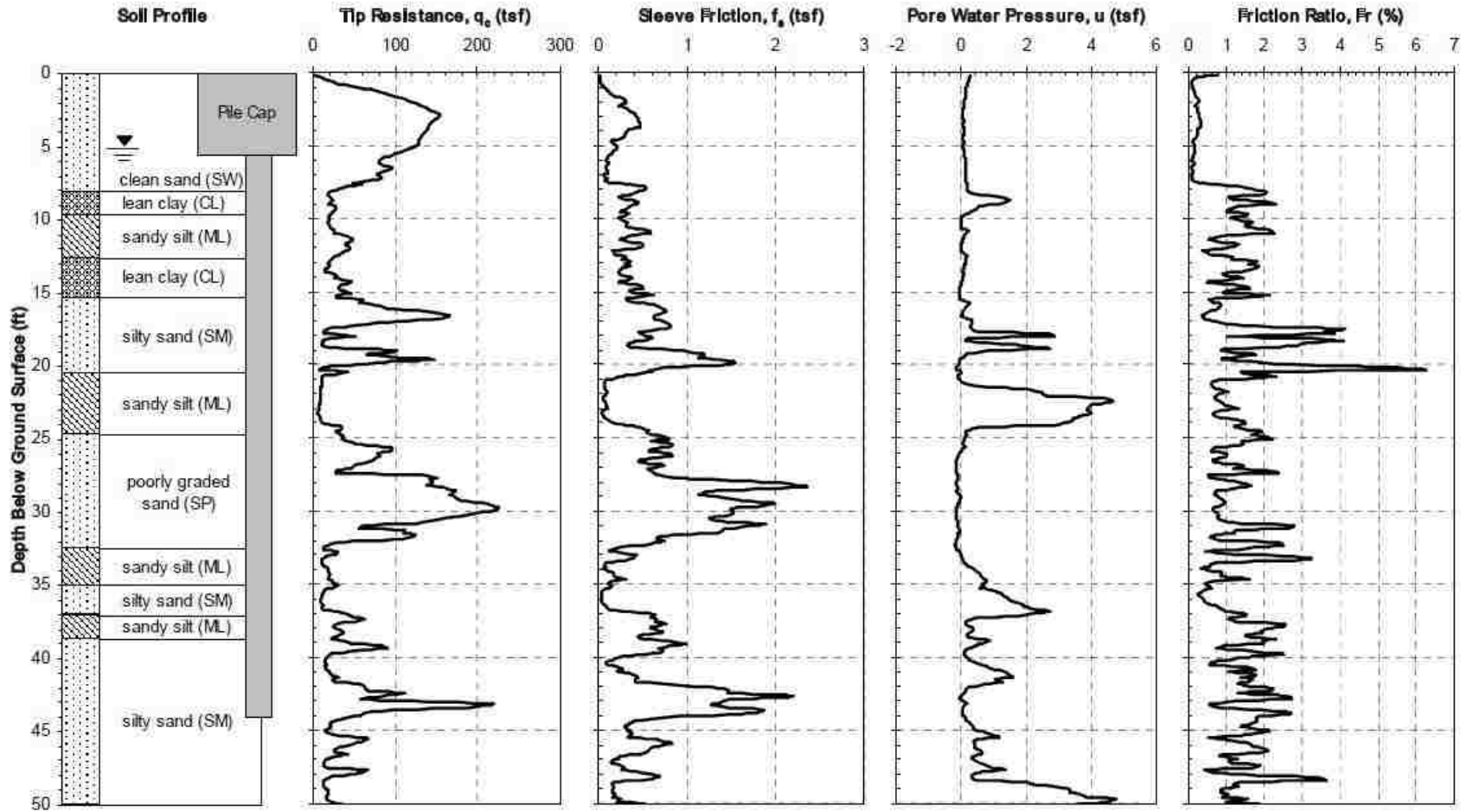
Figure 3-2. Idealized Soil Profile From CPT Test (Rollins et al., 2010).

3.3 Test Layout

Field tests used an existing pile cap to simulate an abutment backwall. The reaction frame, pile cap and its components, loading system, and backfill zone for all four tests are described in this section and illustrated in Figure 3-3 and Figure 3-4. The layout for the transverse load-displacement testing is also outlined here.

3.3.1 Reaction Frame and Foundation

The reaction frame, composed of drilled shafts, a sheet pile wall, and a pair of deep I-beams, is pictured in Figure 3-5. The reinforced concrete drilled shafts were 4 ft (1.2 m) diameter and were spaced 12 ft (3.7 m) east-west on center. They penetrated 70 ft (21.3 m) below the ground surface on the east and 55.2 ft (16.8 m) on the west and were each capped by a 4-ft (1.2-m) square cap, 2 ft (0.6 m) thick. The shafts were reinforced with 18 #11 (~#35M) vertical bars for the upper 35 ft (10.7 m) and 9 #11 (~#35M) bars for the remaining depth, and tied with a #5 (~#15) bar spiral at a pitch of 3 in (7.6 cm) for the upper 35 ft (10.7 m) and a pitch of 12 in (30.5 cm) for the rest. The reinforcement was placed to allow consistent 4.75-in (12.1-cm) cover. The concrete compressive strength was 6,000 psi (41.4 MPa) (Marsh, 2013).

The sheet pile wall was composed of AZ 18 sections and was installed into the natural soil 34 to 36 ft (10-11 m) below the excavated ground surface (Franke, 2013). The two 64-in deep by 28-ft long by 16-in wide I-beams (Palmer, 2013) with several stiffeners (see Figure 3-5) lay flat on either side of the drilled shaft and sheet pile wall.
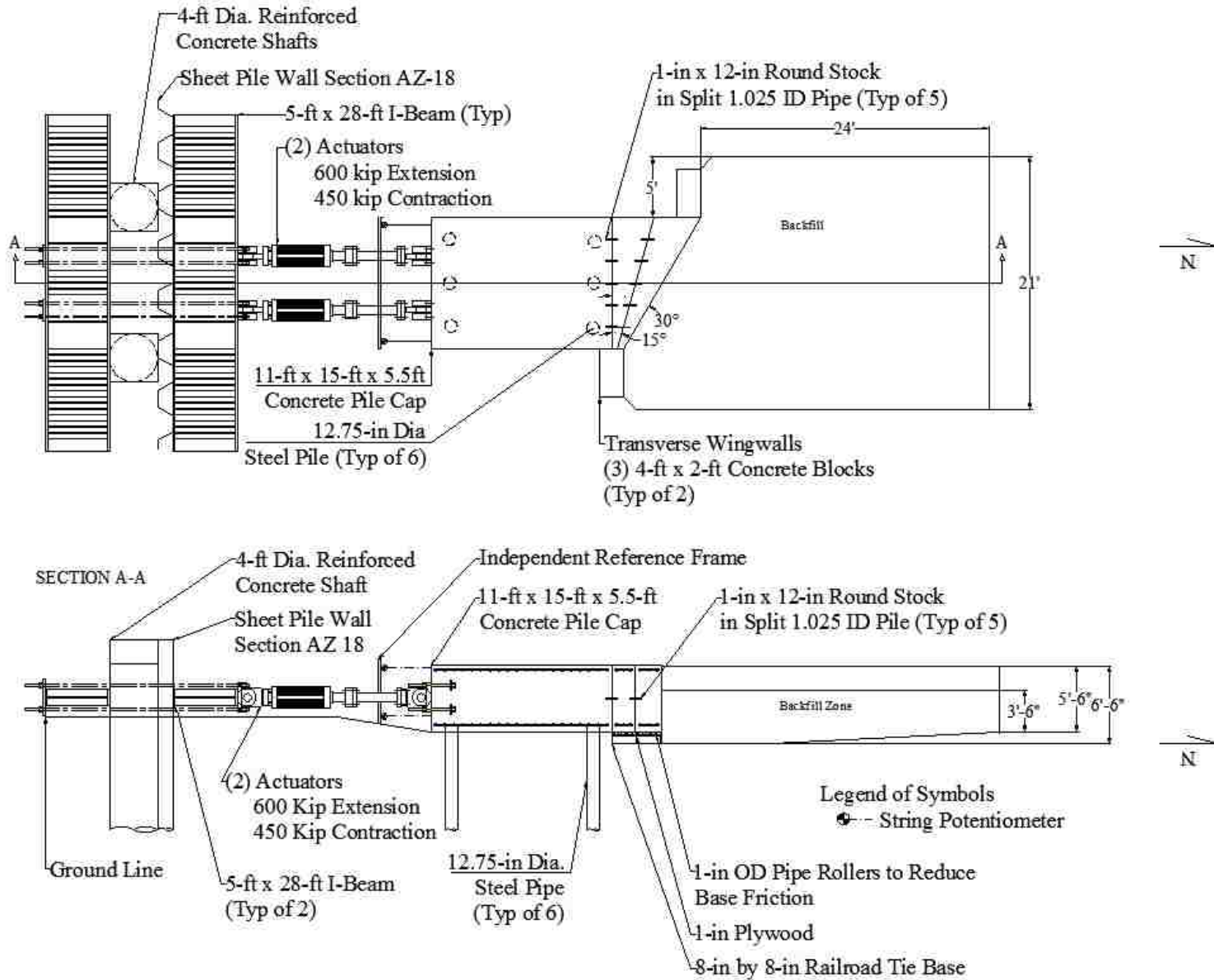
Figure 3-3. Schematic plan and profile drawings of field layout for gravel tests (NOTE 1 ft = 0.305 m).

49
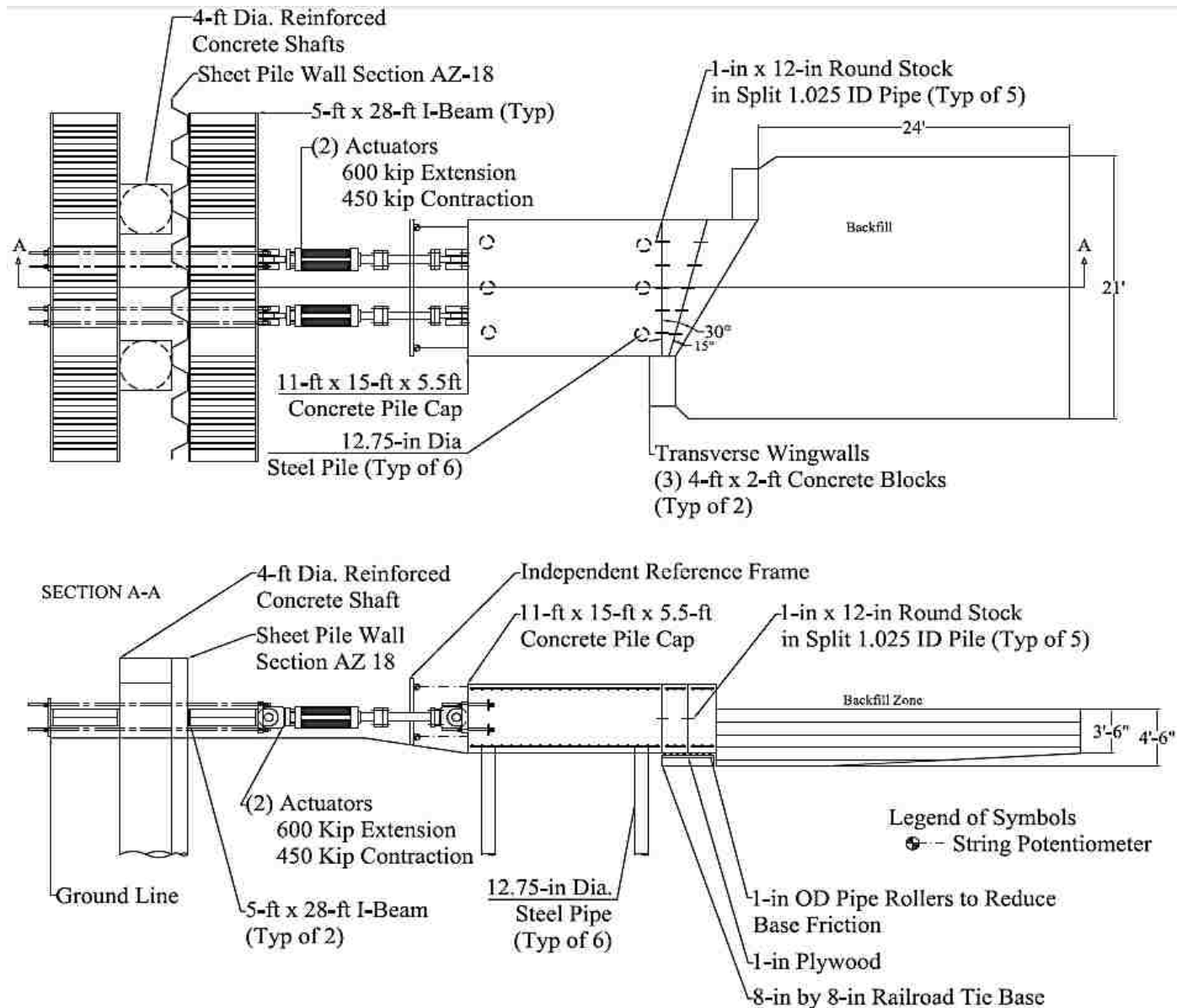
Figure 3-4. Schematic plan and profile drawings of field test layout (NOTE 1 ft = 0.305 m).

Figure 3-5. Reaction foundation.

3.3.2   Loading System

Load was applied in the longitudinal direction with the extension of two MTS hydraulic actuators, pictured in Figure 3-6, which pushed the pile cap into compacted fill. Each actuator had 600-kip (2,670-kN) extension capacity and 450-kip (2000-kN) contraction capacity. The actuators were each tied to the reaction frame with threaded 1.75-in (4.4-cm) DYWIDAG bars. The DYWIDAGs were placed just above and below the two I-beams, threaded through the sheet pile wall, and secured with nuts on each end. The actuators' north attachment to the pile cap was similar with eight threaded DYWIDAG bars embedded in the pile cap securing the actuators.

Figure 3-6. Two 600-kip actuators comprised the loading apparatus.

3.3.3 Model Abutment

An existing 11 ft (3.35 m) wide by 5.7 ft (1.74 m) high by 15 ft (4.57 m) long pile cap was used as a large-scale model of an abutment backwall for the non-skewed tests. Its foundation consisted of two east-west rows of three 12.75-in (32-cm) outer-diameter close-ended steel piles extending about 43 ft (13.1 m) below the ground surface. The wall thickness of the pile was 0.375 in (0.95 cm) of ASTM A252 Grade 3 steel with 57 ksi (393 MPa) yield strength (Marsh, 2013).

The piles were embedded about 6 in (15 cm) into the pile cap and a steel rebar cage was set 13.2 ft (4.02 m) into each pile, extending up 4.8 ft (1.47 m) into the pile cap. The rebar cages were each made using 6 #8 (#25M) vertical bars and a #4 (#13M) spiral at a 6 in (15 cm) pitch (Palmer, 2013). These cages supported the upper horizontal reinforcing mat of reinforcement in the cap. Both upper and lower reinforcing mats were comprised of #5 (#19M) bars in the

52

longitudinal and transverse direction which were spaced 8 in (20.3 cm) on center (Franke, 2013).

Concrete used to fill the piles and construct the pile cap had a 6,000 psi (41.4 MPa) compressive

strength. Within the center pile of each row, inclinometer and shape array pipes were installed to

record pile cap movement. As mentioned in the previous section, eight threaded 1.75-in (4.4-cm)

DYWIDAG bars were embedded in the south side of the pile cap for attachment to the actuators.

To create the 30° skew face, two reinforced concrete wedges were combined and attached

to the front face of the pile cap as shown previously in both Figure 3-3 and Figure 3-4. The

wedges were originally poured for tests that were performed in the spring of 2012 (see Franke,

2013; Marsh, 2013; and Palmer, 2013), shown in Figure 3-7. One-inch (2.54-cm) diameter steel

rollers were placed beneath the wedges to minimize base friction resistance. Since the first

wedge, which created a 15° skew, was already in place due to other testing at the site, the 30°

skew wedge section was re-attached to the 15° skew wedge and the two 30° skew tests were

performed first. Then both wedges were removed to leave the solitary rectangular pile cap to

serve as the two control non-skewed abutment tests.

Concrete in both skewed wedges consisted of 6,000 psi (41.4 MPa) compressive strength

concrete. The reinforcement for the 15° skew only used #4 (#13M) bars. Both top and bottom

grids were oriented against the wedge face such that they were perpendicular or parallel to the

face at an 8 in (20 cm) spacing each way. Horizontal reinforcement on the wedge face was

located at 3, 15, 27, 45, and 64 in (0.08, 0.38, 0.69, 1.14, and 1.63 m) from the base of the wedge

and horizontal reinforcement was limited elsewhere in the wedge (Palmer, 2013). Vertical

reinforcement was only placed as need to hold the horizontal reinforcement in place. A diagram

of the 15° skew rebar cage is shown in Figure 3-8.

Figure 3-7. Simultaneous casting of 15° and 30° wedges, taken from Marsh (2013).
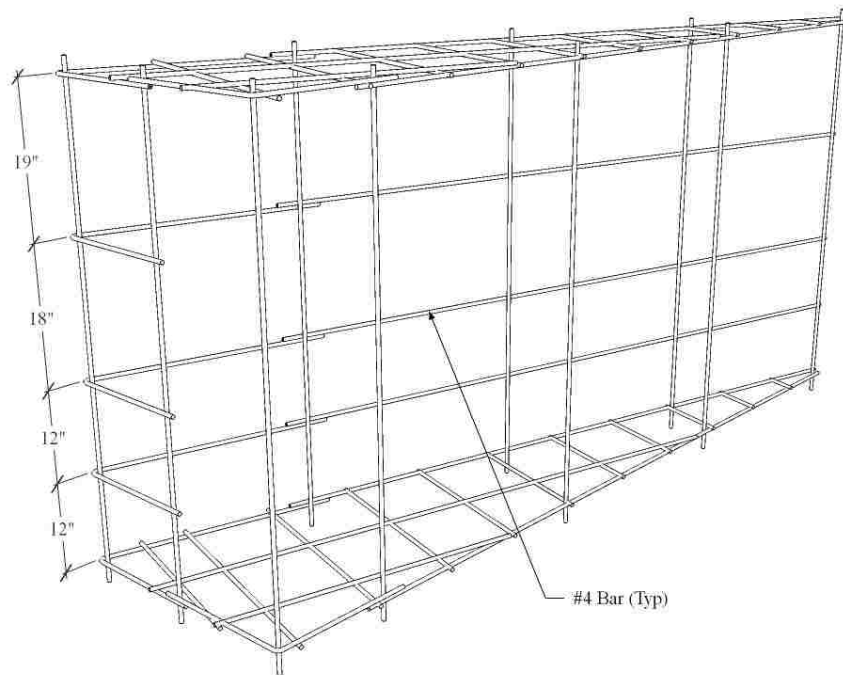
Figure 3-8. Reinforcing grid for 15° wedge (Marsh, 2013).

The 30° wedge reinforcement involved #5 (#16M) bars on both top and bottom grids, again oriented parallel and perpendicular to the wedge face but at 11 in (28 cm) spacing in this case. Horizontal reinforcement consisted of #6 (#19M) bars at 3, 9, and 15 in (0.08, 0.23, and 0.38 m) from the base and #5 bars at 21, 27, 37, 49, and 63 in (0.53, 0.69, 0.94, 1.24, and 1.60 m) from the base. The # 6 (#19M) bars extended 56 in (1.42 m) starting from the acute edge and the #5 (#16M) bars extended 50 in (1.27 m) (Palmer, 2013). Horizontal reinforcement was limited elsewhere in the wedge, and vertical reinforcement was only placed as needed to hold the horizontal bars in place. A diagram of the 30° rebar cage is shown in Figure 3-9.
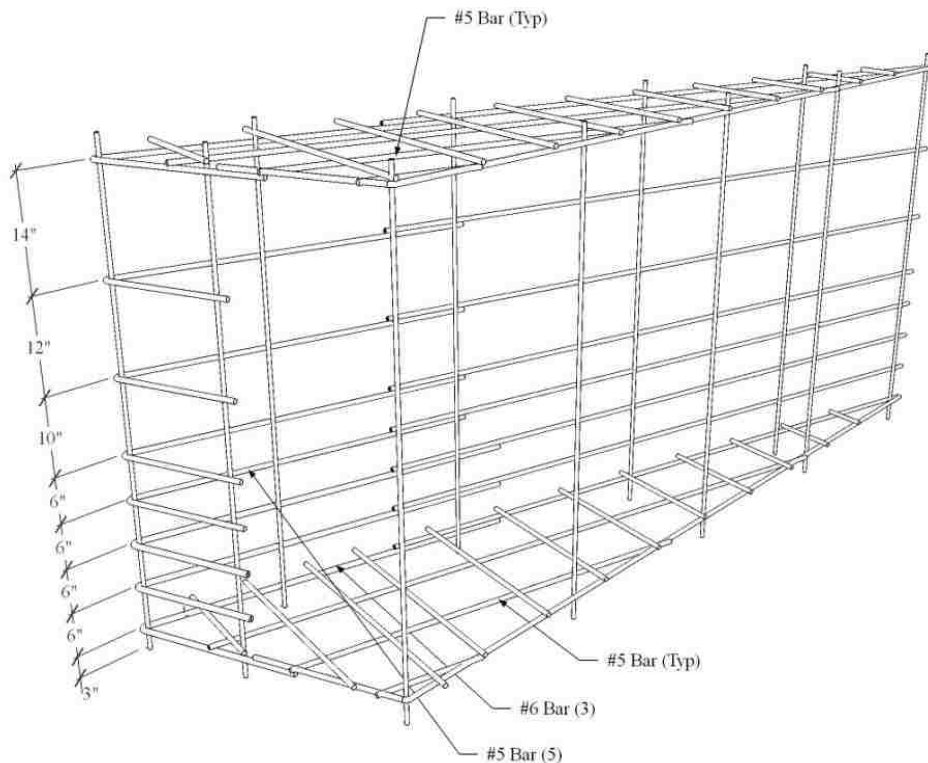
Figure 3-9. Reinforcing grid for 30° skew wedge (Marsh, 2013).

In order to create secure connections for testing that also allowed the skew angle to be altered between tests, metal slip connections were inserted prior to pouring of the wedges. The connections consisted of round stock inside a metal casing which was inserted 6 in (15.2 cm)

into each concrete interface at the time of pouring (Palmer, 2013). Steel plates and anchors embedded in the concrete 1 in (2.54 cm) in diameter and 8 in (20.3 cm) long also secured the wedges to the pile cap. A photo of one of the two plates on the acute side of the wedges is shown in Figure 3-10. Similar connection plates were located on the obtuse side and on the top of the combined, skewed pile cap.
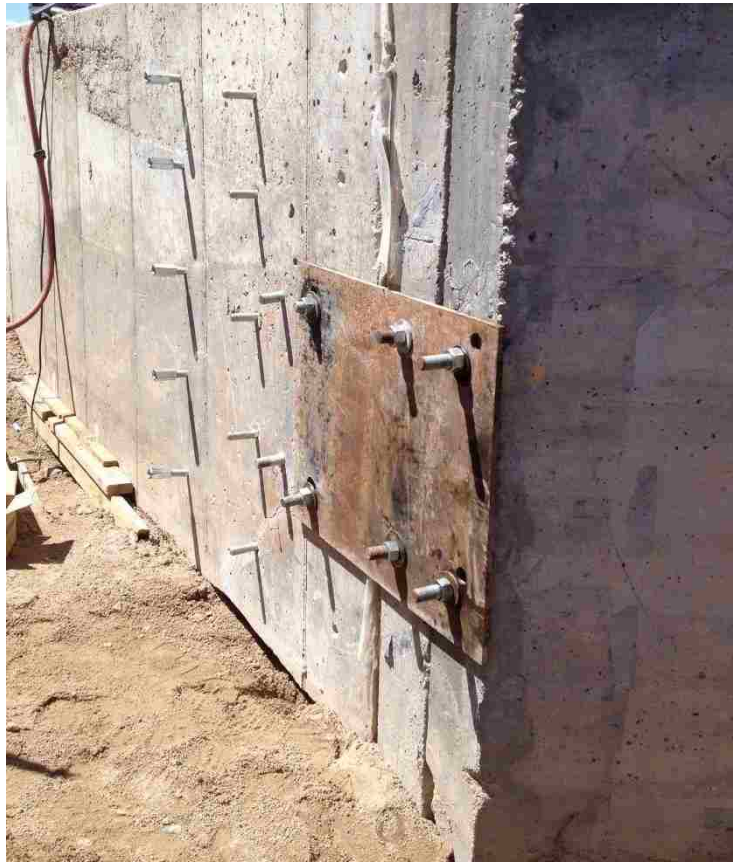
Figure 3-10. Example of metal plate and bolt connection for skew concrete wedges. The plate shown is located on the acute side of the pile cap.

3.3.4 Backfill Zone

Instead of a 2D backfill geometry, the backfill was placed in a test pit that extended a little over 5 ft (1.52 m) out from the sides of the pile cap to the edge of the test pit with transverse concrete wingwalls to allow for the development of a 3D failure geometry. The

56

backfill height was 5.5 ft (1.68 m) above the base of the cap for the 30° skew gravel backfill test and 3.5 ft (1.07 m) for the other three tests. The backfill extended 24 ft (7.32 m) longitudinally from the face of the pile cap. From the face to 10 ft (3.05 m) back into the fill, the fill extended down approximately 1 ft (0.30 m) below the bottom of the cap to contain the potential failure surface. The backfill boundaries were considered to be far enough away from the native soil to not affect the development of a shear surface. Beyond 10 ft (3.05 m), the base of the backfill tapered up to be approximately even with the base of the cap to reduce the required backfill volume.

Backfill gravel was placed in lifts approximately 4- to 6-in (10- to 15-cm) thick and compacted with a smooth-drum vibratory roller and a walk-behind vibratory plate compactor (see Figure 3-11) to an average density greater than approximately 95% of the modified Proctor maximum. The properties of the backfill soil in the tests of this study are summarized in Section 3.5. On the GRS fabric, the gravel was placed in the back first such that no construction equipment drove on the fabric directly.

For the GRS tests, as the backfill was placed and compacted, geotextile fabric layers were placed every 1 ft (0.30 m) starting at 6 in (0.15 m) below the base of the cap (see Figure 3-4). The fabric was laid flat so that the extra fabric on the sides and against the backwall came up vertically (Figure 3-12). The fill was then placed on top of the geofabric sheets. Since the fabric came on a roll with a fixed width, two sheets of fabric were needed to cover the width of the backfill area. The two sheets were overlapped by about 3 ft (0.9 m) in the middle of the backfill zone.

57

Figure 3-11. Vibratory roller compactor used for the bulk of the gravel compaction.

Figure 3-12. Every 1 ft (0.30 m), a new layer of geofabric reinforcement was placed in the backfill area. Overlap of the two sheets of fabric is visible in the top middle of the photo.

At each 1-ft (0.30-m) interval, the fabric against the interface from the previous layer was folded over the fill before placing the new layer of fabric (see Figure 3-13). The fabric was placed such that there was at least 3 ft (0.9 m) of fabric laying on top of the gravel before the next layer was placed, though in many places it was more than 3 ft (0.9 m) for 30° test due to the angled corners of the backwall. Thus the geotextile fabric was double-layered in the 3 ft (0.9-m) or more nearest the backwall for all intermediate layers. The resulting interface between the backfill and the backwall was completely geotextile fabric, similar to what is seen in Figure 3-14. The fabric was folded over the fill similarly on the sides of the backfill zone for the 0° skew test, layer by layer. For the 30° skew test, all layers of fabric on the sides were staked into the native soil until compaction was complete, when the stakes were removed and all the fabric layers were trimmed to a few inches above the fill instead of ever being folded over the fill.

Figure 3-13. Extra geofabric was folded over the 1-ft (0.30-m) gravel layer in the non-skewed GRS test before placement of the next fabric sheet.

59

1 ft (0.3 m)

Figure 3-14. Geotextile fabric layer folds along the front of the backfill, made visible by removing the west transverse wingwall after testing.

3.3.5   Transverse Load-Displacement Tests

For improved evaluation of transverse translation and rotation of the pile cap that was observed during skewed tests, a transverse no-fill baseline test was performed on the pile cap with the 30° skew wedges attached. This test loaded the pile cap from east to west. The main longitudinal testing pushed the pile cap from south to north.

The reaction block was constructed on the native soil east of the pile cap. It consisted of a wall of railroad ties and steel I-beams. Two rows of 4- by 4-in (10.2- by 10.2-cm) wooden blocks supported the horizontal-oriented web of the first steel I-beam. One row of 8-in (20.3-cm) railroad ties sat on top of the web of the first I-beam and was topped by a second steel I-beam. Another two rows of 4x4 (10.2- by 10.2-cm) blocks sat on the web of the second I-beam and supported two more railroad ties. The flanges of the two steel beams and the railroad ties were

made to be as vertical as possible. The slope behind the beams and railroad ties was backfilled with loose native soil and clean sand and two concrete blocks were placed on top to provide a surcharge, as shown in Figure 3-15.
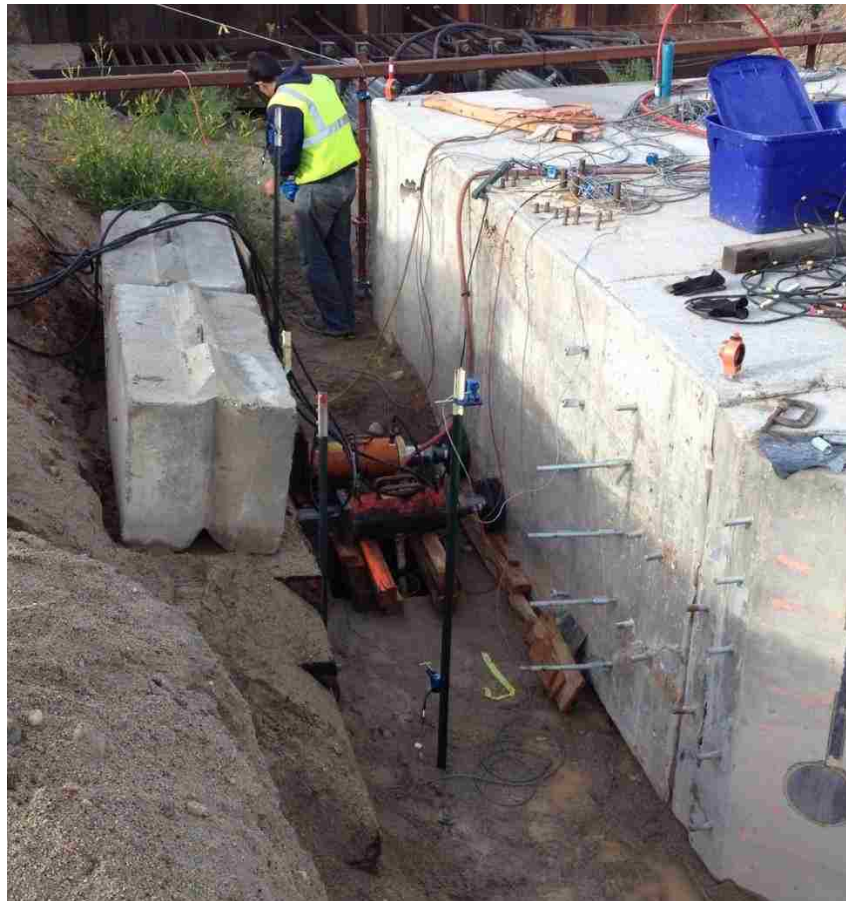
Figure 3-15. The transverse loading test set up when performed on the 45° skew.

The load was applied using two Power Team RD15013 hydraulic jacks, each of which had an extension capacity of 300 kips (1334 kN). Figure 3-15 shows the test of the same kind performed with 45° skew wedge in place. The jacks were centered against the east side of the main pile cap at 23-in (0.58 m) spacing on center; for this study, which had a 30° skew attached to the backwall, the spacing was adjusted to 10-ft (3.0-m) spacing such that the jacks were 30 in (76 cm) from each edge of the rectangular cap. Two pairs of string potentiometers (string pots)

near each corner of the cap were tied to independent vertical stakes and monitored pile cap movement. The load was applied in 0.05-in (0.13-cm) increments up to a displacement of 0.35 in (0.89 cm).

3.4 Instrumentation and Measurement

Longitudinal load was measured using pressure transducers in the actuators. Longitudinal displacement of the pile cap was measured using four string pots located at each corner of the back of the pile cap and were tied to an independent reference frame. As the piles were assumed to provide vertical restraint, vertical movement of the pile cap was not monitored. Longitudinal and transverse deflections versus depth were measured using inclinometers and shape accelerometer arrays (SAAs), which extended approximately 40 ft (14 m) into the center pile in the North and South sides of the pile cap. The shape arrays provided data at 1-ft (0.30-m) vertical intervals while the inclinometers provided data at 2-ft (0.61-m) intervals. Because of the time required to obtain inclinometer readings, the inclinometer measurements were only taken immediately before the start of a test and after the last deflection increment. In contrast, the shape arrays provided profiles at each 0.25-in (0.64-cm) deflection increment because their collection was nearly instantaneous.

To measure backfill heave and displacement, a 2-ft (0.61-m) grid was painted on the backfill surface, shown in Figure 3-16, and the relative elevation of each grid intersection was measured with a survey level and total station prior to and after conducting each test. Surface cracks in the backfill were marked on the backfill surface as they developed at each increment and following the completion of each test.

As an additional measure of backfill movement, eight strings pots secured on top of the pile cap or on its face were connected to stakes pounded into the backfill at 1, 2, or 4 ft (0.30,

0.61, or 1.22 m) intervals to measure longitudinal displacement. The exact locations in the backfill varied from test to test anywhere from 1 ft (0.30 m) to 20 ft (6.1 m) back from the pile cap backwall and are summarized in Table 3-1. Figure 3-17 shows all the backfill displacement monitoring after the non-skewed gravel test and also shows two workers taking post-test inclinometer readings.

In some tests, an optical camera was suspended over the backfill and black and white targets were nailed into the backfill in an attempt to track displacement of the fill surface. Unfortunately, variations in sunlight on the target and backfill washed out some of the photography, making interpretation difficult. Therefore, no results from this optical camera will be discussed in this study.

Figure 3-16. Grid painted at 2 ft by 2 ft (0.61 m by 0.61 m) spacing prior to 30° skew GRS test.

Figure 3-17. Backfill instrumentation and inclinometer readings following 0° skew gravel test.

Table 3-1: Longitudinal Distances [ft (m)] from Pile Cap Backwall
to String Pot Stakes by Test

0° Gravel	30° Gravel	0° GRS	30° GRS
1 (0.3)	2 (0.6)	1 (0.3)	2 (0.6)
2 (0.6)	4 (1.2)	2 (0.6)	4 (1.2)
3 (0.9)	6 (1.8)	3 (0.9)	6 (1.8)
4 (1.2)	8 (2.4)	4 (1.2)	8 (2.4)
6 (1.8)	10 (3.0)	6 (1.8)	10 (3.0)
8 (2.4)	12 (3.7)	8 (2.4)	12 (3.7)
10 (3.0)	16 (4.9)	10 (3.0)	16 (4.9)
12 (3.7)	20 (6.1)	12 (3.7)	20 (6.1)

3.5   Geotechnical Backfill Characterization

Backfill material consisted of a well-graded gravel with silt and sand (GW-GM as

classified by the Unified Soil Classification System or A-1-a according to the AASHTO

64

classification system). Results from two gradation tests on the backfill performed by the supplier and one performed at the BYU Soil Mechanics lab are shown in Figure 3-18. The particle sizes fall within FHWA (2012) specifications, and the particle-size distribution curves generally fall within the gradation bounds specified for these GRS tests by UDOT (2012). They also correlate well to the dense coarse gravel backfill used by Rollins and Cole (2006) coarse gravel but had fewer fines than Rollins and Cole's fine gravel. The particle sizes also had significantly less gravel and greater fines than the poorly-graded fine gravel (GP) backfill used by Pruett (2009).
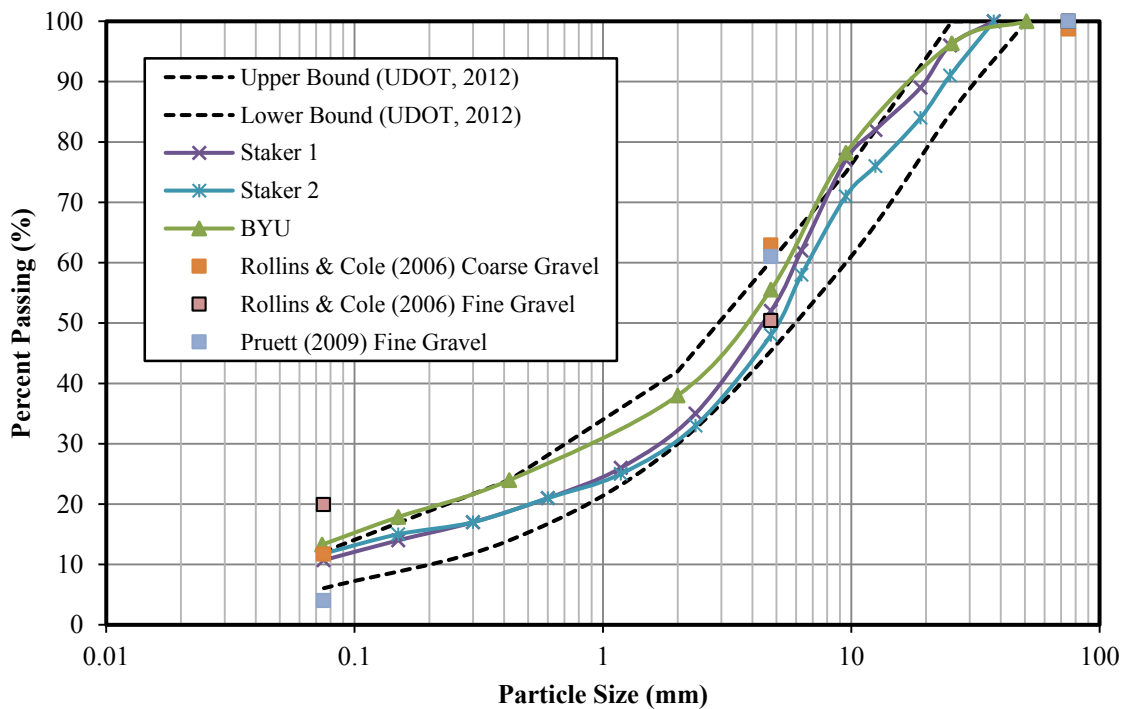
Figure 3-18. Gradation for backfill gravel relative to GRS gradation specification.

3.5.1 Unit Weight and Moisture Content

Maximum dry unit weight according to the modified Proctor compaction test (ASTM D1557) performed prior to testing was 142.0 lb/ft^3 (22.3 kN/m^3) and the optimum moisture content was 6.3%. The target on-site compaction level was 95% of the modified Proctor

maximum. Backfill gravel was placed in lifts approximately 4- to 6-in (15.24-cm) thick and compacted with a smooth-drum vibratory roller and a walk-behind vibratory plate compactor to an average density greater than approximately 95% of the modified Proctor maximum with no values less than 92%. A nuclear density gauge was used to obtain relative compaction and water content data during compaction. The measured dry unit weight and moisture content versus depth for the zero skew test are provided in Figure 3-19 and Figure 3-20, respectively, while similar plots for the 30º skew gravel and two GRS tests are provided in Figure 3-21 through Figure 3-26. Though not shown, the variation of relative compaction was not significant. Relative density was estimated using the empirical relationship between relative density (D_r) and relative compaction (R) for granular materials developed by Lee and Singh (1971) as shown in Equation (3-1) where D_r and R are measured in percent.

$$R = 80 + 0.2D_r \hspace{4cm} (3-1)$$

A summary of the backfill unit weight and water content measurements for the four tests is shown in Table 3-2. The properties of the backfills were generally very consistent. Average mean relative compaction, relative density, and water content for the two gravel tests were 96.3%, 81.5%, and 7.1%, respectively. Average mean relative compaction, relative density, and water content for the two GRS tests were 96.6%, 82.8%, and 6.2%, respectively.

Table 3-2: Summary of Compaction and Water Content Data for Each Test

	Gravel Backfill		GRS Gravel Backfill	
Backfill Soil Properties	**0º Skew**	**30º Skew**	**0º Skew**	**30º Skew**
Minimum Dry Unit Weight [pcf]	133.7	133.7	132.5	130.4
Maximum Dry Unit Weight [pcf]	141.7	139	138.6	140.4
Average Dry Unit Weight [pcf]	136.2	137.3	135.1	136.2
Average Relative Compaction	95.9%	96.7%	96.2%	96.9%
Average Relative Density	79.5%	83.5%	81%	84.5%
Average Moisture Content	6.4%	7.8%	5.8%	6.6%
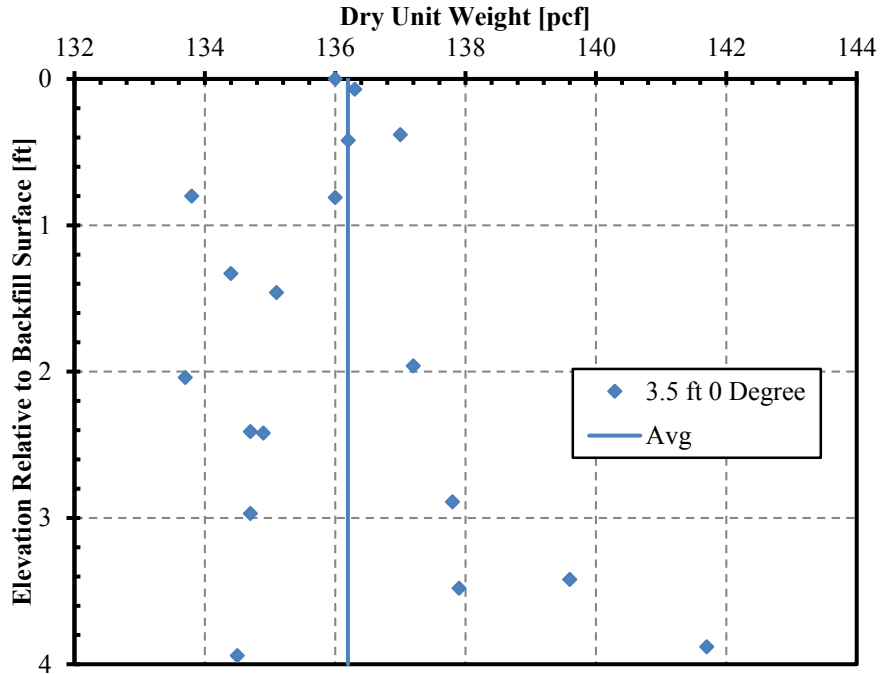
Figure 3-19. Dry unit weights for 0° skew gravel backfill test.
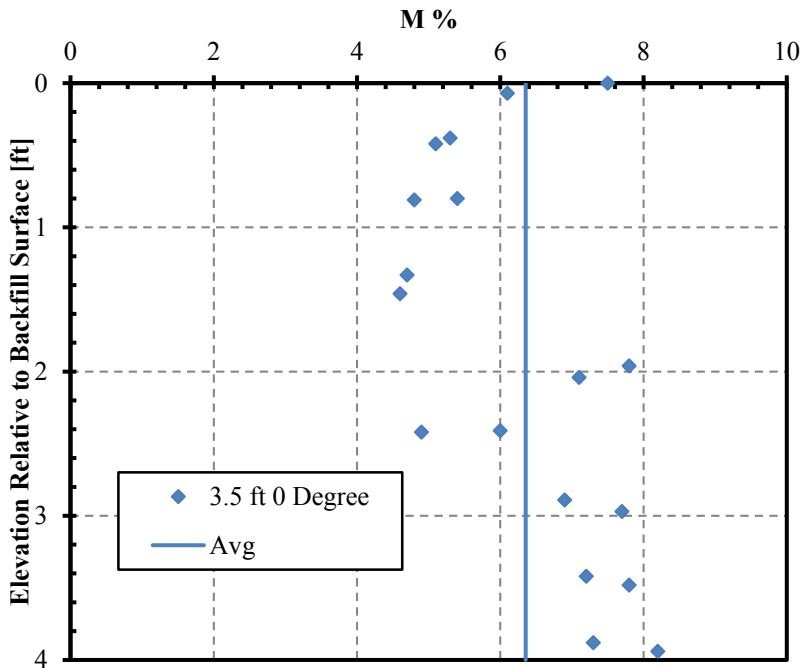
Figure 3-20. Moisture contents for 0° skew gravel backfill test.
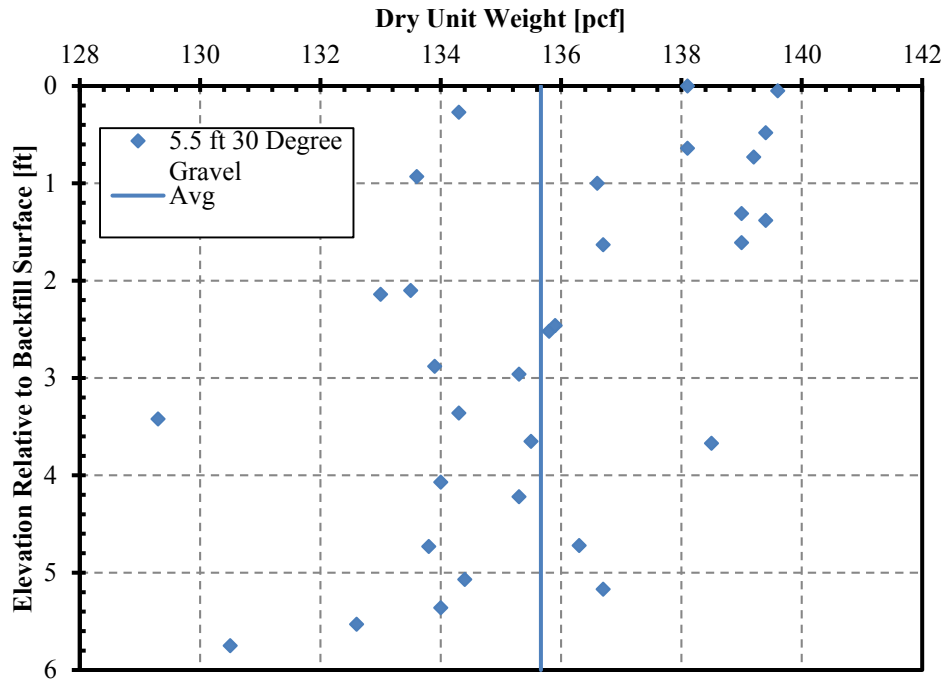
Figure 3-21. Dry unit weights for 30° skew gravel backfill test.
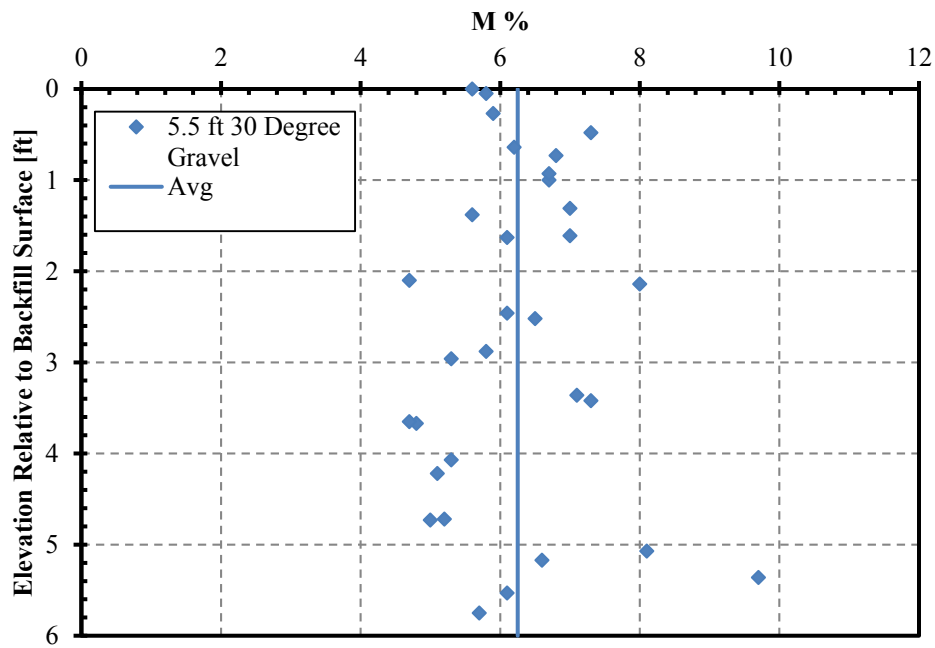
Figure 3-22. Moisture contents for 30° skew gravel backfill test.

68
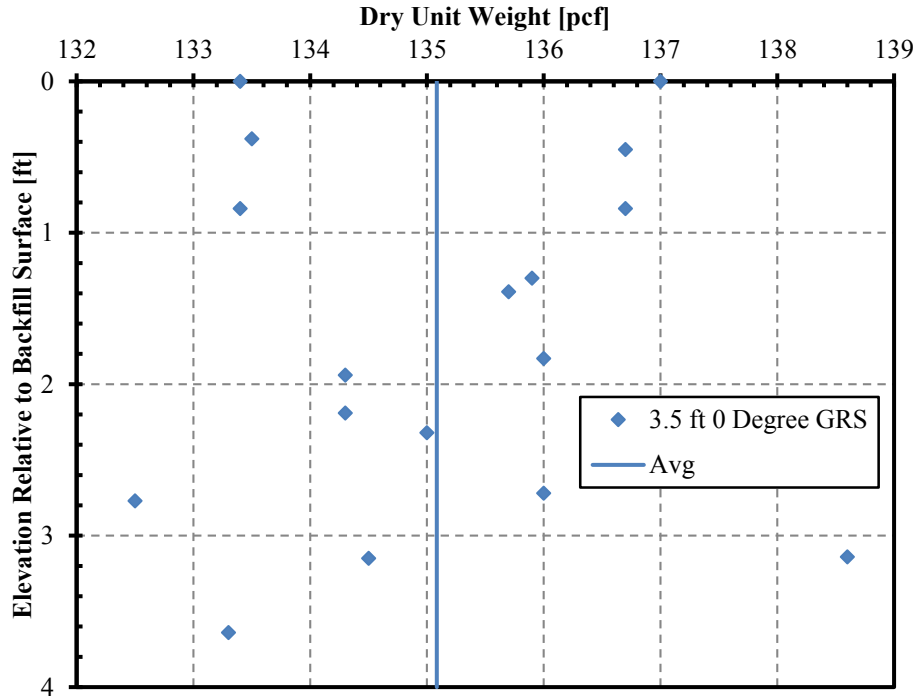
Figure 3-23. Dry unit weights for 0° skew GRS gravel backfill test.
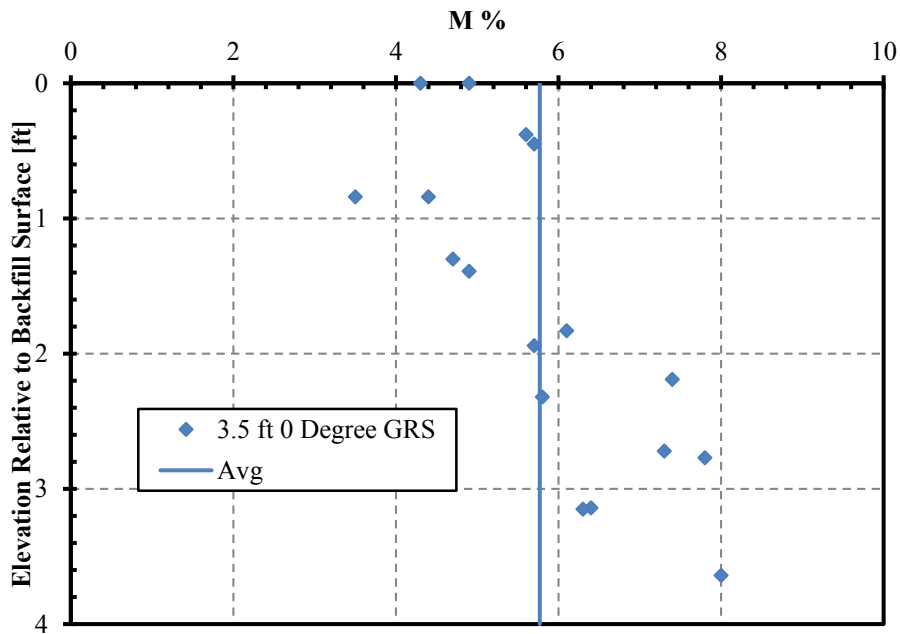
Figure 3-24. Moisture contents for 0° skew GRS gravel backfill test.
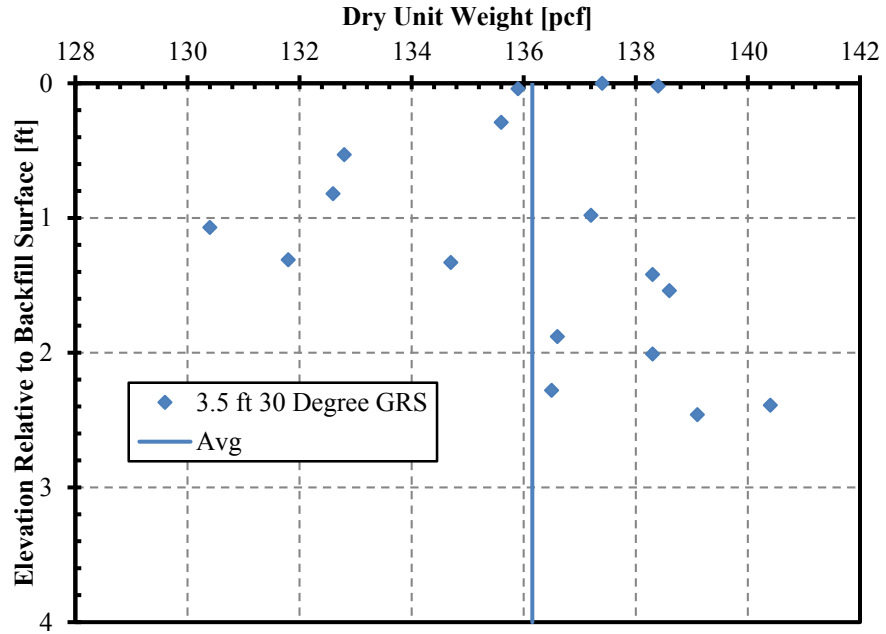
Figure 3-25. Dry unit weights for 30° skew GRS gravel backfill test.
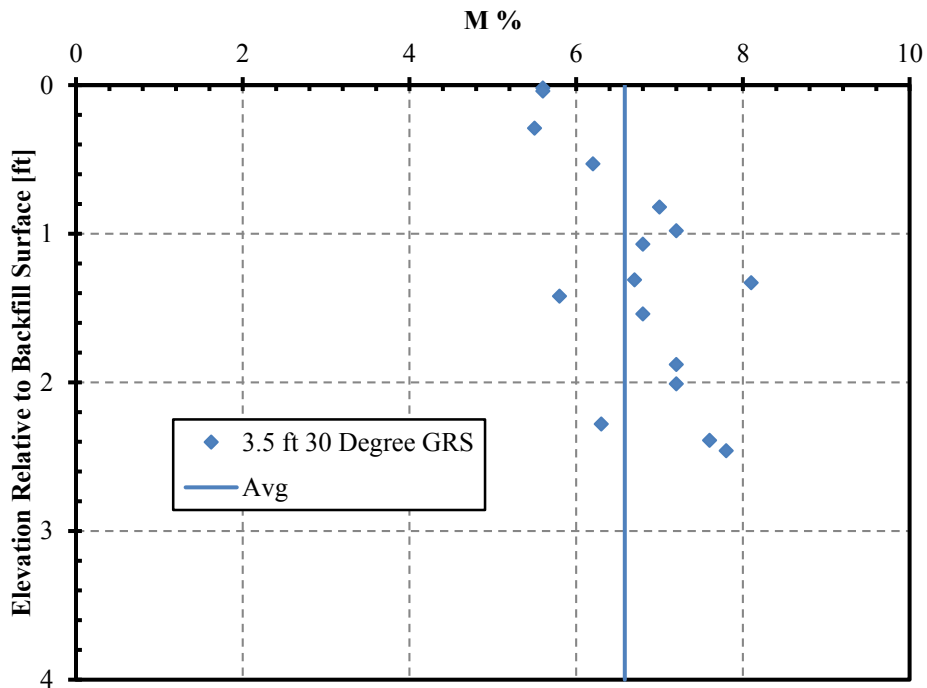
Figure 3-26. Moisture contents for 30° skew GRS gravel backfill test.

70

3.5.2 Shear Strength

3.5.2.1 In Situ Direct Shear in Gravel Backfill

In situ direct shear tests were conducted for the gravel backfill without geofabric. Figure 3-27 shows a photo of the shear tests being performed. The tests were performed after the non-skewed 3.5 ft unconfined gravel test, which had been compacted at 96.3% maximum Proctor density, on average. The box was carefully lowered into place by chipping away the soil around the box and tapping the box downward, into the backfill. Once in place, weights were loaded on top of the soil and a hydraulic jack applied lateral force. Displacement was measured with a dial gauge.

Two separate in situ tests were performed and the results are shown in Figure 3-28. The drained friction angle (ϕ') was found to be 45.8° with a cohesion of 40 lb/ft^2 (6.3 kN/m^2). Previous researchers (Rollins and Cole 2006) conducted direct shear tests and determined that the interface friction angle (δ) between similar coarse gravel soil and concrete was about 75% of the soil friction angle. However, since the GRS tests had the geotextile wrapped around the soil adjacent to the pile cap, there was no soil-concrete interface. Instead, there was a soil-fabric interface and a fabric-concrete interface. The bulk of the movement and, therefore, the resistance likely would have been along the fabric-concrete interface.

71

Figure 3-27. Photo of in-situ direct shear test on gravel backfill
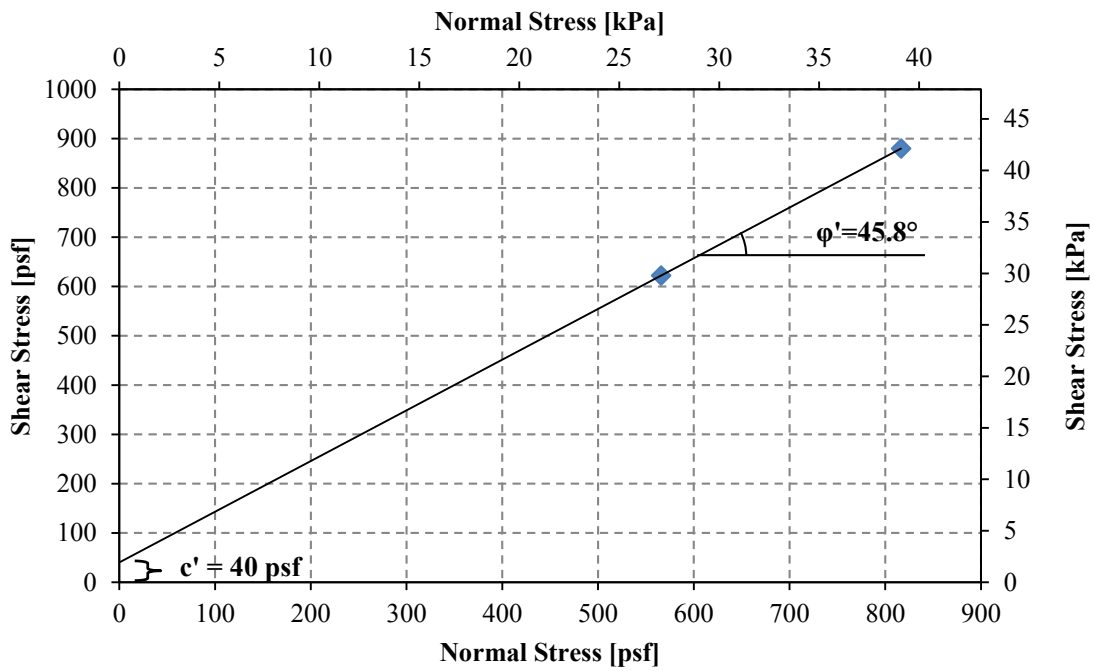
Figure 3-28. In situ direct shear results for gravel backfill

3.5.2.2 Direct Shear Test for Concrete-Fabric Interface

A modified direct shear test in accordance with ASTM D-3080 was performed to determine the interface friction between the geofabric and the concrete pile cap. A standard direct shear machine was used with the 2-in (5.1-cm) thick by 4-in (10.2-cm) diameter circular shear box. The concrete pile cap was cored to obtain a 1-in (2.5 cm) thick by 4-in (5.1-cm) diameter sample core. The outer concrete surface faced up in the lower mold to form the lower interface of the test. A 4-in (5.1-cm) diameter sample of the geofabric was then cut to fit and placed on top of the concrete as the face of the upper mold. Gravel backfill obtained from the test site stockpile filled the space behind the fabric. The soil was screened by the No. 4 sieve, wetted to the average testing moisture content of 6.2%, and placed behind the fabric at the greatest hand compaction possible. The compaction achieved was approximately 99% for the two lower-pressure tests and 94% for the two higher pressure tests. One 0.25-in (0.64-cm) thick porous stone was placed on top. A direct shear test was then performed on each of the four specimens with varying vertical pressures that correlated with the estimated lateral earth pressures against the concrete-fabric interface during testing. The passive earth pressure coefficient assumed was $K_P=10$, and the backfill passive pressure was calculated using the Equation (2-1): $\sigma_p = K_P\gamma H$. Table 3-3 shows how the four vertical loads correspond to loads at varying backfill depths during abutment testing.

Figure 3-29 presents the shear stress vs. displacement curves obtained from the testing. The test with $\sigma_v = 5920$ psf is dashed because the passive earth pressure it represents would occur at 4.0 ft, which is deeper than the backfill used during abutment testing. Similar to stress-strain plots for strain hardening materials, the system had a yield point where tangent stiffness greatly

73

at a slower rate. The capacity of the shear machine prevented greater horizontal displacement to try to obtain an absolute maximum peak from these tests.

Table 3-3: Vertical Loads in Direct Shear Testing and Related Horizontal Forces in GRS Backfill Full-Scale Testing

Backfill Depth [ft]	Passive Pressure Coefficient Assumed, K_P	Moist Unit Weight [pcf]	Passive (Horizontal) Stress in Backfill [psf]	Vertical Stress Applied in Direct Shear Test [psf]	Vertical Load Applied in Direct Shear Test [lb]
1.0	10	144.1	1398	1398	119
1.7	10	144.1	2432	2432	207
3.0	10	144.1	4442	4442	378
4.0	10	144.1	5923	5923	504
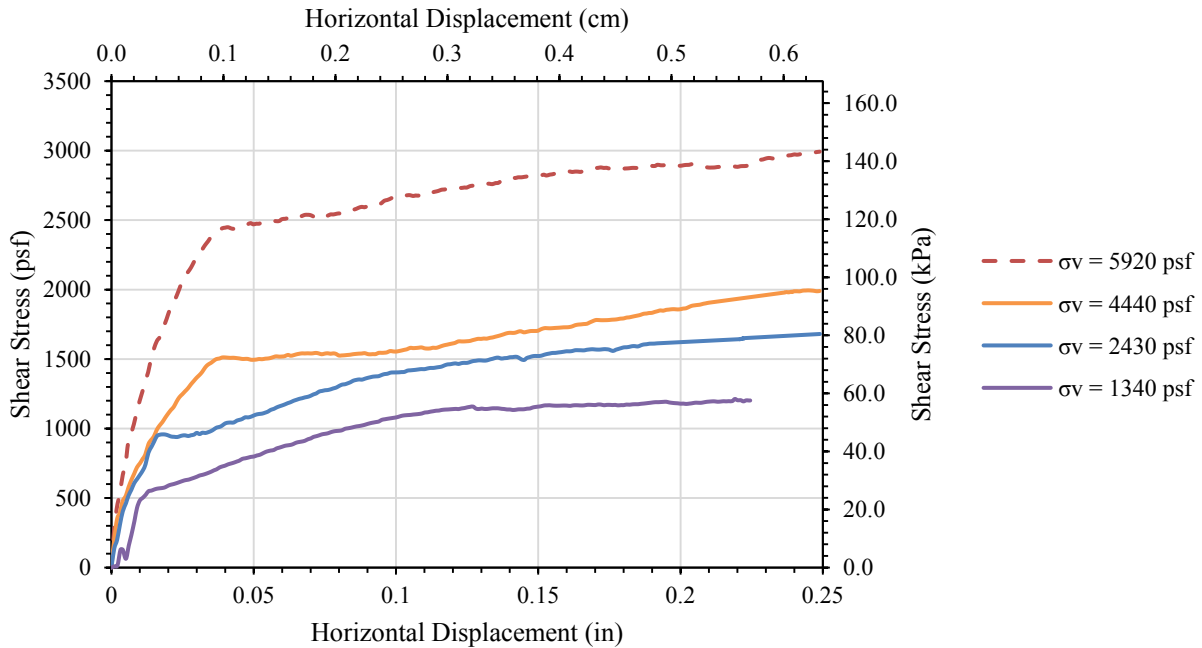
Figure 3-29. Shear stress vs. displacement curves for the four modified direct shear tests performed for the fabric-to-concrete interface.

74

When the peak value was taken at the yield point, the resulting concrete-fabric interface friction angle was 26.1°, about 57% of the friction angle of the gravel used for the backfill, 45.8°, with no apparent cohesion. Because the load steadily increased, an additional friction angle was calculated from the stresses using the last 10 data points of each test, at the approximate horizontal displacement of 0.25 in (0.64 cm). The end-of-test interface friction angle was 20.6°, 45% of the gravel internal friction angle, with an apparent cohesion of 680 psf (32.6 kPa). The measured stress-displacement curves and friction angles seem reasonable based on load test and PYCAP analyses, which will be discussed in Subsection 6.4.1. Figure 3-30 and Figure 3-31 show the shear vs. normal stress plots at these two points of testing.
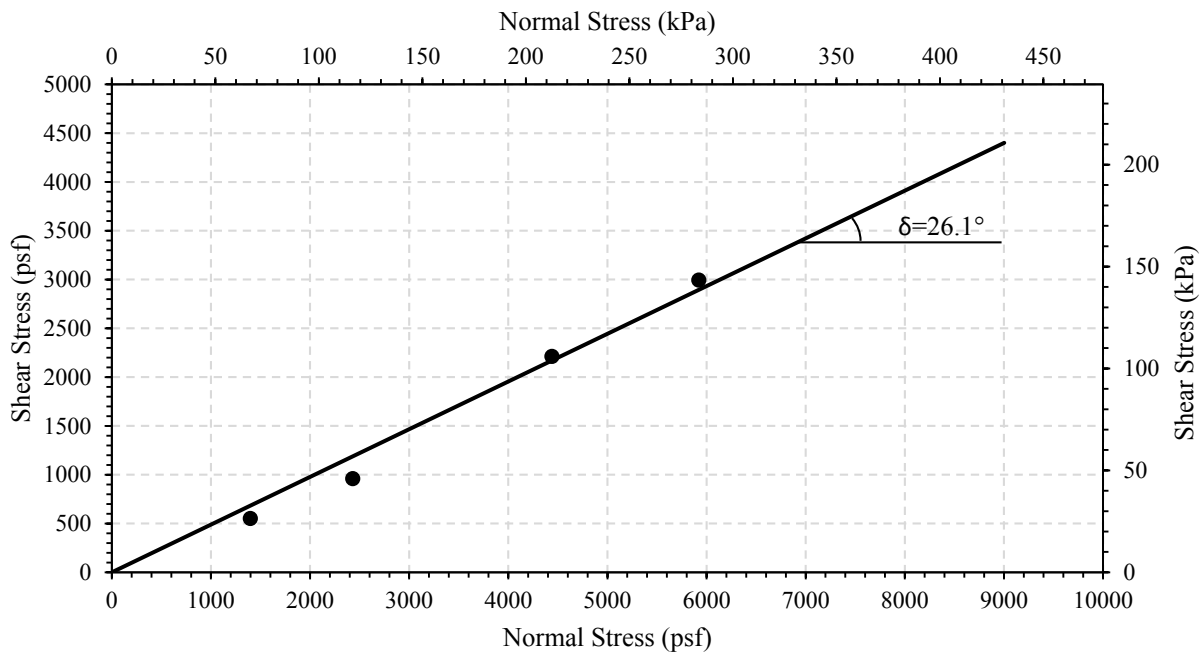
Figure 3-30: Shear vs. normal stress plots for modified direct shear tests using the stresses at the point of yielding.
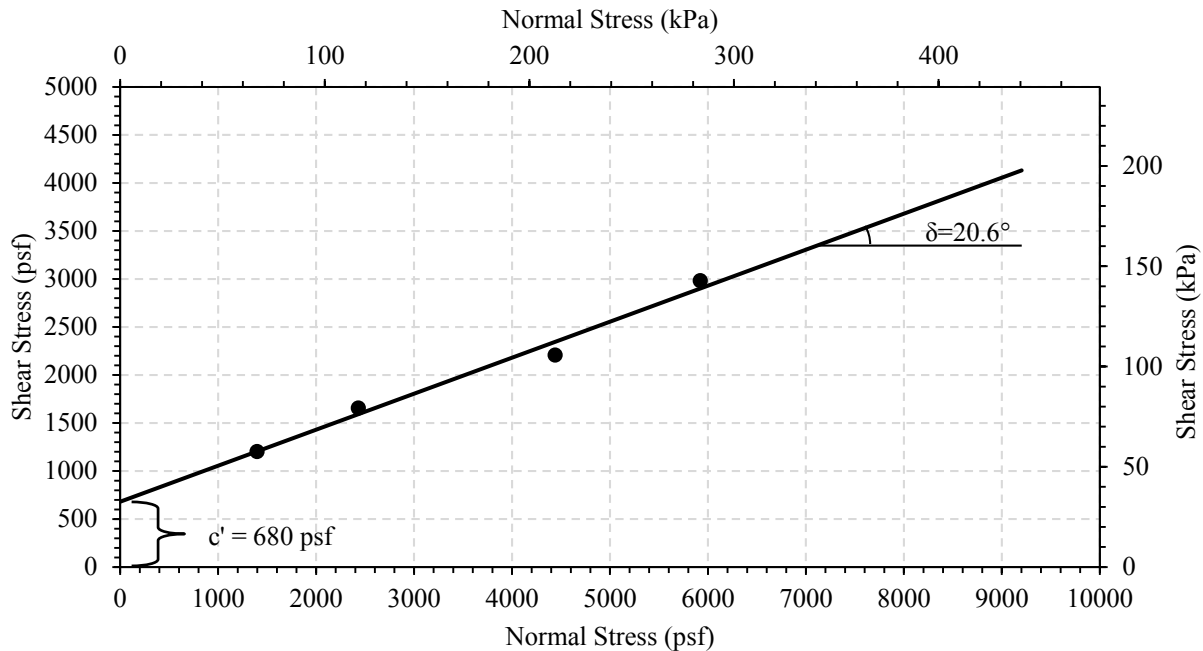
Figure 3-31: Shear vs. normal stress plots for modified direct shear tests using the stresses at the end of testing.

3.5.3   Geosynthetic Fabric Characterization

The geotextile sheet used for the GRS tests was Mirafi® RS380*i* which was donated by Tencate Geosynthetics Americas for this research project. This geotextile is woven from polypropylene (PP) filaments to provide desired strength and soil retention characteristics along with high water flow capacity. Based on test results from the manufacturer, the geotextile has a minimum tensile modulus of 51,000 lb/ft (744 kN/m), which equates to a tensile strength of 2550 lb/ft (37 kN/m) at a strain of 5%. The geotextile has an apparent opening size (AOS) equivalent to a #40 U.S. sieve size (0.43 mm). The pore sizes for O_{95} and O_{50} are 365 and 185 microns, respectively. Permittivity is 0.9/sec and flow rate is 75 gal/min/ft^2 (3056 L/min/m^2). The interface coefficient for sand and gravel is 0.89. A photograph of the woven fabric is provided in Figure 3-32. While FHWA (2012) and UDOT (2012) both specify 4800 lb/ft (70 kN/m) tensile

76

strength, personal communication with Jennifer E. Nicks (2013) recommended using 2400 lb/ft (35 kN/m) as the minimum tensile strength.

Figure 3-32. Photograph of the polypropylene Mirafi® RS380i fabric which was donated by Tencate Geosynthetics Americas for use in this GRS research study.

3.6 General Test Procedures

Prior to testing with the backfill in place, a lateral load test was performed to determine the "baseline" resistance of the pile cap alone, and the pile cap with attached 30° wedge. Because the pile cap had been previously employed for a number of tests, the baseline resistance has become relatively linear. Following the baseline test, backfill was compacted adjacent to the cap, the fabric interlayered in the case of the GRS tests, and a lateral load test was performed to obtain the total resistance. Following backfill compaction, the reference grid was painted and appropriate initial measurements, including relative elevations of the grid points, were recorded.

The backfill material was completely excavated and re-compacted for each individual test. New reinforcement fabric was also placed for each GRS test.

The pile cap (and attached wedge if applicable) was then loaded longitudinally into the backfill zone in 0.25-in (6.35-mm) increments at a velocity of 0.05 in/min (1.27 mm/min) to a final displacement of 3.00 in to 3.75 in (8.30 cm to 9.53 cm) using the two hydraulic actuators. At each 0.25-in (6.35-mm) displacement increment the load was held for approximately 2 minutes to take measurements and observe the reduction in longitudinal force against the backwall as a function of time.

3.7   Cyclic Loading

Cyclic loading was performed at the beginning of the 30° skew 5.5 ft (1.68 m) gravel test. The oscillation pushed and pulled 0.5 in (1.3 cm) both forward and backward from the original starting position for a total range of approximately 1 in (2.5 cm). The test commenced by loading the pile cap at 0.25-in (6.35-mm) increments of displacement according to the standard procedure outlined in the previous section, but after the 0.50 in (1.3 cm) increment, the pile cap was retracted to -0.50 in (-1.3 cm), or 0.50 in (1.3 cm) backward from its original position, and then pushed again past the original position to 0.50 in (1.3 cm) into the backfill to complete the cycle. The pile cap oscillated 20 cycles. After the 20th cycle, the pile cap was continued into the backfill at 0.25-in (6.35-mm) increments for the remainder of the test.

78

4 Gravel Backfill Field Test Results

4.1 Passive Force-Deflection

This section presents the passive force-deflection curves for the two gravel tests and describes how they were calculated.

4.1.1 Total Force-Deflection

As described in Section 3.6, a baseline test was performed at each skew angle to find the baseline resistance of the piles and base friction or other resistance in the system unrelated to passive force. Figure 4-1 shows the total measured actuator force versus longitudinal deflection curves for the non-skewed 3.5 ft (1.07 m) gravel field test alongside the non-skewed baseline test. Figure 4-2 shows a similar graph for the 30° skew 5.5 ft (1.68 m) gravel test and 30° baseline test. The skewed test's significantly higher resistance is due to the extra 2 ft (0.61 m) in fill height. If a 5.5 ft (1.68 m) high gravel backfill had been used for the non-skewed test the capacity of the actuators would have been exceeded. The difference in fill height will be accounted for by scaling down the passive force as discussed subsequently.

Passive force was calculated using Equation (2-12) from Burke Jr (1994) with the longitudinal load (P_L) being the difference of the total actuator load and the appropriate baseline curve. Backwall deflection was computed as the average deflection of the four string pots on the front of the pile cap. Passive force calculations for the 30° test included a height scaling factor.

79
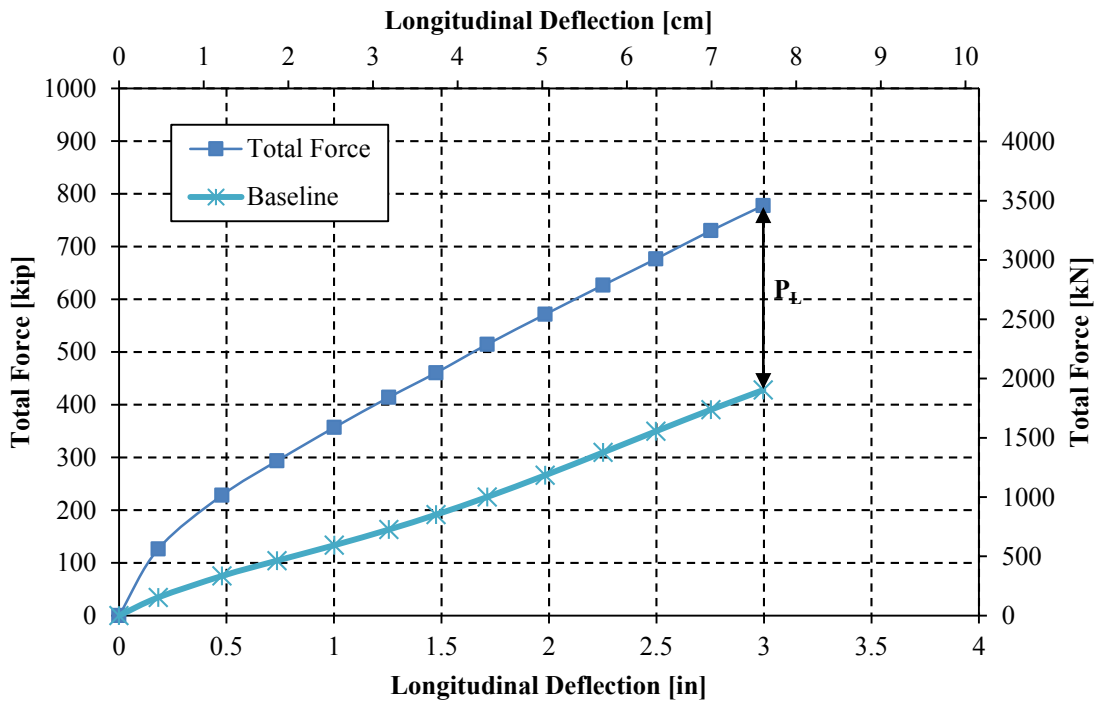
Figure 4-1. Total force and baseline resistance for 0° skew 3.5 ft (1.07 m) gravel test.
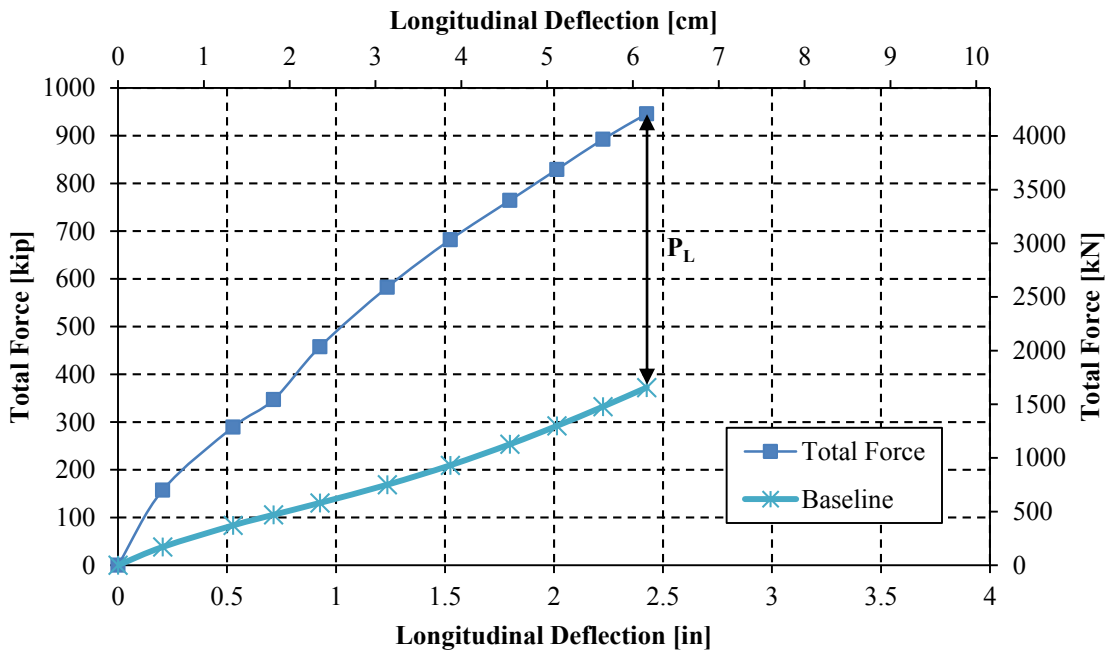
Figure 4-2. Total unadjusted force and baseline resistance for 30° skew 5.5 ft (1.68 m) gravel test.

4.1.2 Baseline Tests

As previously explained, the baseline tests measured the resistance in the system with no backfill, which included any inherent resistance in the actuators, the weight of the piles and pile cap, the passive force behind the pile group, and base friction between the pile cap and the underlying soil. Because the skewed tests had additional concrete wedges that were placed on rollers and attached to the back of the pile cap, the skewed tests had higher baseline curves. This was also observed in the 2012 BYU testing (Marsh, 2013). The baseline tests are vital to isolating passive force in the testing set-up. However, because soil stiffness is generally non-linear and because compression and relaxation take time to develop and to reach equilibrium, measuring a baseline test that is a perfect reflection of the actual resistance the system experiences during a backfill test is nearly impossible. This section seeks to illustrate all BYU baseline tests thus far to evaluate what can be improved for future testing.

Marsh (2013) observed that in the 2012 BYU testing, a key factor that affected each baseline test was the timing of when it was performed in relation to the preceding test. Increased time between tests allowed the soil behind the piles to relax and remold back to its original position. However, disturbance in that soil due to rain or vibrations could settle soil back into gaps that have likely developed behind the piles due to their repetitive loading from testing at the site, thus increasing soil-pile resistance between testing.

To provide context for the 2013 baselines, the BYU baseline tests from 2012 are shown in Figure 4-3 in chronological order. These baseline tests are remarkably similar, within 40 kips of one another for deflections up to 2.75 in (7.0 cm) for five of the tests. For deflections greater than about 2.75 in (7.0 cm), the non-skewed tests drop in stiffness, and the skewed tests more clearly have higher resistances than the non-skewed tests. The low 0° test seen in the figure is

81

low because it was the second baseline test performed in one day. The third 0° test was believed to have extra soil settlement around the piles due to the manner in which the previous test's backfill had been excavated, which increased its resistance. The 15° test and second 30° test were both performed one day after another test had been performed, which is why they exhibit decreased baseline resistance, though they are less decreased than 0° skew #2. Marsh (2013) details each of these baselines in further depth.
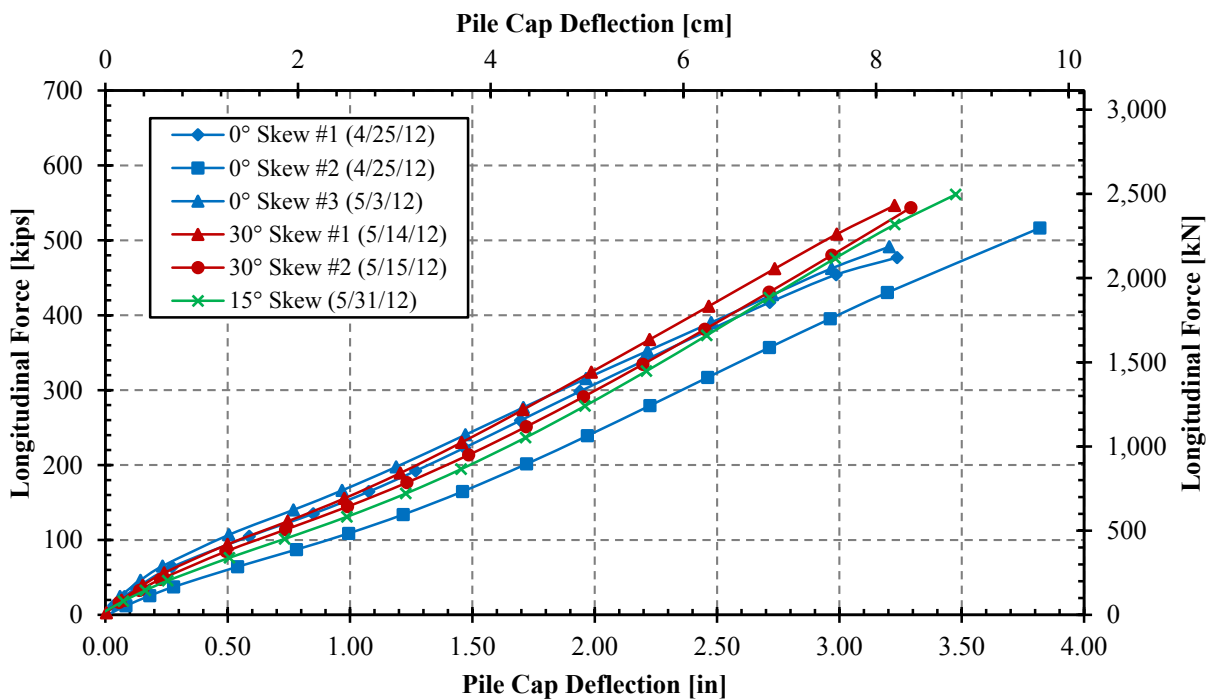
Figure 4-3. Baselines from 2012 BYU testing, labeled in chronological order.

Figure 4-4 plots the baselines for the 2013 BYU testing in chronological order. Testing was performed at skew angles of 0°, 30°, and 45°, beginning with the larger skews and removing skew wedges until the pile cap, or 0° skew, remained. The decrease in resistance between the skew angles is more exaggerated for the 2013 testing compared to the 2012 testing. Another factor at play may be that the overall resistance of the system decreased with continued testing.

Because skew increased over time in the 2012 testing and decreased over time in the 2013, it is possible that such a decrease with increased repetition was present and went unnoticed in the 2012 tests but is more apparent in the 2013 testing. Another factor at play, as previously mentioned, is time between tests.
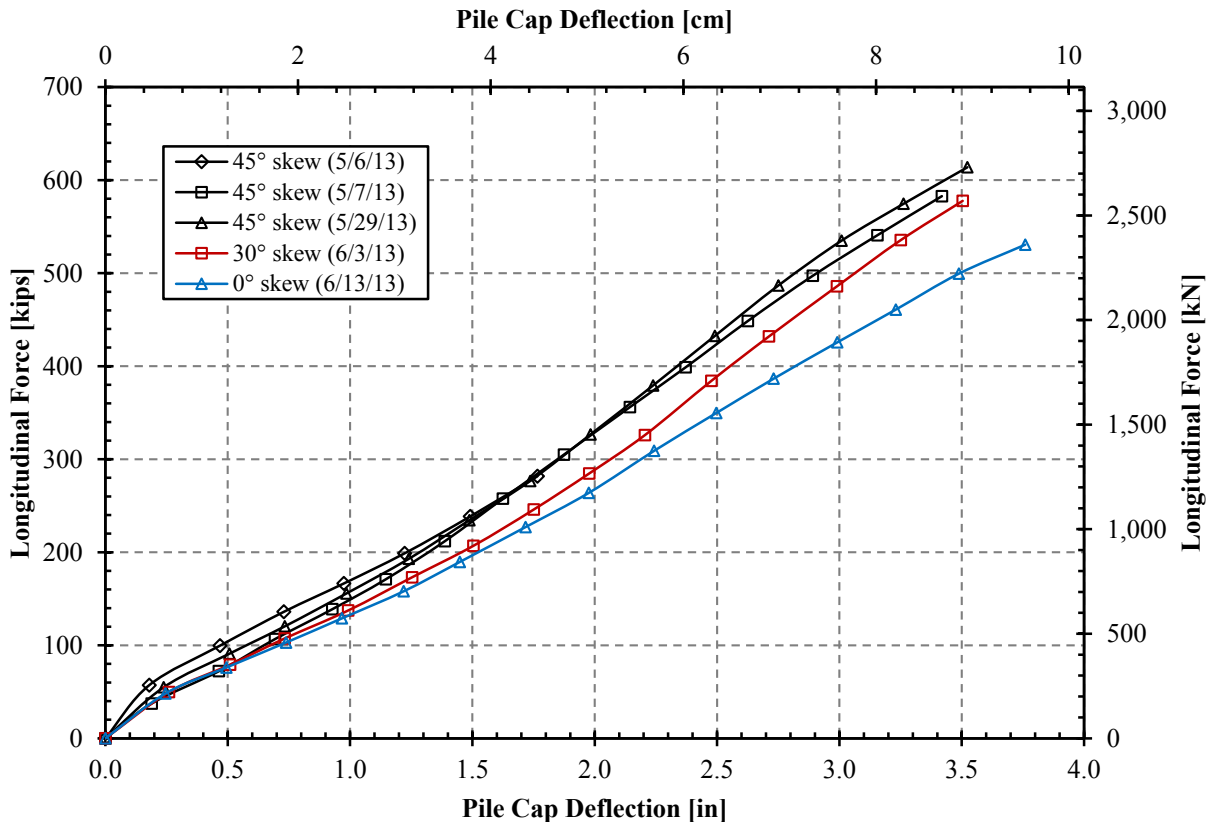
Figure 4-4. Baselines from 2013 BYU testing, labeled in chronological order.

Three 45° skew baseline tests were performed in 2013. The first of these was the first test performed on the system since the previous June, and was performed on May 6, 2013. It had the highest resistance of the five tests and was terminated at just 1.75 inches (4.45 cm). The second was performed the next day and was pushed to 3.5 in (8.9 cm). This baseline had somewhat decreased resistance due to the first baseline test being performed only one day prior.

83

The third 45° test was performed on May 29, 2013, after all four 45° backfill tests had been performed. Six days had passed since the skewed wingwall test had been performed, which allowed the soil to remold itself around the piles. While the 45° side push test had been performed earlier that same day, the side push test was pushed almost exclusively transversely to deflections less than 0.6 in (1.5 cm) (See Subsection 3.3.5). Any effect from the side push was negligible compared to the May 7 test. The difference between the May 7 test, which represents one day of soil remolding, and May 29, which represents 6 days of soil remolding, was about 10 kips at deflections less than 1.5 in and about 20 kips for deflections greater than 2.0-2.5 in (5.1-6.4 cm). Therefore, though there is observable variance in the baseline behavior based on how many days passed between tests, the difference in resistance appears to be small compared to the resisting forces. Also, the increased resistance of the May 29 test shows that the length of time after the previous test likely has more effect on the baseline test than the repetition of the loading. The May 29 test was chosen as the 45° baseline test used to find passive force for all the 45° backfill tests, including the wingwall test by Smith (2014). It was selected because first, the May 29 test appeared to be the most reliable and, second, with the exception of the 3 ft (0.9 m) test, the 45° backfill tests were performed 3-6 days after the previous test, which make comparison with the May 29 test the most reasonable.

Only one 30° baseline was performed in 2013. It showed less baseline resistance for the 30° skew compared to the 45° skew. It was performed five days after the previous test, which was the final 45° baseline test. The 30° 5.5 ft (1.68 m) gravel test was performed two days later, and thus had less time for remolding than it had for the baseline test. Thus the actual baseline behavior for the gravel test may have been up to 10-20 kips lower than measured, based on the

84

45° variance previously discussed. The 30° 3.5 ft (1.07 m) GRS test was performed four days after the previous test.

Only one 0° baseline was performed in 2013. It showed the least resistance of the five tests, particularly at higher deflections, which is consistent with 2012 testing. As mentioned previously, the decreased deflection is believed to be due to less weight and base friction on the pile cap because no skew concrete wedges were attached. The 0° baseline test was performed only two days after the skewed GRS test. The 0° 3.5 ft (1.07 m) gravel test was performed the day after the baseline test. However, because the baseline test only had two days of remolding prior, the difference in actual baseline behavior was probably relatively small. The 3.5 ft (1.07 m) GRS test was performed four days after the previous test, so the actual baseline resistance may have been slightly greater than that measured.

In the previous figure, Figure 4-4, the stiffness in the baseline seems to increase slightly after a deflection of about 2.0-2.5 in (5.1-6.4 cm). The increased stiffness could be due to friction being mobilized in the base rollers or the rollers getting stuck on an obtrusive nail. Though the convexity is more pronounced in the skew curves, it is also observable in the 0° curve. Another explanation, then, is that a gap has formed due to compression of soil behind each of the piles. For all or part of the depth of the piles, the piles may have moved through the gap and become more engaged with the soil at the higher deflections.

Figure 4-5 shows all the baselines from 2012 and 2013 plotted together. The plot shows a general pattern of slightly higher resistances with higher skew. The non-skewed tests had the lowest resistance at higher deflections, but also had the most variability as shown in the separate plot, Figure 4-6. Though the second 2012 0° test was low due to its immediateness after the previous test, the one 2013 test was only about 20-30 kips higher. The 2013 0° test is 40-50 kips

85

lower than the most reliable 2012 non-skewed test. A major factor in the decrease is likely due to the two days only of soil remolding prior to the 2013 0° test. It should also be noted that the 2013 0° test was the final baseline performed at the test site thus far, so repetitious loading could also be a contributing factor to the lower baseline. However, as mentioned previously, the 2013 0° baseline is a good comparison with the backfill tests from 2013 because they share the same repetitious loading characteristics, and the remolding timeframes are similar.
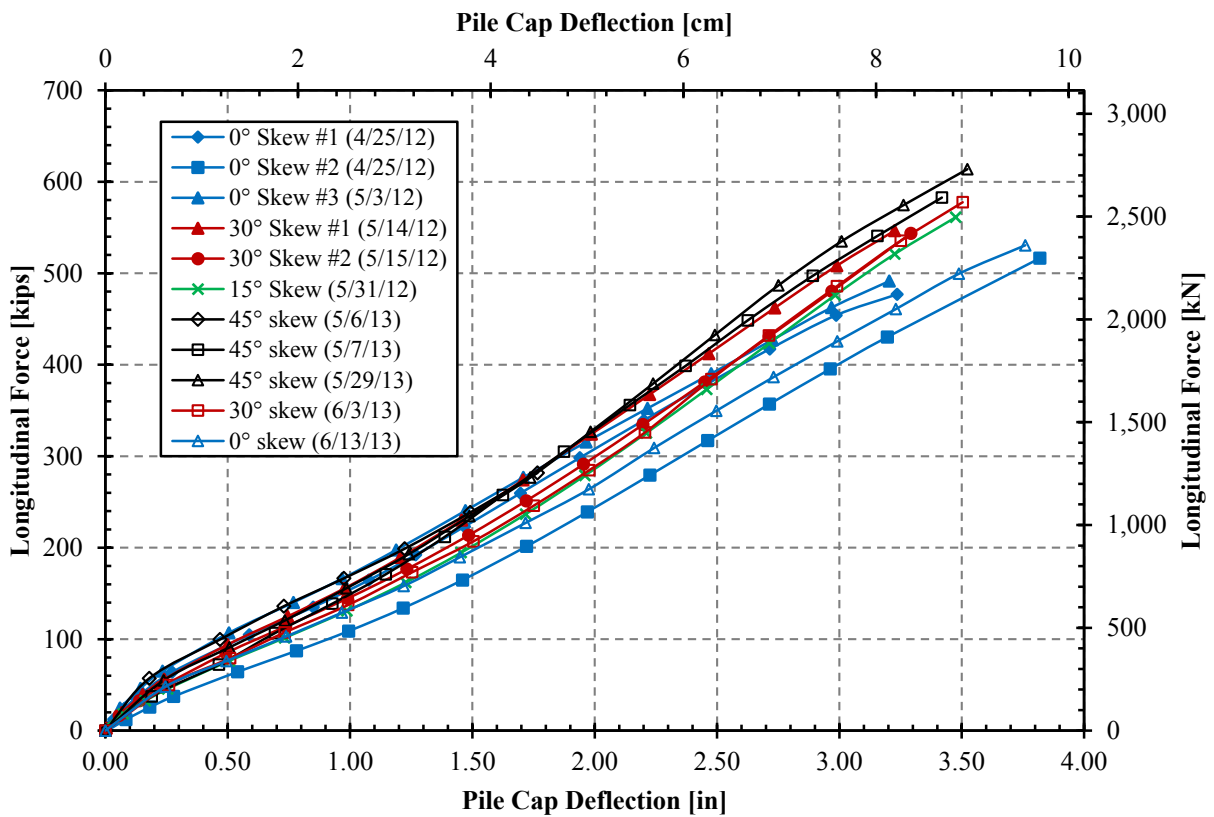
Figure 4-5. Combined 2012 and 2013 baselines show relatively good agreement between years.
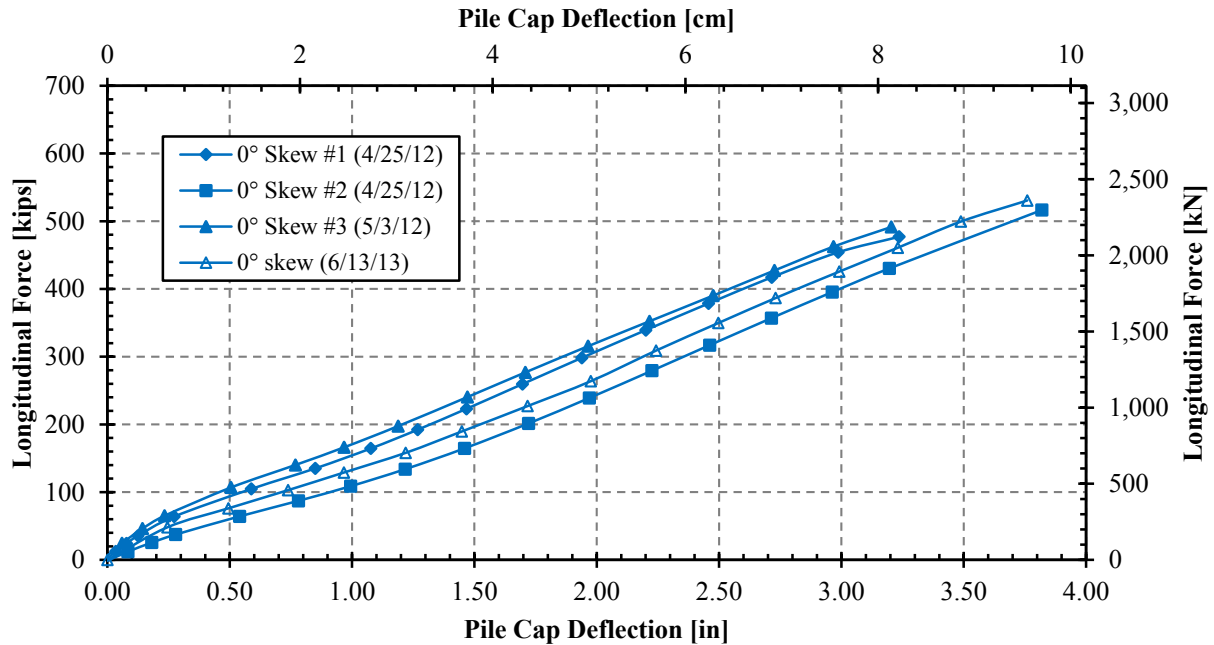
Figure 4-6. Compiled non-skewed baseline tests show the most variation between 2012-2013.

In Figure 4-7, the 2013 30° test was lower than the #1 test from 2012. Despite having a comfortable five days of remolding time prior, the 2013 baseline matched the 2012 #2 test more closely, which had only one day of remolding time. The small difference may again just be the repetitious loading on the system. Another possible explanation is at the end of each test when the pile cap was pulled back, the ending position of the pile cap was not exactly regulated. Therefore, the pile cap may have started at a slightly different position, within about 0.1 in (0.3 cm) from zero deflection.

There are a number of limitations in the baseline tests at present. This section has noted that decreased time between tests noticeably decreases the baseline resistance. There is possible decrease in resistance from 2012 to 2013. Also, exact pile cap ending and starting positions were not necessarily regulated during testing to be at exactly 0.00-inch deflection. In most cases, comparison between consecutive tests should be reasonable, as long as those tests were allowed similar allotments of time between tests for the soil to relax. It is believed that gaps have formed

87

behind each of the piles due to repetitious compression of the soil behind them. Occasionally, due to rain, compaction, or other environment factors, some patches of soil may cave in or otherwise shift between tests. When present, gap intrusion especially affects higher deflections.
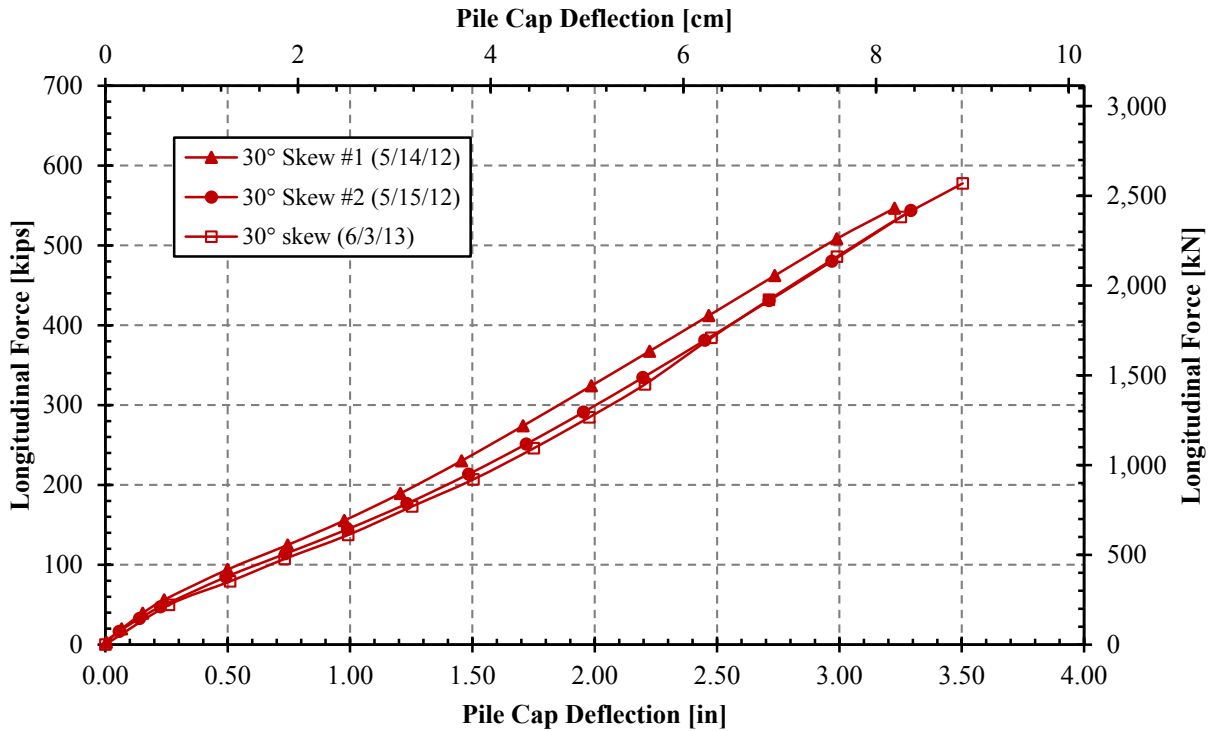
Figure 4-7. Compiled 2012-2013 30° skew tests.

An additional limitation of the baseline testing is transverse movement. Inclinometer and shape array measurements were only taken for some of the baseline tests. The available data showed transverse movements to the west of 0.03 in (0.08 cm) up to 0.07 in (0.18 cm) in one case. Without backfill, the pile cap should have moved forward without transverse movement. Transverse movement in the 0° backfill tests also exhibit transverse movement to the west. This suggests that due to repetitive skew loading, the system tends slightly toward the west, which affects longitudinal directional assumptions. The observed transverse deflections are very small, however. Most backfill tests had much greater transverse deflections than the ones observed for

88

baseline tests. The side push test described in Subsection 3.3.5 only partial addresses this issue, because the longitudinal and transverse deflections occur simultaneously in the backfill tests.

4.1.3 Method of Passive Force-Deflection Scaling for 30° Test

When performing the 30° skew test using a gravel backfill height of 5.5 ft (1.68 m), as was previously done in testing with sand backfill, the west actuator reached its 600 kip (2670 kN) load capacity and shut down, limiting the deflection in the test to approximately 2.50 in (6.4 cm). While the non-skewed tests generally loaded the two actuators more evenly than in the skewed tests, the resulting data suggested that the non-skewed gravel test would likely exceed the 1200 kip (5340 kN) combined load capacity of the two actuators at this fill height. Therefore, for the 0° skew test the gravel backfill was only placed and compacted to a height of 3.5 ft (1.07 m). To allow comparisons between the two tests, the passive forces calculated from the 30° test with the 5.5-ft (1.68-m) thick backfill were scaled down to a 3.5-ft (1.07-m) thickness by the ratio of the square of the heights, H^2, based on the passive force equation described in Equation (2-3). The cohesion measured in the gravel is relatively small so that the second term of Equation (2-3) accounts for only approximately 4% of the passive force equation for this particular gravel soil and test configuration, so it was dropped as a simplification. Also, removing the cohesion in hyperbolic PYCAP analyses caused improved agreement with the measured data (See Subsection 6.4.1). The passive force equation is restated in Equation (4-1) below for a cohesionless soil:

$$(P_P)_{ult} = \frac{1}{2}\gamma H^2 K_P B_e \tag{4-1}$$

where the parameters γ and K_P do not vary between the two gravel tests. The variation in effective width (B_e) is small and the decision to exclude it from the scaling was determined

89

during the checking process, as will be described later in this section. Therefore, the 30° skew 5.5 ft (1.68 m) passive force values were multiplied by the scale factor $(3.5 \text{ ft})^2 / (5.5 \text{ ft})^2$ [$(1.07 \text{ m})^2 / (1.68 \text{ m})^2$], or approximately 40.5%, to obtain the scaled 3.5 ft (1.07 m) passive force values for the 30° test. The mathematical derivation for the scaling, Equation (4-2), is illustrated below.

$$\frac{P_{P(3.5\text{ft})}}{P_{P(5.5\text{ft})}} = \frac{\frac{1}{2}\gamma(3.5\text{ft})^2 K_P B_e}{\frac{1}{2}\gamma(5.5\text{ft})^2 K_P B_e}$$

$$P_{P(3.5\text{ft})} = \left[\frac{(3.5\text{ft})^2}{(5.5\text{ft})^2}\right] P_{P(5.5\text{ft})} \tag{4-2}$$

When calculated by hand for ultimate or peak conditions using log spiral passive force factors, removal of the cohesion term only affected the scaling results by about 1%.

Additionally, as described by Potyondy (1961), the required deflection to reach peak passive force is largely determined by the height of the backfill. It is assumed that all displacements are similarly correlated. Therefore, the displacements (d) were also scaled, as illustrated in Equation (4-3) below.

$$\frac{d_{(3.5\text{ft})}}{H_{(3.5\text{ft})}} = \frac{d_{(5.5\text{ft})}}{H_{(5.5\text{ft})}}$$

$$\frac{d_{(3.5\text{ft})}}{3.5 \text{ ft}} = \frac{d_{(5.5\text{ft})}}{5.5 \text{ ft}}$$

$$d_{(3.5\text{ft})} = \left[\frac{3.5\text{ft}}{5.5\text{ft}}\right] d_{(5.5\text{ft})} \tag{4-3}$$

The method of scaling the passive force as described was checked in two ways. The first check used Duncan and Mokwa's (2001) PYCAP program, and the second check used true test data from the unconfined sand tests performed in 2012. First, PYCAP was used to scale the 3.5 ft (1.07 m) non-skewed gravel test data from this study to estimate data for a 5.5 ft (1.68 m) fill.

90

The input parameters were calibrated to match the 3.5 ft (1.07 m) non-skewed gravel data before changing the backfill parameter to 5.5 ft (1.68 m). For comparison, the test data was then scaled as described in Equations (4-2) and (4-3), except from 3.5 ft (1.07 m) up to 5.5 ft (1.68 m) instead of vice versa. The resulting curves are shown in Figure 4-8 and correspond reasonably well with the PYCAP predicted curve, which includes effective width differences.
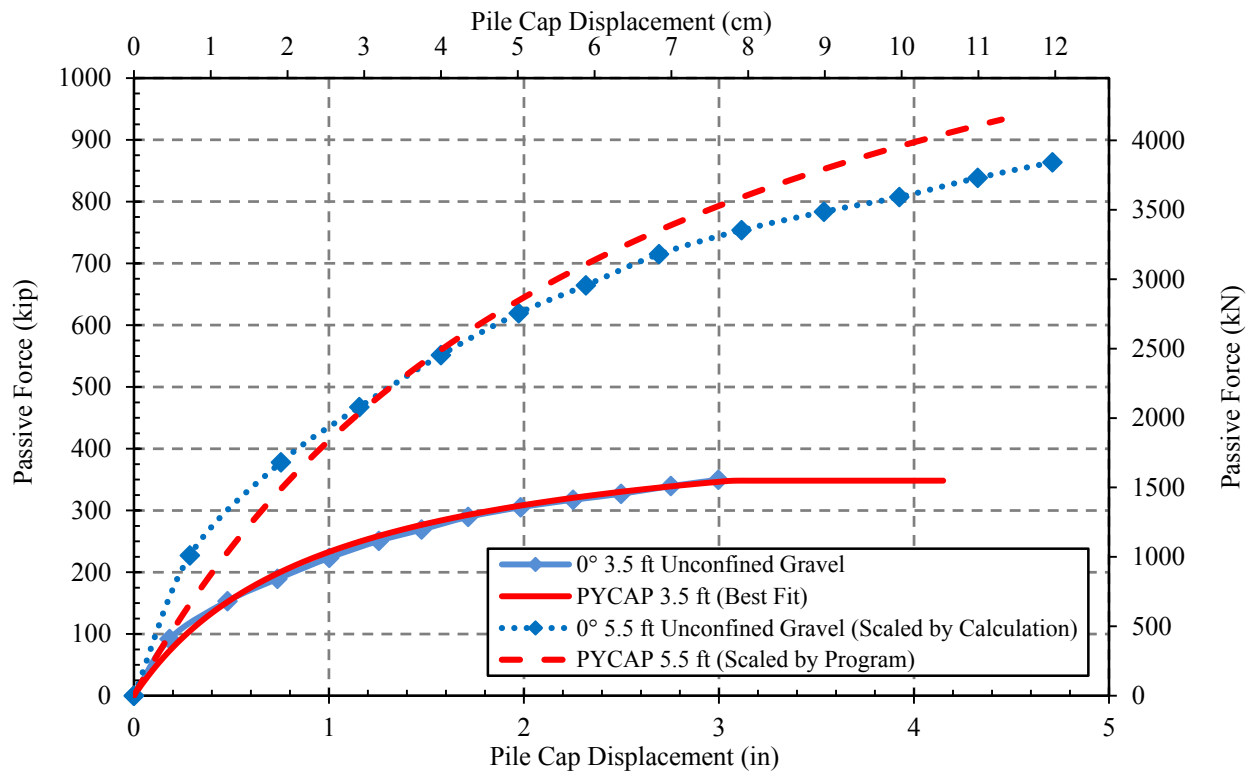
Figure 4-8. Trial of proposed scaling method using PYCAP and data from the 0° 3.5 ft (1.07 m) unconfined gravel test.

Unconfined sand tests from 2012 (Marsh, 2013; Palmer, 2013) from the same test site as this study also included tests with the same configuration and backfill sand material but two different fill heights: 3.0 ft (0.91 m) and 5.5 ft (1.68 m). To confirm that the proposed scaling method described is practical for skewed tests, it was applied to the data from all four skew angles 0°, 15°, 30°, and 45° for each fill height, so that the 3.0 ft (0.91 m) data was scaled up to

estimate 5.5 ft (1.68 m) data and the 5.5 ft (1.68 m) data was scaled down to estimate a 3.0 ft (0.91 m) passive force-deflection curve. These results for the 30° data are shown in Figure 4-9. Again, the agreement is not exact but is reasonably close, within about 10% for both cases. As such, the magnitude of difference is smaller scaling down than scaling up. Scaling from 5.5 ft (1.68 m) down to 3.0 ft (0.91 m) only produced a magnitude difference of 8 kips (36 kN). Scaling with the data from the other three sets of tests had similar agreement, but even more, since the proposed scaling method underpredicted in one case and overpredicted in three other cases, the split shows that the scaling method is a good estimation.
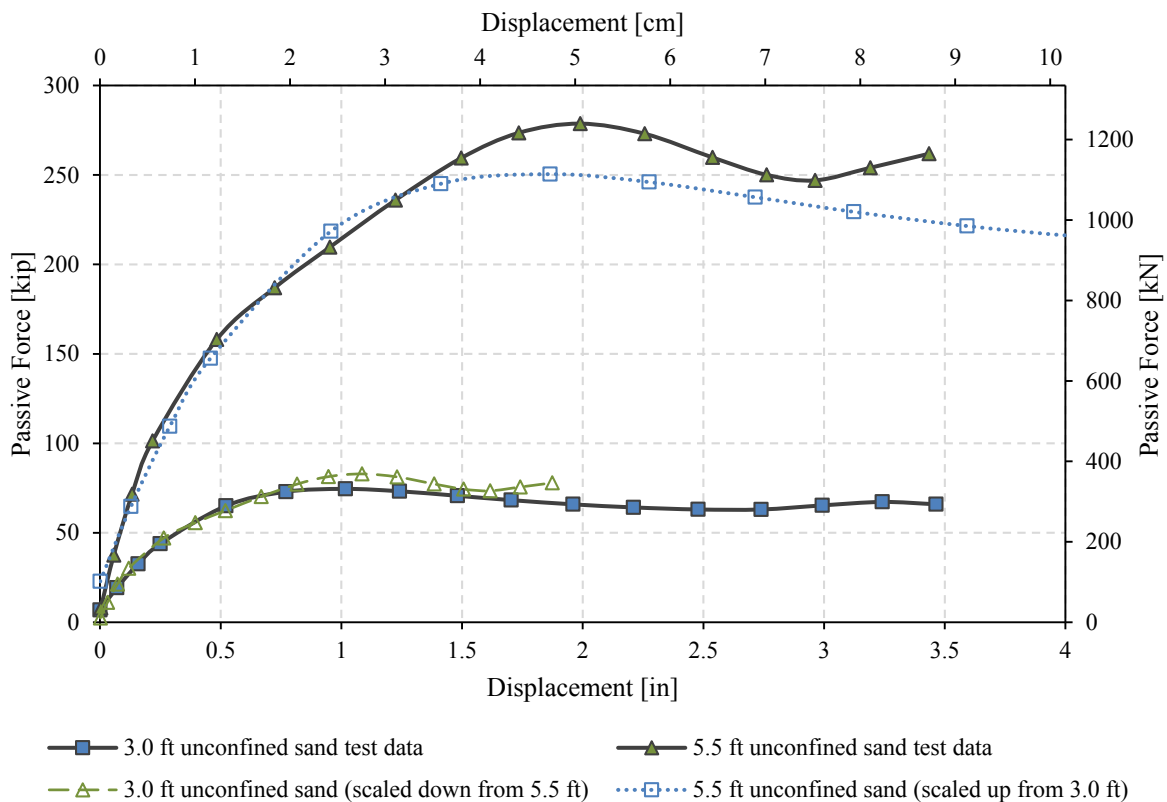
Figure 4-9. Trial of proposed scaling method using 30° skewed unconfined sand test data from Marsh (2013) and Palmer (2013).

In general, when the Brinch Hansen (1966) 3D factor as calculated by PYCAP was included as a term in the scaling, the predicted scaled data made the scaling significantly less accurate in most cases. However, the Brinch Hansen (1966) 3D factor was created using tests with non-skewed pile caps, and there is little data that addresses effective width in passive force for skewed data. As an additional simplification which the author believes to be more accurate, the 3D-factor was estimated to be approximately equivalent at both fill heights and therefore confirmed the elimination of the effective width factor from the passive force scaling equations. The assessments summarized above verified to the author that the scaling method of the skewed 5.5 ft (1.68 m) passive force data is satisfactory and within the variability of these types of tests. Figure 4-10 shows the unscaled and scaled passive force-deflection curve for the 30° gravel test, which will be explained further in the following subsection.
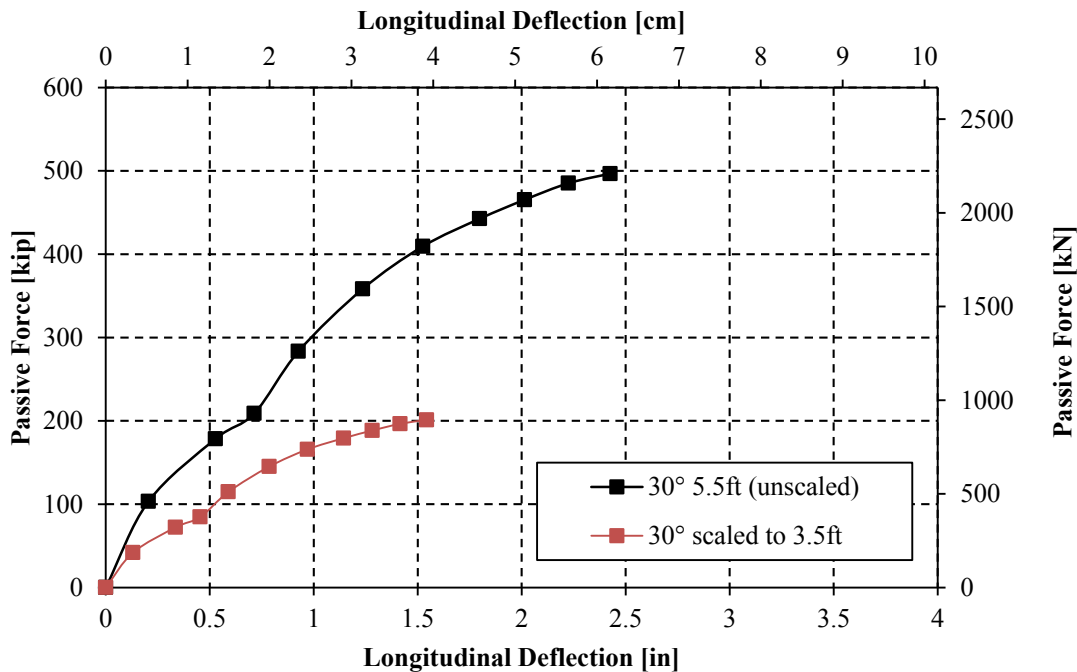
Figure 4-10. Scaling of 30° unconfined gravel test data from 5.5 ft (1.68 m) backfill height to 3.5 ft (1.07 m) backfill height.

4.1.4 Passive Force-Deflection Results and Reduction Factor

Figure 4-11 shows passive force versus longitudinal deflection curves for both tests with the 30° skew test data scaled. While neither test peaked within the available deflection, the 30° skew test may have been nearing its peak resistance at the end of the test. Maximum passive force was 350 kip (1557 kN) for the 0° test and 201 kip (894 kN) for the 30° test. The displacement of the skewed test was limited to 2.43 in (6.17 cm) due to the overheated actuator system, therefore the scaled displacement data for this test only extends to 1.54 in (3.91 cm) displacement, which is about 3.7% of the wall height.
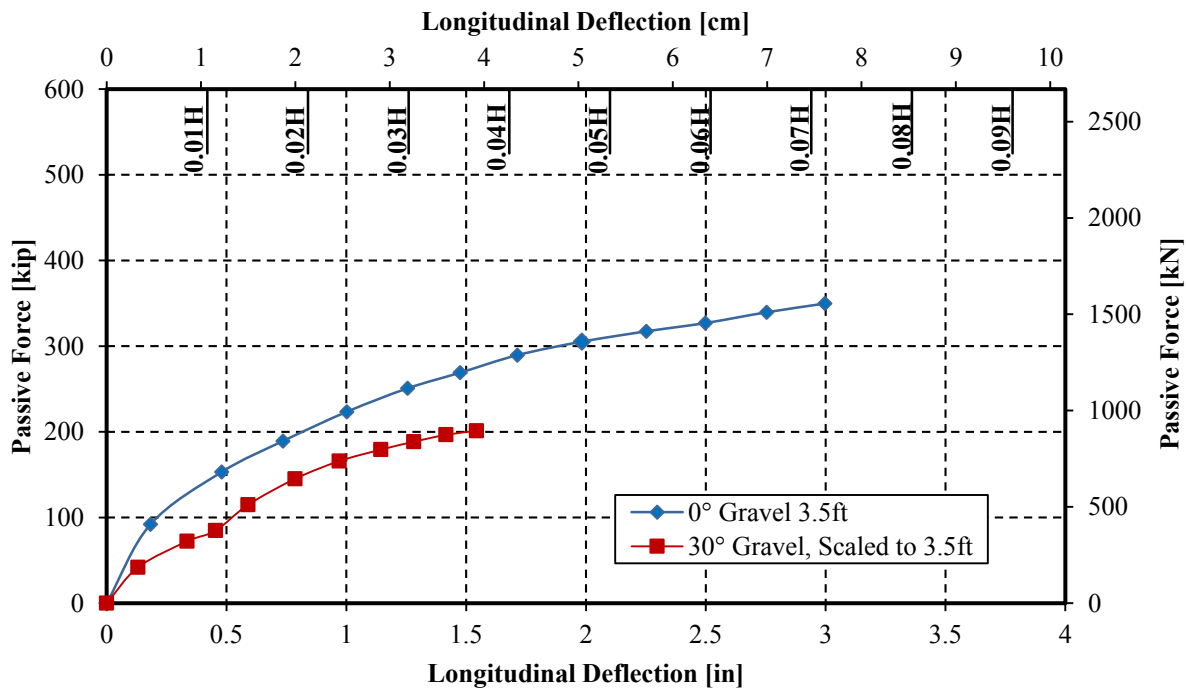
Figure 4-11. Comparison of passive force versus longitudinal deflection for 0° and 30° skew gravel tests.

The first two data points for the skewed test in Figure 4-11 represent the initial loading prior to cyclic loading. Cyclic loading was performed after pushing to 0.5 in (1.3 cm) unscaled displacement, during which both a transverse shift of the pile cap and, likely, some compaction

94

occurred to change the slope in the total force curve in Figure 4-2 between 0.5 and 0.75 in (1.3 and 1.9 cm) and in the scaled passive force curve in Figure 4-11 between 0.34 and 0.45 in (0.9 and 1.1 cm). This accounts for the small irregularity between those displacements. Cyclic loading will be further described in the next subsection, and transverse pile movement touching this case will be discussed in Subsection 4.3.

For the 0° skew test, the passive peak was not reached, although the cap displacement had already reached 7.1% of the 3.5 ft (1.07 m) wall height. The actual non-skewed test was performed to 3.75 in (9.5 cm), which is the maximum displacement allowed by this testing system and is about 9% of this test's backfill height. From 3.00 to 3.75 in (7.6 to 9.5 cm), the passive force data continued to increase steadily without significant change of stiffness. Deflections of more than 5 or 6% of the backfill height are rarely seen, much less at 9% displacement, as evidenced by the data in the compilation of studies shown in Section 2.5 (Meyer, 2012). Behavior of this kind is more typical of looser soils in that compilation of passive force curves, but the magnitude of the failures are stiff enough for dense material. Also, this test was compacted at approximately 95.9% modified Proctor compaction and therefore had a relative density (D_r) of about 80%. Without a peak at 0.09H displacement, it is inconsistent with other test results.

The PYCAP Excel program (Duncan & Mokwa, 2001) was used to attempt to back-calculate a hyperbolic passive force-deflection curve to fit the non-skewed unconfined gravel data to 3.75 in (9.5 cm) deflection. However, no PYCAP adjustments based on the gravel backfill characteristics could fit the data. Shown in Figure 4-12 is the best fit curve for 3.0 in (7.6 cm) deflection, with input parameters chosen as explained in Section 6.4, including specifying the peak displacement at 7.3% of the backfill height (0.73H). The most variable of the unknown

95

input parameters, or the most sensitive parameter not directly measured by any soil testing for this study, is the wall interface friction angle. A second hyperbolic curve was calculated in PYCAP with the peak developing at 10.0% of the backfill height (0.10*H) and by increasing the interface wall friction from 28.9° to 30.7° (0.63*φ to 0.67*φ) and is shown in Figure 4-13. Note that 10% of the backfill height as the maximum displacement is unsupported by any data as gathered by the author, and was only chosen to see if doing so would fit the data in this case. While most of the computed curve matches the data quite closely, it still diverges off of the last three points, which are the points at deflections greater than 3.0 in (7.6 cm). In general, the passive force-deflection data for this test fits the hyperbolic curve very closely, except for the deflections about 3.0 in (7.6 cm), which demonstrates possible inconsistency at the larger deflections. Because of this inconsistency, the non-skewed baseline curve was examined as a possible cause, particularly beyond 3.0 in (7.6 cm).

Linearity at the higher displacements allowed by the test configuration (3.0-3.75 in [7.6-9.5 cm]) was seen in all tests using the 0° baseline from the summer of 2013, including the 0° test reported in Smith (2014). For this reason, as explained by Smith (2014), the baseline curve was judged as somewhat questionable beyond 3.0 in (7.6 cm), perhaps due to stiffening of the soil from the repetitive loading or perhaps due to an error in the baseline. It is possible that soil infiltrated the gaps behind the six piles after the baseline test during vibratory compaction or rainstorms and increased the pile resistance not represented in the baseline curve. A number of other reasons could explain the linearity. Because of the inconsistency of the data at large deflections, the non-skewed data is reported only up to longitudinal deflections of 3.0 in (7.6 cm) for the purposes of this study, as was seen in Figure 4-11.
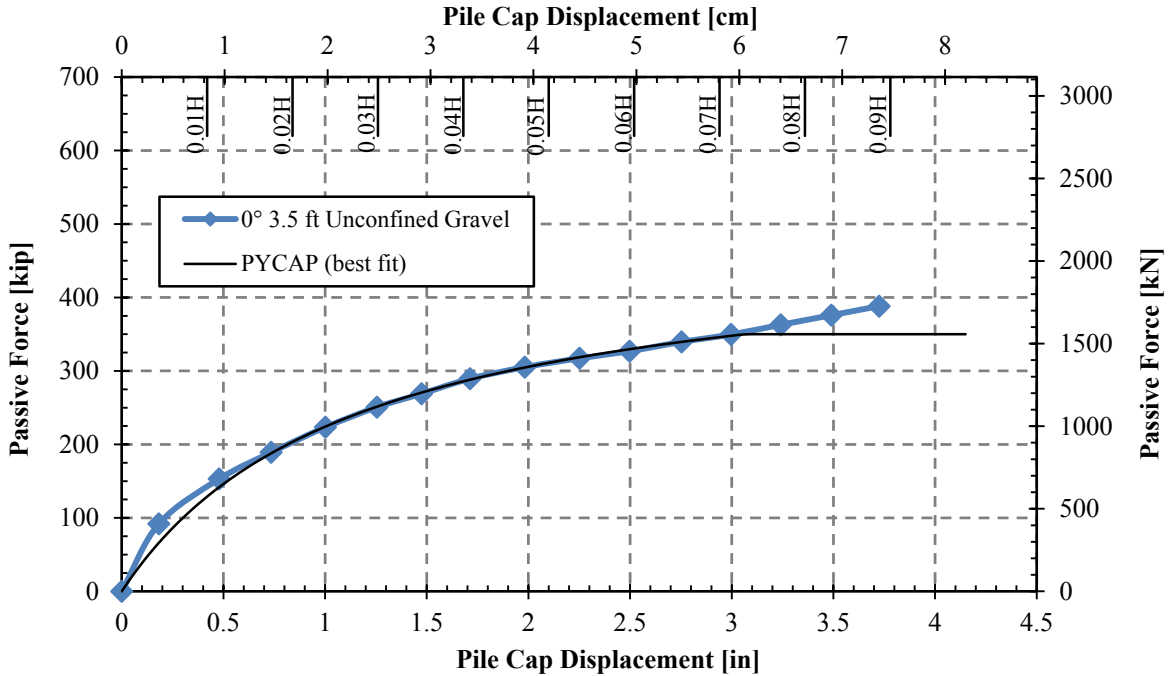
Figure 4-12. Best fit PYCAP hyperbola using 0° skew 3.5 ft (1.07 m) unconfined gravel parameters, limited to 0.073H to develop peak displacement, compared to 0° skew passive force-deflection data up to 3.75 in (9.5 cm) displacement.
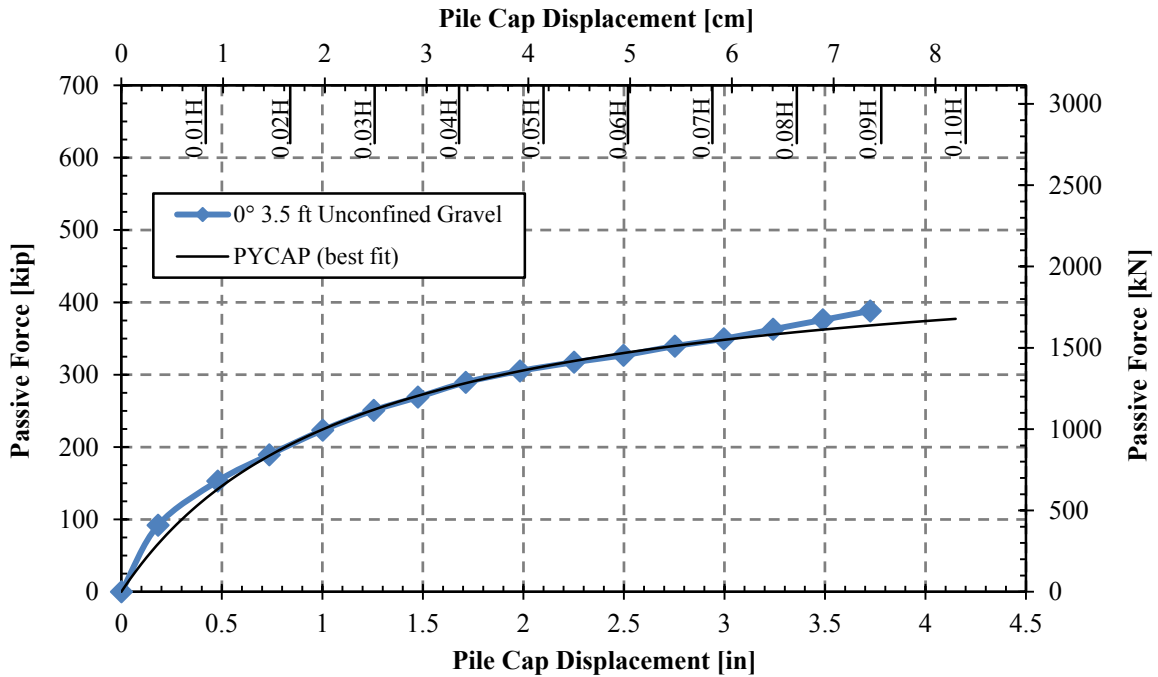
Figure 4-13. PYCAP best fit hyperbola using 0° skew 3.5 ft (1.07 m) unconfined gravel parameters, assuming 0.010H to develop peak displacement and adjusting wall interface friction angle, compared to 0° skew passive force-deflection data up to 3.75 in (9.5 cm) displacement.

97

Figure 4-14 plots the passive force reduction factor versus skew angle for the lab tests conducted by Rollins and Jessee (2013), the numerical models reported by Shamsabadi et al. (2006), and the results of this study with gravel backfill. If the peak values for the 0° and 30° skew tests are used, as has been done in previous tests, a reduction factor of 58% is obtained when comparing the 30° skew test to the 0° skew test at 3.0-in (7.6-cm) displacement. However, due to the actuators overloading in the 30° test and to baseline uncertainty for the 0° test, though both tests appear to be nearing their peak, neither had developed peak passive force. Particularly, because the 30° skew test at 5.5 ft (1.68 m) fill was only pushed 2.5 in (6.4 cm) into the backfill, it is more likely that the peak for that test had not been developed, which would result in a higher reduction factor than shown by the current data. Based on the shapes of the curves, the two tests do not appear to be peaking at the same displacements, but if, for example, the reduction is taken at 1.5 in (3.8 cm) instead of at the available measured peaks, the reduction factor would be higher, at 73%. However, the reduction factor equation was designed from peak passive force values, so 58% is believed to be the most reasonable estimate based on the measured data. As shown, Equation (1-1) predicts that at the 30° skew angle the passive force reduction factor to be about 53% when compared to the 0° skew case in gravel. These results suggest that the force reduction factor equation is generally applicable for gravel but may require some fine tuning because of increased stiffness and friction angle in gravel backfill compared to sand backfill.
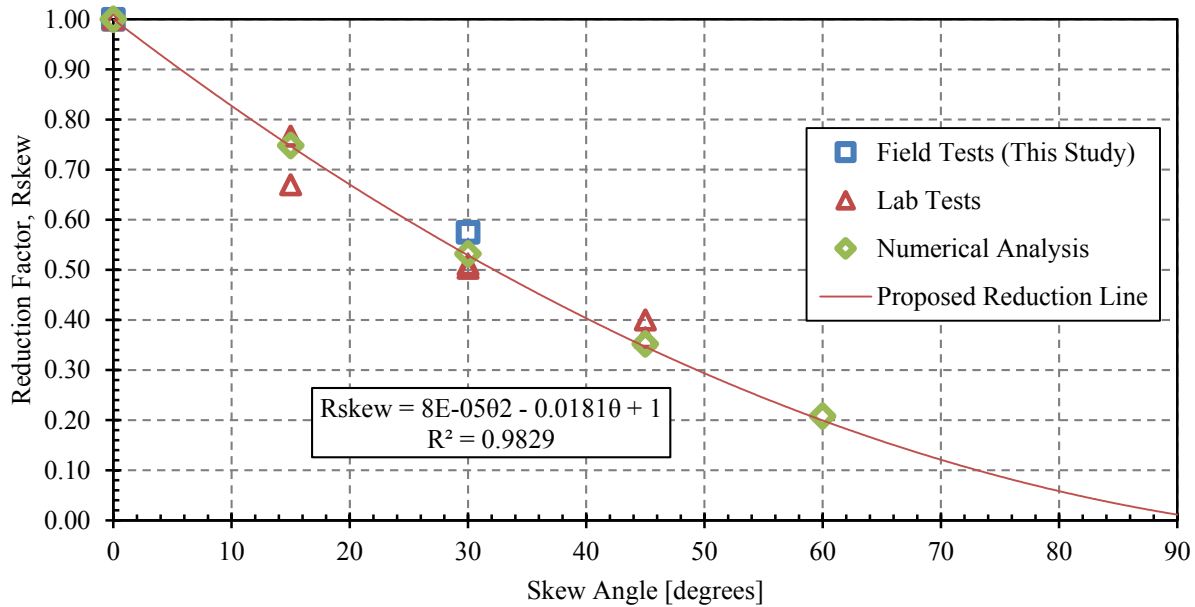
Figure 4-14. Reduction factor, R_{skew} (passive force for a given skew angle normalized by passive force with no skew) plotted versus skew angle based on lab tests (Rollins and Jessee 2013), numerical analyses (Shamsabadi et al. 2006) and results from field tests in this study.

4.1.5 Cyclic Loading

Figure 4-15 demonstrates the total force versus deflection behavior of the 30° skew 5.5 ft (1.68 m) gravel test under 21 oscillations of cyclic loading. Included in the figure is the initial total loading for the first two 0.25-in (6.35-mm) increments of the test prior to the commencement of the cyclic loading. Figure 4-15 shows total force since no baseline was recorded for pile cap movements in the negative direction, or away from the backfill. The cycles are differentiated by color as noted.

In Figure 4-15, the soil stiffness decreased dramatically in the first cycle, as was also seen in Smith (2014). This reduction is likely due to the formation of a gap between the backfill gravel and the pile cap. The gravel had sufficient apparent cohesion to maintain a small gap during cyclic loading. The gap leads to a concave upward force-deflection curve shape rather than the typical concave downward shape typical of initial loading. Following each of the second

and third cycles, there were additional noticeable, though less dramatic, decreases in stiffness. After the third cycle the stiffness remained rather consistent.
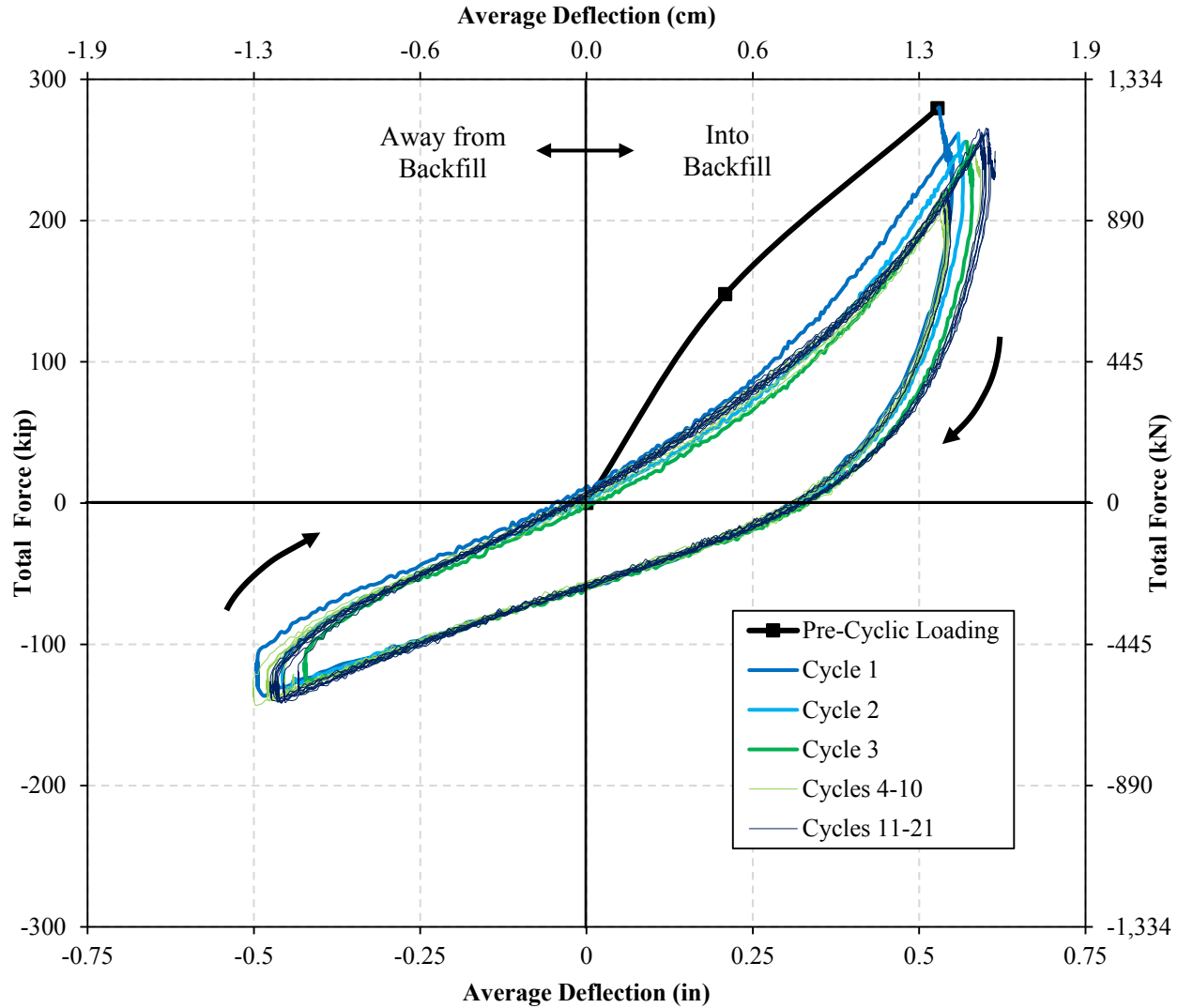
Figure 4-15. Total force-deflection of cyclic loading during 30° skew 5.5 ft (1.68 m) gravel backfill test.

Figure 4-16 shows the calculated, scaled cyclic passive force in the positive direction (into the fill) in relation to the scaled peak passive values from the longitudinal loading of the 30° 5.5 ft (1.68 m) skew test. The figure confirms that decreased stiffness from the cyclic loading resulted in the irregularity in the passive curve between the scaled 0.34 and 0.45 in (0.9 and 1.9

100

cm) increments. Apparently, the relatively small incremental displacement 0.11 in (0.3 cm) was insufficient to bring the passive force-deflection curve back to the virgin loading curve. At greater displacements the virgin curve was again reached and the curve shape appears consistent from this point onward.
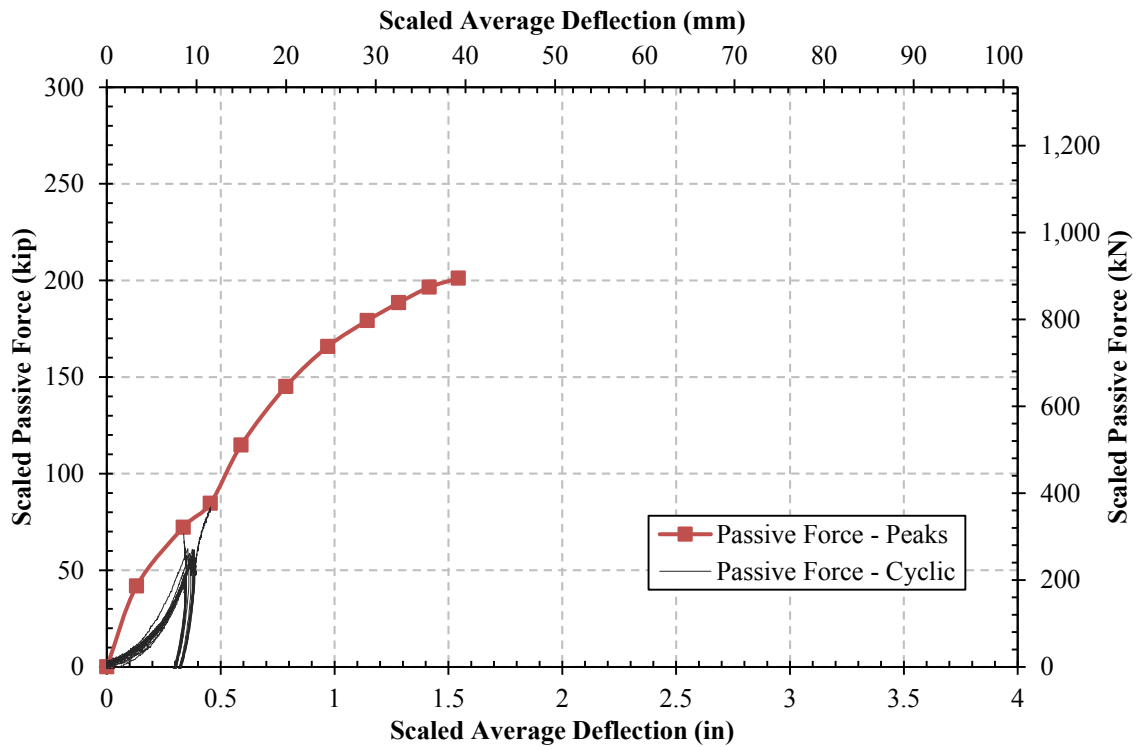
Figure 4-16. Scaled passive force-deflection 30° skew 3.5 ft gravel test including positive-direction cyclic loading data.

4.1.6   Transverse Effects

Force-deflection baseline curves were measured from the side push tests described in Subsection 3.3.5 and are plotted in Figure 4-17. These tests measured transverse resistance against small transverse movement for the skewed test configuration. In the plot, "North Piles" plots the average deflection of the north string pots versus the north actuator loads and "South Piles" likewise plots the average deflection of the south string pots versus the south actuator loads. The actual load-deflection curves for each set of piles is probably the same; the difference

101

between the plotted resistances of the two pile groups is likely due to the frictional resistance of the wedge. This plot shown is for the 45° skew side push. Accounting for transverse resistance may increase or decrease the passive force calculated by Burke Jr's (1994) equations (see Subsection 2.4.3.1), which do not take transverse abutment resistance into account. Preliminary investigation suggested that the passive force reduction factor increases slightly when transverse movements and resistances are taken into account. Future studies will need to calibrate these baseline curves to investigate further the effects of the transverse movements and rotations observed in these skewed abutment tests.

Figure 4-17. Raw baseline force-deflection curves from transverse loading tests (Smith, 2014).

4.2 Pile Cap Movement

Pile cap movement was monitored in both the longitudinal and transverse directions. As described in Section 3.4, longitudinal movement was measured throughout testing using four string pots on the front wall of the pile cap, one on each corner. The average of these four string

102

pots was the displacement value used for each data point in all the total and passive force-deflection curves shown in Section 4.1. Additionally, an inclinometer and two shape accelerometer arrays (SAAs) measured both longitudinal and transverse displacements. This section describes the pile cap movement data gathered from these three methods of measurement.

4.2.1   Longitudinal Movement

Figure 4-18 and Figure 4-19 provide longitudinal deflection versus depth profiles obtained from string pots, inclinometer, and shape array in the central pile of the north pile group for the 0º and 30° skew tests, respectively. Figure 4-19 excludes the inclinometer reading for the 30° test due to the actuator overheating and releasing its load and deflection before a reading could be taken. Both profiles represent pile cap behavior for the final longitudinal displacement of the test. Depths are referenced to the top of the cap. Figure 4-18 demonstrates that the measurements for the three systems are reasonably accurate and aligned with each other. For example, the percent difference between the inclinometer and shape array profiles for the non-skewed test from the top of the cap to a depth of 16 ft (4.9 m) ranges between 0.03% and 13% with an average of median of approximately 5%. For displacements located below a depth of 16 ft (4.9 m) the percent error increases but is not particularly meaningful because the displacements are very small

The measurements indicate a relatively linear deflection profile within the pile cap and small cap rotations. Below the base of the cap, the piles deflect in a non-linear fashion with the deflections reaching a point of counterflexure at depth of approximately 22 ft (6.7 m) and a point of fixity at about 30 ft (9.1 m). Agreement between the north and south inclinometers was generally very good.

103
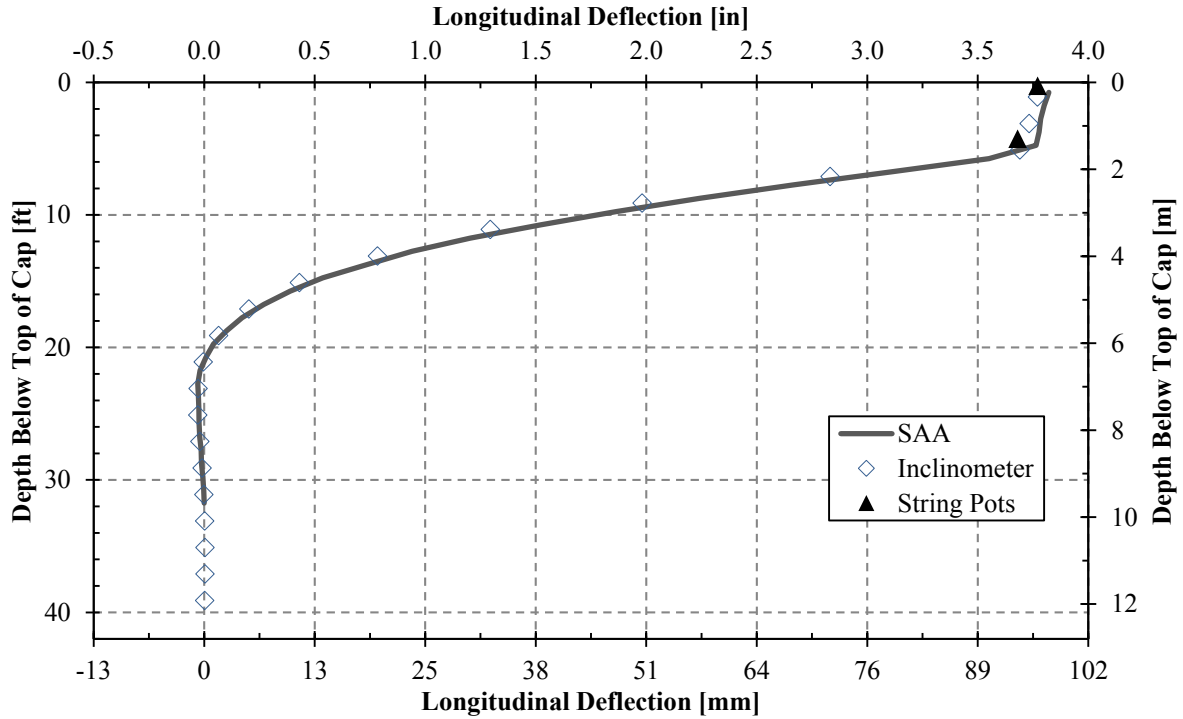
Figure 4-18. North 3.5-ft gravel backfill 0° skew final deflection comparing inclinometer, shape array, and string pots.
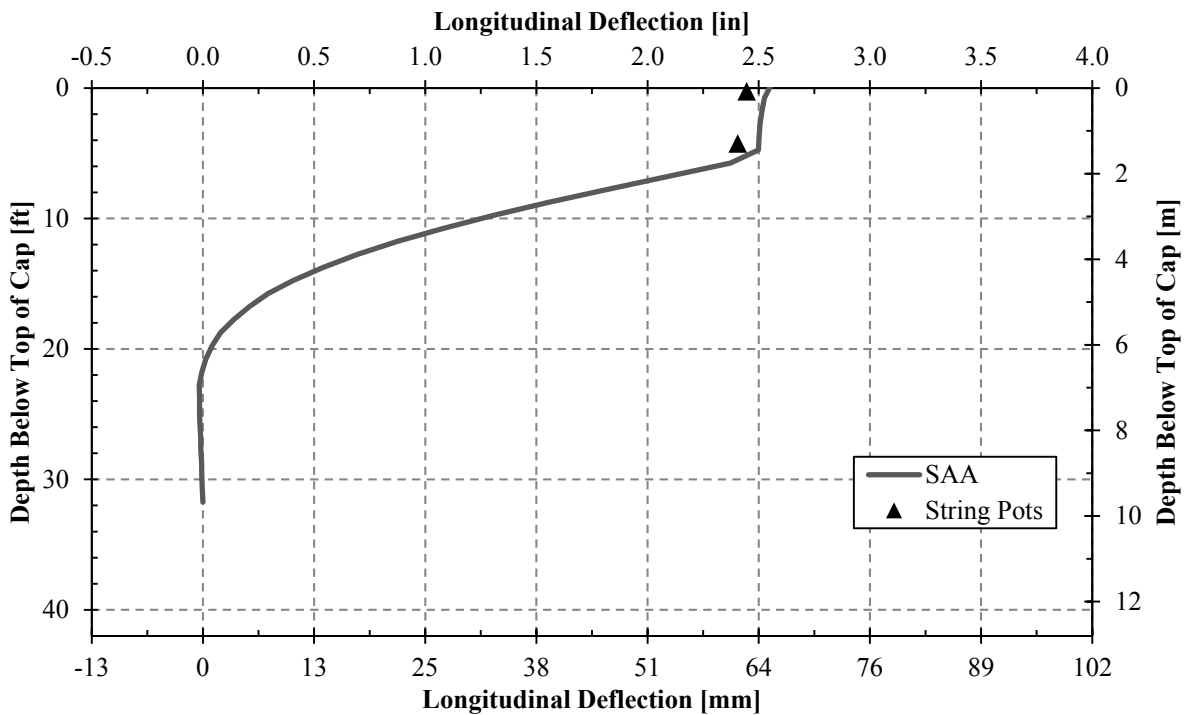
Figure 4-19. North 5.5-ft gravel backfill 30° skew final deflection comparing shape array and string pots.

Although the inclinometer readings were only taken at the maximum deflection for each load test, shape array profiles in the longitudinal and transverse directions were obtained at each deflection increment for each test. Figure 4-20 and Figure 4-21 show profiles of longitudinal deflection vs. depth for each deflection increment for each of the two tests. As the deflection level increases, the deflection of the pile cap remains linear, the rotation progressively increases, and the depth to the point of fixity increases. At smaller deflection levels there are some variations associated with the small measurement errors; however at larger deflections, the data was accurate and useful in visualizing the pile movement. The small variation in the 30° test (Figure 4-21) between the shape array and string pot data at some increments is likely an effect from missing the inclinometer reading from this test as previously discussed. An inclinometer reading is necessary to calibrate the rotational orientation of the shape array data most accurately.
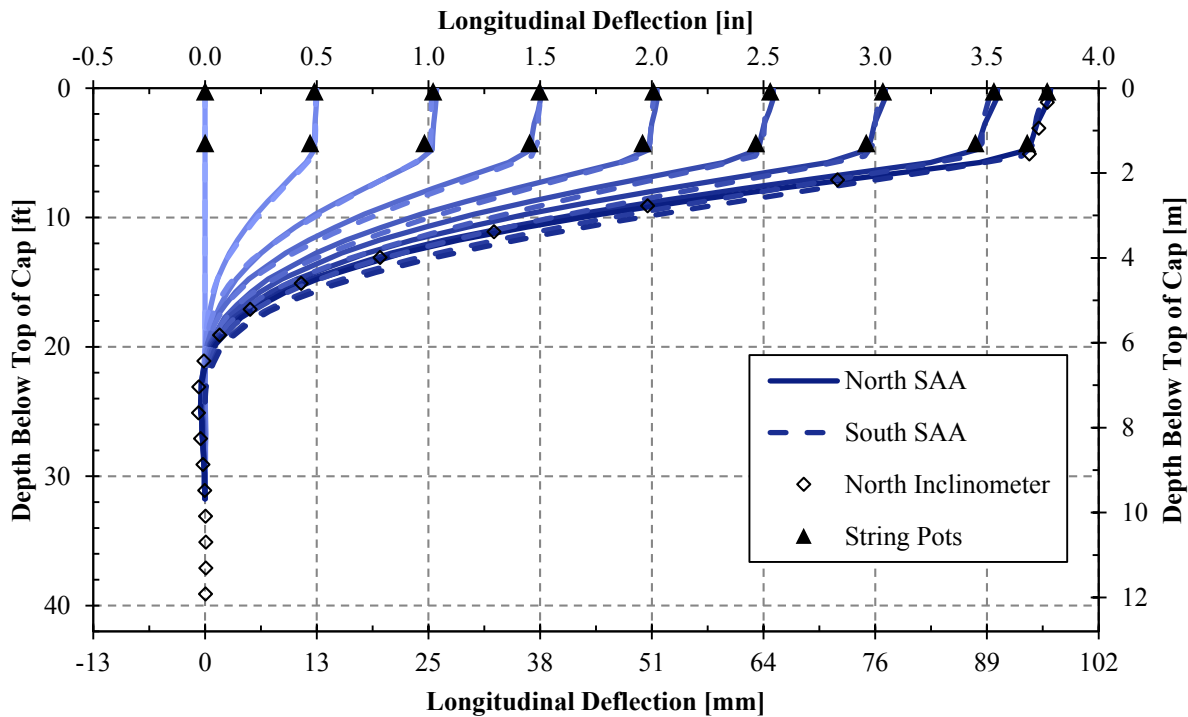
Figure 4-20. Longitudinal deflection vs. depth curves for 0° skew 3.5 ft gravel test from string pot and SAA data at various deflection increments and the final north inclinometer reading.
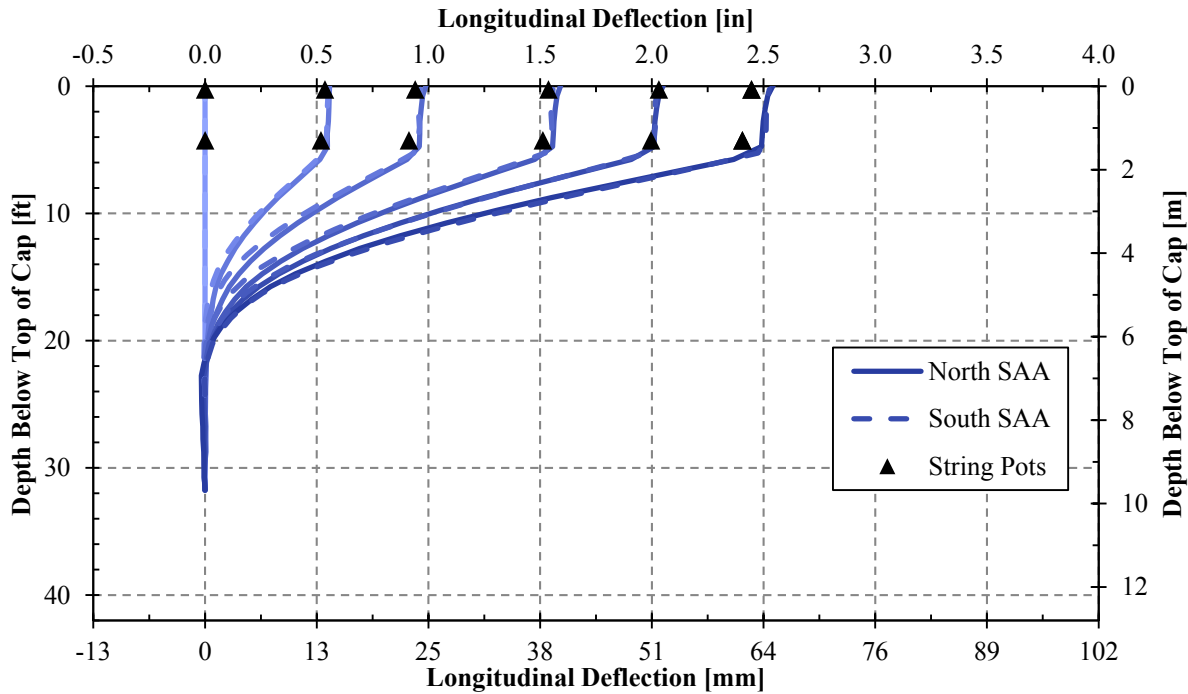
Figure 4-21. Longitudinal deflection vs. depth curves for 30° skew 5.5 ft gravel test from string pot and SAA data at various deflection increments.

4.2.2 Transverse Movement and Rotation

Although deflections of both actuators were kept relatively constant throughout the test, rotation and transverse deflection were still affected by the skew angle. Transverse deflection versus depth profiles for the pile cap, recorded by shape array and inclinometer, are plotted in Figure 4-22 and Figure 4-23. Plotted on a smaller scale, the percent error between the instruments seems larger than the longitudinal error though the magnitude difference is very small. As observed for the deflections below 16 ft (4.9 m) in the longitudinal test, the percent difference in agreement is exaggerated due to the smaller displacements. The difference is within the error thresholds of each instrument (±1.5 mm/30 m for shape array and ±1.24 mm/30m for inclinometer) (Rollins et al. 2009). Once again, the shape of the deflection profile indicates essentially linear deflection in the pile cap and very small rotations. The deflection in the piles is non-linear and decreases to zero at a deflection of about 30 ft (9.1 m).

106
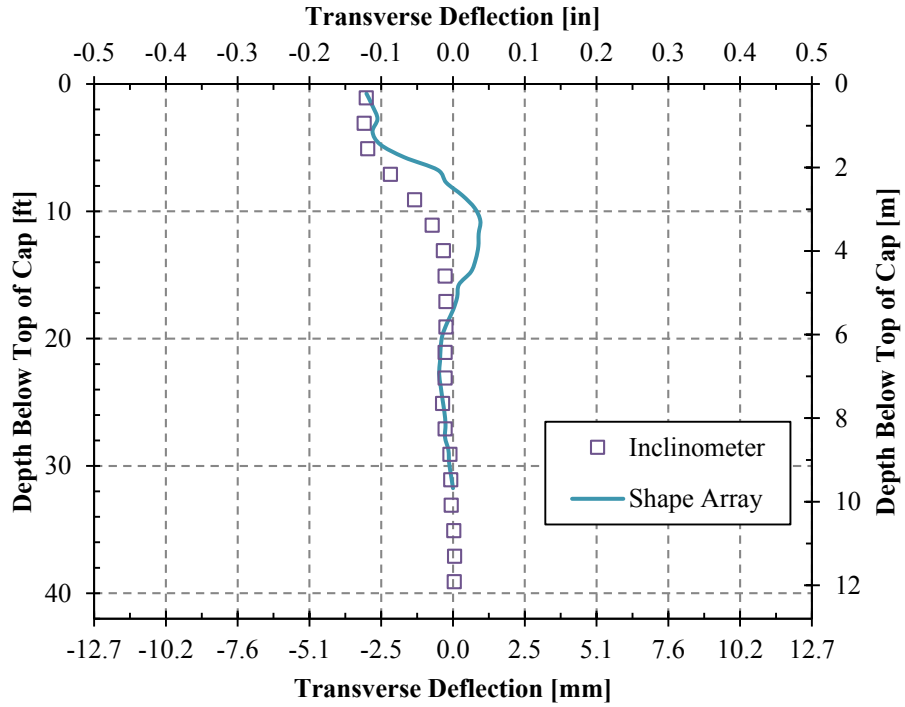
Figure 4-22. North 3.5-ft gravel backfill 0° skew final transverse deflections with depth, comparing inclinometer and shape array.
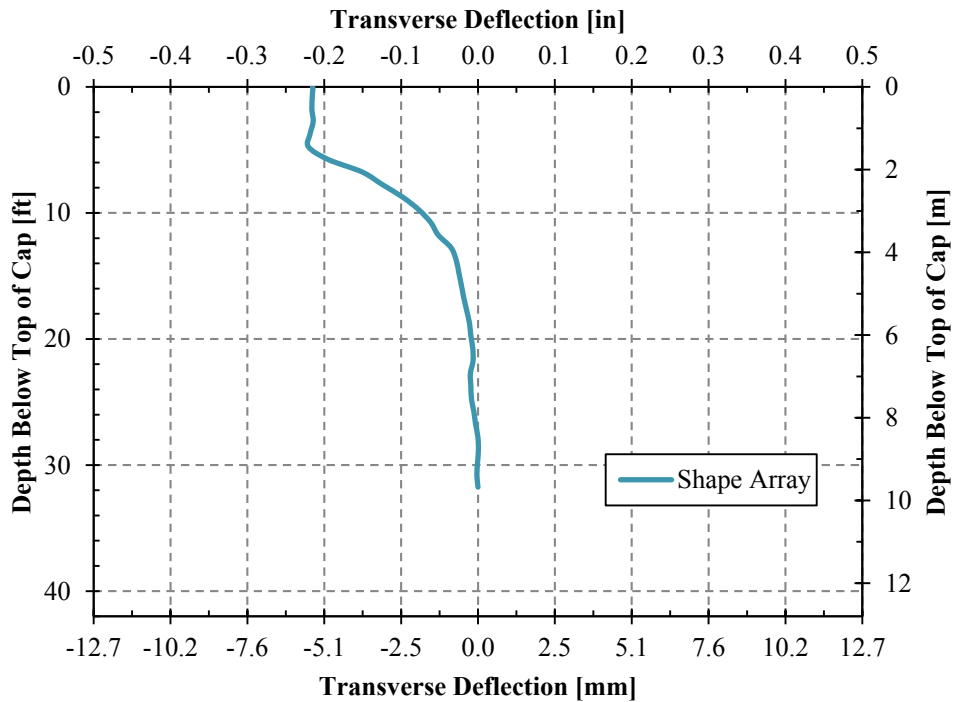
Figure 4-23. North 5.5-ft gravel backfill 30° skew final transverse deflections with depth using shape array measurements.

107

The final north and south measured transverse deflections for each test at the surface of the pile cap, as measured by inclinometer and shape arrays, are plotted in Figure 4-24 from a plan view perspective. The transverse deflection is again exaggerated compared to the length of the pile cap, which also exaggerates the angles of rotation, but the plot allows for a comparison of deflection and rotation between the two tests. As seen in Figure 4-24, the pile cap ultimately shifted to the west (in the direction of the acute skew corner) for both the 0° and 30° skew tests by approximately 0.09 and 0.15 in (0.22 and 0.38 cm), respectively, and rotated in a counterclockwise direction approximately 0.02° and 0.05°, respectively. At 5.5 ft (1.68 m), the backfill height of the skewed test was 57% greater than the non-skewed test, but its final longitudinal displacement was only 67% of that of the non-skewed test. Still, the skewed test had noticeably greater drift to the west. The transverse movement of the 0° test may be attributed to the number of skewed tests performed on the piles that have likely weakened the resistance to pile movement to the west as the cap is pushed north.

As the actuator loading progressed and the pile cap was pushed north into the backfill, movements in the cap to the east and west were detected with the shape arrays at each loading increment. The development of pile cap displacement as the test took place is shown in plan view for each of the 0° and 30° skew tests in Figure 4-25 and Figure 4-26, respectively. Like Figure 4-24, the figures were created with shape array data from the point closest to the surface of the pile cap.
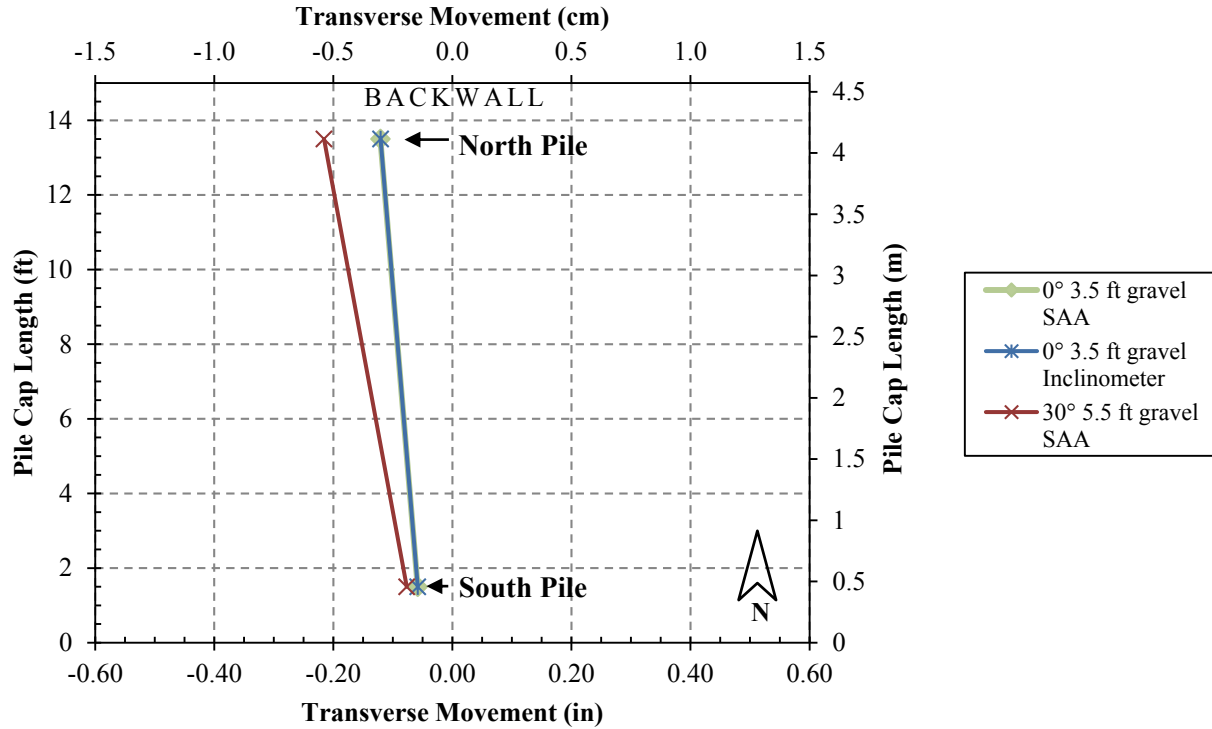
Figure 4-24. Transverse pile cap deflection and rotation at the end of both gravel tests, as determined by north and south shape array and inclinometer data.

In the non-skewed test in Figure 4-25, the pile cap stayed relatively straight, with small-magnitude drifts back and forth east and west on the south end. However, the north pile stayed mostly true to center, and the end transverse movement was still very small on both ends, averaging approximately 0.09 in (0.22 cm) to the west, as stated before. The 30° test, shown in Figure 4-26, had greater transverse deflections, averaging 0.15 in (0.38 cm) deflection to the west, which was toward the acute corner of the skew, by the end of the test. Though the 0.75 in (1.9) data point was omitted in the graph due to the slow process of processing the shape array data, the shift to the east that occurred due to the cyclic loading is still visible between the 0.5 and 1.0 in (1.9 and 2.5) longitudinal displacements. After the first inch (2.5 cm), the deflection to the west became more pronounced, particularly in the north pile, so that a small rotation of 0.05° developed as discussed earlier.

109
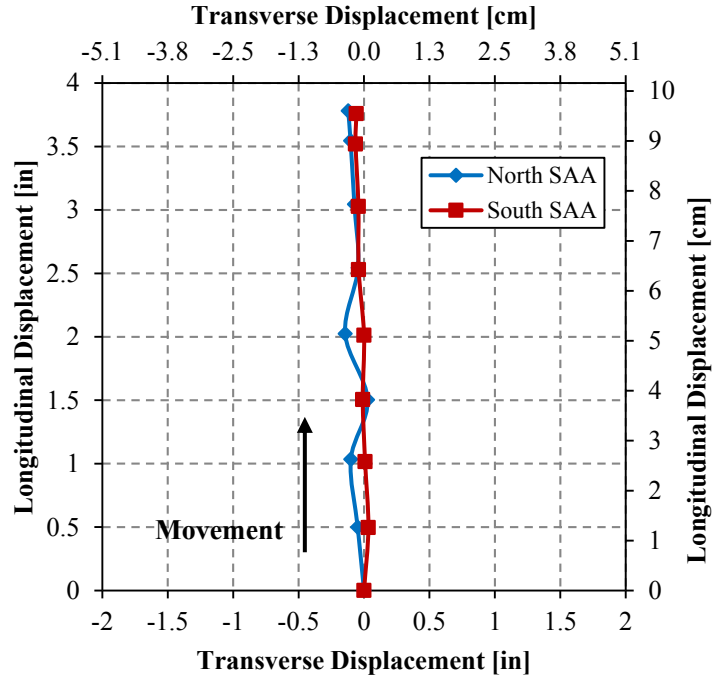
Figure 4-25. Longitudinal and transverse displacements of pile cap in plan view over the course of the non- skewed unconfined gravel test, as determined by north and south shape array data.
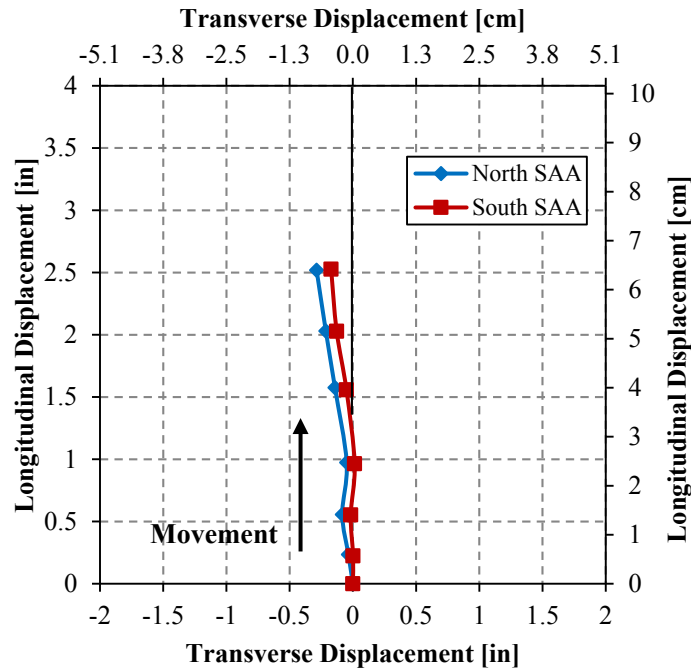
Figure 4-26. Longitudinal and transverse displacements of pile cap in plan view over the course of the 30° skewed unconfined gravel test, as determined by north and south shape array data.

110

4.3 Applied Shear Force vs. Transverse Displacement

The relationship between the applied shear force (P_T) and transverse displacement is plotted in Figure 4-27 for the 30º skew test. The applied shear force was scaled by substituting Equation (2-12) into Equation (2-13) to create Equation (4-4).

$$P_T = P_P \tan \theta \qquad\qquad\qquad (4\text{-}4)$$

Transverse displacements were also scaled; data was scaled by height as done for the longitudinal displacements as described in Equation (4-3). Original transverse displacement values were based on measurements recorded from the north shape array during testing. Maximum shear force was 114 kip (507 kN) and occurred at the maximum displacement for the test, which was approximately 1.5 in (3.8 cm) longitudinal scaled displacement.

As mentioned previously, the unusual decrease in transverse displacement is due to the cyclic loading performed at 0.5 inch (1.27 cm) longitudinal displacement (0.05 in [0.13 cm] transverse displacement and 38 kip [169 kN] shear force). When shape array measurements were resumed at 0.75 inch (1.9 cm) longitudinal displacement, transverse displacement had shifted some to the positive direction, the east. The 0.75 in (1.9 cm) point was omitted for this plot, instead the shift is visible at the 1.0 in (2.5 cm) point (0.03 in [0.08 cm] transverse displacement and 63 kip [280 kN] shear force). The data showed a consistent shear force-displacement curve despite the shift from the cyclic loading and appeared to be approaching a peak when testing finished, similar to the passive force for this test. A comparison between this test and the GRS 30° skew test will be included, along with calculated shear resistances for both tests, in Subsection 6.1.2.

111
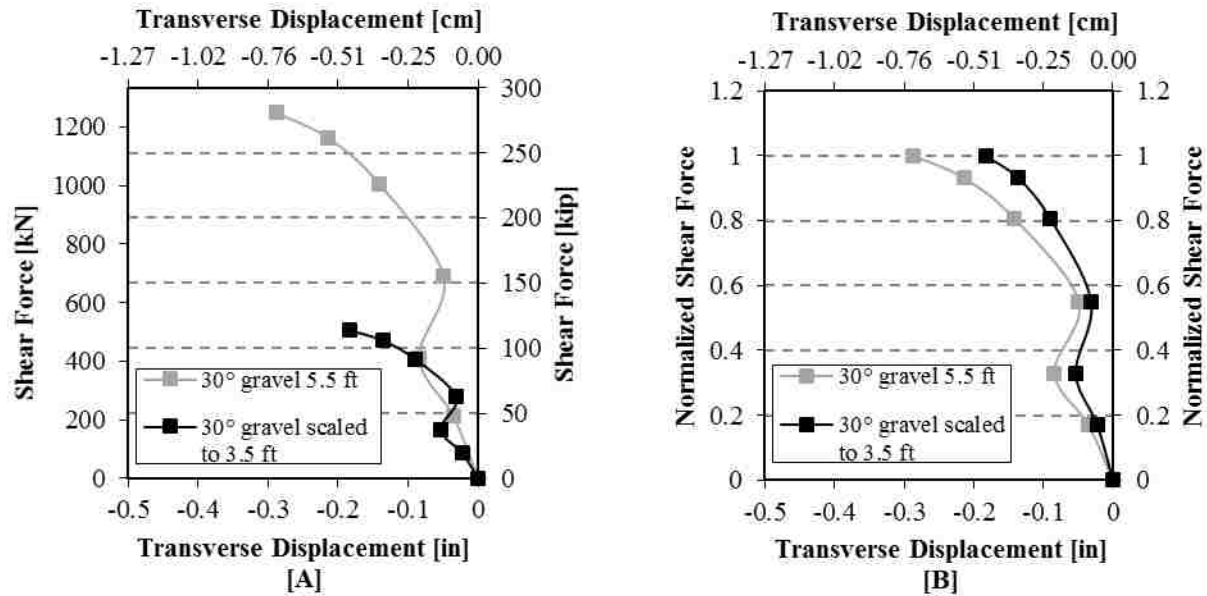
Figure 4-27. For the 30° skew gravel data scaled for 3.5 ft (1.07 m) fill: [A] Applied shear force vs. transverse displacement; [B] Normalized applied shear force vs. transverse displacement.

4.4 Backfill Response/Failure Surface Geometry

The displacements in all the tests of this study were of such magnitude that plastic deformations in the backfill were detectable through surface cracks and soil heave. A failed soil mass will have both surface cracks and vertical heave in the approximate shape of a "bulb" behind the backwall. Because neither gravel test displaced beyond the failure state, neither backfill had a completely defined failure surface. Experience in previous tests indicates that failure surfaces do not generally manifest themselves at the surface until the displacement clearly exceeds that required for peak resistance or when there is a decrease in passive force toward a residual value. Surface cracks were spray painted in the soil as they occurred during testing and vertical displacements, or heave, was measured by the level and total station before and after testing. The total station also measured lateral displacements in the backfill, as did string pots. A photo from the 0° gravel test is shown in Figure 4-28. Unfortunately, no photo was taken at the

112

end of the 30° gravel test. This section describes the lateral and vertical displacements of the backfill due to the pile cap loading.

Figure 4-28. Backfill surface at end of non-skewed 3.5 ft (1.07 m) gravel test, viewed from the east side.

4.4.1 Vertical Heave and Failure Surface Geometry

Backfill heave contours and surface cracks for the non-skewed and 30° skewed tests are illustrated in Figure 4-29 and Figure 4-30. Surface cracks for the non-skewed test were pictured earlier in Figure 4-28. Heave contours for the non-skewed abutment were generally symmetrical with maximum heave of 4.4 in (11.2 cm) occurring 2 ft (0.6 m) from the backwall near the abutment edges. In contrast, the maximum heave from the 3 ft (0.9 m) sand tests was about 2 in (5.1 cm) for the 0°, 15°, and 30° tests (Palmer, 2012) for 3.25 to 3.5 in (8.3 to 8.9 cm) longitudinal displacement and about 2.5 in (6.4 cm) for the 45° skew test at 3.75 in (9.5 cm)

longitudinal displacement. In previous tests where the failure surface was fully mobilize the surface was often associated with heaves in the 0.5 to 0.75 in (1.3 to 1.9 cm) range. For the non-skewed case this would indicate that the failure surface would ultimately develop at a distance of around 10 ft from the backwall. Cracking and heaving extended to about 10 to 12 ft (3.1 to 3.7 m) back from the pile cap; some cracks developed as far as 14 ft (4.3 m). Effective width was about 19 ft (5.8 m).

As visible in the photo of the failure surface in Figure 4-28, longitudinal cracks developed at each of the string pot stakes at 6, 8, 10, and 12 ft (1.8, 2.4, 3.1, and 3.7 m) from the pile cap. The magnitude of these cracks decreased as the distance from the pile cap increased. It is possible that driving the stakes may have caused stress concentrations that led to localized crack formation. If so, this likely explains the smaller cracks at 10 and 12 ft (3.1 and 3.7 m), and could have also initiated the transverse cracks seen at 6 and 8 ft (1.8 and 2.4 m).

As shown in Figure 4-30, considerably less heave occurred and far fewer surface cracks were observed in the 5.5 ft (1.68 m) backfill for the 30° skewed test compared to the 3.5 ft (1.07 m) backfill for the non-skewed test, likely due to the increased resistance of the greater backfill height. Additionally, the 30° test was only pushed to approximately 2.5 in (6.4 cm), which is only 67% of the 3.75 in (9.5 cm) displacement in the 0° test. Maximum heave of approximately 0.5 in (1.3 cm) was observed near the acute side of the abutment 4 to 6 ft (1.2 to 1.8 m) behind the backwall. In contrast to the symmetrical heave and crack pattern observed for the non-skewed test, the heave pattern for the 30° skew test was asymmetric with greater heave concentrated near the acute corner of the cap. Shear cracks near the acute corner began tangent with backwall while shear cracks at the obtuse corner were normal to the backwall. Effective width appears to have been about 18 ft (5.5 m).

114
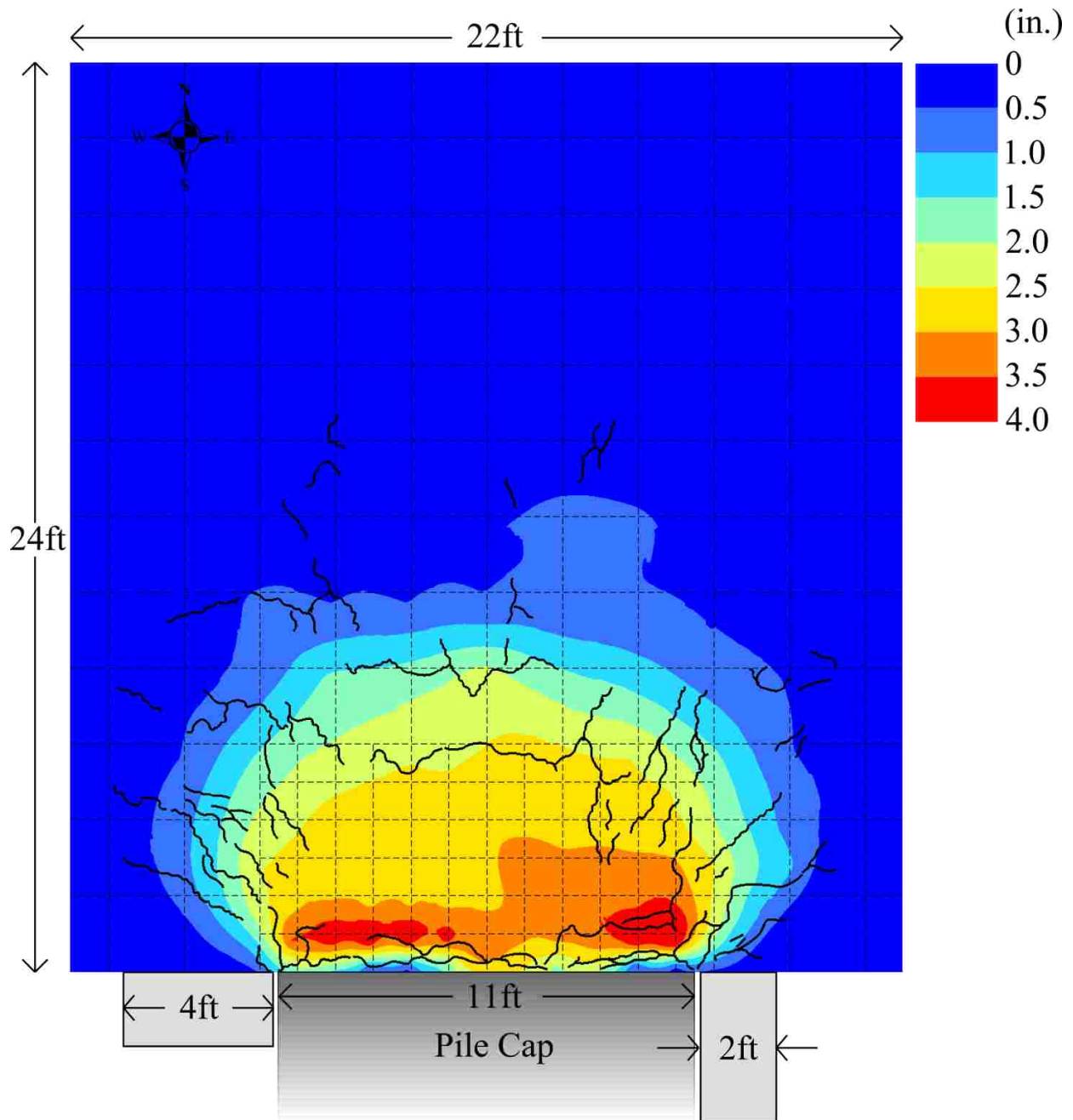
Figure 4-29. Vertical heave contours and surface cracks at 3.75 in (9.5 cm) of longitudinal displacement (test completion) for 3.5 ft (1.07 m) 0° skew gravel test (NOTE: 1 in = 2.54 cm; 2 ft [0.6 m] grid is refined to a 1 ft [0.3 m] grid in the 6 ft [1.8 m] nearest to the backwall).
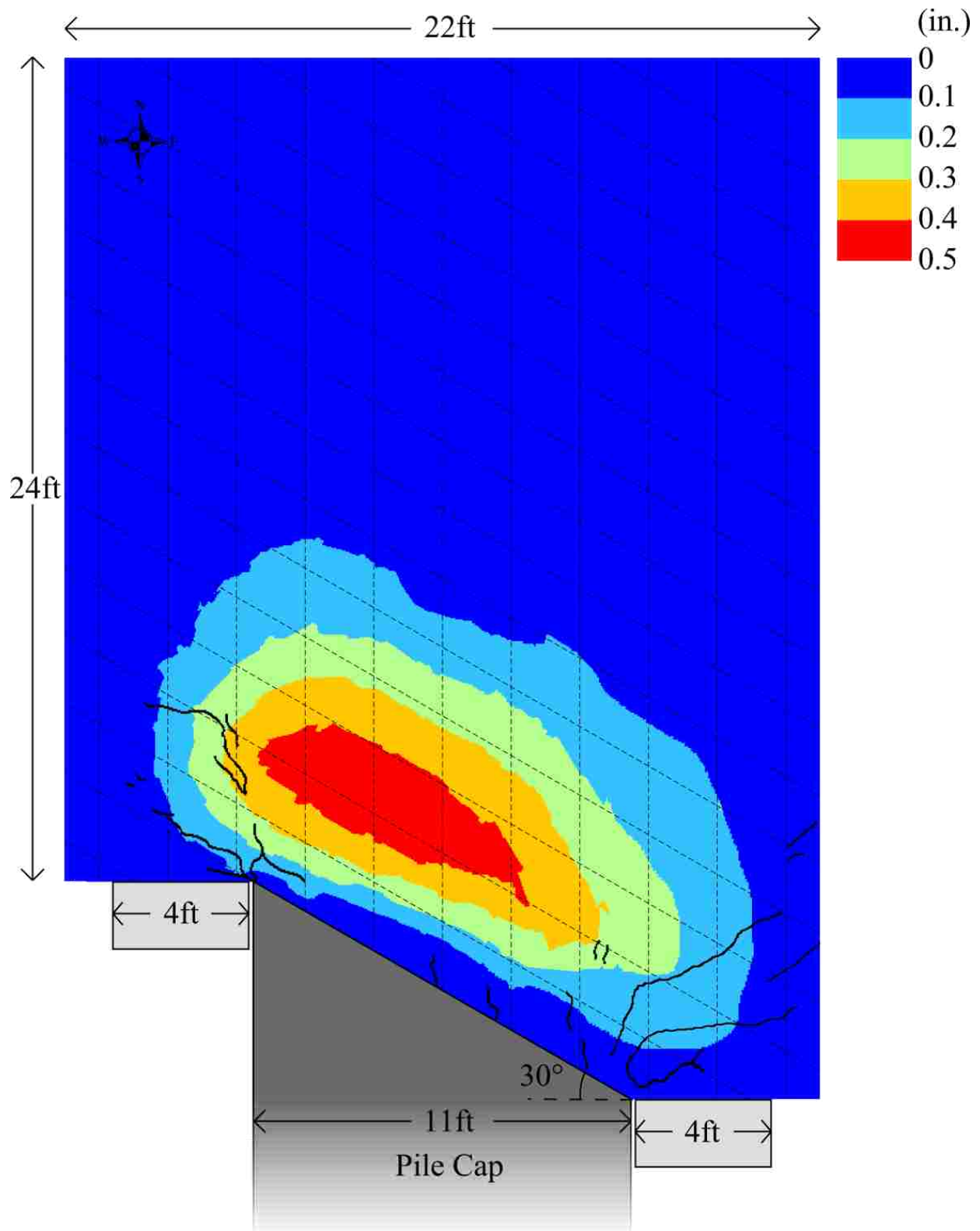
Figure 4-30. Vertical heave contours and surface cracks at 2.5 in (7.61 cm) of longitudinal displacement (test completion) for 5.5 ft (1.68 m) 30° skew gravel test (NOTE: 1 in = 2.54 cm; 2 ft [0.6 m] grid is refined to a 1 ft [0.3 m] grid in the 6 ft [1.8 m] nearest to the backwall).

4.4.2 Lateral Displacement and Strain

Horizontal backfill displacements for the 0° and 30° skew abutments from total station data are illustrated in Figure 4-31 and Figure 4-32. Displacement vectors for the non-skewed test demonstrate generally longitudinal movement in the backfill with an outward component behind the edges of the backwall. This agrees with the non-skewed backfill movement with wingwalls described by Smith (2014). In contrast, the displacement vectors for the 30º skew backfill typically show a significant transverse component toward the acute side of the pile cap. This is particularly pronounced near the face of the wall and decreases somewhat with distance from the backwall. However, the uniformity of the displacement vectors to the west does not agree with any other 30° or even 45° skew tests, including the 30° skew GRS test in this study (Section 5.3). It is believed that the total station may have been laterally bumped for this test and the significance of all the displacement vectors leaning west can be disregarded.

As described in Section 3.4, eight string potentiometers secured on or near the backwall face and attached to driven stakes in the backfill measured longitudinal displacement of the backfill soil as the test progressed. Some variability in the data cast uncertainty on a handful of data points. Possible reasons for small variations in the data include (1) a developing shear plane crossing the stake beneath the surface, causing the stake to lean either forward or backward (Franke, 2013; see Figure 4-33), or (2) the stake was not driven to a stable depth to begin with. Despite small variations observed in the data, general trends were detectable.

117
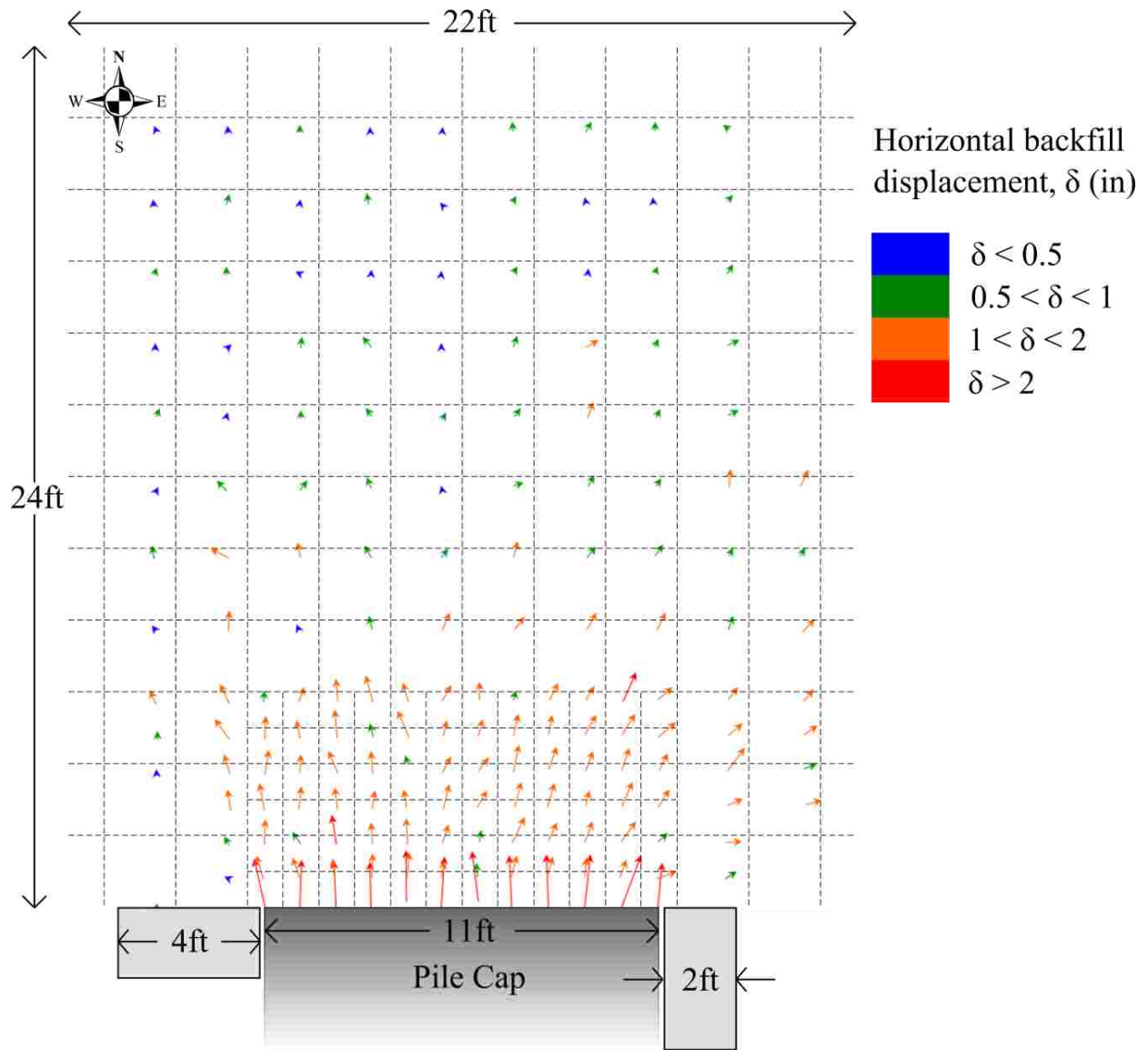
Figure 4-31. Soil displacement for 0° skew 3.5 ft (1.07 m) gravel unconfined backfill.
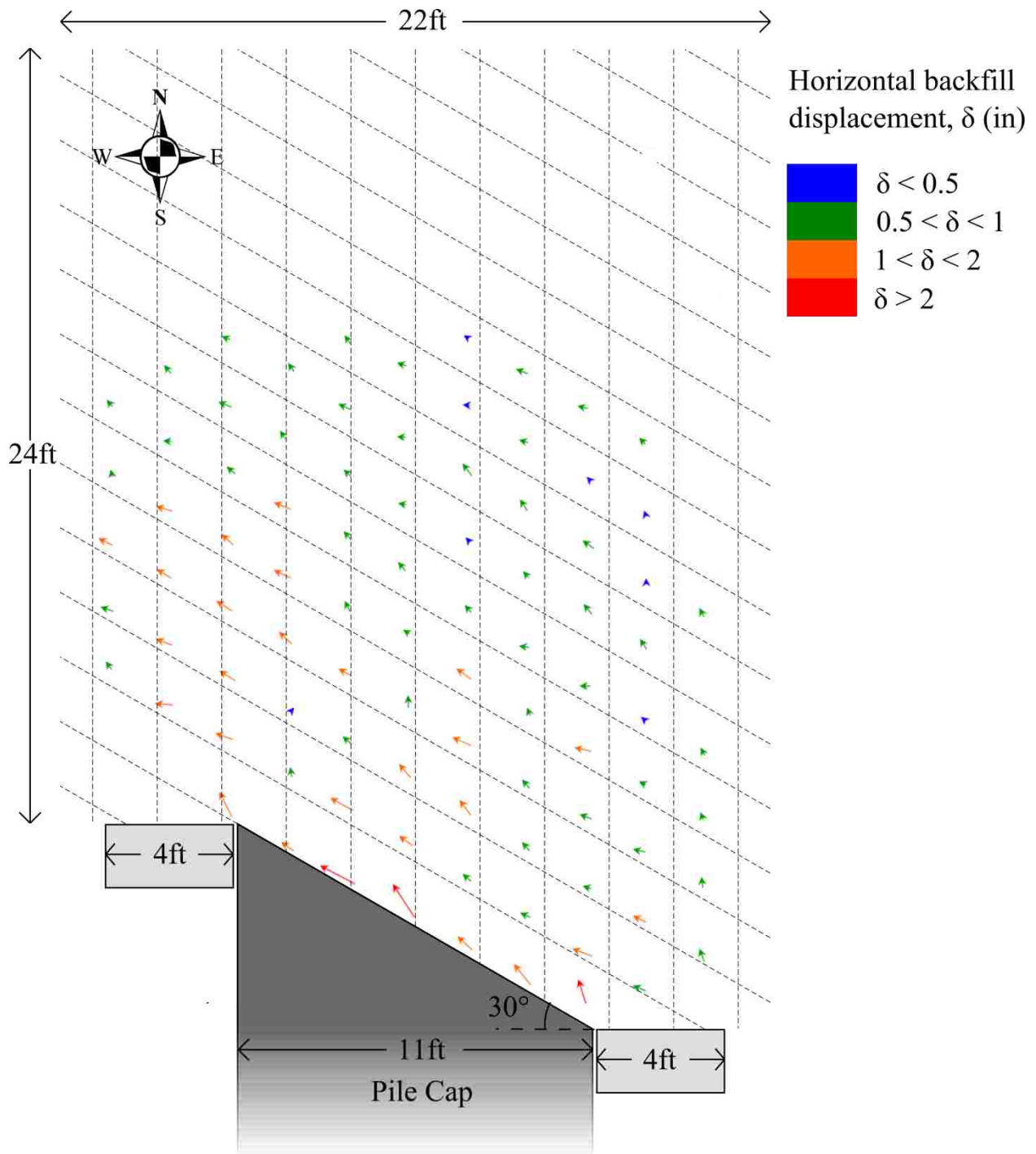
Figure 4-32. Soil displacement for 30° skew 5.5 ft. gravel unconfined backfill.

119
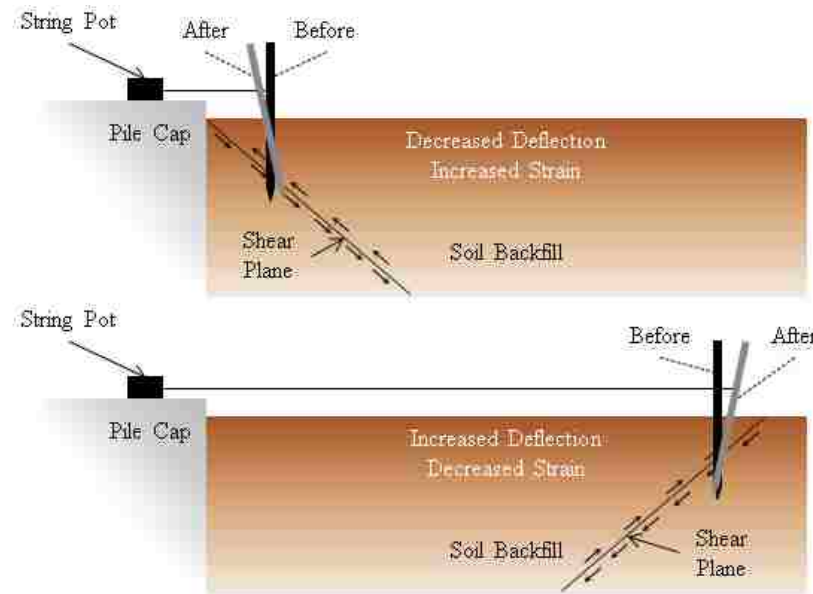
Figure 4-33. Stake-shear plane interaction with string potentiometers (Franke, 2013).

For the 0° 3.5 ft (1.07 m) test, the string pots were generally placed at close distances to determine the behavior near the pile cap. However, more string pots closer to the pile cap meant fewer string pots to place at greater distances from the pile cap. The string pots for this test only extended 12.0 ft (3.66 m) from the backwall. The 30° skew 5.5 ft (1.68 m) test, on the other hand, had fewer string pots closer to the pile cap so that the farthest string pot was 20.0 ft (6.09 m) from the backwall. Figure 4-34 and Figure 4-35 show the displacements in the backfill for the 0° skew 3.5 ft (1.07 m) and the 30° skew 5.5 ft (1.68 m) tests, respectively, at selected increments of pile cap displacement during the test. The final displacements are in bold. In general, the backfill displaced less with increased distance from the pile cap.

For the 0° 3.5 ft (1.07 m) test seen in Figure 4-34, small variability in the data is observed between 4.0 and 8.0 ft (1.22 and 2.44 m) from the backwall. However, the displacements follow the general pattern of decreasing with increased distance from the pile cap and drop after about

120

8.0 ft (2.44 m). This could suggest that a shear surface was developing somewhere between 8.0 and 10.0 ft (2.44 and 3.05 m), which could account for the artificially high displacement seen at 8.0 ft (2.44 m). Displacements drops in the 3 ft (0.91 m) unconfined sand tests were at similar distances, between 8.0 and 12.0 ft (2.44 and 3.66 m).

Perhaps coincidentally, a similar drop in displacement is seen at the same distance in the 30° skew test shown in Figure 4-35, despite the 57% increase in fill height for this test. In the 30° test, the drop in displacement at 8.0 ft (2.44 m) reverses to an increase at 16.0 ft (4.88 m) and then only drops slightly at 20.0 ft (6.10 m) distance. It is unknown whether the 0° skew had similar behavior at these distances. Whether the drop in the 30° test between 8.0 and 10.0 ft (2.44 and 3.05 m) or the rise at 16 ft (4.88 m) was the anomaly is difficult to distinguish. At 8.0 ft (2.44 m), the drop is nearer to the pile cap than in the 5.5 ft (1.68 m) unconfined sand tests, which were between 10 and 18 ft (3.05 and 5.49 m) (Marsh, 2013).

Fewer string pots closer to the cap prevented a better explanation for the drop of displacement at 2.0 ft (0.61 m). However, a drop in the data at 2.0 ft (0.61 m) occurred for 2-3 out of the three 3 ft (0.91 m) unconfined sand tests (Palmer, 2013) and was likely a case of stake-shear plane interaction with a downward shear plane.

Strain in the backfill were calculated using the backfill string potentiometer data. For example, the first string pot of the 0° skew test, placed 1 ft (0.30 m) back from the pile cap, moved 2.29 in (5.82 cm) compared to the pile cap's 3.73 in (9.47 cm) (see Figure 4-34). In other words, at the surface of the backfill, the first foot (0.30 m) closest to the pile cap compressed 1.43 in (3.63 cm), or had a compressive strain of 12%.

121
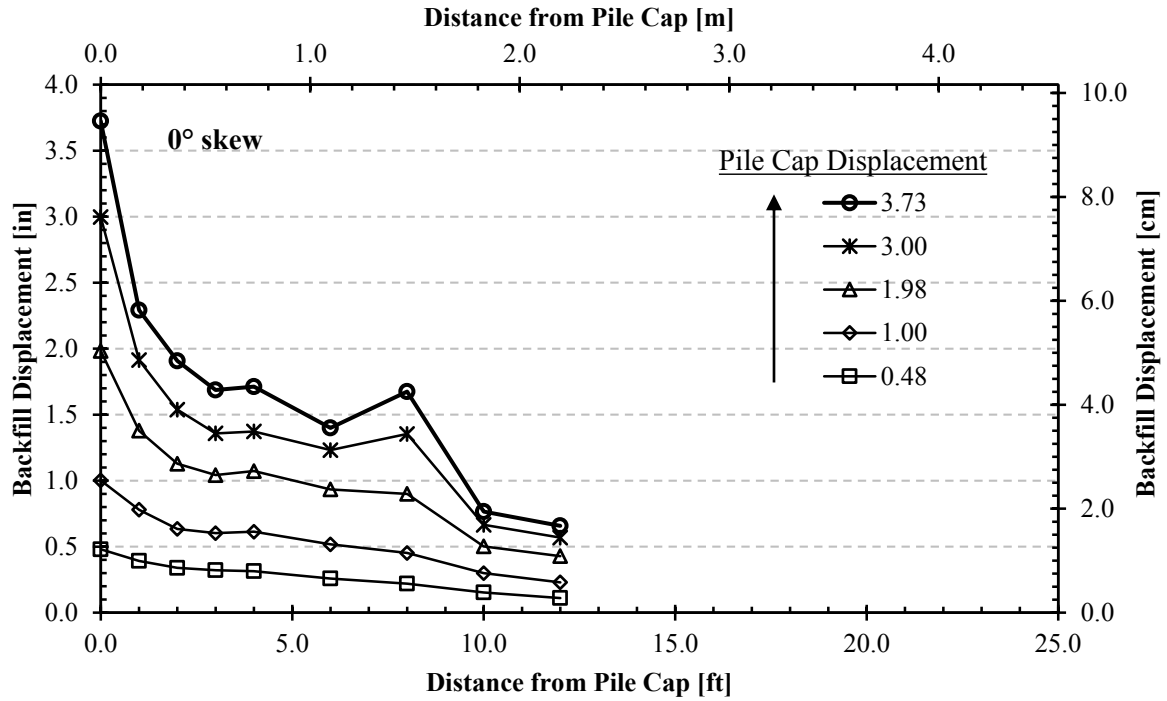
Figure 4-34. Development of displacement in the backfill of the 0° skew 3.5 ft (1.07 m) gravel test with increasing distance from the backwall face.
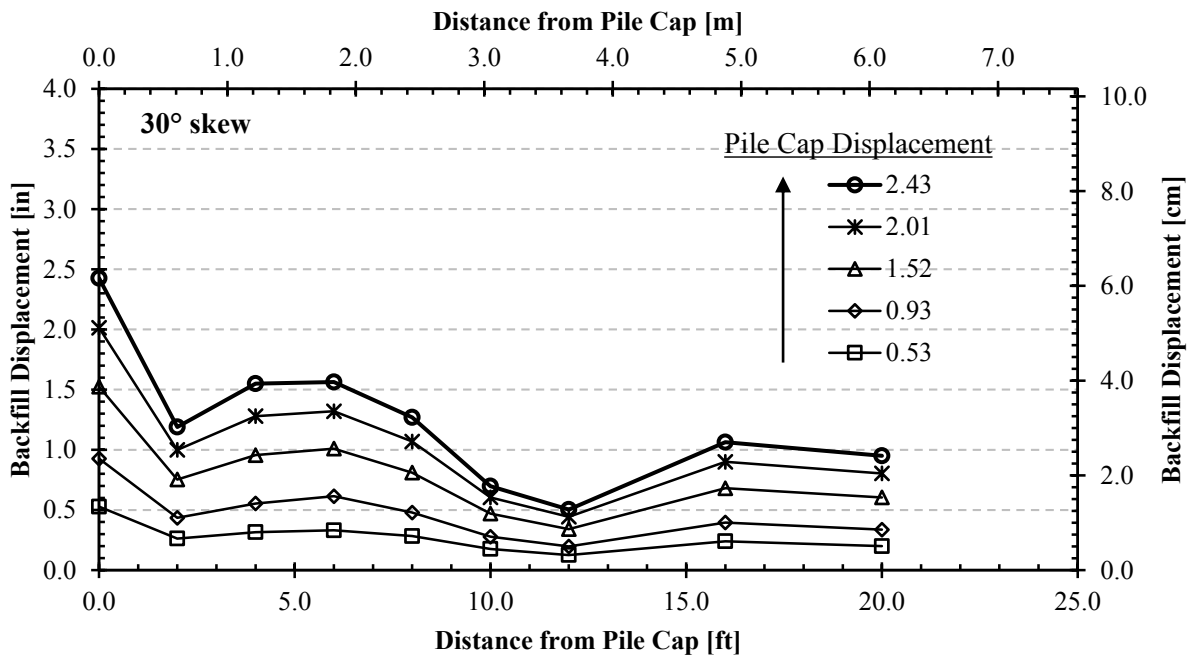
Figure 4-35. Development of displacement in the backfill of the 30° skew 5.5 ft (1.68 m) gravel test with increasing distance from the backwall face.

122

Strain for both tests is shown in Figure 4-36. The maximum strain in the first 1-2 ft (0.3-0.6 m) was the most pronounced in both tests, with 12% for the non-skewed test and 5.2 % for the 30° skew test. For the 0° skew test, the remaining strains varied from -1.1% at approximately 7 ft (2.1 m) to 3.8% at approximately 9 ft (2.7 m). For the 30° skew test, the remaining strains varied from -1.5% at approximately 3 ft (0.9 m) to 2.4% at approximately 9 ft (2.7 m). Both tests had strains between 0-0.5% at their farthest distance.
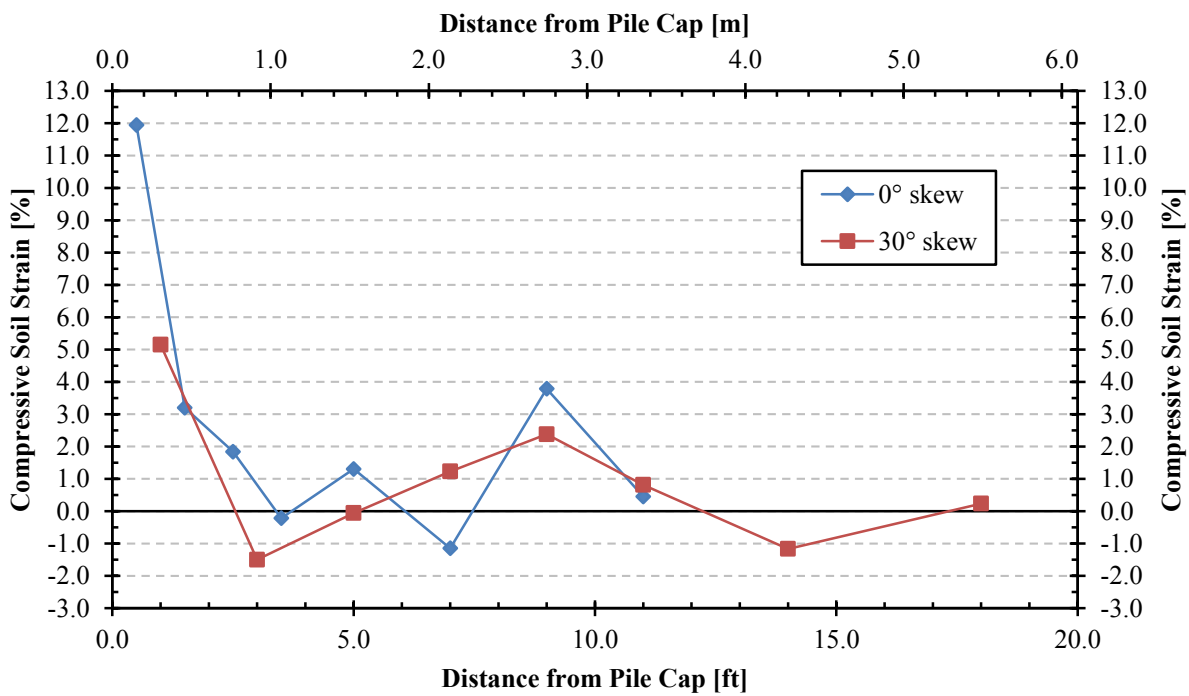
Figure 4-36. Compressive soil strain for gravel tests according to backfill string pot data.

123

5   GRS Backfill Field Test Results

5.1   Passive Force-Deflection

This section presents the passive force-deflection curves for the two GRS backfill tests and describes how they were calculated. A possible correction due to transverse movement is also outlined in this section.

5.1.1   Total Force-Deflection

As described in Section 3.6, a baseline test was performed at each skew angle to find the baseline resistance of the piles, base friction, and any other resistance in the system unrelated to passive force. See Subsection 4.1.2 for a full description of all the 2012-2013 BYU baseline testing and its corresponding limitations. Figure 5-1 shows the total measured actuator force versus longitudinal deflection curves for the non-skewed 3.5 ft (1.07 m) GRS field test alongside the non-skewed baseline test. Figure 5-2 shows a similar graph for the 30° skew 3.5 ft (1.07 m) GRS test and the 30° baseline test. Total force is defined as the total measured loading applied by the combined actuators. Passive force was calculated using Equation (2-12) from Burke Jr (1994) with the longitudinal load (P_L) on the backfill being the difference between the total actuator load and the appropriate baseline curve, as shown in the following figures. Backwall deflection was computed as the average deflection of the four string pots on the front of the pile cap.

125
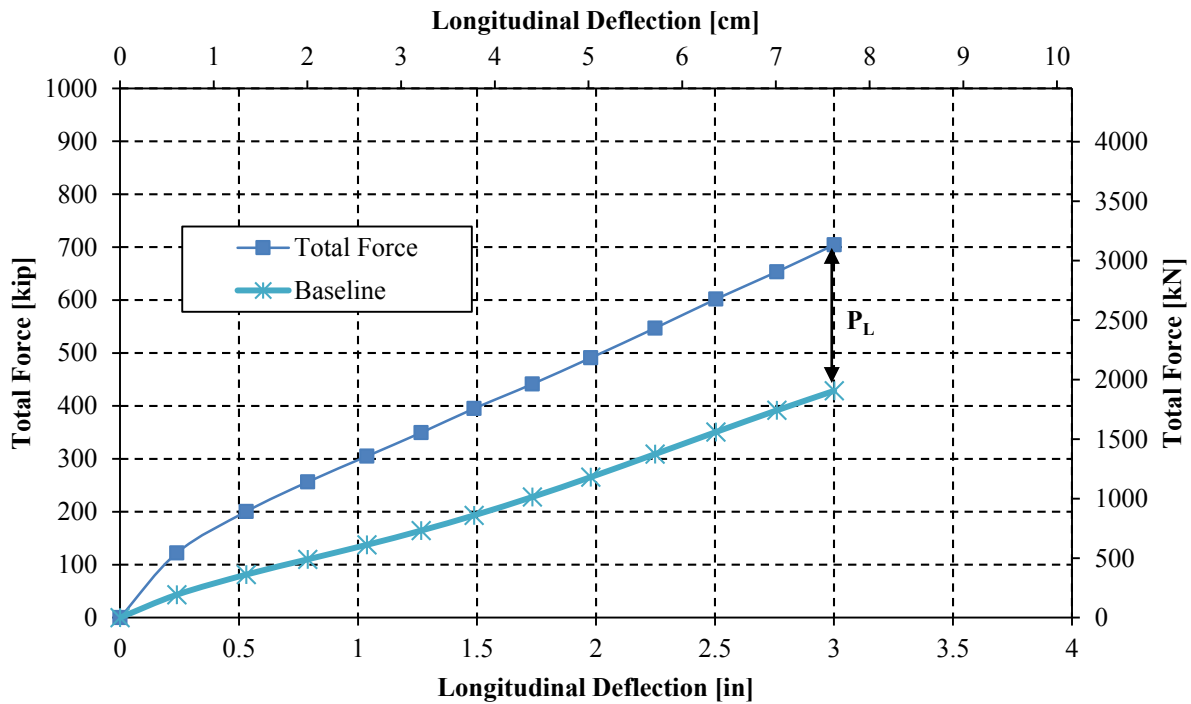
Figure 5-1. Total force and baseline resistance for 0° skew test.
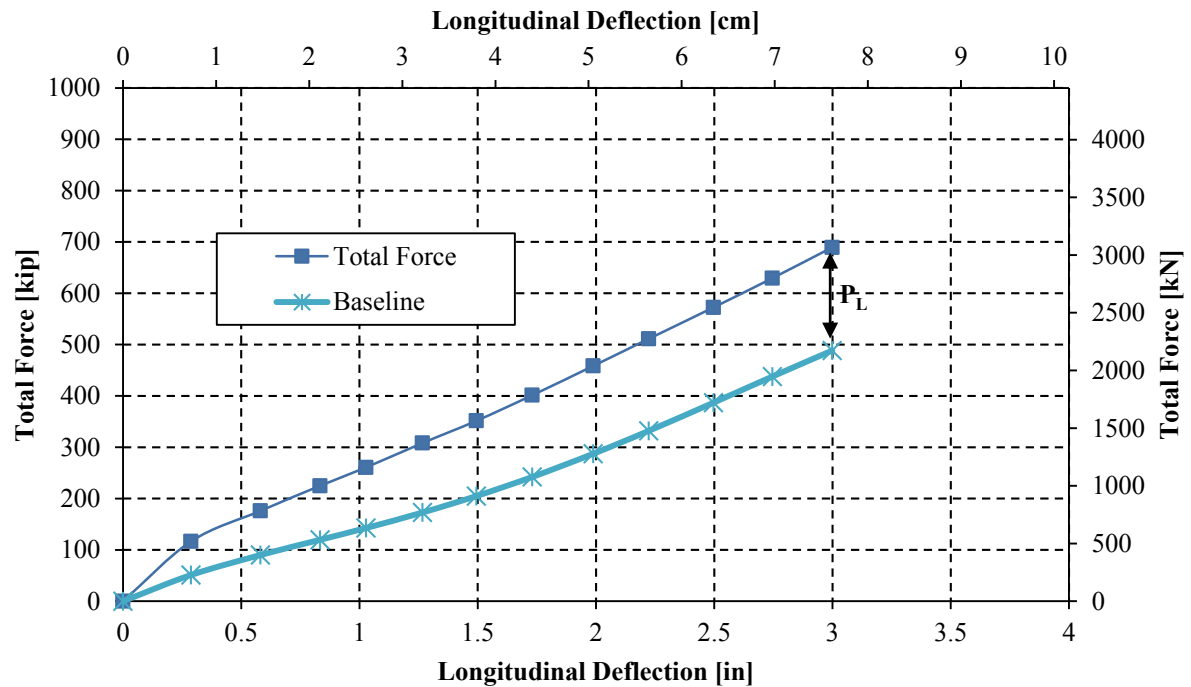
Figure 5-2. Total force and baseline resistance for 30° skew test.

126

5.1.2 Passive Force-Deflection Results and Reduction Factor

Both GRS tests were performed to 3.75 in (9.5 cm). The calculated passive force to full deflection for both GRS tests is shown in Figure 5-3. As was explained in Subsection 4.1.4, the baseline for the 0° skew past 3.0 in (7.6 cm) was deemed to underpredict the actual resistance, and the linearity as was seen previously for the 0° gravel test beyond 3.0 in (7.6 cm) was also seen in the 0° GRS test, as shown in this plot. Therefore, the deflections beyond 3.0 in (7.6 cm) for the non-skewed GRS test were disregarded as discussed. For comparison's sake, the same deflections were dropped from future plots for the 30° skewed test as well.
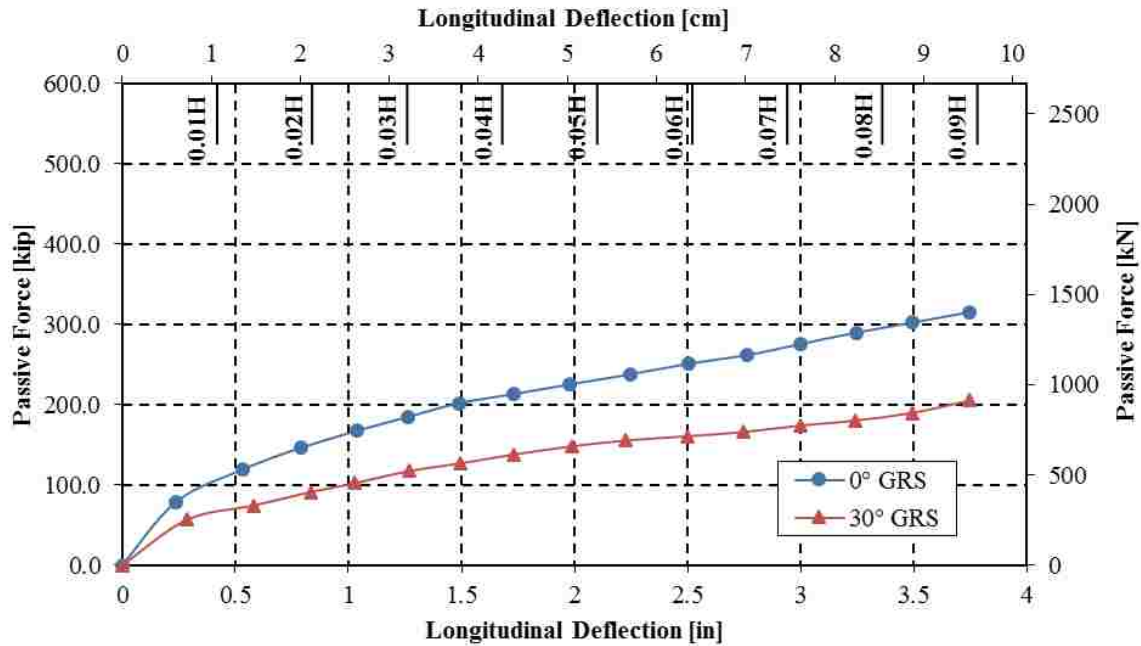
Figure 5-3. Passive force-deflection curves shown to maximum 3.75 in (9.5 cm) deflections for 0° and 30° skew GRS 3.5 ft (1.07 m) tests.

Figure 5-4 shows the passive force-deflection curves for the 0° and 30° skew GRS tests. Passive force was calculated using Equation (2-12) as described previously. Backwall deflection was computed as the average deflection of the four string pots on the back of the pile cap. For

127

both tests, the peak passive force does not reach a clear peak even at displacements as high as 3.0 in (7.6 cm). Although the rate of increase in resistance appears to decrease, there is still a gradual increase in resistance with displacement for normalized displacements beyond 7% of the wall height. In contrast, most tests with unreinforced soil backfill reach a peak resistance at deflections between approximately 0.01H and 0.05H (Clough and Duncan, 1991; see also Subsection 2.5). Additional movement might have been required to fully mobilize the resistance provided by the geotextile sheets as was observed in the interface shear testing described in Subsection 3.5.2.2.
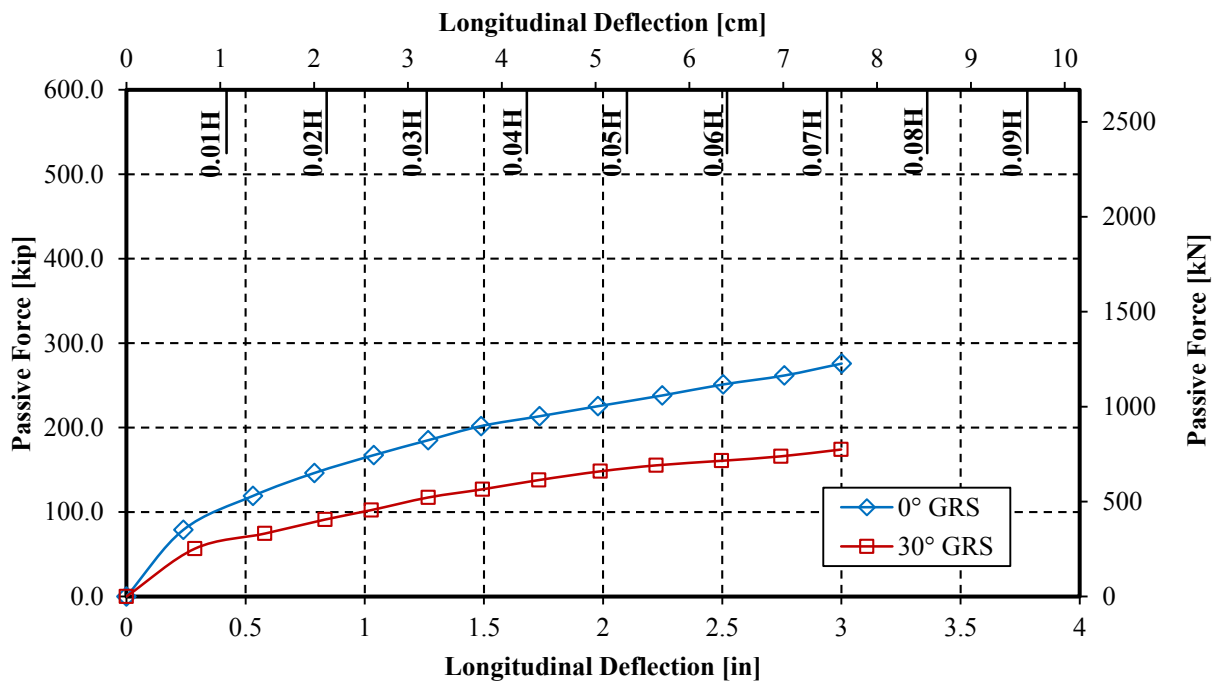
Figure 5-4. Comparison of passive force-deflection curves for 0° and 30° skew GRS 3.5 ft (1.07 m) tests.

Figure 5-5 plots the passive force reduction factor versus skew angle obtained from these tests in comparison with the lab tests conducted by Rollins and Jessee (2013) and the numerical models reported by Shamsabadi et al. (2006). As can be seen from Figure 5-5, Equation (1-1)

128

predicts 53% for a 30° skew angle as the passive force reduction factor compared to the 0° skew case. The measured reduction factor at 3.0 in (7.6 cm) was 63%, however; this value is similar to and slightly higher than the 58% reduction observed for the gravel backfill. If the reduction is calculated at displacements lower than 3.0 in (7.6 cm), the reduction is still approximately 63%. These results suggest that the reduction factor might be somewhat higher for gravel than for sands. Comparisons between the passive force results for GRS and gravel backfills and other skewed tests will be discussed in Section 6.1.
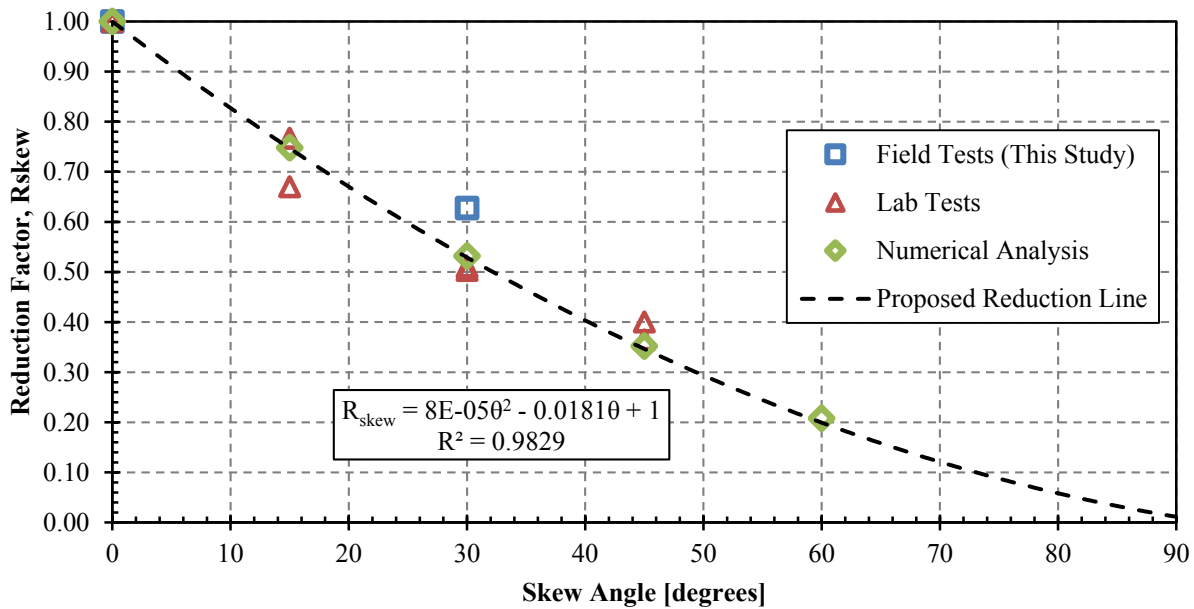
Figure 5-5. Reduction factor, R_{skew} (passive force for a given skew angle normalized by passive force with no skew) plotted versus skew angle based on lab tests (Rollins and Jessee 2013), numerical analyses (Shamsabadi et al. 2006), and results from field tests in this study.

5.1.3   GRS-IBS vs. This Study

As outlined in Section 2.6, GRS backfill is designed to be used in conjunction with a GRS-IBS bridge system, where geotextile reinforces the abutment and the deep foundation as well as the backfill under the approach slab known as the integrated approach. This study was

129

modeled as the integrated approach of the GRS-IBS system, with the pile cap modeling the bridge superstructure. However, the test set up for this study was not a perfect model for the GRS-IBS integrated slab due to the pile group used in this set up. Though not directly monitored in this test, pile groups usually restrain vertical movement of pile caps. One assumption of the pile group set-up is that any vertical component of passive force would be absorbed by the weight and friction of the piles. However, a GRS-IBS abutment is not vertically restrained with a deep foundation, and therefore may experience vertical movement due to the upward component of passive force (see Figure 2-2). It is possible that the weight of the GRS-IBS superstructure with a span of less than 140 ft (43 m) may be light enough to experience this passive force uplift, and further investigation is required.

5.1.4 Transverse Effects

Force-deflection baseline curves were measured from the side push tests described in Subsection 3.3.5 and are plotted in Figure 5-6. These tests measured transverse resistance against small transverse movement for the skewed test configuration. In the plot, "North Piles" plots the average deflection of the north string pots versus the north actuator loads and "South Piles" likewise plots the average deflection of the south string pots versus the south actuator loads. The actual load-deflection curves for each set of piles is probably the same; the difference between the plotted resistances of the two pile groups is likely due to the frictional resistance of the wedge. This plot shown is for the 45° skew side push. Accounting for transverse resistance may increase or decrease the passive force calculated by Burke Jr's (1994) equations (see Subsection 2.4.3.1), which do not take transverse abutment resistance into account. Preliminary investigation suggested that the passive force reduction factor increases slightly when transverse movements and resistances are taken into account. Future studies will need to calibrate these baseline curves

to investigate further the effects of the transverse movements and rotations observed in these skewed abutment tests.

Figure 5-6. Raw baseline force-deflection curves from transverse loading tests (Smith, 2014).

5.2 Pile Cap Movement

Pile cap movement was monitored in both the longitudinal and transverse directions. As described in Section 3.4, The average of the four string pots on the front wall of the pile cap was the longitudinal displacement value used for each data point in all the total and passive force-deflection curves shown in Section 5.1. Additionally, an inclinometer and two shape accelerometer arrays (SAAs) measured both longitudinal and transverse displacements. This section describes the pile cap movement data gathered from these three methods of measurement.

131

5.2.1 Longitudinal Movement

Figure 5-7 and Figure 5-8 provide longitudinal deflection versus depth profiles obtained from both an inclinometer and SAA for the non-skewed test and the 30° skew test, respectively. Both profiles represent pile cap behavior for the final longitudinal displacement of the test. The depths are referenced to the top of the cap. The average deflection measured by the string pots at two elevations on the pile cap are also shown for comparison purposes. The graphs demonstrate that the measurements for the three systems were reasonably consistent and aligned with each other. For the non-skewed test, the percent difference between the north inclinometer and shape array profiles from the top of the cap to a depth of 15 ft (4.6 m) ranged between 0.6 and 12.7% with a median of 3.4%. For the 30° skewed test, the percent difference between the north inclinometer and shape array profiles from the top of the cap to a depth of 15 ft (4.6 m) ranged between 0.9 and 7.7% with a median of 3.6%. For displacements located below a depth of 15 ft (4.6 m) the percent error became very high but because displacements in this zone were versy small at 0.05 in (0.13 cm) or less, the percent error is not particularly meaningful.

The measurements indicate a relatively linear deflection profile within the pile cap and small cap rotations. Below the base of the cap, the piles deflect in a non-linear fashion with the deflections reaching a point of counterflexture at depth of approximately 21 ft (6.3 m) and a point of fixity at about 31 ft (9.45 m). Agreement between the north and south inclinometers was generally very good.

Although the inclinometer readings were only taken at the maximum deflection for each load test, shape array profiles in the longitudinal and transverse directions were obtained at each deflection increment for each test. Figure 5-9 and Figure 5-10 show profiles of longitudinal deflection vs. depth for each deflection increment. As the deflection level increases the

132

deflection of the pile cap remains linear but the rotation progressively increases while the depth to the point of fixity increases. Similar curves were obtained in the transverse direction.
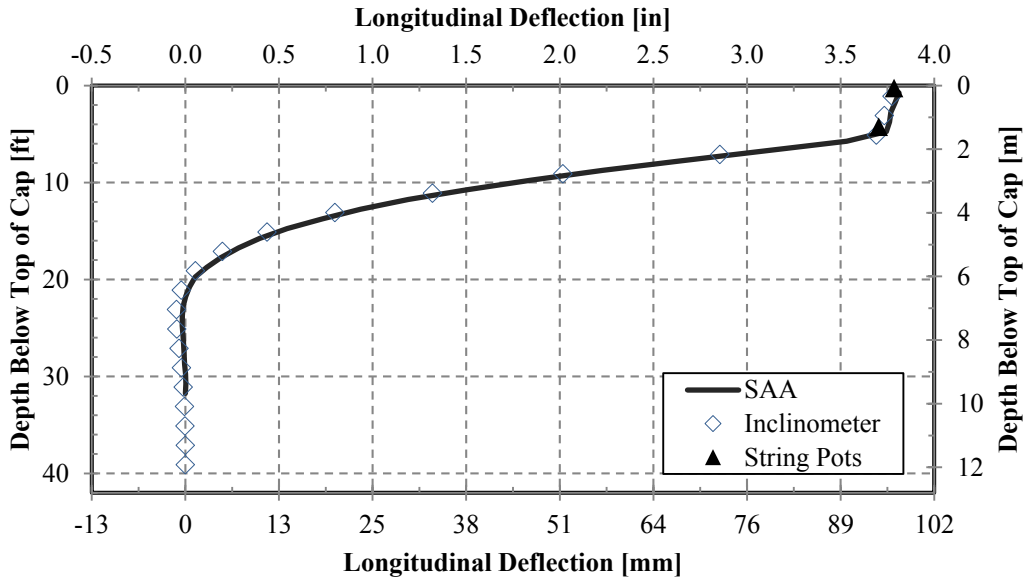
Figure 5-7. North 3.5-ft GRS gravel backfill 0° skew final deflection comparing inclinometer, shape array, and string potentiometers
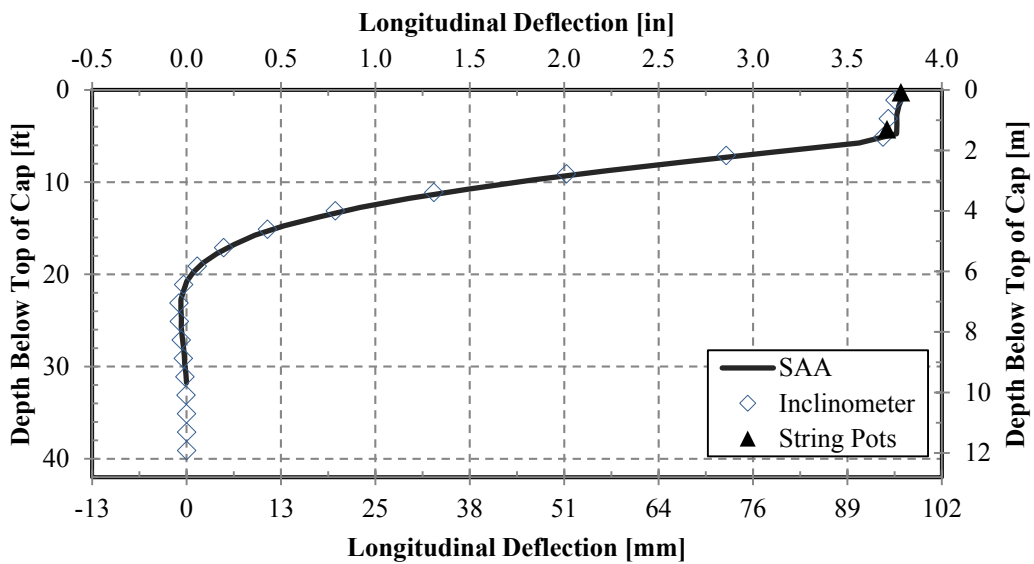
Figure 5-8. North 3.5-ft GRS gravel backfill 30° skew final deflection comparing inclinometer, shape array, and string potentiometers

133
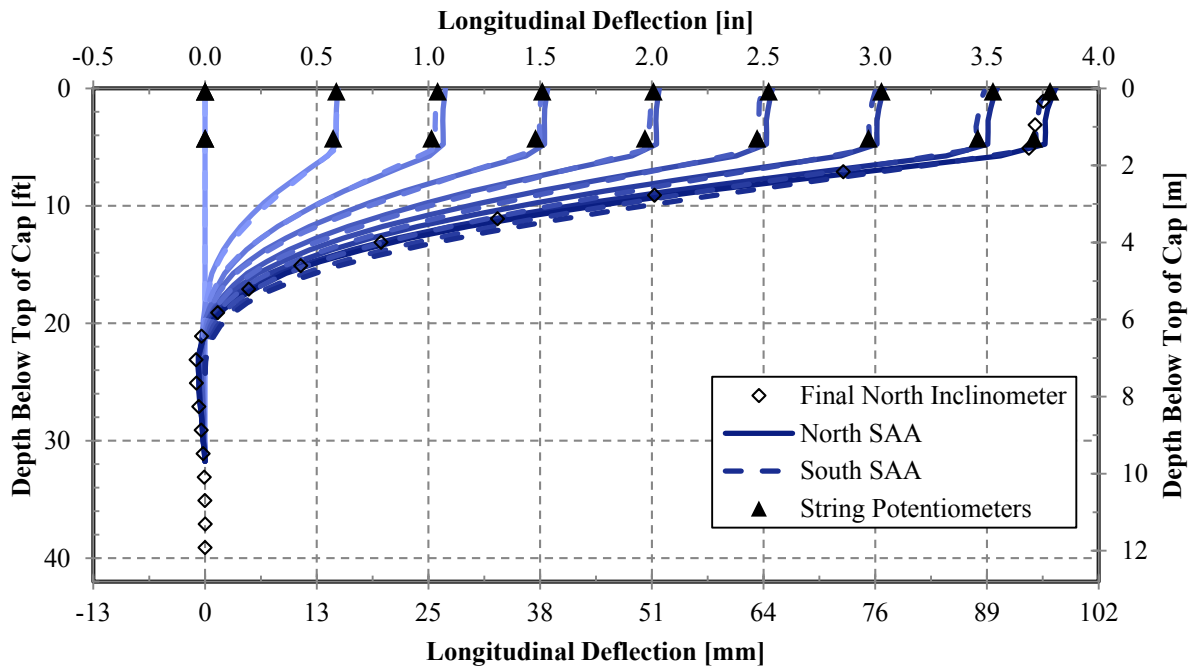
Figure 5-9. Longitudinal deflection vs. depth curves from SAA and string potentiometer data at various deflection increments for 0° skew test.
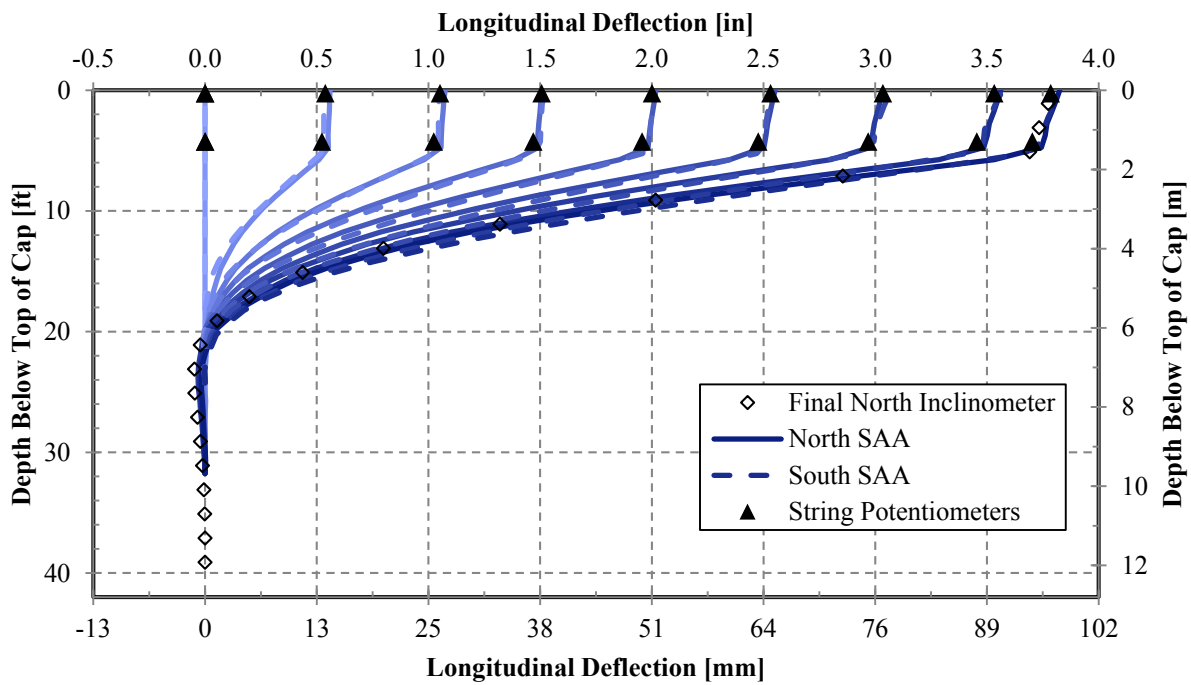
Figure 5-10. Longitudinal deflection vs. depth curves from SAA and string potentiometer data at various deflection increments for 30° skew test.

134

5.2.2 Transverse Movement and Rotation

Transverse deflection versus depth profiles for the pile cap, also recorded by shape array and inclinometer, are plotted in Figure 5-11 and Figure 5-12. Plotted on a smaller scale, the error is more pronounced though the magnitude difference is still small. As observed for the deflections below 15 ft (4.6 m) in the longitudinal test, the percent difference is exaggerated due to the smaller scale. The percent difference is within the error thresholds of each instrument (±1.5 mm/30 m for shape array, and ±1.24 mm/30m for inclinometer) (Rollins et al. 2009) and confirms that shape arrays are not particularly reliable for very small deflections. Once again, the shape of the deflection profile indicates essentially linear deflection in the pile cap and very small rotations. The deflection in the piles is non-linear and decreases to zero at a deflection of about 30 ft (9 m).
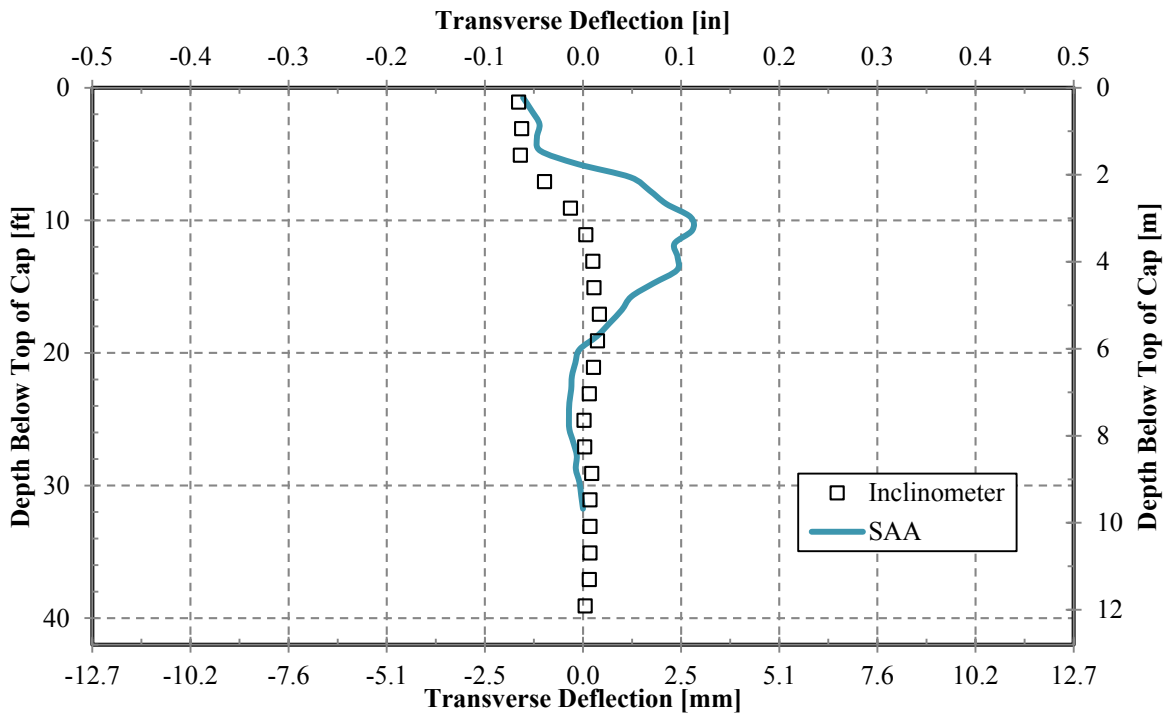
Figure 5-11. North 3.5-ft GRS gravel backfill 0° skew final deflections comparing inclinometer and shape array

135
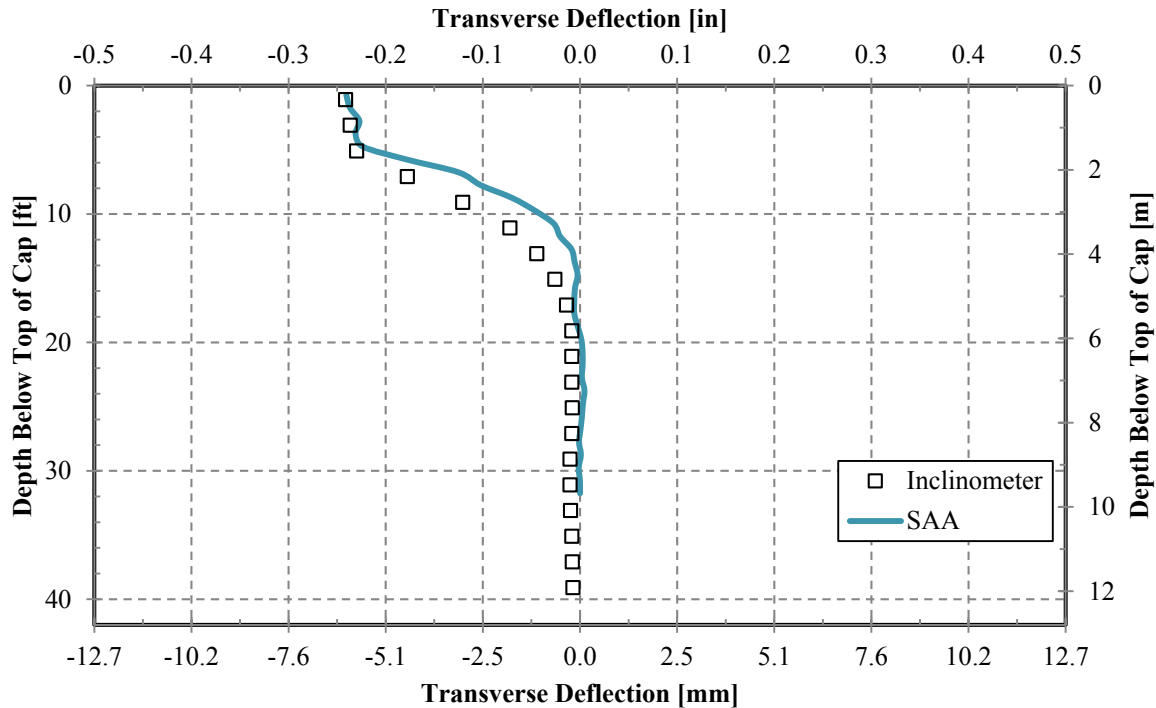
Figure 5-12. North 3.5-ft GRS gravel backfill 30° skew final deflections comparing inclinometer and shape array

The final north and south measured transverse deflections for each test at the surface of the pile cap, as measured by inclinometer and shape arrays, are plotted in Figure 5-13 from a plan view perspective. The transverse deflection is again exaggerated compared to the length of the pile cap, which also exaggerates the angles of rotation, but the plot allows for a comparison of deflection and rotation between the two tests. Although deflections of both actuators were kept relatively constant throughout the test, rotation and transverse deflection were still affected by skew angle. As seen in Figure 5-13, for both the 0° and 30° skews the pile cap ultimately shifted to the west (the direction of the acute corner of the skew) by approximately 0.04 and 0.21 in (0.1 and 0.5 cm), respectively. The transverse movement of the non-skewed test may be attributed to the number of skewed tests performed on the piles that have likely weakened the

136

resistance to pile movement to the west as the cap is pushed north. Both tests rotated the pile cap approximately 0.02° in the counter-clockwise direction.
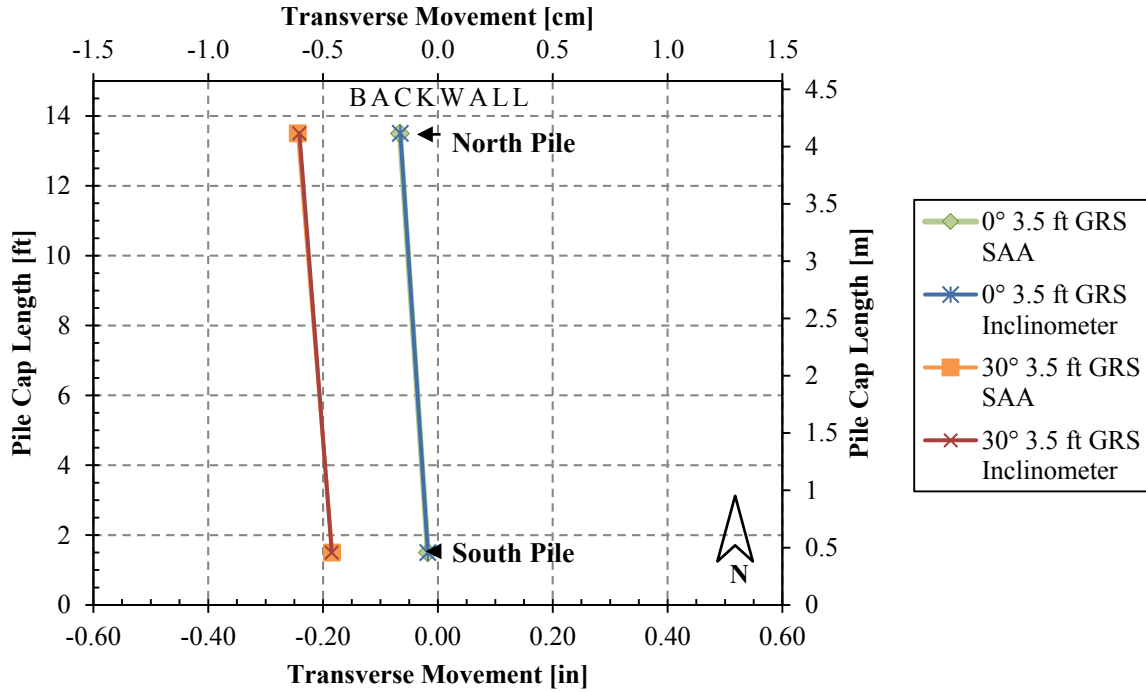
Figure 5-13. Transverse pile cap deflection and rotation determined between north and south shape array and inclinometer data.

As the actuator loading progressed and the pile cap was pushed north into the backfill, movements in the cap to the east and west were detected with the shape arrays at each loading increment. The development of pile cap displacement as the test took place is shown for each of the 0° and 30° skew tests in plan view in Figure 4-25 and Figure 4-26, respectively. Like Figure 4-24, the figures were created with shape array data from the point closest to the surface of the pile cap.

In the non-skewed test in Figure 4-25, the pile cap stayed relatively straight, with small-magnitude drifts back and forth east and west on the south end. However, the north pile stayed mostly true to center, and the final transverse movement was still very small on both ends,

137

averaging approximately 0.04 in (0.1 cm) to the west and rotating counterclockwise about 0.02°, as stated previously. The 30° test, shown in Figure 4-26, had greater transverse deflections, averaging 0.21 in (0.5 cm) deflection to the west, which was toward the acute corner of the skew, by the end of the test. This is also the direction along which the shear force was applied by the longitudinal loading. Though the final rotation was 0.02° counterclockwise, the rotation of the pile cap ranged from 0.03° to 0.05° for the entire test prior to the final 0.25 in (0.6 cm) of longitudinal deflection.
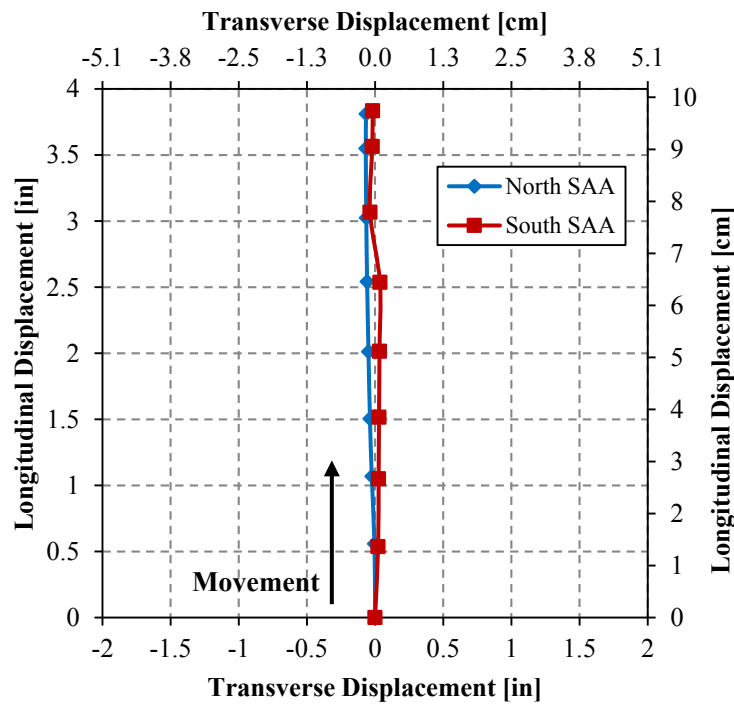
Figure 5-14. Longitudinal and transverse displacements of pile cap in plan view over the course of the non-skewed GRS test, as determined by north and south shape array data.
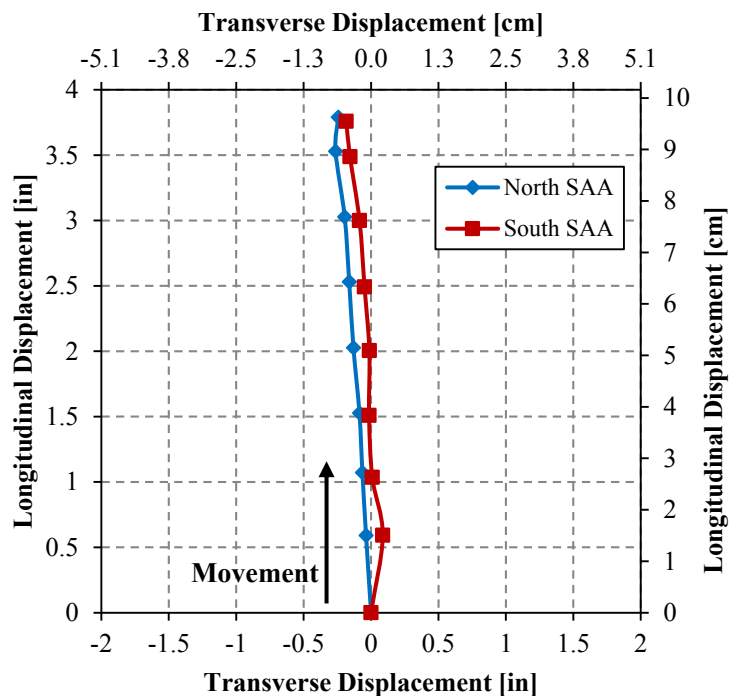
Figure 5-15. Longitudinal and transverse displacements of
pile cap in plan view over the course of the 30° skewed GRS
test, as determined by north and south shape array data.

5.3 Applied Shear vs. Transverse Displacement

The relationship between the applied shear force (P_T) and transverse displacement for the 30° skewed GRS test is plotted in Figure 6-4A. The applied shear force was computed using Equation (2-5) and displacement values were based on measurements recorded from the north shape array during testing. The transverse stiffness of the backfill seemed to have distinct stages during the test. The most distinct change occurred after transverse movement of 0.1 in (0.25 cm), when the stiffness dropped slightly. Duncan and Mokwa (2001) specify the minimal movement to develop interface friction to be 0.1-0.25 in (0.25-1.3 cm). However, because longitudinal movement was occurring simultaneously, more than 0.1 in (0.25 cm) movement had actually occurred transversely, or parallel to the plane of the backwall. Likely the soil was simply beginning to fail. The maximum shear force was 100 kip (445 kN) and occurred at about 3.0 in

(7.6 cm) of longitudinal displacement for the GRS test. In Figure 6-4B the shear force has been normalized by the maximum shear force. A comparison between this test and the scaled gravel 30° skew test will be included, along with calculated shear resistances for both tests, in Subsection 6.1.2.
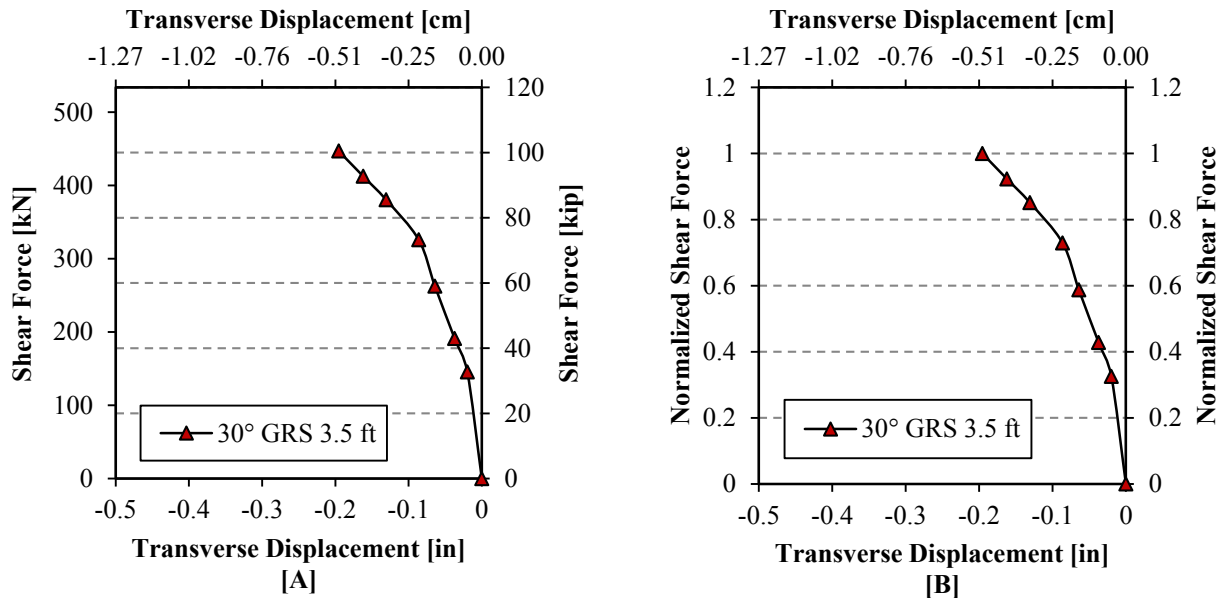
Figure 5-16. [A] Applied shear force versus transverse displacement; [B] Normalized applied shear force versus transverse displacement.

5.4 Backfill Response

The displacements in all the tests of this study were of such magnitude that plastic deformations in the backfill were detectable through surface cracks and soil heave. A failed soil mass will have both surface cracks and vertical heave in the approximate shape of a "bulb" behind the backwall. Experience in previous tests indicates that failure surfaces do not generally manifest themselves fully until the displacement clearly exceeds that required for peak resistance or when there is a decrease in passive force toward a residual value. Though neither of the GRS tests reached a definitive peak in passive force indicating failure, substantial backfill heave and

140

surface cracks were observed. Shamsabadi (2007) described this phenomenon as failure from the top down, or that intermediate passive wedges formed prior to the ultimate failure surface appearing. Thus if the testing layout had allowed more displacement, addition heave and surface cracks would have been observed for further displacements until the ultimate failure surface developed.

Surface cracks were spray painted in the soil as they occurred during testing and vertical displacements, or heave, were measured by the level and total station before and after testing. The total station also measured lateral displacements in the backfill, as did string potentiometers. A photo from the 0° gravel test is shown in Figure 5-17. Unfortunately, no photo was taken at the end of the 30° GRS test. This section describes the lateral and vertical displacement behavior of the backfill due to the pile cap loading.
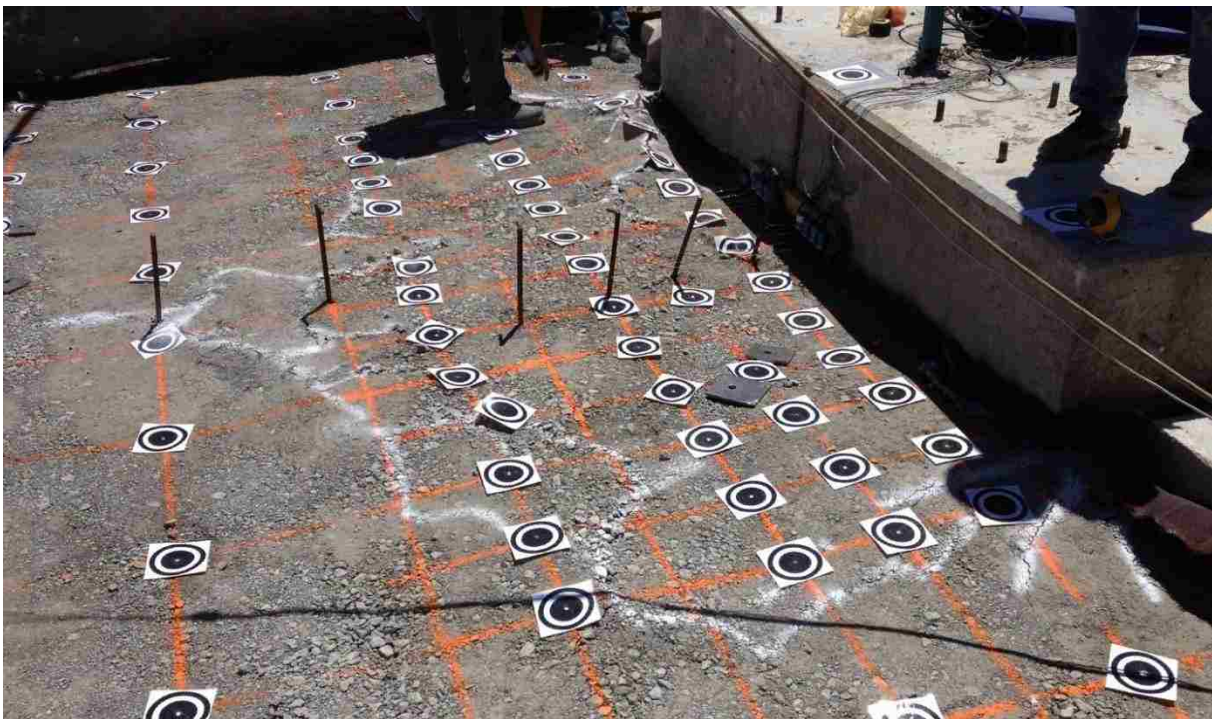
Figure 5-17. Backfill surface at end of non-skewed 3.5 ft (1.07 m) GRS test.

5.4.1 Vertical Heave and Failure Surface Geometry

Backfill heave contours and surface cracks for the non-skewed and 30° skewed abutments are illustrated in Figure 5-18 and Figure 5-19. Heave contours for the non-skewed abutment have generally been symmetrical in other non-skewed tests; however, in this case, the maximum heave was 1.0 in (2.5 cm) greater behind the east side of the backwall relative to the west side. One potential cause for this asymmetry is the placement of the 2-ft (0.6-m) wide pre-cast block wingwall on the east side of the wall to accommodate a reaction wall for transverse load testing. This orientation may have restrained southward movement of the backfill relative to the wingwall on the west side of the cap, leading to additional heave. It is interesting to note that the heave contours were also higher on the east side for the 0° skew test with gravel backfill when this same wingwall geometry was used (see Figure 4-29). An additional possibility is that the pile cap and failure surface caught on one or more of the geotextile sheets and some part of that interaction caused the soil to heave on that side. Another possibility is small variances in compaction, in addition to the slight rotation of the pile cap as discussed in Subsection 5.2.2 could produce greater maximum heave. It should be noted, however, that the heave contours for smaller heave values are relatively symmetrical.

The heave for the GRS tests, like for the gravel tests, was very high compared to similar tests in sand (Marsh, 2013, Palmer, 2013). The maximum heave was 4.9 in (12.4 cm) for the 0° test and occurred near the east abutment edge, 1 ft (0.3 m) from the backwall. The maximum heave for the 30° test was 2.8 in (7.1 cm) and was found 1 ft (0.3 m) behind the middle of the backwall toward the obtuse corner. Surface cracks typically developed about 4 to 8 ft (1.2 to 2.4 m) longitudinally behind the wall for both the non-skewed backwall and for the 30° test. However, heave contours greater than about 0.75 in (1.9 cm) extended to distances of 8 to 10 ft

142

(2.4 to 3.0 m) longitudinally behind the backwall. In previous tests, surface cracking was often associated with surface heaves of approximately 0.5 to 0.75 inches (1.3 to 1.9 cm), as observed here with both GRS tests. For example, for the unreinforced gravel test, surface cracks were manifest at distances of 10 to 12 feet (3.0 to 3.7 m) behind the wall (see Figure 4-29 and Figure 4-30). Effective widths for the GRS tests were approximately 16 and 17 ft (4.9 and 5.2 m) for the 0° and 30° tests, respectively.

Unlike other forms of confinement (i.e. concrete wingwalls, MSE wingwalls), the geotextile reinforcement allowed the failure wedge to extend beyond the edge of the pile cap walls. Thus, the effective width of the failure wedge extended about 3-4 ft (0.9-1.2 m) for both tests beyond the edge of the abutment on either side, similar to an otherwise unconfined test. As was demonstrated by other unconfined backfill geometries (Smith, 2014), the developing 30° failure surface extending perpendicular to the obtuse corner of the pile cap and tangent to the acute corner.

143
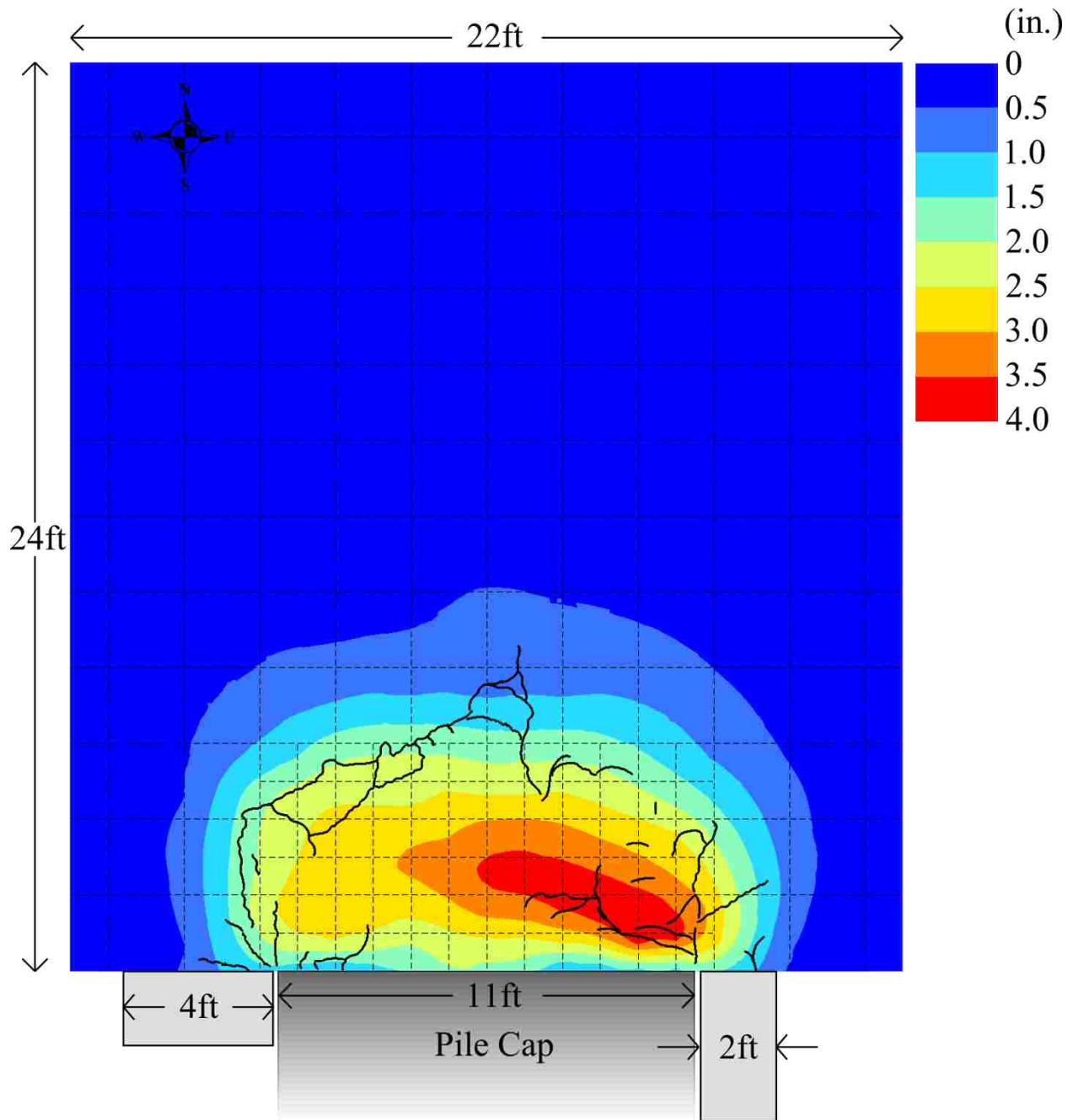
Figure 5-18. Vertical heave contours and surface cracks at 3.74 in (9.51 cm) of longitudinal displacement (test completion) for 3.5 ft (1.07 m) 0° skew GRS test (NOTE: 1 in = 2.54 cm); 2 ft [0.6 m] grid is refined to a 1 ft [0.3 m] grid in the 6 ft [1.8 m] nearest to the backwall).
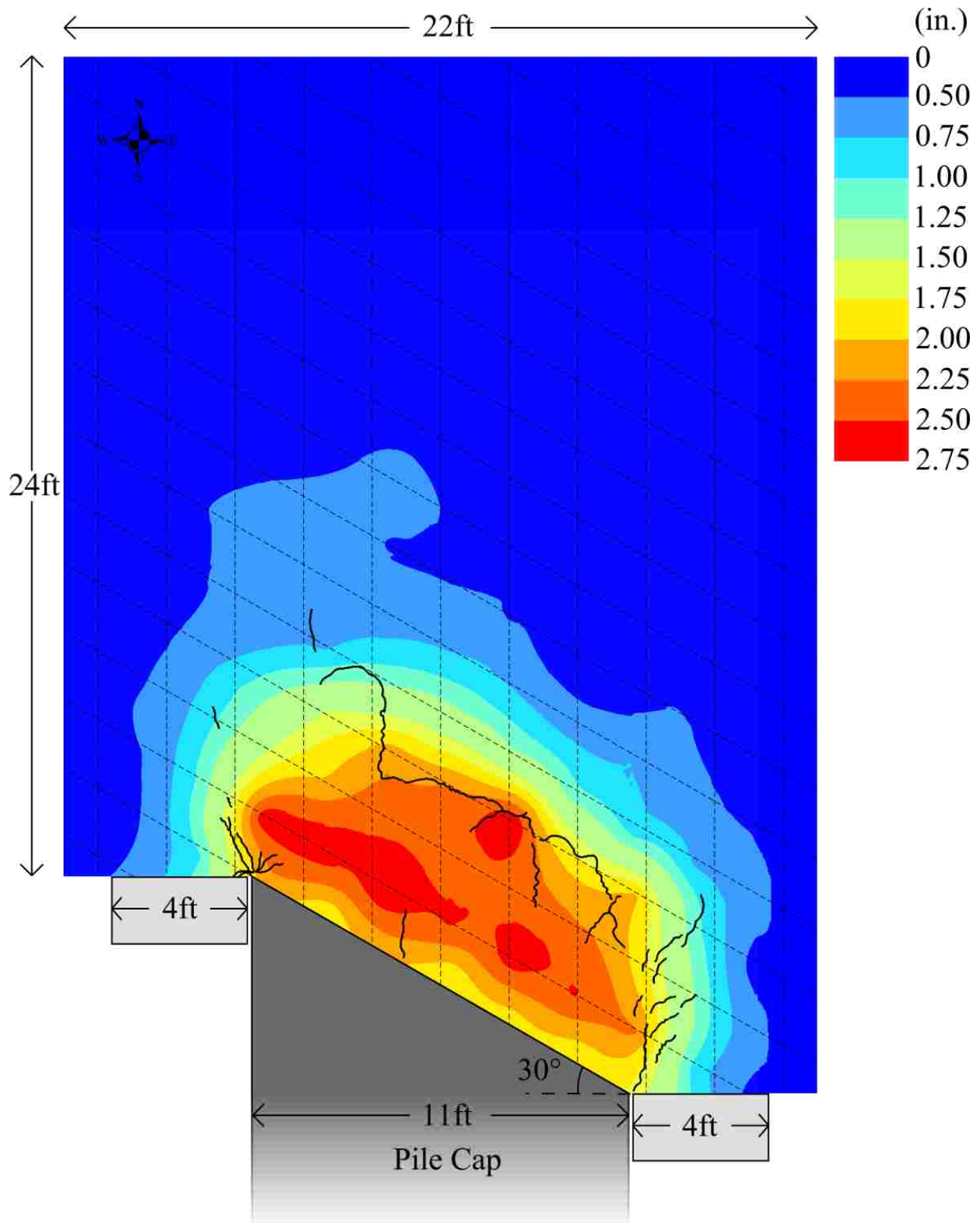
Figure 5-19. Vertical heave contours and surface cracks at 3.75 in (9.53 cm) of longitudinal displacement (test completion) for 3.5 ft (1.07 m) 0° skew GRS test (NOTE: 1 in = 2.54 cm; grid is 2 ft by 2 ft [0.6 m by 0.6 m]).

5.4.2   Lateral Displacement and Strain

Figure 5-20 and Figure 5-21 show horizontal backfill displacements for the non-skewed and 30° skewed abutments. In contrast to the heave plots, the displacement vectors show symmetric movement on the east and west sides of the wall for the non-skewed test. Displacement vectors for both tests generally indicate longitudinal movement of the backfill with an outward component near the edges of the backwall. However, the outward movement component is somewhat larger near the acute side of the wall for the 30º skew tests. Small variations in vector direction are typical of the similar diagrams from other tests. Displacement vector magnitudes are generally less than about 0.5 inch (1.3 cm) beyond distances of 14 to 16 ft (4.3 to 4.9 m) for both the non-skewed and 30° walls.

As described in Section 3.4, eight string pots secured on or near the backwall face and attached to stakes driven into the backfill measured longitudinal displacement of the backfill soil, or its compression, as the test progressed. Some variability in the data cast uncertainty on a handful of data points. Possible reasons for small variations in the data include (1) a developing shear plane crossing the stake beneath the surface, causing the stake to lean either forward or backward (Franke, 2013; see Figure 4-33), or (2) the stake was not driven to a stable depth to begin with. Despite small variations observed in the data, general trends were detectable.

146
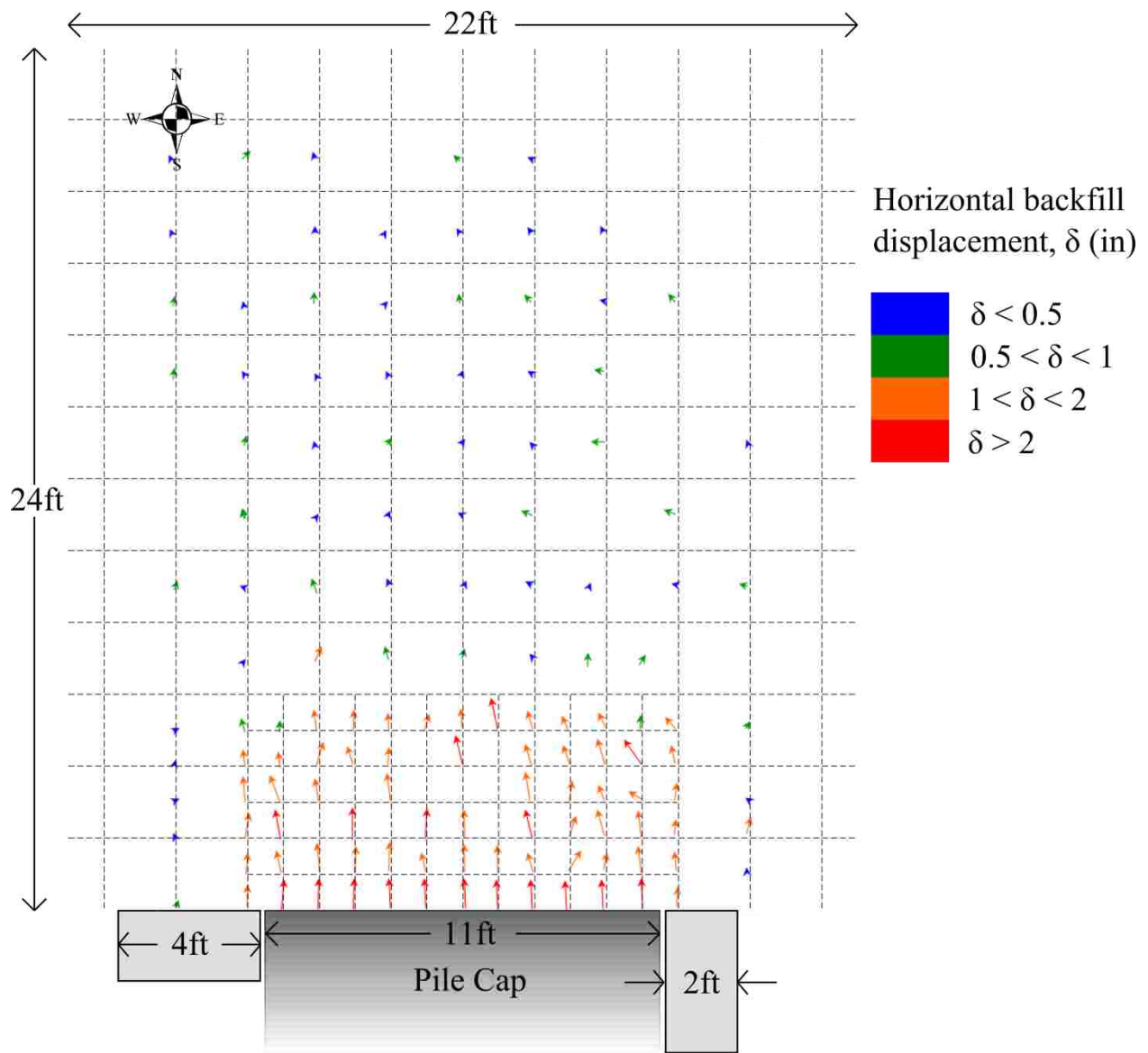
Figure 5-20. Soil displacement for 0° skew 3.5 ft (1.07 m) GRS backfill.
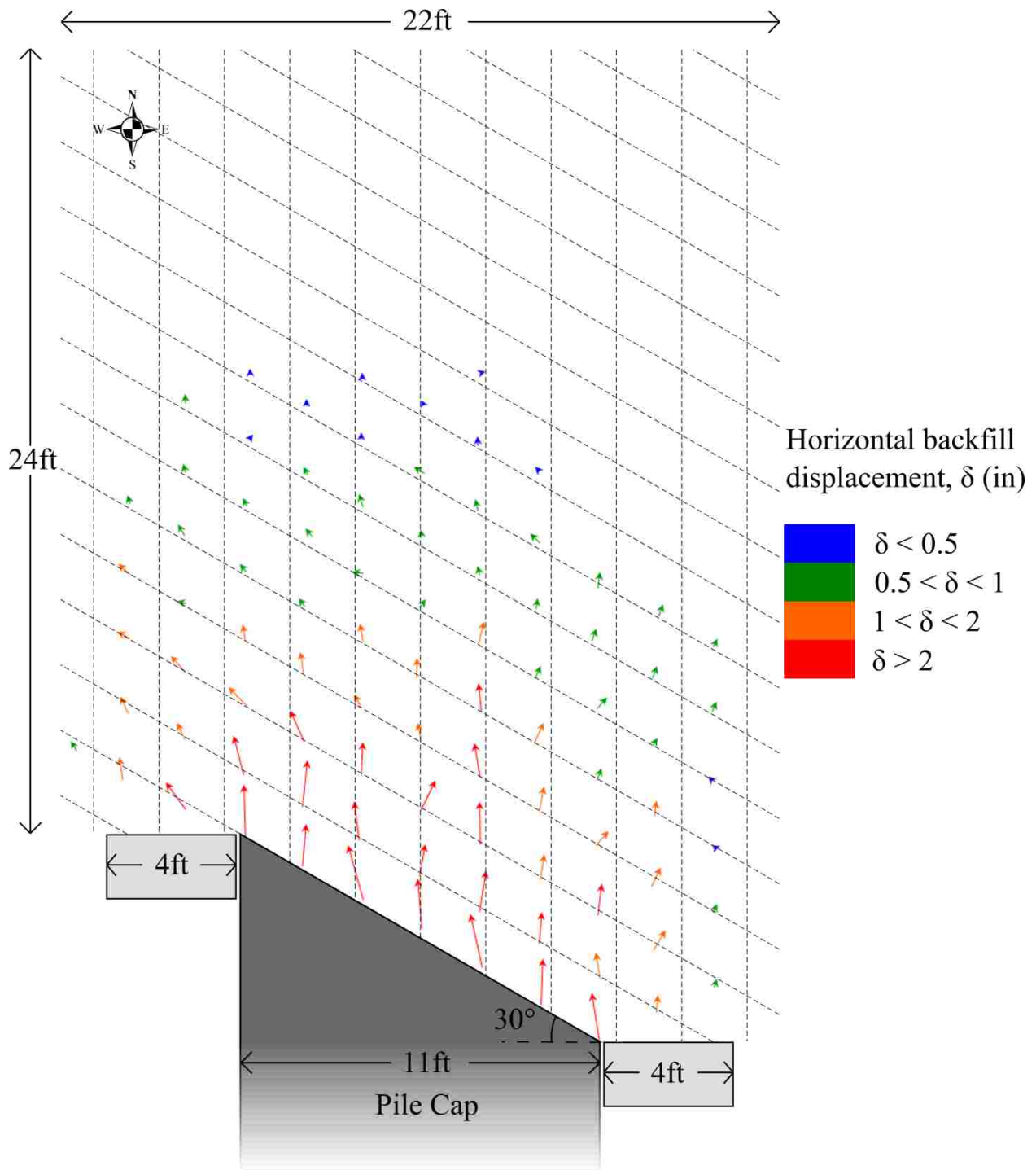
Figure 5-21. Soil displacement for 30° skew 5.5 ft. GRS backfill.

For the 0° 3.5 ft (1.07 m) test, the string pots were generally placed at close distances to determine the behavior near the pile cap. However, more string pots closer to the pile cap meant fewer string pots to place at greater distances from the pile cap. The string pots for this test only extended 12.0 ft (3.66 m) from the backwall. The 30° skew 3.5 ft (1.68 m) test, on the other hand, had fewer string pots closer to the pile cap so that the farthest string pot was 20.0 ft (6.09 m) from the backwall. In other words, string pots were placed at the same distances as in the unreinforced gravel tests. Figure 5-22 and Figure 5-23 show the displacements in the backfill for the 0° skew 3.5 ft (1.07 m) and the 30° skew 3.5 ft (1.68 m) tests, respectively, at selected increments of pile cap displacement during the test. The final displacements are in bold. The left axis represents the pile cap backwall. In general, the backfill displaced or compressed less with increased distance from the pile cap.

For the 0° 3.5 ft (1.07 m) test seen in Figure 5-22, compression in the backfill in the first inch (2.5 cm) of pile cap displacement followed the pattern of decreased compression with greater distance from the pile cap backwall. At pile cap displacements beyond 1 in (2.5 cm), compression closest to the pile cap increased less with increasing distance up to 6 ft (1.8 m), where the string pot stake displaced the most horizontally. Significant cracking suggests a shear surface was developing between 6 and 8 ft (1.8 and 2.4 m) of the pile cap (see Figure 5-18), which likely explains why at 8 ft (2.4 m) and greater distances only significantly reduced compressions were observed in the backfill. It also means that stake-shear plane interaction with a downward shear plane could have caused the peak in compression at 6 ft (1.8 m).

The extraordinary heave from the non-skewed test (see Figure 5-18) up to about 6 ft (1.8 m) was likely related to the abnormal behavior in the string pot stakes within 6 ft (1.8 m) of the pile cap. The post-test pictures (see Figure 5-17) shows significant leaning of the first two string

pot stakes at 1 and 2 ft (0.3 and 0.6 m) distances toward the pile cap, which explain their small

displacements. Slight leaning was also visible in the 3 ft (0.9 m) stake.
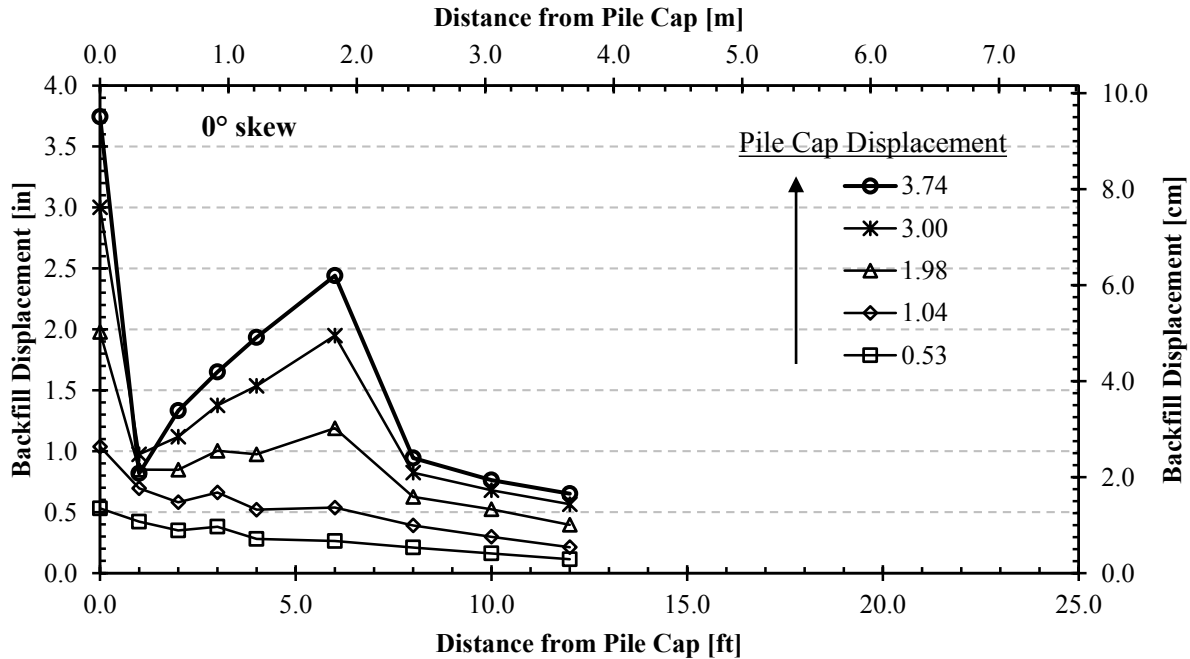
Figure 5-22. Development of displacement in the backfill of the 0° skew 3.5 ft (1.07 m) GRS test with increasing distance from the backwall face.

Compression in the 30° skew test shown in Figure 5-23 almost uniformly follows the rule

of less compression with increased distance from the cap. The only bump in the data is seen at 6

ft from the pile cap, which is where cracking was observed (see Figure 5-19). Thus, like the non-

skewed GRS test, the slightly increased compression at 6 ft (1.8 m) was likely artificial due to

stake-shear plane interaction with a downward shear plane.
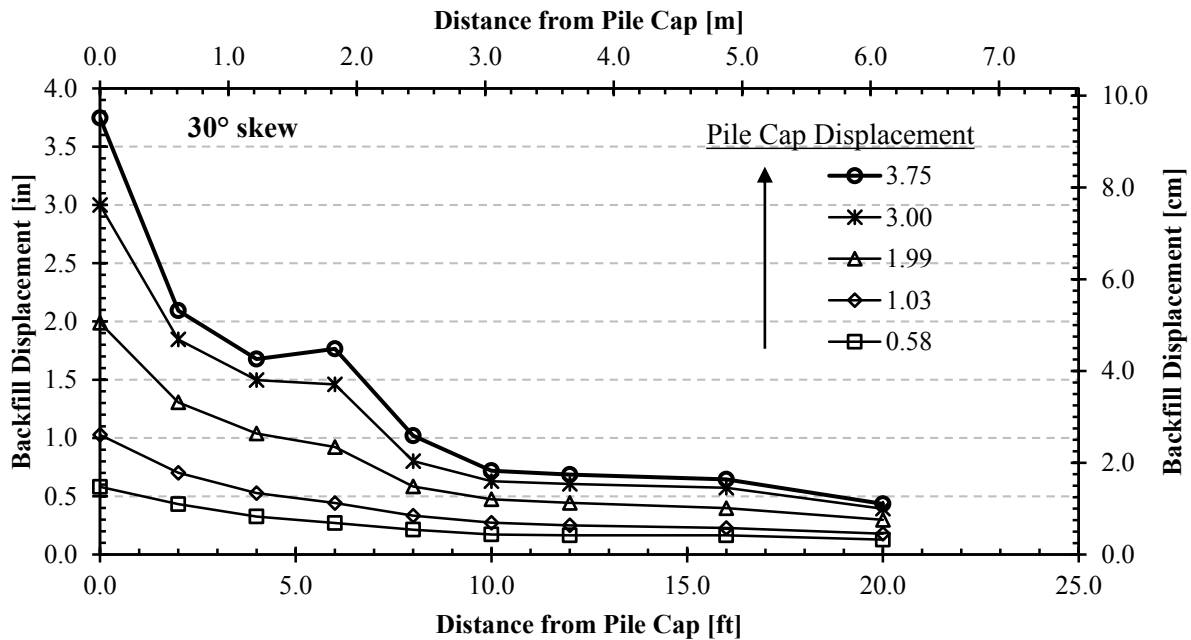
Figure 5-23. Development of displacement in the backfill of the 30° skew 3.5 ft (1.07 m) GRS test with increasing distance from the backwall face.

Strain for both tests is shown in Figure 5-24. The maximum strain in the first 1-2 ft (0.3-0.6 m) was the most pronounced in both tests, with 24% for the non-skewed test and 6.9 % for the 30° skew test. For the 0° skew test, the remaining strains varied from -4.3% at approximately 3 ft (0.9 m) to 6.2% at approximately 7 ft (2.1 m). For the 30° skew test, the remaining strains had a smaller range; they varied from -0.4% at approximately 5 ft (1.5 m) to 3.1% at approximately 7 ft (2.1 m). Both tests had strains between 0-0.5% at distances of 11 ft (3.4 m) and greater.

The typical pattern appears to be that compressive strain is highest within a short distance behind the pile cap, then strain becomes relatively uniform further back as the failure wedge tends to move more as a block. As the failure surface daylights in the backfill, the compressive strain also tends to increase as the failure wedge is compressed against the backfill behind the more stationary wedge further back.

151
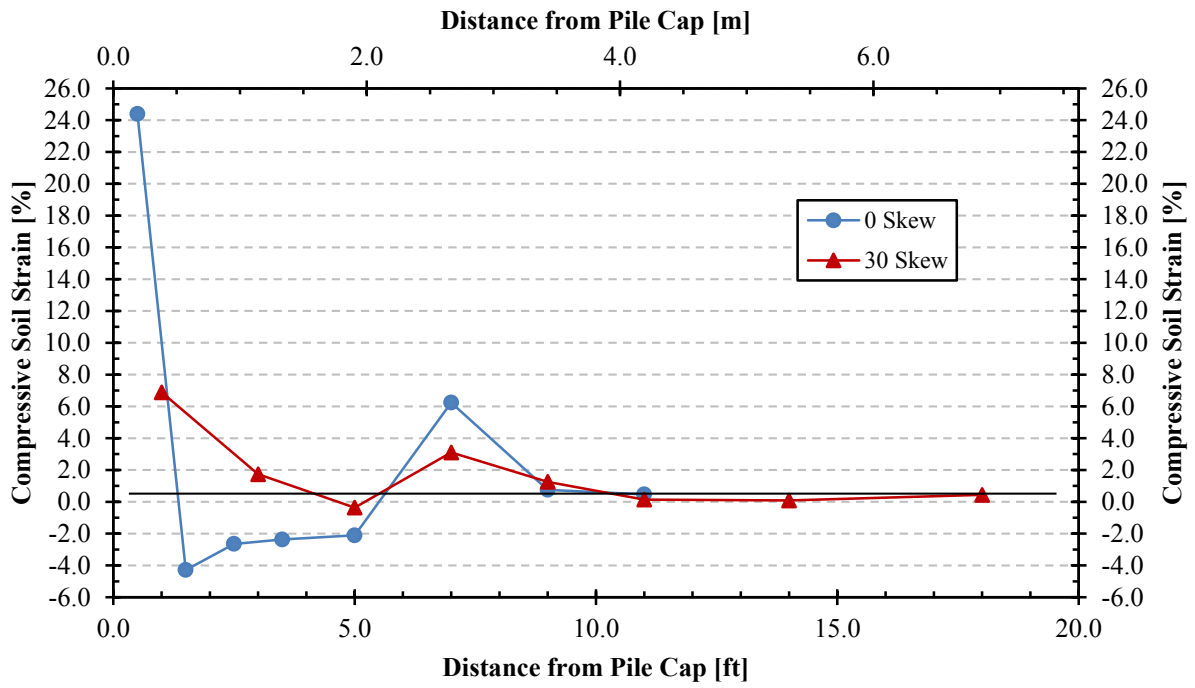
Figure 5-24. Compressive soil strain for GRS tests according to backfill string pot data.

6 Analysis of Passive Force-Deflection Results

6.1 Comparison of Results

This section will put context to the passive force results of this study by comparison. The section contains comparisons of the gravel and GRS passive force-deflection results with each other and with data from other sand and gravel tests. In particular, it will compare the results of this study with previously performed skewed abutment testing.

6.1.1 Comparison between Gravel and GRS Results

Passive force-deflection results from the four tests of this study are all plotted together in Figure 6-1. As previously illustrated, both pairs of tests showed clear reduction in passive force due to skew angle—58% for the gravel tests and 63% for the GRS tests. This plot reveals that there was also some reduction in passive resistance due to the geotextile reinforcement. Perhaps most significantly, there was a decrease in stiffness in the GRS backfill, so that significantly higher deflections were required to reach equivalent passive resistances compared to the unreinforced gravel. This backfill elasticity is favorable in the GRS-IBS abutment configuration because it allows thermal movement without developing excessive induced stresses in the bridge superstructure. Though it is possible that the GRS backfills would have developed similar ultimate passive forces to the gravel backfills if allowed to deflect further, computer analyses in Section 6.4 agree that the reduction does pertain to both stiffness and ultimate passive force.

153

GRS soil was expected to yield higher passive resistance than unreinforced backfills because the shear failure plane would need to develop by passing through each textile layer. However, that was not the case for this set of tests. The reduction in passive force due to the GRS backfill compared to gravel was 79% at 3.0 in (7.6 cm) for the 0º tests and 87% for the 30º tests. Combined with the reduction from skew angle, the 30° GRS test reached only 50% of the passive resistance reached by the 0° gravel test at 3.0 in (7.6 cm) of deflection.
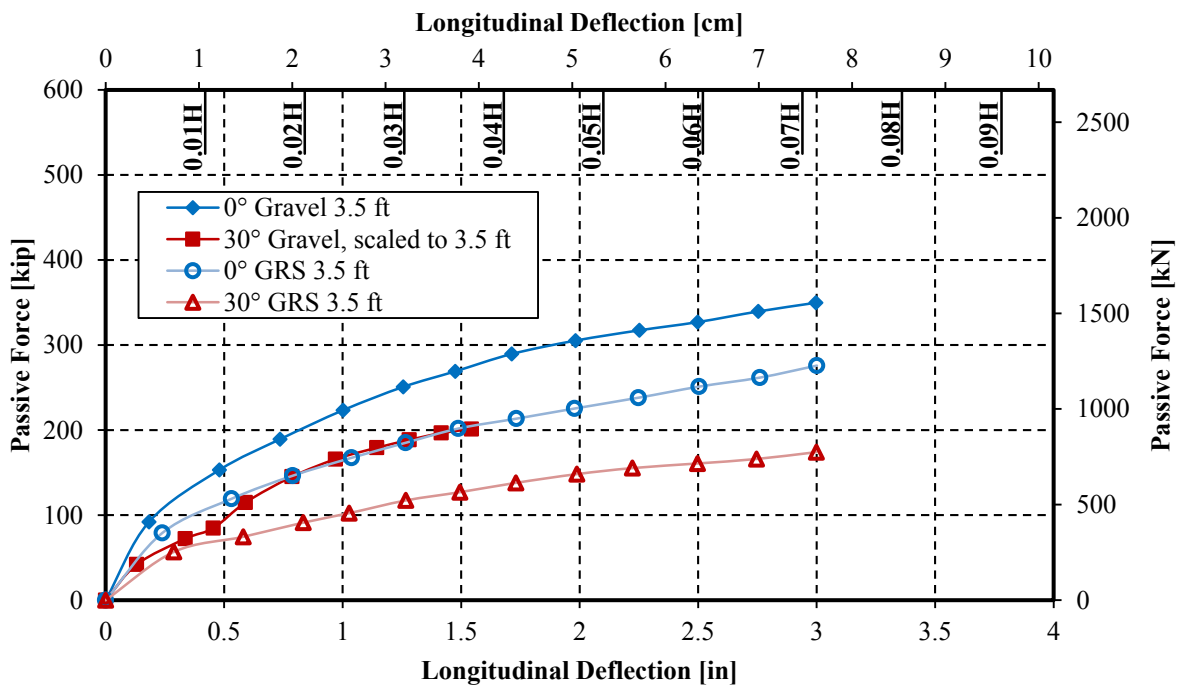
Figure 6-1. Comparison of passive force-deflection curves for unconfined gravel and GRS tests.

When comparing at equivalent displacements instead of at the peak passive force (i.e. the GRS passive force at 0.25 in [0.64 cm] compared to the gravel passive force at 0.25 in [0.64 cm]), the passive force in the GRS backfill for the non-skewed test ranged from 74-86% compared to gravel, with mean and median of 77% and 76%, respectively. The 86% comparison was at 0.25 in (0.64 cm) and the 74% comparison was at three of the four points between 1.25

154

and 2.0 in (3.2 and 5.1 cm). When comparing the 30° tests at equivalent displacements up to 1.5 in (6.4 cm), the GRS passive force ranged from 60-88% compared to gravel, with mean and median respectively 67% and 63%. The 88% reduction occurred again at the 0.25 in (0.64 cm) deflection, and the 60% comparison was from 0.75 to 1.0 in (1.9-2.5 cm).

The overlap of the skewed gravel curve and the non-skewed GRS curve in Figure 6-1 is interesting, but to the best of the author's knowledge, it is probably coincidental. It represents that compared to a non-skewed abutment with gravel backfill, either a 30° skewed abutment or GRS reinforcement will lower passive force resistance by about the same proportion up to 1.5 in (3.8 cm); otherwise there is little significance of the correlation between the two tests.

Of the possible explanations for the reduced resistance in these GRS tests, one major consideration is the possibility that the friction at the concrete-fabric interface was lower than the friction between the concrete and the soil. The direct shear test on fabric (Subsection 3.5.2.2) and PYCAP analyses (Section 6.4) confirm this. Because the ultimate passive force is highly dependent on the interface friction on the wall, a decrease in wall friction would likely lead to a significant reduction in passive force. Although the geotextile may have increased the passive resistance as the shear surface moved through the backfill as desired, the reduction in the wall friction might have ultimately decreased the resistance. Though not investigated directly in this study, based on the work of Tuna and Altun (2012), a reduction of internal friction due to the geotextile-gravel interface may have been present as well. Internal friction reduction along the fabric-soil interface may have introduced shear planes prematurely into the backfill along the planes of the geotextile.

Additionally, GRS reinforcing becomes more beneficial as confining pressures increase due to increased friction (Tuna and Altun, 2012); however in the relatively shallow depth of soil

155

directly behind a bridge abutment, those confining pressures were likely relatively small. Therefore, the fabric in the GRS may not have contributed to the extent desired. Lastly, while geotextile is very strong in tension, but buckles under compression. It is possible that bending of the geosynthetic sheets may have occurred as the shear plane intersected the sheets and movement at the intersection may have been insufficient to fully mobilize the tensile resistance of the fabric, as illustrated in Figure 6-2. Possible local buckling next to the pile cap may have also been present. Also, compaction was difficult near the backwall, particularly near both skew corners due to the geometry of the sheets prior to folding and could have been compromised. Other factors may apply, but these four mechanisms appear to be reasonable causes for the observed variation.
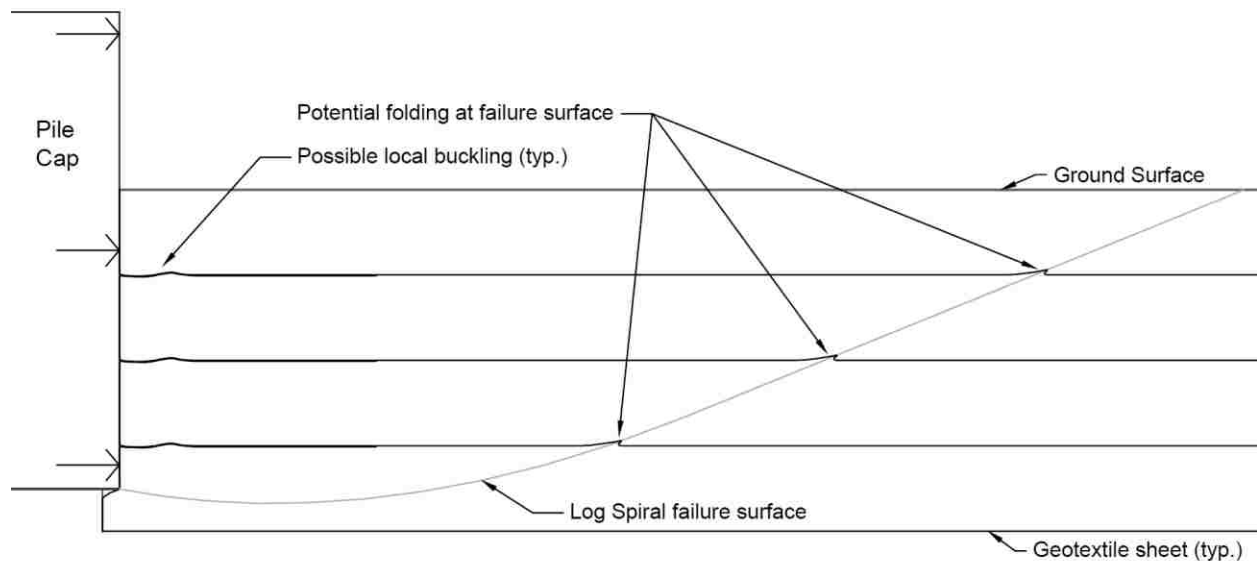
Figure 6-2. Schematic of possible bending in geotextile sheets along failure surface and possible buckling in fabric adjacent to pile cap.

Figure 6-3 shows the passive force reduction factor chart showing the reduction curve from Rollins and Jessee (2013) including the reduction factors from both sets of gravel field tests

156

from this study. As explained previously, the skew reduction factors from the measured data for the unconfined gravel tests was 0.58 and for the GRS tests was 0.63. As can be seen from Figure 6-3, Equation (1-1) predicts 53% for a 30° skew angle as the passive force reduction factor compared to the 0° skew case. These results suggest that the reduction factor might be somewhat higher for gravel than for sands. Comparison of these results with skewed field tests in sand will be at the end of this comparison section, in Subsection 6.1.4.
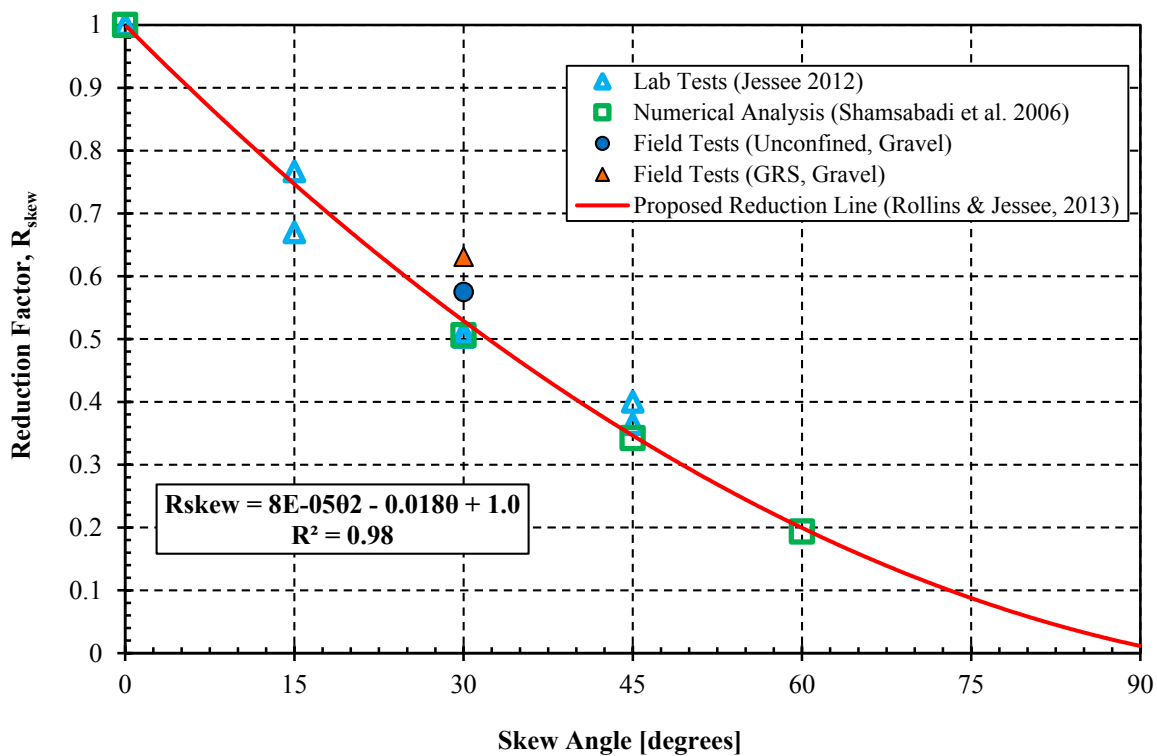
Figure 6-3. Reduction factor, R_{skew} (passive force for a given skew angle normalized by passive force with no skew) plotted versus skew angle based on lab tests (Rollins and Jessee 2013), numerical analyses (Shamsabadi et al. 2006), and results from field tests in this study.

6.1.2   Shear Forces vs. Transverse Displacement

Figure 6-4 shows the relationship between the applied shear force (P_T) and pile cap shear resistance (P_R) versus transverse pile cap displacement for both 30° skewed tests. The shear force

and shear resistance for the gravel test were calculated from the scaled passive force, and the displacements were scaled by wall height to 3.5 ft (1.07 m) fill, as explained in Section 4.3. The applied shear force was computed using Equation (2-5) and the shear resistance was calculated using Equation (2-11), as explained previously. Ignoring the back and forth in the transverse displacement for the gravel test from the cyclic loading, the stiffnesses of the applied shear force are somewhat similar beyond 0.1 in (0.25 cm) transverse movement. Because passive force and transverse force are related according to the equations of Burke Jr (1994), the passive force reduction in the GRS test compared to the gravel test is also visible in the shear forces.

Each point shown in Figure 6-4 represents 0.5 in (1.3 cm) of longitudinal movement, except for one additional point at 0.25 in (0.6 cm) longitudinal displacement for each test, included to better identify initial stiffnesses. The maximum applied shear force occurred at about 1.5 in (3.8 cm) of longitudinal scaled displacement for the gravel test and about 3.0 in (7.6 cm) of longitudinal displacement for the GRS test. By assuming no cohesion in the gravel, as will be discussed in the PYCAP discussion in Subsection 6.4.1, the only difference in the applied shear force and shear resistance equations is that shear force is based on the angle of the skew (θ) and the shear resistance is based on the angle of wall friction, (δ). So, for the gravel, which was assumed to have an interface friction angle of 30.2°, the shear resistance was a little bit greater than the applied shear force at the 30° skew. On the other hand, The 25.8° wall friction angle assumed for the GRS interface was smaller than the skew angle of 30°, so the GRS shear resistance was lower than the applied shear force. Therefore, it would be expected for the GRS test, which had lower shear resistance, to displace more transversely with increased applied force than the gravel test. However, this was not the case. It is interesting to note that despite the GRS test doubling the scaled longitudinal movement of the gravel test, the maximum applied shear

158

force was developed with displacements of approximately 0.2 in (0.5 cm) for both tests. Therefore, there must be more to the transverse movements and resistances than is understood at this time.
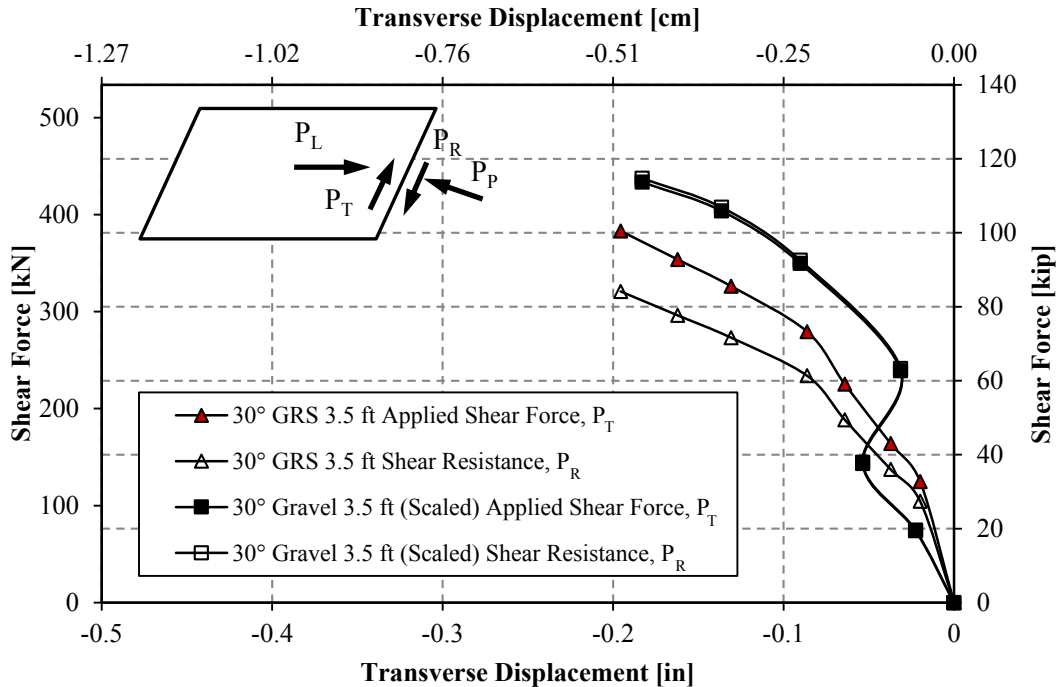
Figure 6-4. Applied shear force and pile cap shear resistance versus transverse displacement for the 30° skew tests.

6.1.3   Comparison to Other Granular Soil Backfills

The gray and blue shaded areas of Figure 6-5 represent normalized dense sand and gravel data, respectively, as gathered by Meyer (2012) and explained in Section 2.5. The shaded bands represent the general shape of previous testing. On the y-axis, passive force is normalized by the maximum passive force of each individual test, and the on the x-axis, lateral deflection (y) is normalized by wall height (H). As can be seen in Figure 6-5, previous testing peaked within the range of approximately 2-5.5% of wall height.

159
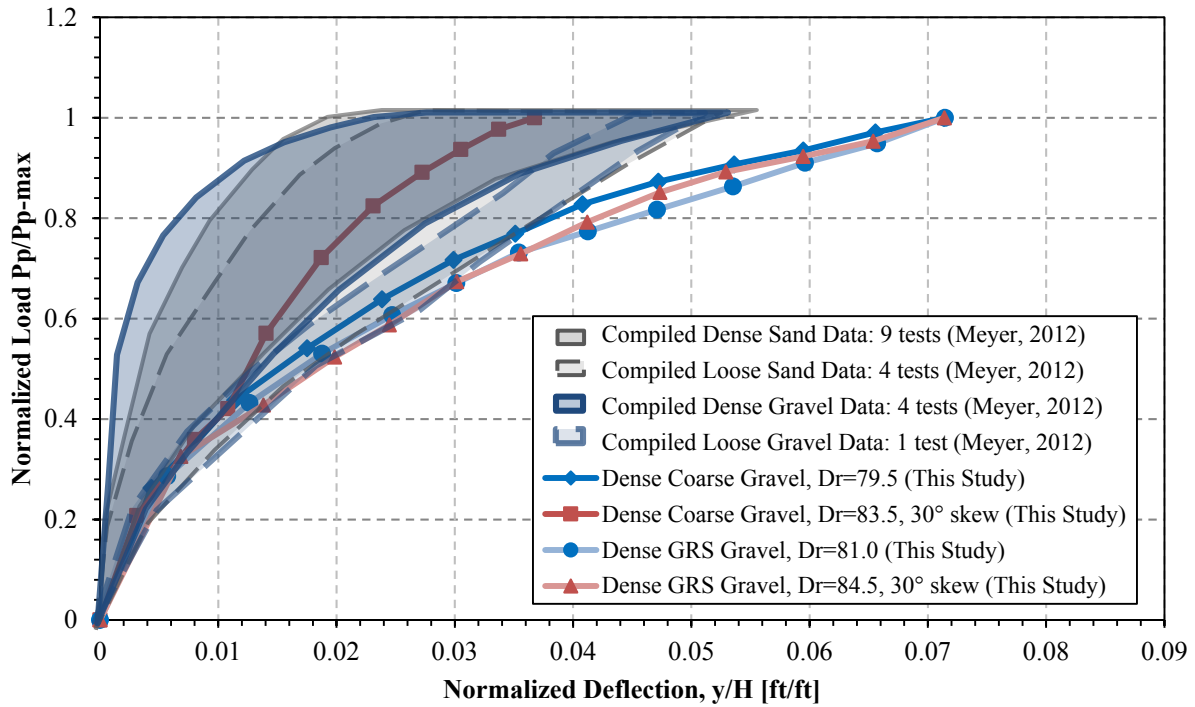
Figure 6-5. Normalized test results compared to other normalized sand and gravel results (see Section 2.5)

Of the four tests, only the skewed gravel test reached or nearly reached its peak within the shaded bands in Figure 6-5. The other three tests were outside the general pattern of previous testing in dense materials due to their failure to peak before 7% of wall height. This demonstrates that the high deflection required for failure in these tests was unusual, particularly for the unreinforced gravel. Of the three tests, the shallower slope of the non-skewed gravel test at maximum deflection suggests it was somewhat closer to failing than the GRS tests. Why the gravel took greater deflection to develop in this test is unknown. Possible errors in the baseline as previously discussed could be a major contributing factor. The increase of deflection required for passive force failure in the GRS gravel was likely due to lower stiffness, as discussed previously.

160

It is interesting to note the very close agreement between the two GRS curves when normalized by maximum passive force. This suggests the only reason for the actual reduction in passive force is the skew. Beyond initial stiffness, there is not similar agreement for the unconfined gravel tests.

6.1.4   Comparison to Previous Skewed Tests in Sand

Skewed abutment testing previously performed at the BYU test site consisted of several configurations of poorly graded sand (SP) backfills: 5.5 ft (1.68 m) tall unconfined (Marsh, 2013), 3.0 ft (0.91 m) unconfined (Palmer, 2013), 5.5 ft (1.68 m) MSE walls (Franke, 2013), and 5.5 ft (1.68 m) reinforced concrete (RC) wingwalls (Smith, 2014). The tests performed thus far have ranged from non-skewed to 45° skews. The results of the non-skewed tests are combined in Figure 6-6 with the non-skewed 3.5 ft (1.07 m) unconfined gravel tests and the GRS tests from this study. Despite the lower backfill height, the unconfined gravel developed greater passive resistance than did the RC wingwall test in sand up to 3.0 in (7.6 cm) of deflection.

For improved comparison, the gravel and GRS tests were scaled up in the manner described in Chapter 4 to project what the passive resistance would have been for 5.5 ft (1.68 m) of fill. Because Equations (4-2) and (4-3) were manipulated to scale 5.5 ft (1.68 m) data down to 3.5 ft (1.09 m), they were re-manipulated to scale 3.5 ft (1.07 m) data up to 5.5 ft (1.68 m) data in Equations (6-1) and (6-2).

$$P_{P(5.5ft)} = \left[\frac{(5.5\text{ft})^2}{(3.5\text{ft})^2}\right] P_{P(3.5ft)} \tag{6-1}$$

$$d_{(5.5ft)} = \left[\frac{5.5\text{ft}}{3.5\text{ft}}\right] d_{(3.5ft)} \tag{6-2}$$

161

The 3.0 ft (0.91 m) sand test was not scaled to 5.5 ft (1.68 m) for comparison because there is already data for a test of 5.5 ft (1.68 m) of unconfined sand.
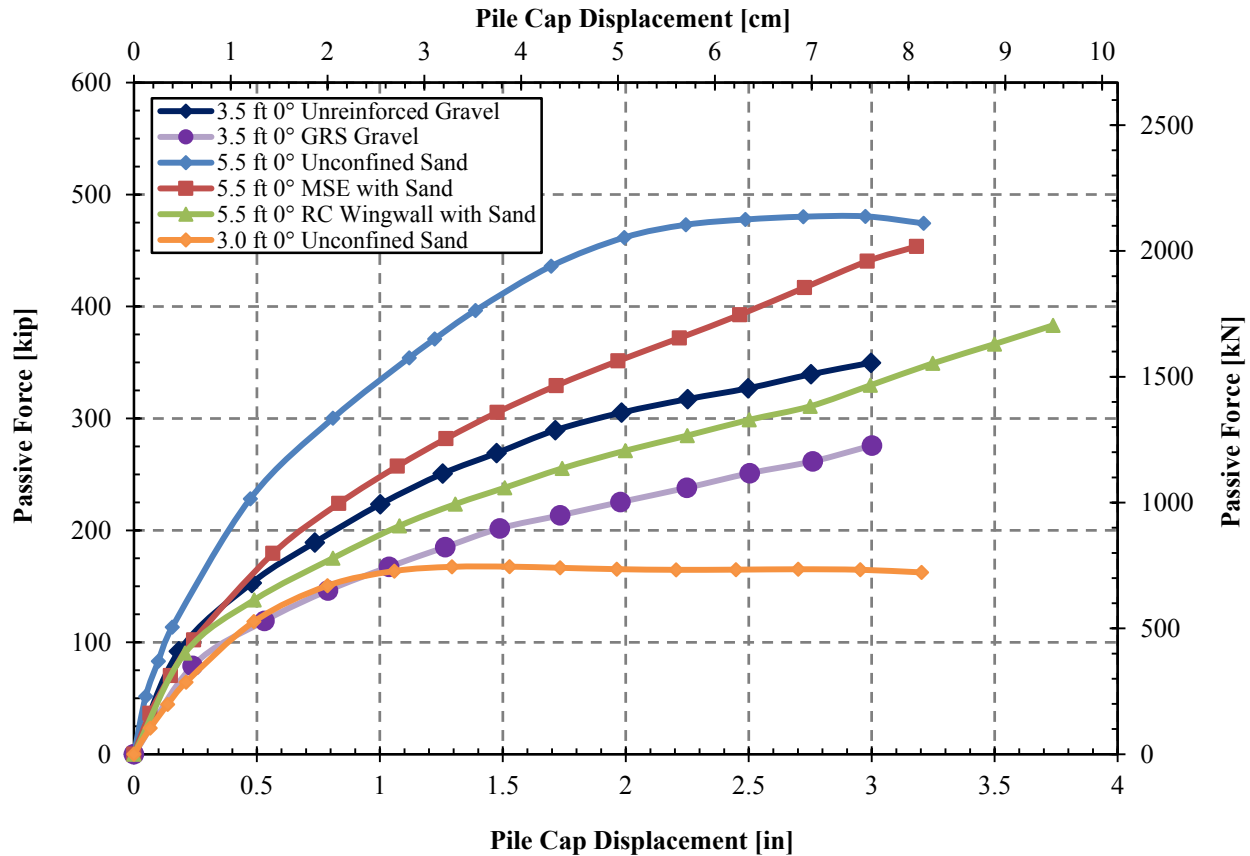
Figure 6-6. Comparison of passive force-deflection curves for all non-skewed tests performed at the BYU test site. Tests were performed at varying heights.

Figure 6-7 shows the six non-skewed tests standardized to 5.5 ft (1.68 m) of fill. The unreinforced gravel test is clearly the strongest at all displacements. At 4.7 in (12.0 cm) of scaled displacement, the gravel test would be expected to developed approximately 860 kips (3840 kN) of passive resistance and the GRS test would have developed approximately 680 kips (3030 kN). In contrast, the unconfined sand test reached a maximum passive force of 480 kips (2140 kN), the MSE wall test a maximum of 450 kips (2000 kN), and the RC wall test a maximum of 380 kips (1700 kN). Thus the unconfined gravel exhibited 80% more passive resistance than the

unconfined sand test. At its peak, the GRS backfill exhibited 42% more passive resistance than the unconfined sand test. However, the unconfined sand curve and the scaled GRS passive force curve match each other very closely up to 2.0 in (5.8 cm) of deflection, when the stiffness of the unconfined sand backfill decreased significantly and then peaked. On the other hand, the GRS backfill continued to develop passive resistance with increasing deflection, and more closely resembles the shape of the tests with MSE and RC walls. Thus, though the geotextile seems to have decreased the internal and interface friction of the gravel, the benefits of the reinforcement are seen with increased deflections. Further comparisons between the tests are summarized in Table 6-1. The table is read so that the test on the left is compared to the test in each column as a ratio. For example, since the GRS peak passive force was 79% of the unconfined gravel peak, the ratio is 0.79.

Table 6-1: Comparisons of Peak Passive Force for 0° Skew Tests Standardized to 5.5 ft (1.68 m) Backfill Height

Test	Peak Passive Force [kip (kN)]	Test Comparison				
		Unconfined Gravel (GW)	GRS with Gravel (GW)	**Unconfined Sand (SP)**	MSE Walls in Sand (SP)	RC Wingwalls in Sand (SP)
Unconfined Gravel (GW)	864 (3843)	1	1.27	**1.80**	1.92	2.26
GRS with Gravel (GW)	681 (3030)	0.79	1	**1.42**	1.51	1.78
Unconfined Sand (SP)	480 (2140)	0.56	0.70	**1**	1.07	1.25
MSE Walls in Sand (SP)	450 (2000)	0.52	0.66	**0.94**	1	1.17
RC Wingwalls in Sand (SP)	383 (1700)	0.44	0.56	**0.80**	0.85	1

163
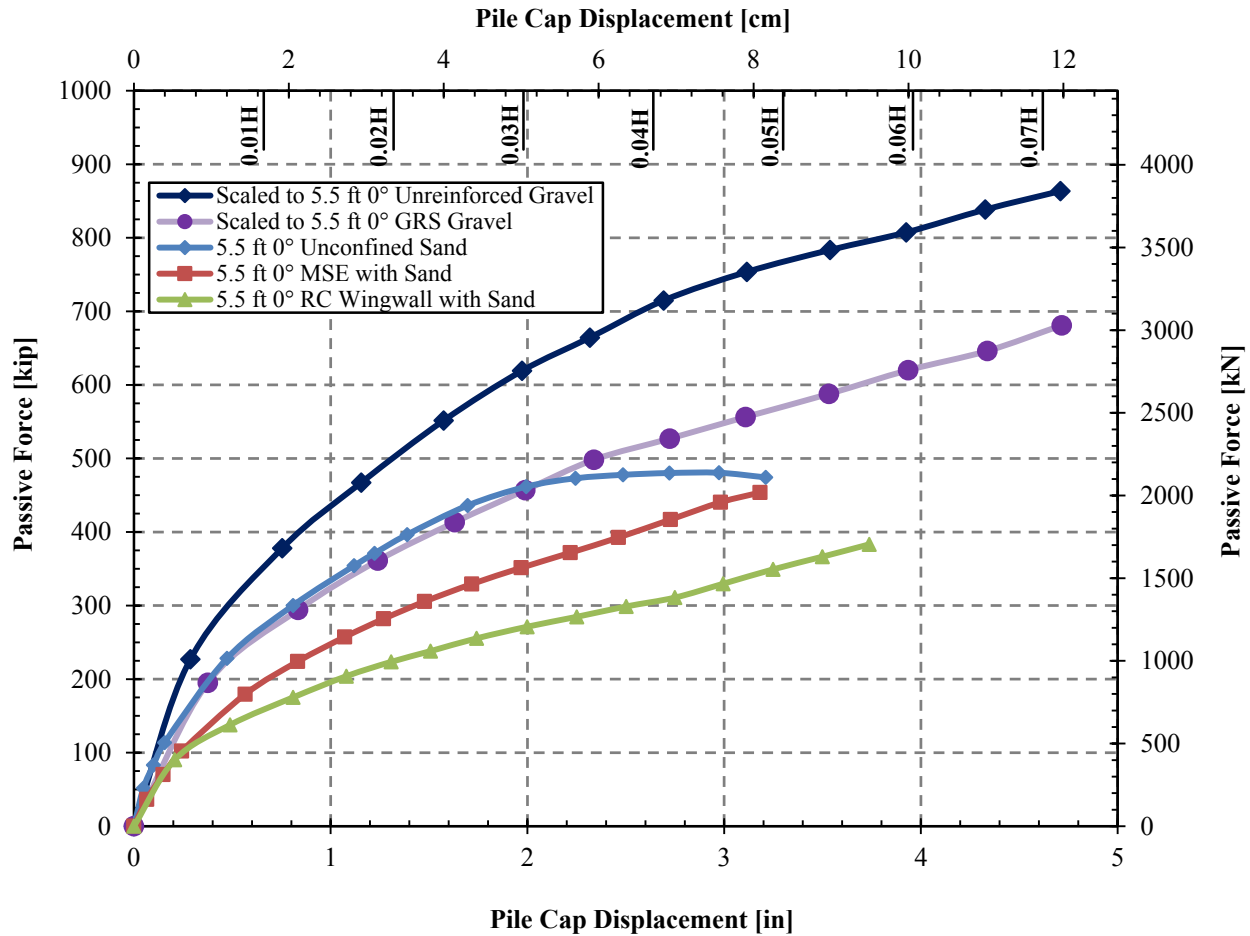
Figure 6-7. Comparison of passive force-deflection curves for non-skewed tests performed at the BYU test site. Gravel and GRS tests were scaled to 5.5 ft (1.68 m) backfill heights.

All of the previously mentioned test configurations in sand backfill were also tested with a 30° skew backwall except for the RC wingwall configuration. The results of the three 30° tests in sand and two 30° tests in gravel are shown in Figure 6-8. For consistency's sake, the unreinforced gravel test is shown with its scaled data. Again, though the unconfined gravel test was at a lower backfill height, its peak passive resistance was considerably close to the resistances of the sand tests. Both the tests with gravel had higher resistances than the 3.0 ft (0.91 m) test in sand.

164
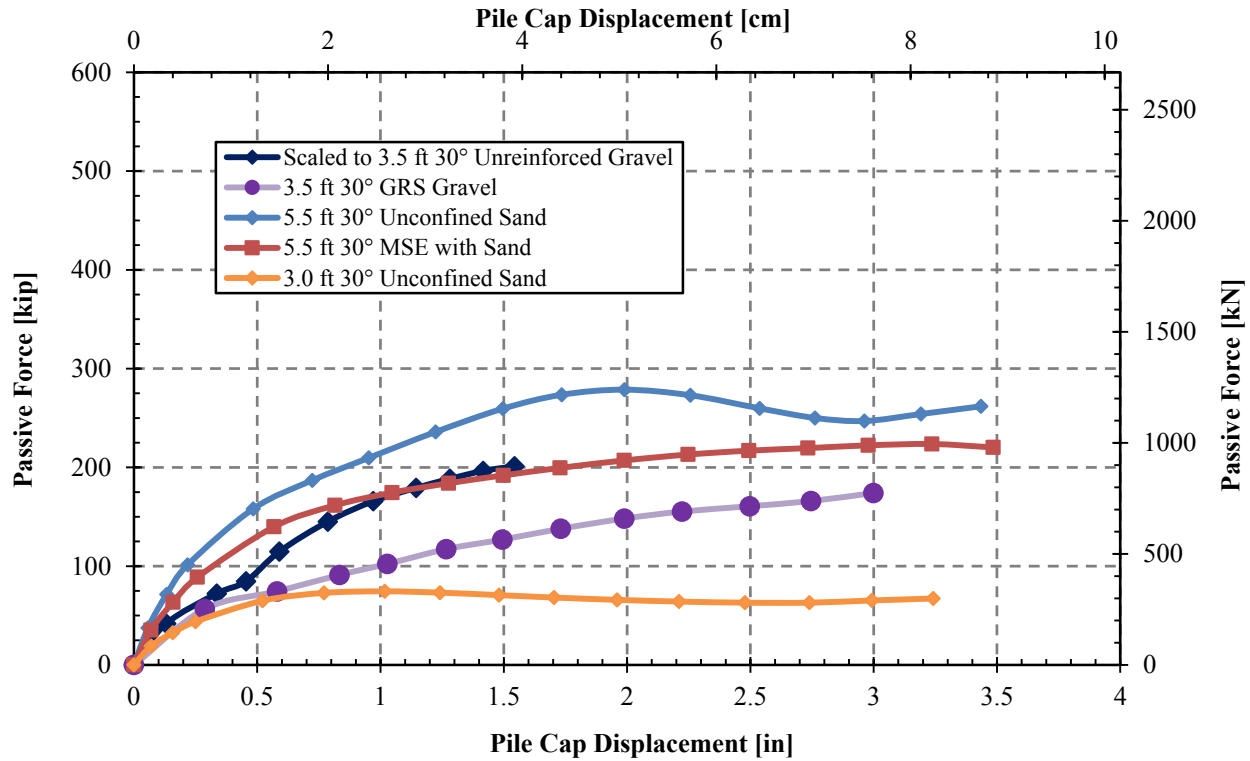
Figure 6-8. Comparison of passive force-deflection curves for all 30° skewed tests performed at the BYU test site. Tests were performed at varying fill heights.

Figure 6-9 shows the results of the 30° tests, standardized to 5.5 ft (1.68 m) of fill. Because the skewed unconfined gravel test was originally tested to 5.5 ft (1.68 m), it is shown in this figure as measured. The GRS data was scaled with Equations (6-1) and (6-2) as it was for the non-skewed tests in Figure 6-7. The unconfined gravel test once again had the highest passive resistance, 497 kips (2210 kN) at its peak, which was 78% higher than the unconfined sand peak at 279 kips (1240 kN). The scaled GRS data was 430 kips (1910 kN) at its peak at 4.7 in (11.9 cm) deflection. The GRS developed approximately 54% more passive resistance than the unconfined sand test and 92% more than the MSE wall test. Further comparisons between the tests are shown in Table 6-2 on page 166. Again, each test on the left is compared against the test at the column heading in ratio form, so that, for example, the peak passive force for the 30° GRS test divided by the peak for the unconfined gravel test was 0.87.

165

Table 6-2: Comparisons of Peak Passive Force for 30° Skew Tests Standardized to 5.5 ft (1.68 m) Backfill Height

Test	Peak Passive Force [kip (kN)]	Unconfined Gravel (GW)	GRS with Gravel (GW)	**Unconfined Sand (SP)**	MSE Walls in Sand (SP)
			Test Comparison		
Unconfined Gravel (GW)	497 (2210)	1	1.16	**1.78**	2.22
GRS with Gravel (GW)	430 (1910)	0.87	1	**1.54**	1.92
Unconfined Sand (SP)	279 (1240)	0.56	0.65	**1**	1.25
MSE Walls in Sand (SP)	224 (996)	0.45	0.52	**0.80**	1
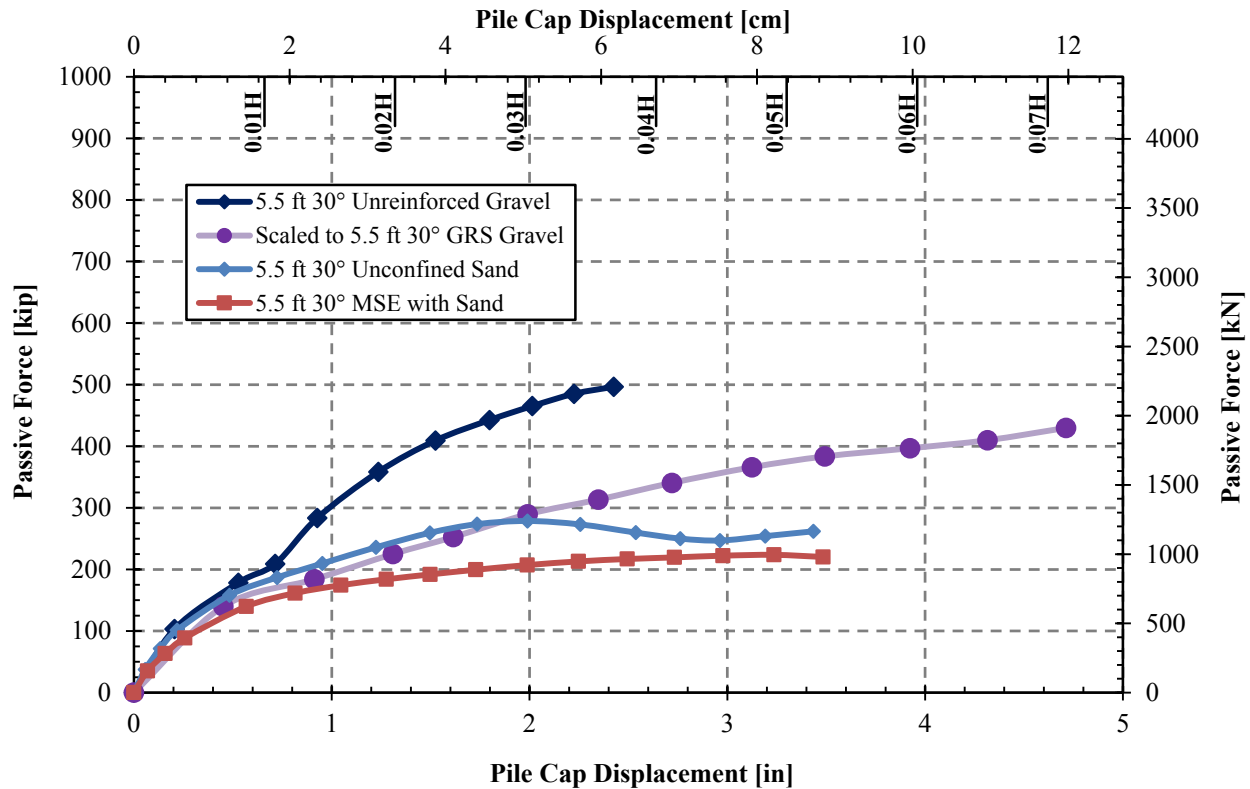
Figure 6-9. Comparison of passive force-deflection curves for 30° skewed tests performed at the BYU test site. The GRS test was scaled to backfill height 5.5 ft (1.68 m).

Figure 6-10 shows the passive force reduction factor chart showing the reduction curve from Rollins and Jessee (2013) and the passive force reduction factor, R_{skew}, plotted against skew angle for all skewed tests performed. Included in the figure are lab tests from Jessee (2012), all

field tests, and the numerical analysis performed by Shamsabadi et al. (2006). The results from this study suggest that R_{skew} may be somewhat higher backfills using gravel. However, this plot reveals that the variation of the gravel and GRS tests from the predicted passive force reduction curve is well within the scatter of test results. Additional tests with gravel backfill would be necessary to fully reveal whether the higher reduction values in this study are an indication of necessary adjustments to R_{skew} for gravel backfills or simply a result of statistical scatter.

Passive force reductions among field, laboratory, and numerical analyses agree very well. Table 6-3 summarizes the mean of the laboratory and the field tests individually and collectively. The collective mean weighs the field tests more heavily due to more field tests having been performed; however, each test is equally weighted. In lab and field testing, the average 15°, 30°, and 45° passive force reductions due to skew were 72%, 53%, and 36%, respectively. Also shown in Table 6-3 are the predicted values from Rollins and Jessee (2013) and the difference between the test average and the predicted average. Remarkably, the predicted 15°, 30°, and 45° reductions due to skew were 75%, 53%, and 35%, respectively. The difference between the actual and predicted reductions due to skew for the 15°, 30°, and 45° skews were 3%, 0%, and 1%, respectively. The average error between predicted and measured values was 2.3%.

Table 6-3: Summary of Mean R_{skew} Values for Lab and Field Tests Compared to Predicted Values from Equation (1-1)

Angle of Skew	Average (Lab Tests)	Average (Field Tests)	Average (All Tests)	Predicted	Difference	*% Error*
0°	1	1	**1**	**1**	**0.00**	*0.0*
15°	0.72	0.72	**0.72**	**0.75**	**0.03**	*4.0*
30°	0.51	0.54	**0.53**	**0.53**	**0.00**	*0.0*
45°	0.38	0.35	**0.36**	**0.35**	**0.01**	*2.9*
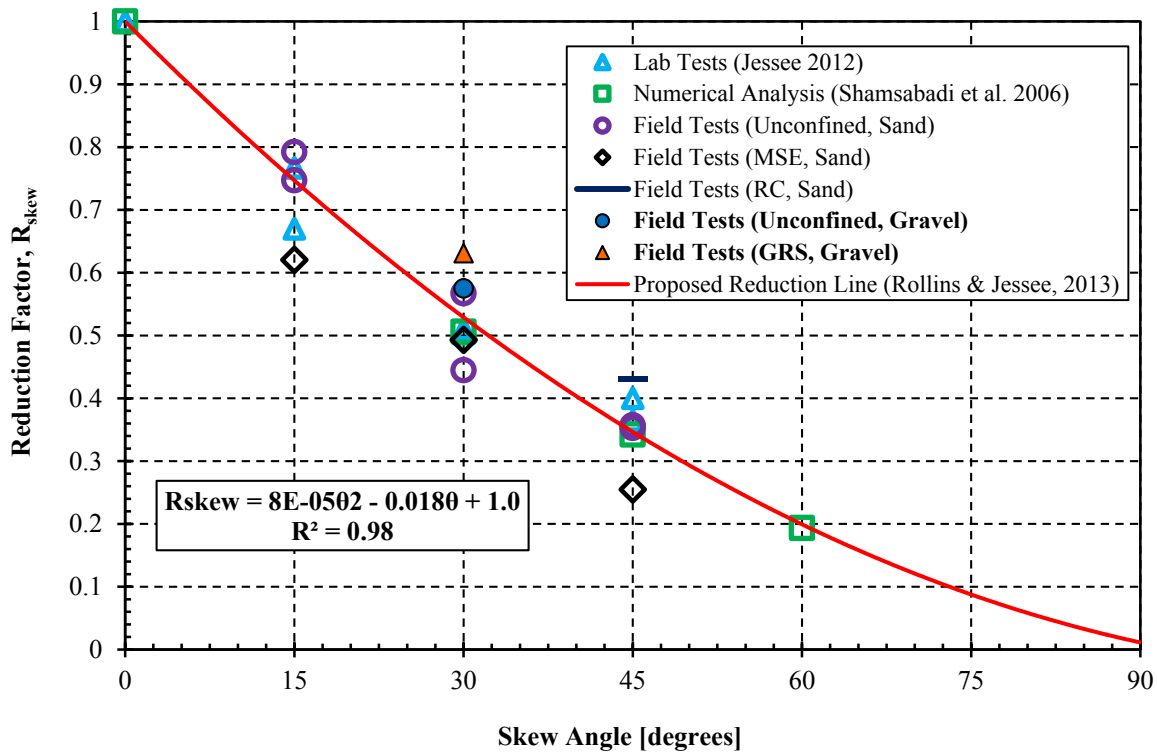
Figure 6-10. Summary of passive force reduction factors for all skewed tests compared to the reduction line proposed by Rollins and Jessee (2013).

6.2 A Short Note about Conservatism in Passive Force Design

When predicting passive force, it is best to be as accurate as possible for all deflections. Many design engineers are accustomed to the idea that to under-predict passive force behavior is a more conservative approach for passive force design. This assumption is valid for classic passive force conditions: When there is uncertainty in movement of the bridge in relation to the soil, it is better to have more passive force capacity available than expected than it is to have less. However, in cases of lateral spreading under each abutment, the soil will be moving in relation to the structure, and too much passive force capacity will damage the bridge foundations. In these cases, excessive passive force capacity is more likely to cause damage to the bridge, and overpredicting passive force would actually be the more conservative design.

168

While most design engineers are worried about the former, more classic case of bridge movement in relation to unmoving soil, it should be noted that excessive passive force capacity is actually unfavorable. It is better to be as close to be as accurate as possible for passive force design. Thus, comments on the conservatism of each of the following design methods will be withheld, and discussion will instead address error through either underprediction or overprediction of passive force.

6.3 Bilinear Design Curves

Caltrans and AASHTO are two bilinear methods commonly used for passive force-deflection design. This section will compare the passive force results from this study to the predicted passive force-deflection curves from Caltrans (2010) and AASHTO (2014). For both methods, the effective width was applied simply as the width of the backwall because it is Caltrans (2010) designates it as such in and AASHTO (2014) leaves it unspecified.

6.3.1 Caltrans (2010) Design

Caltrans recommends a bilinear method to define the passive force-deflection curve for design of bridge abutments. Due to relative densities of 79-85% and a friction angle over 45°, the gravel soil was well within the Caltrans specifications of 30+ blow counts at deeper depths (Caltrans, 2010; Meyerhof, 1956) and therefore qualified for the higher K_i stiffness of 50 kip/in/ft (28.70 kN/mm/m). The lower stiffness (25 kip/in/ft, 14.35 kN/mm/m) will also be shown for reference. Bilinear passive-force deflection curves with both stiffnesses are plotted in Figure 6-11 against the results of the four tests from this study. The higher design stiffness matched the initial stiffnesses of the non-skewed tests rather closely—a little low for the gravel test and a little high for the GRS test. The lower rather than the higher stiffness matched the 30°

169

gravel test more closely. However, even the lower stiffness was about twice the measured stiffness of the 30° skewed GRS test.

The ultimate passive pressure force was calculated by the Caltrans method was 122.5 kip (539.2 kN) by using the wall width as the effective width, as illustrated in the Caltrans (2010) Seismic Design Manual. The error from using actual width instead of effective width would be proportionally smaller on an actual abutment, which are generally much longer than the 11 ft (3.35 m) width of the pile cap used in this study. The observed effective widths of 16-19 ft (4.9-5.8 m) for the four tests in this study compared to the actual width of the pile cap, 11 ft (3.35 m), agrees well with PYCAP's predicted 3D factor of about 1.7. To find the passive force using the effective width, multiply the passive force calculated from the actual width, shown in this section, and multiply it by 1.7 (see Equation (2-3).
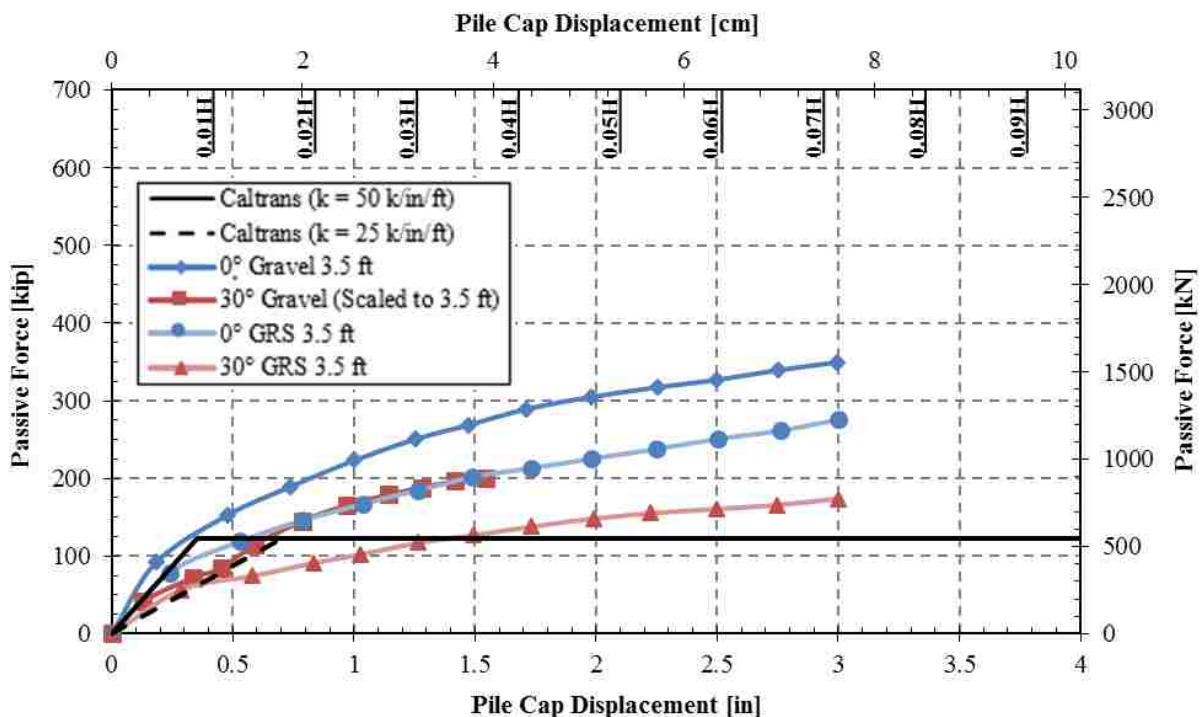
Figure 6-11. Comparison of Caltrans (2010) design passive force-deflection to measured data.

Because the Caltrans (2010) is based primarily on sand backfills and does not account for gravel in its calculation of ultimate passive force, it predicted ultimate passive force very low for all four tests in this series due to the high strength of the gravel. The Caltrans approach is designed to be conservative, but underpredicting passive force is not always conservative, as discussed in Section 6.2. The measured resistance ranged from 42% to 185% above the ultimate peak force. Therefore, the Caltrans approach underpredicts ultimate passive force for all four gravel backfills in this study and extremely underpredicts passive force for non-skewed gravel-backfill abutments.

6.3.2 AASHTO (2014) Design

AASHTO (2014) does not specify a value of Δ/H for development of peak passive pressure for gravel. For dense sand it is specified as 0.01, or 0.05 as an estimate assumed to be traditionally conservative. As with the Caltrans (2010) method, several stiffnesses will be compared, corresponding to Δ/H values from 0.01 to 0.05. Also, AASHTO only gives a passive pressure equation; it does not outline what should be used to define the effective width. The actual pile cap width is used as the effective width in this section. As mentioned in the previous section, using the actual width versus the effective width has less effect on very wide structures. The pile cap used in this study is a much shorter structure than an actual bridge abutment. The observed effective widths of 16-19 ft (4.9-5.8 m) for the four tests in this study compared to the actual width of the pile cap, 11 ft (3.35 m), agrees well with PYCAP's predicted 3D factor of about 1.7. To find the passive force using the effective width, multiply the passive force calculate from the actual width, shown in this section, and multiply it by 1.7 (see Equation (2-3).

The AASHTO (2014) design method, in contrast to the Caltrans (2010) method, does take soil properties into consideration when designing for passive force by using the log spiral

171

method, which is dictated by both interface and soil friction angles. The log spiral method was calculated using the graphical method; however, the log spiral graph in Figure 3.11.5.4-2 of AASHTO (2014) only includes friction angles up to 45°. Thus, 45° was used as the friction angle to determine the coefficient of passive pressure, K_p.

AASHTO (2014) recommends using an interface friction angle ranging 22° to 26° for the interface between formed concrete and gravel mixtures (see Table 2-2). On the other hand, Potyondy (1961) found 0.76 to be the minimal δ/φ ratio for sand. Figure 6-12 shows the AASHTO design with a wall friction angle of 26° ($\delta/\varphi=0.58$) while Figure 6-13 shows it with a wall friction of 32° ($\delta/\varphi=0.7$). PYCAP analyses suggest actual wall friction angles for this study were approximately 30° ($\delta/\varphi=0.66$) for gravel and 26° ($\delta/\varphi=0.58$) for GRS backfills.

For the GRS wall friction angle of 26° ($\delta/\varphi=0.58$) shown in Figure 6-12, the ultimate passive force calculated was 187 kips (832 kN). This value corresponds well with both skewed tests in this study, within 10% low of the gravel test and 10% high of the GRS test. The gravel and GRS non-skewed tests were 47% and 87% above this estimate, respectively. Δ/H values to develop peak resistance were above 0.01 in all cases, and all but the skewed GRS test were stiffer than a Δ/H value of 0.05. The non-skewed gravel test corresponded to a stiffness with Δ/H between 0.01 and 0.02. The skewed gravel and non-skewed GRS tests both corresponded to stiffnesses with Δ/H a little higher than 0.02.
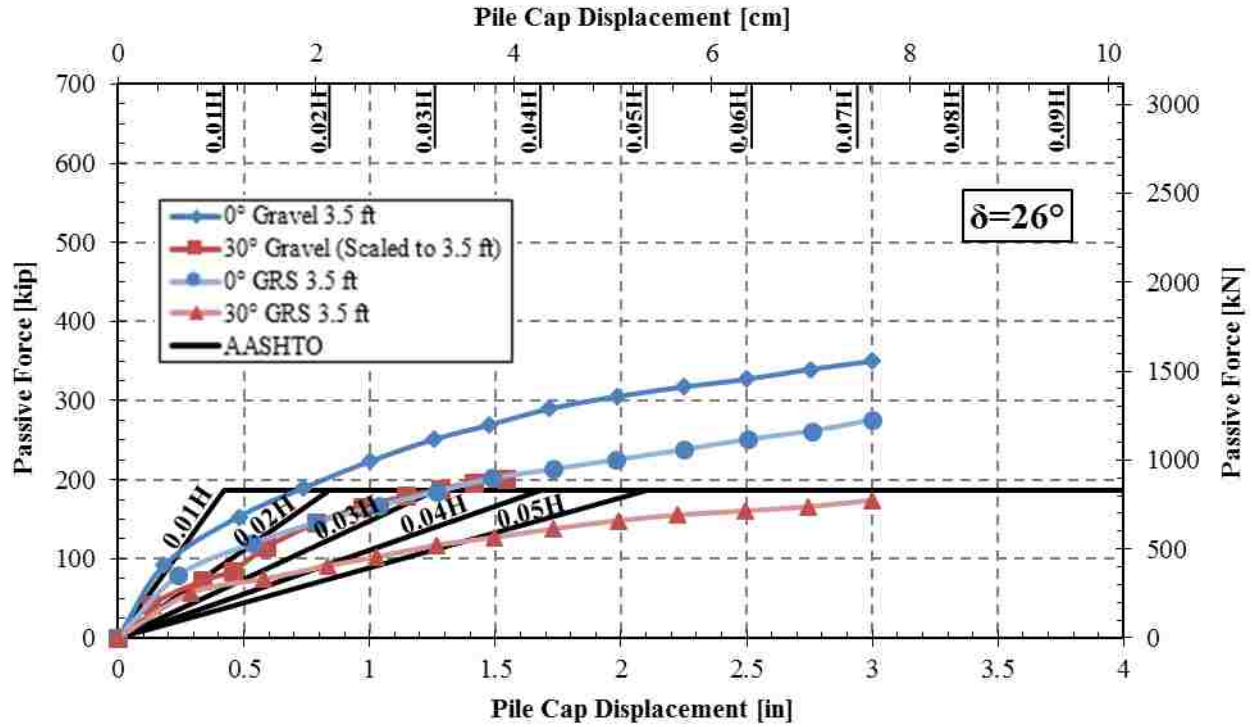
Figure 6-12. Comparison of AASHTO (2014) design passive force-deflection to measured data for δ=26° (δ/φ=0.58) with varying Δ$_{max}$ values.

For the gravel wall friction angle of 32° (δ/φ=0.7) shown in Figure 6-13, the ultimate passive force calculated was 231 kips (1028 kN). This value reflected better the higher strength of the gravel, only underestimating the ultimate passive force for the non-skewed gravel test by 51% and the non-skewed GRS test by 19%. Both 30° skewed tests were under this AASHTO design curve—the gravel by 13% and the GRS by 25%. Δ/H values to develop peak resistance were again between 0.01 and 0.05 in all cases except the 30° skewed GRS test. The non-skewed gravel test corresponded to a stiffness with Δ/H about 0.02. The skewed gravel and non-skewed GRS tests both corresponded to stiffnesses with Δ/H between 0.03 and 0.04.
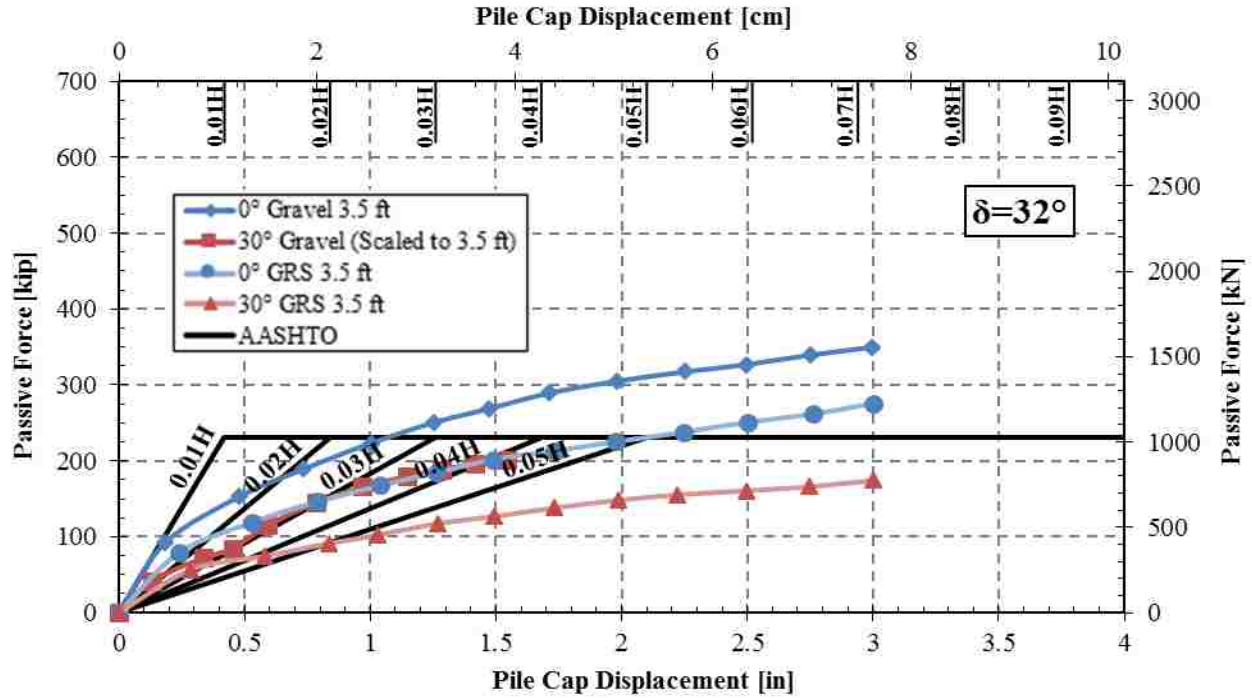
Figure 6-13. Comparison of AASHTO (2014) design passive force-deflection to measured data for δ=32° (δ/φ=0.7) with varying Δ_{max} values.

Thus, 0.02H to 0.03H proved to be a more accurate deflection estimate for developing AASHTO (2014) design passive force in dense gravel. By using the log spiral method to calculate ultimate passive force, AASHTO's estimates were close to the measured peak. The AASHTO peak passive force, however, clearly needs adjustment for the effects of skew. Caltrans (2010) extremely overpredicted ultimate passive force in non-skewed gravel due to its design curve ignoring soil type beyond the initial stiffness. Caltrans approach could be improved if it included some guidelines based on backfill soil type. Although the current design curve was conservative enough for the skewed tests because of the high strength of the gravel, an improved Caltrans design code would also account for skew. Lastly, Caltrans initial stiffnesses were found to be suitable, but skewed tests likely need to use the lower stiffness in order to have better accuracy.

174

6.4   **Computer Program Analyses**

Two computer programs, PYCAP (Duncan and Mokwa, 2001) and ABUTMENT (Shamsabadi et al., 2007), have been developed which use hyperbolic functions based on soil parameters to model passive force-deflection curves. These two programs will be used to compare the data from the two non-skewed tests in this study, both to find which parameter inputs best fit the data and to see how well these methods predict passive force-deflection.

6.4.1   PYCAP

6.4.1.1   Best-Fit Analysis

When performing the PYCAP analysis (Duncan and Mokwa, 2001), most of the input parameters for the best-fit case were determined by the test site configuration or by field or laboratory testing. Table 6-4 shows the inputs used for best-fit curves for both the gravel and GRS tests. The friction angle of the gravel (45.8°) was determined with a field direct shear test (Subsection 3.5.2.1) with only two data points; however, the value makes sense for the type of gravel and fit well in PYCAP. The cohesion measured in the field shear test in gravel was small at 40 psf (1.9 kPa). In order to match parameters with the GRS inputs and the interface direct shear test (Subsection 3.5.2.2), the cohesion was removed completely. The computed curve fit the data favorably without the cohesion term. Poisson's ratio was calculated by PYCAP using Equation (2-7) and the deflection required to reach ultimate resistance ($D_{max}/H = 0.06$) was chosen based on where the measured data peaked. Figure 6-14 shows the best-fit PYCAP curves for both non-skewed tests compared to the measured data.

The two parameters in the gravel test not previously determined through testing were the wall friction angle (δ) and the initial soil modulus (E_i). Because a direct shear test was performed for the GRS interface (Subsection 3.5.2.2), the only unknown for GRS was the initial soil

175

modulus. The wall friction for the GRS tests was lowered from 26.1° from the peak data points of the direct shear test (see Figure 3-30) to 25.8° due to the end-of-test friction angle from the direct shear (see Figure 3-31) being so low and because the slightly lower value fit the data well. The values shown represent δ/φ ratios of 0.66 and 0.56, respectively, which are lower than Potyondy's (1961) minimal values for sand.

The initial soil modulus was best fit to the data. The value recommended by Duncan and Mokwa (2001) for dense compacted sands and gravels is 600 psf (28.7 kPa). Though the initial modulus in the gravel test data was about 550 psf (26.3 kPa), the lower value of 310 psf (14.8 kPa) was selected to match the bulk of the data curve. Similarly, an E_i of 350 psf (16.8 kPa) fit the initial slope of the GRS curve but was lowered to 200 psf (9.6 kPa).

Table 6-4: Best Fit PYCAP Input Values for Gravel and GRS Tests

Soil Strength Parameter	Units	0° Gravel Inputs	0° GRS Inputs
Cap Width, b	ft (m)	11.0 (3.35)	11.0 (3.35)
Cap Height, H	ft (m)	3.5 (1.07)	3.5 (1.07)
Cohesion, c	lb/ft^2 (kPa)	0	0
Soil Friction Angle, ϕ	deg	45.8	45.8
Wall Friction Angle, δ	deg	30.2	25.8
Initial Soil Modulus, E_i	lb/ft^2 (kPa)	310 (14.8)	200 (9.6)
Poisson's Ratio, ν	–	0.22	0.22
Soil Unit Weight, γ_m	lb/ft^3 (N/m^3)	144.9 (18.25)	144.9 (18.25)
Δ_{max}/H at Failure	–	0.06	0.073

176

Figure 6-14. PYCAP best fit passive force deflection curves for non-skewed gravel and GRS tests.

6.4.1.2 Sensitivity Analysis

To illustrate the difference of properties between the gravel and GRS soils, the best-fit PYCAP hyperbola for the unconfined gravel is compared to the GRS test results and the previously outlined GRS best-fit curve in Figure 6-15. The only modification to the unconfined gravel PYCAP curve was changing Δ_{max}/H from 0.06 to 0.073. Once again, a lower initial modulus and wall friction were required to fit the GRS data. In some analyses lowering the internal soil friction angle (φ) instead of the wall friction also brought the hyperbola to close agreement with the GRS curve.

177
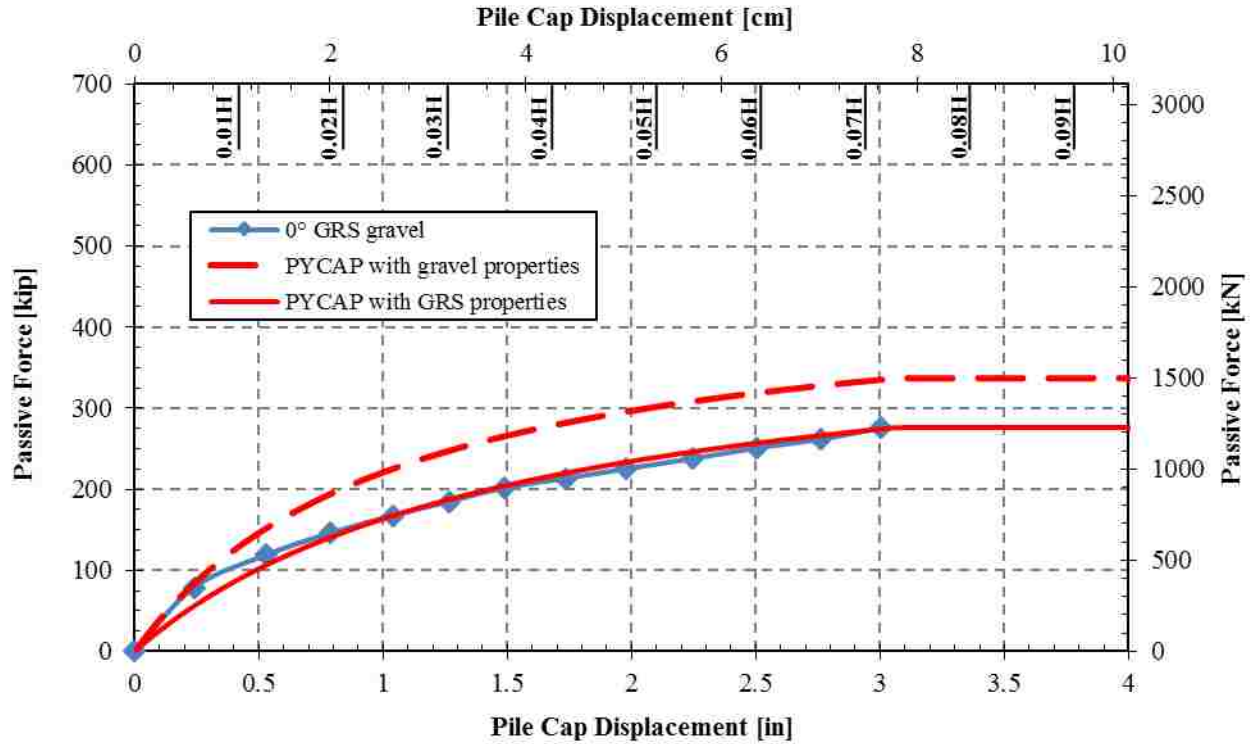
Figure 6-15. PYCAP comparison of gravel backfill properties compared to 0° GRS measured data.

The gravel for this study had both a higher unit weight (γ) and a higher friction angle (φ) compared to the sand used in previous BYU skewed testing. The gravel also had lower cohesion. To determine whether increased unit weight or increased friction angle was more vital to the increased stiffness observed in the gravel compared to the previous sand tests (see Subsection 6.1.4), a sensitivity analysis was performed in PYCAP. In addition to moist unit weight and internal friction angle, wall friction (δ) and cohesion (c) were also included in the sensitivity analysis. The Δ_{max}/H factor at failure for all the analyses was kept at 0.05. The passive force sensitivity results are shown in Table for English units and Table 6-6.

178

Table 6-5: Ultimate Passive Force Sensitivity Analysis Based on Several PYCAP Inputs
(English Units)

P_{ult} (kips)		γ=117.0pcf		γ=144.9pcf	
		c=0psf	c=100psf	c=0psf	c=100psf
φ=42.0°	δ=28.8°	169	**227[1]**	209	267
φ=45.8°	δ=28.8°	256	332	316	394
	δ=30.2°	272	352	**336[2]**	417

[1] – Corresponds to ultimate passive force using properties of BYU sand at Δ_{max}/H = 0.05.
[2] – Corresponds to ultimate passive force using properties of BYU gravel at Δ_{max}/H = 0.05.

Table 6-6: Ultimate Passive Force Sensitivity Analysis Based on Several PYCAP Inputs
(SI Units)

P_{ult} (kN)		γ=14.74N/m^3		γ=18.25N/m^3	
		c=0kPa	c=4.79kPa	c=0kPa	c=4.79kPa
φ=42.0°	δ=28.8°	752	**1010[1]**	927	1188
φ=45.8°	δ=28.8°	1139	1477	1406	1753
	δ=30.2°	1210	1566	**1495[2]**	1855

[1] – Corresponds to ultimate passive force using properties of BYU sand at Δ_{max}/H = 0.05.
[2] – Corresponds to ultimate passive force using properties of BYU gravel at Δ_{max}/H = 0.05.

The sensitivity analysis showed that the increase in moist unit weight from the sand to the gravel had moderate impact on the passive force. Interface friction (δ) also had less, but still moderate, effect on the passive force. The two most sensitive PYCAP inputs, however, were cohesion, c, and internal friction angle, φ. The decreased cohesion in the gravel actually decreased the stiffness by 60-80 kips (265-355 kN), so the sensitivity of the cohesion does not explain the gravel's increased strength compared to sand. The small increase of internal friction angle, from 42.0° to 45.8°, accounted alone for an increase of approximately 90-125 kips (400-555 kN) of passive force. An increase of internal friction usually also signifies an increase in interface friction (Potyondy, 1961). The increased interface friction angle accounted for an additional 15-20 kips (65-90 kN) of passive force. The relatively large increase of moist unit weight from sand (117.0 pcf or 14.74 N/m^3) to gravel (144.9 pcf or 18.25 N/m^3) accounted for an increase of 40-65 kips (180-290 kN). Therefore, both increased friction angle and

179

increased unit weight were responsible for the increased passive strength observed in the gravel, with friction angle having about twice the effect of the unit weight.

6.4.1.3 Skew

Because PYCAP has no evaluation of skew, a manual reduction of the PYCAP curve was calculated with the R_{skew} factor (Rollins and Jessee, 2013) and compared with the skewed test data. Otherwise the inputs remained the same, except for the Δ_{max}/H factor for the skewed gravel test. The resulting curves are shown in Figure 6-16 for the gravel results and Figure 6-17 for the GRS results. Though R_{skew} is based on peak passive force values, the agreement across the whole curve was very good in both cases. For the gravel tests in Figure 6-16, the Δ_{max}/H factor was changed to 0.35 prior to applying the reduction factor to the data. All four best-fit PYCAP curves are plotted with the measured data in Figure 6-18.
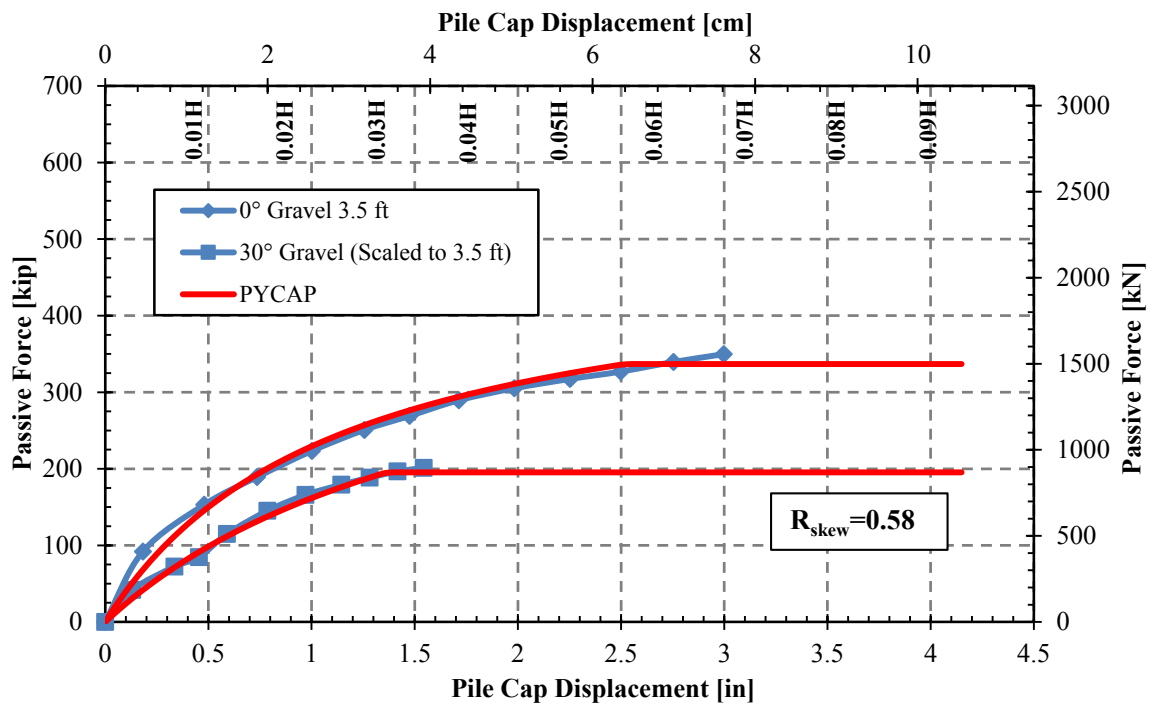
Figure 6-16. Gravel PYCAP curves with R_{skew} based on peaks and 0° and 30° data.

180
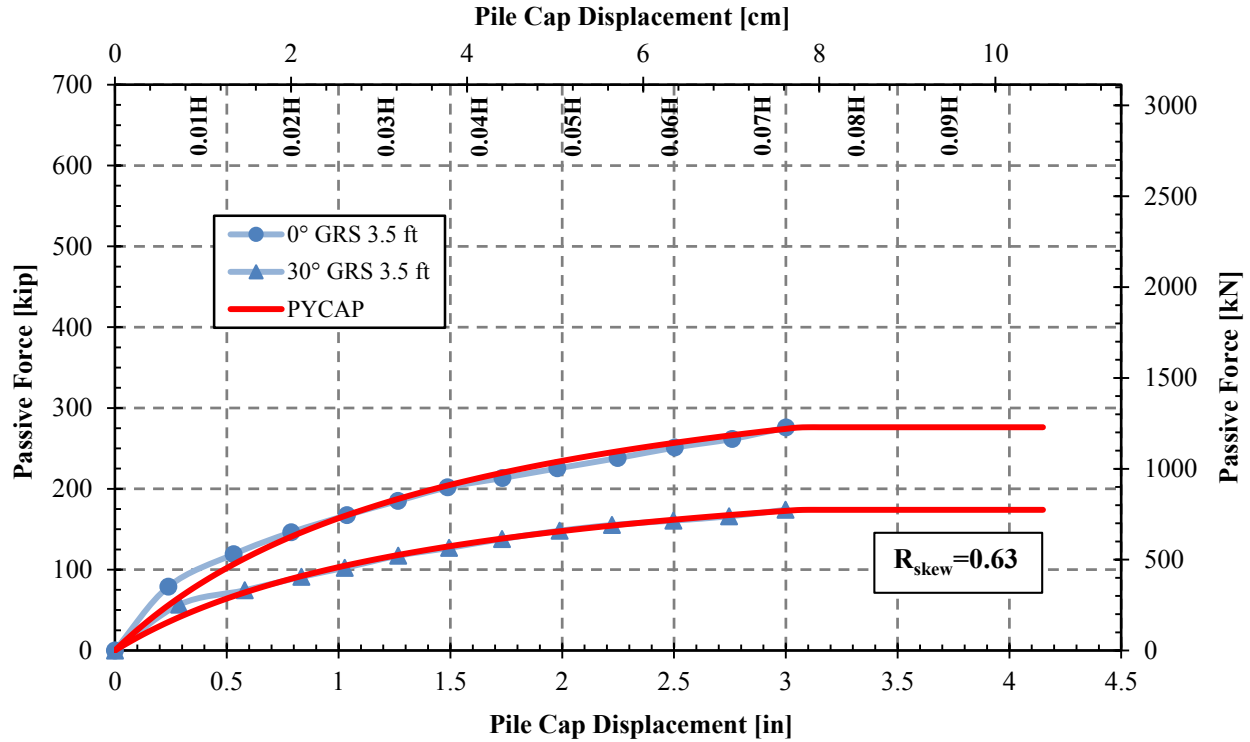
Figure 6-17. GRS PYCAP curves with R_{skew} and 0° and 30° data.

Table 6-7: Best Fit PYCAP Input Values for 30° Gravel and GRS Tests

Soil Strength Parameter	Units	30° Gravel Inputs	30° GRS Inputs
Cap Width, b	ft (m)	11.0 (3.35)	11.0 (3.35)
Cap Height, H	ft (m)	3.5 (1.07)	3.5 (1.07)
Cohesion, c	lb/ft^2 (kPa)	0	0
Soil Friction Angle, ϕ	deg	45.8	45.8
Wall Friction Angle, δ	deg	30.2	25.8
Initial Soil Modulus, E_i	lb/ft^2 (kPa)	310 (14.8)	200 (9.6)
Poisson's Ratio, ν	–	0.22	0.22
Soil Unit Weight, γ_m	lb/ft^2 (N/m^3)	144.9 (18.25)	144.9 (18.25)
Δ_{max}/H at Failure	–	0.0325	0.073
R_{skew}	–	0.58	0.63

181
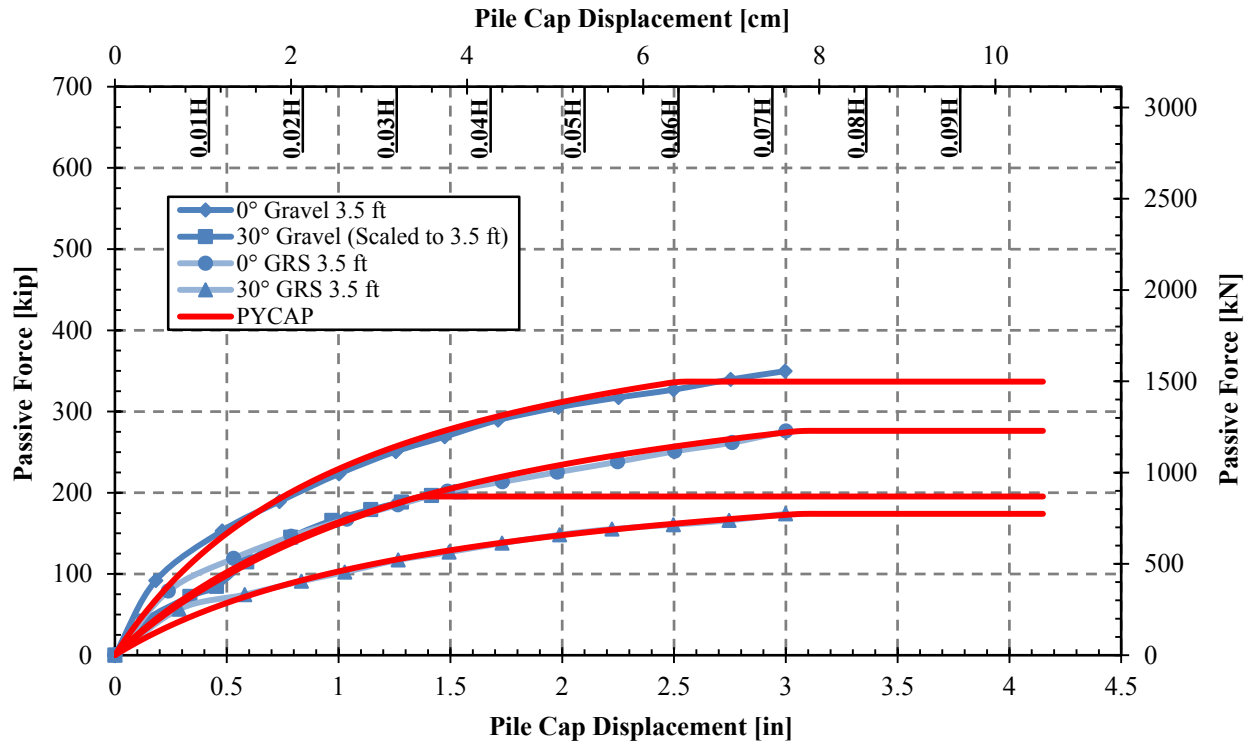
Figure 6-18. All four gravel and GRS PYCAP best fit curves.

6.4.1.4 Design

The PYCAP curves shown so far were back-calculated from measured results. However, when predicting passive force, estimates need to be made based on the properties of the soil and recommended values by Duncan and Mokwa (2001). Figure 6-19 shows a design PYCAP curve based on the soil parameters that would be known in a design situation. The unknowns would be the wall friction angle (δ) and the initial soil modulus (E_i). Based on recommendations by Potyondy (1961), δ was estimated as 0.7H, or 32.1°. Cohesion was included as reported by the gravel shear tests. For E_i, Duncan and Mokwa suggest 600 ksf (28.7 MPa) as the low end of the range for a dense compacted soil (Dr≈80%). However, previous BYU studies have found 400 ksf (19.2 MPa) a more accurate value for unconfined tests and 300 ksf (14.4 MPa) a more accurate value for the MSE tests, which is shown for comparison to the GRS tests. The Δ_{max}/H factor was

182

assumed to be 0.05 based on previous studies including Rollins and Jessee (2013) and the conservative recommendation by AASHTO (2014). The effective width factor was automatically calculated by PYCAP as 1.80. Therefore the calculated predicted effective width for the 11.0 ft [3.35 m] pile cap was 19.8 ft [6.04 m]. The recommended inputs are summarized in Table 6-8 on page 184 next to the best fit inputs for each non-skewed test.
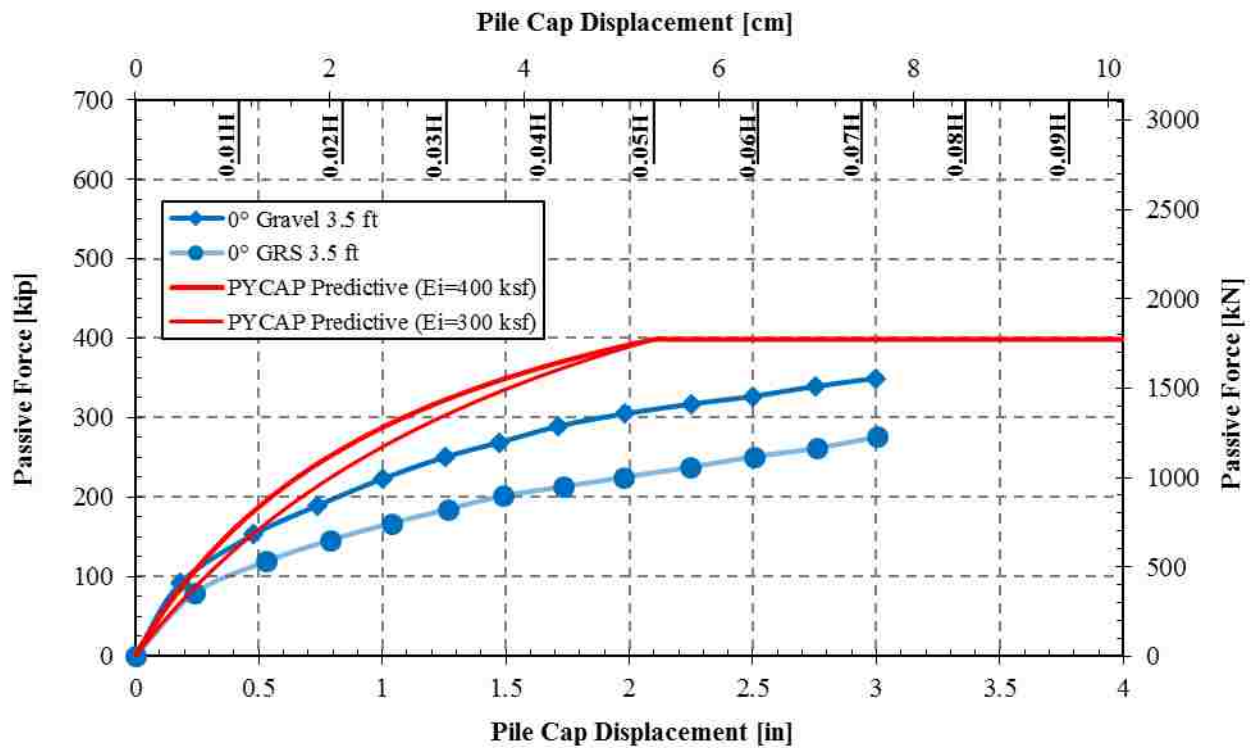
Figure 6-19. PYCAP passive force-deflection hyperbola based on recommended values compared to testing results.

The resulting hyperbolic curve predicts a maximum passive force of 399 kips. This value is 14% greater than the ultimate passive force measured in the gravel and 45% greater than the ultimate passive force measured in the GRS. The most sensitive factor to increase the ultimate passive force in the PYCAP curve is the increase in the wall friction angle. Thus, using 0.70H for the wall friction was a reasonable estimate for the gravel test, but was less so for the GRS test.

183

The curvature of the hyperbola is largely governed by the initial modulus (E_i). Using the E_i values recommended for normally loaded granular soils rather than for compacted soils produced an initial stiffness that more closely matched the actual data. The Δ_{max}/H value for the unconfined gravel test was already shown to be unusually high, therefore, the Δ_{max}/H value of 0.05H would be reasonable for most cases. However, the data suggests this value would likely be more accurate if increased to at least 0.07H for GRS backfills.

Table 6-8: Recommended PYCAP Input Values for Design in Gravel Backfill Compared to Best Fit Input Values

Soil Strength Parameter	Units	Gravel Recommended Inputs	0° Gravel Inputs	0° GRS Inputs
Cap Width, b	ft (m)	11.0 (3.35)	11.0 (3.35)	11.0 (3.35)
Cap Height, H	ft (m)	3.5 (1.07)	3.5 (1.07)	3.5 (1.07)
Cohesion, c	lb/ft^2 (kPa)	40	0	0
Soil Friction Angle, ϕ	deg	45.8	45.8	45.8
Wall Friction Angle, δ	deg	32.1	30.2	25.8
Initial Soil Modulus, E_i	lb/ft^2 (kPa)	300 (14.4), 400 (19.2)	310 (14.8)	200 (9.6)
Poisson's Ratio, ν	–	0.22	0.22	0.22
Soil Unit Weight, γ_m	lb/ft^3 (N/m^3)	144.9 (18.25)	144.9 (18.25)	144.9 (18.25)
Δ_{max}/H at Failure	–	0.05	0.06	0.073

6.4.2 ABUTMENT

Agreement with the ABUTMENT computer program (Shamsabadi et al., 2007) was also investigated. Like PYCAP, ABUTMENT also models the passive force-deflection curve hyperbolically but is based more on forces than on moments (See Subsection 2.3.4). The method specified in the program was Log Spiral Forces Method Composite, and 3D geometry was

184

selected. Failure planes were specified from the top down, and stress/strain was calculated with the modified hyperbolic method.
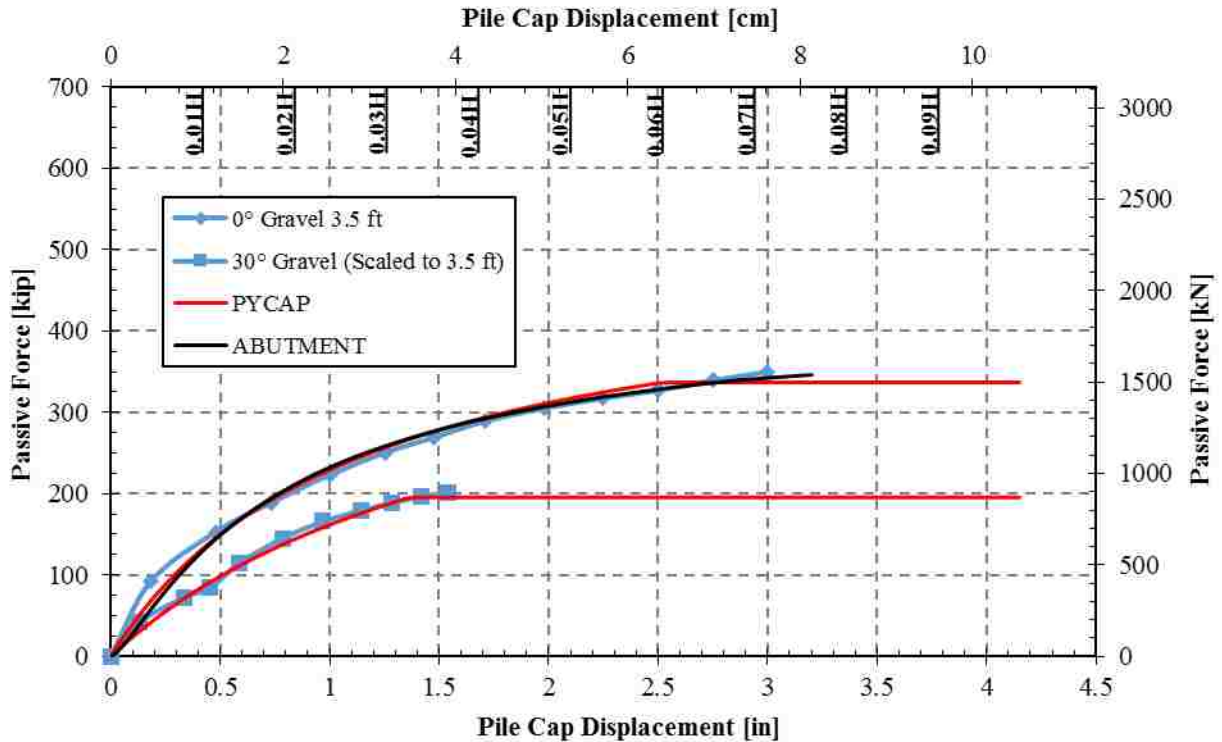
Figure 6-20. ABUTMENT best fit curve with 0° skew 3.5 ft gravel test data.

The results from ABUTMENT provided very good agreement with the gravel test data and with PYCAP results (see Figure 6-20) with very little adjustment of soil parameters and ABUTMENT default values. The curve is shown in Figure 6-20, and the inputs are listed in Table 6-9. The adjustment to the soil friction angle from 45.8° to 45.6° was very small and well within the variability allowed by using only two direct shear field test points. The wall interface friction angle ratio (δ/φ) was kept at 66%. Remaining soil parameters are equivalent to those input into PYCAP.

The parameter ε_{50} represents the strain at which 50% of the ultimate passive force is reached. Shamsabadi et al. (2007) recommends a range of 0.001 to 0.005 for gravels. The ε_{50}

185

value that best fit the data was 0.0075, which is indicative that the large displacements required to push this test without peaking were unusual, as previously discussed. A row in Table 6-9 shows the percentage above the highest ε_{50} value recommended for gravel, which is 0.005, of the best-fit ε_{50} value used. The recommended range for the failure ratio is 0.94 to 0.98; 0.955 fits comfortably within that range. Adjusting the Δ_{max}/H value in ABUTMENT with the ε_{50} value was more difficult than in PYCAP, thus the skew reduction was excluded from this case.

Table 6-9: ABUTMENT Input Values for Gravel and GRS Tests

Soil Strength Parameter	Units	0° Gravel Inputs	0° GRS Inputs
Cap Width, b	ft (m)	11.0 (3.35)	11.0 (3.35)
Cap Height, H	ft (m)	3.5 (1.07)	3.5 (1.07)
Soil Friction Angle, ϕ	deg	45.6	45.8
Wall Friction Angle, δ	deg	30.1	25.8
Cohesion, c	ksf (MPa)	0	0
Abutment Adhesion, C_a	ksf (MPa)	0	0
Soil Density, γ	kcf (kN/m^3)	0.1449 (0.01825)	0.1449 (0.01825)
ε_{50}	–	0.0075	0.010
% Above Recommended ε_{50}	%	50	100
Poisson's Ratio, ν	–	0.22	0.22
Failure Ratio, R_f	–	0.955	0.965
Surcharge, q	ksf (MPa)	0	0

The ABUTMENT analysis inputs for the GRS tests are also included in Table 6-9. The ABUTMENT analysis for GRS used the same soil and wall friction angles used in the PYCAP analysis of 45.8° and 25.8°, respectively. It also used a higher ε_{50} horizontal strain value (0.010) and higher failure ratio (R_f=0.965) than the gravel analysis as an effort to fit the shallower slope of the curve. Still, the shallow slope of the curve was difficult to match in ABUTMENT, as seen

in Figure 6-21. This analysis confirms the likelihood that the reduced passive resistance in the GRS tests was due to both lower wall friction and greater displacement required to develop full passive resistance. The R_{skew} value of 0.63 was used with the ABUTMENT data to reduce it for a 30° skew analysis, which also had nearly as good agreement as PYCAP.
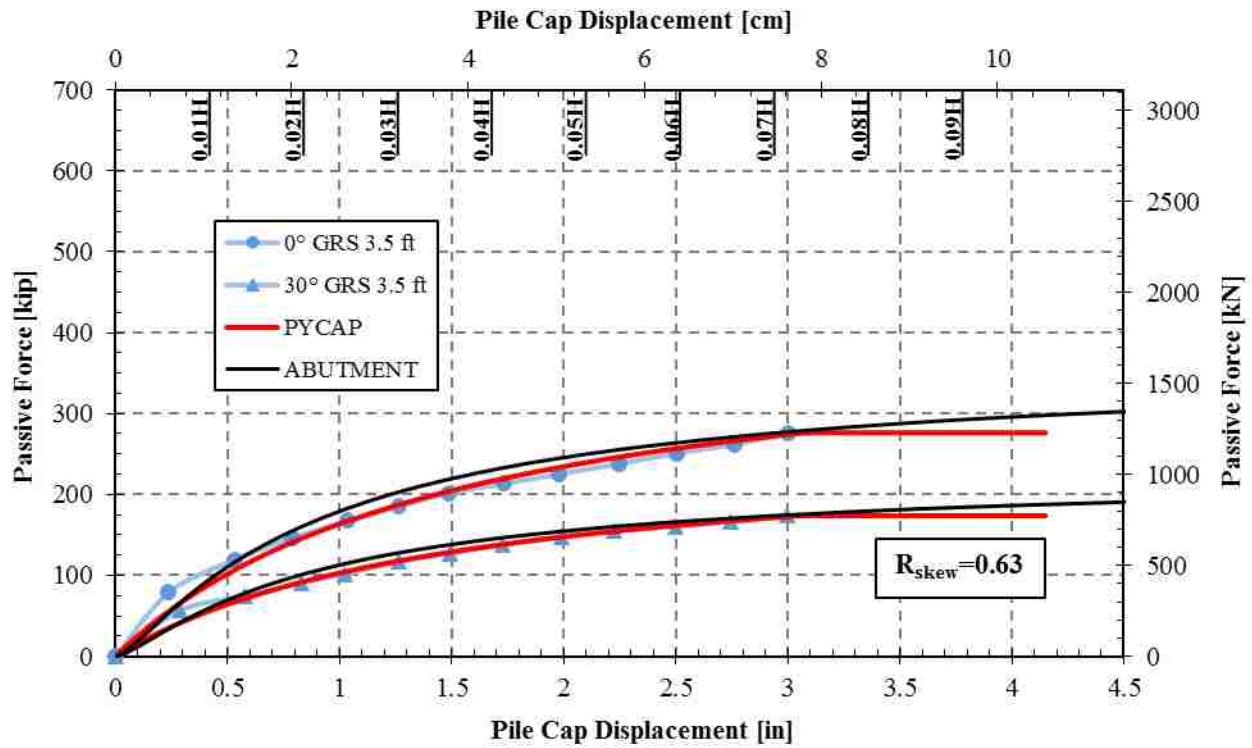
Figure 6-21. ABUTMENT analysis for GRS tests using PYCAP inputs and ε_{50}=0.010.

7   Conclusions

The following conclusions were developed as a result of this study.

1. Results from this study confirm that the passive force reduction factor equation (Rollins and Jessee, 2013) is generally applicable for gravel and GRS backfills but suggest the equation may require some fine tuning due to increased stiffness, higher friction angles, and increased unit weight in gravel backfills compared to sand backfills. However, the higher reduction factors observed in this study are within the range of statistical scatter based on all 26 abutment tests conducted to this point. Further testing is needed to determine if the higher passive force reduction factors observed in this study are an indication of needed adjustments to R_{skew} for gravel backfills.

2. Based on the 18 large-scale tests and the 8 laboratory-scale skewed abutment tests performed to date, the average passive force reductions due to skew are within about 3% of the predicted values from the passive force reduction factor equation developed by Rollins and Jessee (2013).

3. Within the range of longitudinal deflections investigated (0 to 0.06H), the GRS backfill typically produced about 40% lower passive resistance than the backfill consisting only of gravel. The reduction is likely attributable to lower interface friction between the concrete backwall and the geosynthetic and possible reduction of composite friction for the GRS backfill noted by previous researchers (Tuna & Altun, 2012).

189

4. Lower stiffnesses were observed in GRS backfills at small deflections. However, the geotextile also reinforced the soil so that stiffness only decreased slightly at higher deflections.

5. Results suggest a reduction in ultimate passive force in GRS backfills compared to unreinforced gravel backfills, but movement limitations at the test site prevented conclusive evidence. The actual reduction may be an effect of the greater deflections required to develop the same passive resistance, or in other words, the decreased stiffness.

6. When normalized by backfill height, both unconfined gravel and GRS-gravel backfills had significantly higher passive resistances than previous field tests performed with sand backfills. Some of the increase was due to the higher unit weight of the gravel relative to the sand; however, about two thirds of the additional resistance was associated with the strength properties of the gravel.

7. By using the log spiral method to calculate ultimate passive force, AASHTO's estimates were close to the measured peak. The AASHTO peak passive force, however, likely needs adjustment for the effects of skew. Δ_{max}/H values recommended by AASHTO for dense sand were slightly to moderately low for the dense gravel backfills tested in this study, but the lower bound of 0.05 was also moderately high, but not unreasonable.

8. The Caltrans passive force design approach underestimated the passive forces in gravel and GRS backfills, except in skewed GRS backfill. The higher initial stiffness was sufficient for the non-skewed unconfined gravel, but the non-skewed GRS and the skewed unconfined gravel stiffnesses matched the lower stiffness more consistently. The skewed GRS initial stiffness was below Caltrans recommendations. Based on these test

190

results and other conducted in the overall study, we recommend a modification to the Caltrans to account for observed reduction in stiffness and ultimate passive resistance associated with different backfill types as well as abutment skew angle.

9. Baseline tests showed that baseline resistance decreased with decreased time between tests. It also appears that baseline resistance may have decreased from the year before due to the volume and repetition of the loading that has occurred at the test site. Starting position of the pile cap may have also affected the baseline comparison. Because the baseline is integral to the calculation of passive force, it is recommended that future studies investigate further what factors cause the baseline resistance to change. Other skew studies should take multiple baseline tests at each skew angle whenever possible.

10. Preliminary investigations into effects from the transverse movements observed during testing showed that the passive force reduction factor may be higher when accounting for transverse movements. Future skewed abutment testing should more closely examine the impact of these transverse movements on how passive force is calculated.

REFERENCES

AASHTO (2014). "Guide Specifications for LRFD Seismic Bridge Design." 3-99 to 3-107.

Adams, M.T., Nicks, J.E., Stabile, T., Wu, J.T.H., Schlatter, W., and Hartmann, J. (2011). "Geosynthetic Reinforced Soil Integrated Bridge System—Synthesis Report." Report No. FHWA-HRT-11-027, *Federal Highway Administration*, McLean, VA.

Adams, M., Nicks, J. E., Stabile, T., Wu, J., Schlatter, W., and Hartmann, J. (2012). "Geosynthetic Reinforced Soil Integrated Bridge System Interim Implementation Guide." Report No. FHWA-HRT-11-026, *Federal Highway Administration*, Washington, DC.

Apirakyorapinit, P., Mohammadi, J., and Shen, J. (2012). "Analytical Investigation of Potential Seismic Damage to a Skewed Bridge." *Practice Periodical on Structural Design and Construction*, 16(1), 5-12.

Bathurst, R. J., Allen. T. M., and Walters, D. L. (2005). "Reinforcement Loads in Geosynthetic Walls and the Case for a New Working Stress Design Method." *Geotextiles and Geomembranes*, Vol. 23, No. 4, 287-322.

Brinch Hansen, J. (1966). "Resistance of a rectangular anchor slab." *Bull. No. 21*, Danish Geotechnical Institute, Copenhagen, 12-13.

Bryant, B. (1990). "Geologic Map of the Salt Lake City 30' x 60' Quadrangle, North-Central Utah, and Uinta County, Wyoming." *USGS,* Denver, CO.

Burke Jr., M. P. (1994). "Semi-Integral Bridges: Movements and Forces." *Transportation Research Record 1450,* 1-7.

Buke Jr., M. P., and Gloyd, C. S. (1997). "Emergence of Semi-Integral Bridges." *Transportation Research Record 1594,* 179-186.

Caltrans (2010). "Seismic Design Criteria Version 1.6." *California Department of Transportation*, Sacramento, California.

Clough, G. W., and Duncan, J. M. (1991). *Foundation Engineering Handbook*, 2nd Ed., H. Y. Fang, ed., Chapman and Hall, New York.

Cole, R. T., and Rollins, K. M. (2006). "Passive Earth Pressure Mobilization during Cyclic Loading." *Journal of Geotechnical and Geoenvironmental Engineering*, ASCE, 132(9), 1154-1164.

Cummins, C. R. (2009). "Behavior of a Full-Scale Pile Cap with Loosely and Densely Compacted Clean Sand Backfill Under Cyclic and Dynamic Loadings." *M.S. Thesis*, Department of Civil and Environmental Engineering, Brigham Young University, Provo, UT.

193

Duncan, J. M., and Mokwa, R. L. (2001). "Passive Earth Pressures: Theories and Tests." *Journal of Geotechnical and Geoenvironmental Engineering, ASCE*, 127(3), 248-257.

Elnashai, A. S., Gencturk, B., Kwon, O., Al-Qadi, I. L., Hashash, Y., Roesler, J. R., Kim, S. J., Jeong, S., Dukes, J., and Valdivia, A. (2010). "The Maule (Chile) Earthquake of February 27, 2010: Consequence Assessment and Case Studies." Department of Civil and Environmental Engineering, University of Illinois at Urbana-Champaign, 190.

FHWA. (2012). "Sample Guide Specifications for Construction of Geosynthetic Reinforced Soil-Integrated Bridge System (GRS-IBS)." Report No. FHWA-HRT-12-051, *Federal Highway Administration*, Washington, DC.

Franke, B. W. (2013). "Passive Force on Skewed Abutments with Mechanically Stabilized Earth (MSE) Wingwalls Based on Large-Scale Tests." M.S., Brigham Young University, Provo, Utah.

Helwany, S., Wu, J., Meinholz, P. (2012). "Seismic Design of Geosynthetic–Reinforced Soil (GRS) Bridge Abutments with Flexible Facing." *National Cooperative Highway Research Project 12–59(01). Transportation Research Board,* Washington, DC.

Horvath, J. S. (2005). "Integral-Abutment Bridges: Geotechnical Problems and Solutions Using Geosynthetics and Ground Improvement." *2005 FHWA Conference on Integral Abutment and Jointless Bridges*, Baltimore, Maryland, USA: 287-297.

Jessee, S. J. (2012). "Skew Effects on Passive Earth Pressures Based on Large-Scale Tests." M.S., Brigham Young University, Provo, Utah.

Lee, K. L., and Singh, A. (1971). "Relative Density and Relative Compaction." *Journal of Soil Mechanics and Foundations Design*, 97(7), 1049-1052.

Marsh, A. K. (2013). "Evaluation of Passive Force on Skewed Bridge Abutments with Large-Scale Tests." Master of Science, Brigham Young University, Provo, Utah.

Meyer, R. D. (2012). "Passive Earth Pressures: Design Parameters for Common Force-Displacement Approaches." M.S. Project, Brigham Young University, Provo, UT.

Meyerhof, G. G. (1956). "Penetration tests and bearing capacity of cohesionless soils." *Journal of Soils Mechanics and Foundation Division, ASCE*, 82(SM1).

Mokwa, R. L., and Duncan, J. M. (2001). "Experimental Evaluation of Lateral-Load Resistance of Pile Caps." *Journal of Geotechnical and Geoenvironmental Engineering, ASCE*, 127(2), 185-192.

Nicks, J. E., Adams, M., and Wu, J., "A new approach to the design of closely spaced geosynthetic reinforced soil for load bearing applications," TRB Annual Compendium of Papers, Transportation Research Board, Washington D.C., 2013a.

Ovesen, N. K. (1964). "Anchor slabs, calculation methods, and model tests," *Bull. No. 16*, Danish Geotechnical Institute, Copenhagen, 5-39.

Palmer, K. N. (2013). "Large-Scale Testing of Passive Force Behavior For Skewed Abutments with High Width-Height Ratios." M.S. Thesis, Brigham Young University, Provo, UT.

Potyondy, J. G. (1961). "Skin Friction between Various Soils and Construction Materials." *Geotechnique*, 11(4), 339-353.

Pruett, J. M. (2009). "Performance of a Full-Scale Lateral Foundation with Fine and Coarse Gravel Backfills Subjected to Static, Cyclic, and Dynamic Lateral Loads." M.S. Thesis, Brigham Young University, Provo, UT.

Rollins, K. M., and Cole, R. T. (2006). "Cyclic Lateral Load Behavior of a Pile Cap and Backfill." *Journal of Geotechnical and Geoenvironmental Engineering, ASCE*, 132(9), 1143-1153.

Rollins, K. M., Gerber, T., Cummins, C., and Herbst, M. (2009). "Monitoring Displacement vs. Depth in Lateral Pile Load Tests with Shape Accelerometer Arrays." *Proceedings of 17th International on Soil Mechanics & Geotechnical Engineering*, 3, 2016-2019.

Rollins, K. M., Gerber, T. M., and Heiner, L. (2010). "Passive Force-Deflection Behavior for Abutments with MSE Confined Approach Fills." *Report No. UT-10.15*, Utah Department of Transportation.

Rollins, K. M., and Jessee, S. (2013). "Passive Force-Deflection Curves for Skewed Abutments." *Journal of Bridge Engineering*, 17(5).

Rollins, K. M., and Sparks, A. E. (2002). "Lateral Load Capacity of a Full-Scale Fixed-Head Pile Group." *Journal of Geotechnical and Geoenvironmental Engineering, ASCE*, 128(9), 711-723.

Runnels, I. K. (2007). "Dynamic Full-Scale Testing of a Pile Cap with Loose Silty Sand Backfill." M.S. Thesis, Brigham Young University, Provo, UT.

Sandford, T. C., and Elgaaly, M. (1993). "Skew Effects on Backfill Pressures at Frame Bridge Abutments." *Transportation Research Record: Journal of the Transportation Research Board*, 1-11.

Shamsabadi, A., Kapuskar, M., and Zand, A. (2006). "Three-Dimensional Nonlinear Finite-Element Soil-Abutment Structure Interaction Model for Skewed Bridges." *5th National Seismic Conference On Bridges and Highways*, FHWA, ed. San Francisco, CA, 1-10.

Shamsabadi, A., Rollins, K. M., and Kapaskur, M. (2007). "Nonlinear Soil-Abutment-Bridge Structure Interaction for Seismic Performance-Based Design." *Journal of Geotechnical and Geoenvironmental Engineering, ASCE*, 133(6), 707-720.

195

Shinoda, M., and Bathurst, R. J. (2004). "Lateral and axial deformation of PP, HDPE and PET geogrids under tensile load." *Geotextiles and Geomembranes,* Vol. 22, 205-222.

Smith, K. M. (2014). "Passive Force on Skewed Bridge Abutments with Reinforced Concrete Wingwalls Based on Large-Scale Tests." M.S. Thesis, Brigham Young University, Provo, UT.

Steinberg, E., and Sargand, S. (2010). "Forces in Wingwalls from Thermal Expansion of Skewed Semi-Integral Bridges." *Report No. FHWA/OH-2010/16*, Prepared by Ohio University for Ohio Department of Transportation, Athens, OH, 87.

Strassburg, A. N. (2010). "Influence of Relative Compaction on Passive Resistance of Abutments with Mechanical Stabilized Earth (MSE) Wingwalls." M.S. Thesis, Brigham Young University, Provo, UT.

Tuna, S. C., and Altun, S. (2012). "Mechanical Behaviour of Sand-Geotextile Interface." *Scientia Iranica, Transactions A: Civil Engineering,* Sharif University of Technology, 196 (4), 1044-1051.

Unjoh, S. (2012). "Repair and Retrofit of Bridges Damaged by the 2010 Chile, Maule Earthquake." *Proc., International Symposium on Engineering Lessons Learned from the 2011 Great East Japan Earthquake*.

UDOT. (2012). "GRS Abutment and Wingwall." *Utah Department of Transportation*, Section 02871S, Project #F-I84-6(109)119, PIN #10182, Salt Lake City, UT.

Valentine, T. J. (2007). "Dynamic Testing of a Full-Scale Pile Cap with Dense Silty Sand Backfill." M.S. Thesis, Brigham Young University, Provo, UT.

Warren, K. A., Whelan, M. J., Hite, J., and Adams, M. (2014). "Three Year Evaluation of Thermally Induced Strain and Corresponding Lateral End Pressures for a GRS IBS in Ohio." *Geo-Congress 2014 Technical Papers, ASCE,* GSP 234, 4238-4251.